Accelerator based production of medically useful isotopes – ^{99}Mo/^{99m}Tc and ^{64,67}Cu

By

Arjun Gopalakrishna

Enrolment No PHYS01201304021

Bhabha Atomic Research Centre

A thesis submitted to the

Board of Studies in Physical Sciences

In partial fulfillment of requirements

for the Degree of

DOCTOR OF PHILOSOPHY

of

HOMI BHABHA NATIONAL INSTITUTE

December 2018

Homi Bhabha National Institute[1]

Recommendations of the Viva Voce Committee

As members of the Viva Voce Committee, we certify that we have read the dissertation prepared by Arjun Gopalakrishna entitled ***Accelerator based production of medically useful isotopes – $^{99}Mo/^{99m}Tc$ and $^{64,67}Cu$*** and recommend that it may be accepted as fulfilling the thesis requirement for the award of Degree of Doctor of Philosophy.

Chairman – Dr. B. S. Tomar		**Date:** 7/6/2019
Guide / Convener – Dr B.K.Nayak		**Date:** 7/06/2019
Examiner – Dr. S.K.Mukherjee		**Date:** 7/6/2019
Member 1- Dr. Sharmila Banerjee		**Date:** 7/6/19
Member 2- Dr. D.D.Deshpande		**Date:** 7/6/2019
Member 3- Dr R.Tripathi		**Date:** 7/6/19

Final approval and acceptance of this thesis is contingent upon the candidate's submission of the final copies of the thesis to HBNI.

I/We hereby certify that I/we have read this thesis prepared under my/our direction and recommend that it may be accepted as fulfilling the thesis requirement.

Date: 7/6/19

Place: Mumbai

Dr. B.K.Nayak

(Guide)

Annexure I

CERTIFICATION ON ACADEMIC INTEGRITY

1. I **Arjun Gopalakrishna** (name of the student) hereby, HBNI Enrolment No. **PHYS01201304021** undertake that, the thesis titled ***Accelerator based production of medically useful isotopes – $^{99}Mo/^{99m}Tc$ and $^{64,67}Cu$*** is prepared by me and is the original work undertaken by me and free of any plagiarism. That the document has been duly checked through a plagiarism detection tool and the document is plagiarism free.
2. I am aware and undertake that if plagiarism is detected in my thesis at any stage in future, suitable penalty will be imposed as per the applicable guidelines of the Institute / UGC.

Arjun G

Signature of the Student

Endorsed by the Thesis Supervisor:

(I certify that the work done by the Researcher is plagiarism free)

Signature (with date) B.K.Nayak 17/07/2019

Name: B.K.Nayak

Designation: Head NPD

Department / Centre: NPD, BARC

Name of the CI / OCC : BARC

STATEMENT BY AUTHOR

This dissertation has been submitted in partial fulfillment of requirements for an advanced degree at Homi Bhabha National Institute (HBNI) and is deposited in the Library to be made available to borrowers under rules of the HBNI.

Brief quotations from this dissertation are allowable without special permission, provided that accurate acknowledgement of source is made. Requests for permission for extended quotation from or reproduction of this manuscript in whole or in part may be granted by the Competent Authority of HBNI when in his or her judgment the proposed use of the material is in the interests of scholarship. In all other instances, however, permission must be obtained from the author.

Arjun Gopalakrishna

DECLARATION

I, hereby declare that the investigation presented in the thesis has been carried out by me. The work is original and has not been submitted earlier as a whole or in part for a degree / diploma at this or any other Institution / University.

Arjun Gopalakrishna

List of Publications arising from the thesis

Publications in Refereed Journal:

a. Published

1) Preparation of ^{99}Mo from the ^{100}Mo(γ, n) reaction and chemical separation of ^{99m}Tc, A.Gopalakrishna, H. Naik, S.V. Suryanarayana, Y. Naik, V.T. Nimje, B.K. Nayak, S.K. Sarkar, S. Padmanabhan, C. Kothalkar, P. Naskar, A.C. Dey, A. Goswami J Radioanal Nucl Chem 308: 431–438 (2016)

2) Production, separation and supply prospects of ^{67}Cu with the development of fast neutron sources and photonuclear technology, Arjun Gopalakrishna, Saraswatula Venkata Suryanarayana, Haladhara Naik, Tanuja Sushant Dixit, Basant Kumar Nayak, Amit Kumar, Pravind Maletha, Kiran Thakur,Abhay Deshpande, Ramamoorthy Krishnan, Kamaldeep, Sharmila Banerjee and Alok Saxena, Radiochim. Acta, 106(7): 549-558 (2018)

3) Measurement of ^{99}Mo production cross-section from the ^{100}Mo(n,2n) reaction with quasi mono-energetic neutron based on the ^{9}Be(p,n) reaction , A.Gopalakrishna, G.N. Kim, H. Naik, K. Kim, B.K. Nayak, Muhammad Zaman, J Radioanal Nucl Chem 316:561–569 (2018)

4) Production of ^{99}Mo and ^{64}Cu in a mixed field of photons and neutrons in a clinical electron linear accelerator, A. Gopalakrishna, S.V.Suryanarayana, H.Naik, B.K.Nayak, B.J.Patil, S.Devraju, R.R.Upreti, R.Kinhikar, D.D.Deshpande, P.Maletha, Kamaldeep, S.Banerjee, A.Saxena J Radioanal Nucl Chem 317 (3) ; 1409-1417 (2018)

b. Communicated

1) Direct production of ^{99m}Tc via the ^{100}Mo(p,2n) reaction: estimation of clinical shelf life of pertechnetate . A. Gopalakrishna, S.V. Suryanarayana, B. K. Nayak, H. Naik, A.A.Shanbhag, Kamaldeep, G.L.Vispute, E. T Mirgulae, D. Sarkar, S.C.Sharma, P.Maletha, S.Banerjee.

Other Publications:

a. Conference/Symposium

1) Investigation on the feasibility of ^{99m}Tc production from ^{100}Mo(p,2n) reaction at existing Medical Cyclotron Facilities, Arjun Gopalakrishna, D Sarkar, S.V Suryanarayana, B.K Nayak, E.T Mirgulae , H Naik, A Saxena
Proceedings of the 60th DAE-BRNS Symposium on Nuclear Physics 2015

2) Development of ^{99}Mo/^{99m}Tc generator via the ^{100}Mo(γ,n)^{99}Mo reaction A. Gopalakrishna, H. Naik, S.V. Suryanarayana, B. K. Nayak, Devraju, R.Khinikar, D.Deshpande
Proceedings of the seventh DAE-BRNS biennial symposium on emerging trends in separation science and technology 2016

3) Radioisotopic purity of ^{99m}Tc produced via ^{100}Mo(p,2n)^{99m}Tc as a function of proton irradiation energy, A. Gopalakrishna, S.V. Suryanarayana, B. K. Nayak, E. T. Mirgule, D. Sarkar, S.C. Sharma, Kamaldeep, P. Maletha, H. Naik, S. Banerjee, A. Saxena
Proceedings of the 61st DAE-BRNS Symposium on Nuclear Physics 2016

4) Production of ^{67}Cu at electron linacs - development of photonuclear technology A.Gopalakrishna, S.V.Suryanarayana, T.S.Dixit, Abhay Deshpande, B.K.Nayak, H.Naik, R. Krishnan, K.Thakur, P.Maletha, Kamaldeep, S.Banerjee, A.Saxena
Proceedings of the thirteenth DAE-BRNS nuclear and radiochemistry symposium 2017

5) Radioisotopic purity of ^{99m}Tc produced via ^{100}Mo(p,2n)^{99m}Tc, A . Gopalakrishna, S.V. Suryanarayana, B. K. Nayak, H. Naik E. T. Mirgule, D. Sarkar, S.C. Sharma, Kamaldeep, P. Maletha, , S. Banerjee, A. Saxena
Proceedings of the NAARRI International conference, NICSTAR 2018

6) Low specific activity ^{64}Cu ions – biomarker for melanoma, A. Gopalakrishna, S.Chakraborty, A.Chakraborty, Y. Pawar, B.Mohanty, M.Tawate, K. V. Vimalnath, R. Chakravarty, S.Banerjee, B.K.Nayak, S.V.Suryanarayana, H.Naik, P.C.Chaudhari, A. Kumar, P.Maletha, Kamaldeep, A.Dash, , ARCEBS 2018

Arjun Gopalakrishna

Dedicated

to

Bhaikaka

ACKNOWLEDGEMENTS

At the foremost, I would like to thank my guide Dr B.K.Nayak for his support and guidance.

This thesis could not have been completed without the help and support of Dr S.V.Suryanarayana and Dr H.Naik .

I thank the Doctoral Committee members Dr B.S.Tomar, Dr D.D.Deshpandhe, Dr S.Banerjee, Dr R.Tripathi, for their suggestions and comments.

I thank Shri Shanbhag, Shri Sharma, Shri Rohan, Dr Mirgule, Shri D.Sarkar, Head NPD BARC, Head RCD BARC & all operating personnel, for their support in the pelletron experiments.

I thank Shri Devraju, Shri Khinikhar, Shri Ritu Raj & all operating personnel for their support in the Clinical Linac experiments and Dr B.J.Patil for his help in Fluka simulations.

I thank Dr Tanuja Dixit, Dr Abhay Deshpande, Dr Y. Naik , Dr V.T. Nimje , Dr Krishnan and all operating personnel for their support in the experiments at EBC, Kharghar & SAMEER:

For the fast neutron experiments at Purnima BARC and at KIRAMS, I would like to thank Smt Saroj Bishnoi, Shri Tarun Dr G.N.Kim, Dr K.Kim, Dr M.Zaman & all operating personnel

I would like to thank my colleagues at Column generator production facility, BRIT : Dr Sarkar, Dr Saraswathy, Shri C.Kothalkar, Shri P. Naskar, Shri A.C.Dey, for their help in preparation of ZrMo gel.

My colleagues at The Medical Cyclotron Facility have been a great help and support. I would like to thank, Dr N.Lakshminarayanan, Shri Amit Kumar, Shri Pravind, Shri Kamaldeep, Shri Mitra, Shri Rahul Shri Rajesh W, Shri B.K.Sharma, Shri Yuv Raj, Dr Nandy, Shri Nayak, Dr Rajesh, Smt Kanchan, Shri Abhinav, and others at RMC

For the animal studies, I would like to thank Dr Sudipta Chakraborty, Dr K. V. Vimalnath, Dr Rubel Chakravarty , Dr Avik Chakraborty, Dr Yogita Pawar, Ms Megha Tawate, Shri Bhabani Mohanty, Dr P.C.Chaudhari, and Head RpHD BARC

I would like to thank Dr Rajan, Dr Meera Venkatesh and Dr N.Ramamoorthy for their words of wisdom over the years.

Ms Bioletty, Ms Reetu , Ms Sylvia of NEHU are acknowledged for their help. The training course (OCES-57) was a smooth experience, due to the help received from Shri Swayam Kesari, Shri Sushant, Ms Saheli Ms P.Biswas, Shri D.Sarkar, Shri Raj Narayan, Shri Swapan, Smt Nirupama, Smt Sangeetha, Shri Kanse, Shri Naveen, Shri Paramjeet.

I would like to thank my Late mother, Smt Nalini, my mother in law, Smt Meera and maid Smt Savitri, for their help in taking care of my responsibilities towards my son. The families of my brother Lt Col Chetan, my sister Smt Indira, my brother in law Shri Naresh, and sister in law Smt Binda are acknowledged for their support.

This work has been only possible, with the full support of my wife Dr (Smt) Chanda, who left me free to carry out this work, and due to the grace of Sadhguru.

CONTENTS

Homi Bhabha National Institute

SYNOPSIS OF Ph. D. THESIS

1. **Name of the Student: Arjun Gopalakrishna**
2. **Name of the Constituent Institution: BARC**
3. **Enrolment No. : PHYS01201304021**
4. **Title of the Thesis:** Accelerator based production of medically useful isotopes – ^{99}Mo/^{99m}Tc and ^{64,67}Cu
5. **Board of Studies: Physical Sciences**

SYNOPSIS

Nuclear medicine today is a well-established field, with radionuclides and radiopharmaceuticals playing key roles, in diagnostic investigations and therapy.

Technetium-99m (^{99m}Tc) is used in approximately 85% of nuclear medicine diagnostic imaging procedures worldwide. Almost all the ^{99m}Tc used for this purpose is obtained from the radioactive decay of molybdenum-99 (^{99}Mo), which is produced by processing irradiated uranium targets in Belgium (IRE), Canada (AECL/Nordion), the Netherlands (Covidien) and South Africa (NTP). After irradiation, the uranium targets are processed to extract ^{99}Mo, which in turn is purified for use in ^{99}Mo / ^{99m}Tc generators that are shipped to radiopharmacies, hospitals and clinics. The research reactors used to irradiate targets that produce most of the world's supply of ^{99}Mo are over 40 years old. Planned and unplanned shutdowns of some of these reactors have resulted in several recent ^{99}Mo / ^{99m}Tc supply interruptions. These interruptions coupled with promoting the conversion of ^{99}Mo production from highly enriched uranium (HEU) to low enriched uranium (LEU), to eliminate HEU use in civilian applications have prompted

global efforts to develop alternative production methods for the parent radionuclide ^{99}Mo as well as the desired product ^{99m}Tc.

Major alternative non-HEU ^{99}Mo /^{99m}Tc production methods, routes independent of a reactor [1] , being considered are

a) Charged-particle induced reactions ^{100}Mo(p,pn) ^{99}Mo, ^{100}Mo(p,2n) ^{99m}Tc,

b) Photon induced reactions ^{nat}U(γ,f) ^{99}Mo and ^{100}Mo(γ,n) ^{99}Mo and

c) Neutron induced reaction ^{100}Mo(n,2n) ^{99}Mo.

Copper (Cu) is a transition metal with atomic number 29. In humans, copper plays a role as a cofactor for numerous enzymes, such as Cu/Zn-superoxide dismutase, cytochrome c oxidase, tyrosinase, ceruloplasmin, and other proteins, crucial for respiration, iron transport and metabolism, cell growth, and hemostasis

Natural copper comprises two stable isotopes, ^{63}Cu (69.17%) and ^{65}Cu (30.83%), and 27 known radioisotopes, five of them are particularly interesting for molecular imaging applications (^{60}Cu, ^{61}Cu, ^{62}Cu, and^{64}Cu), and in vivo targeted radiation therapy (^{64}Cu and ^{67}Cu). Copper radionuclides offer a varying range of half-lives and decay modes.

^{64}Cu is an attractive radionuclide in nuclear medicine for both positron emission tomography and radiotherapy, because of its intermediate half-life and a characteristic decay process ($T_{1/2}$ = 12.7 h; β^+ 17.6%, β^- 38.5%, and EC 43.9%). ^{67}Cu is a promising therapeutic radionuclide, suitable for Single Photon Emission Computed Tomography (SPECT) due to its soft gamma-ray emission (Eγ = 184.58 keV, 48.6%) and for the therapeutic effect due to its average 141 keV β- particle (0.61 mm tissue range). The half-life of ^{67}Cu (2.58 d) is shorter, compared to those of clinically established radiotherapeutic radionuclides ^{131}I(8.04 d) and ^{177}Lu (6.65 d), and thus ^{67}Cu can be used to label molecules that exhibit a more rapid washout from tumor tissues.

Despite the presence of favorable factors- the overexpression of the human copper transporter protein (hCtr1) in a variety of cancers, the specific role of copper as a trace

metal in various metabolic pathways of human physiology and ready availability of chelators, the growth and use of ^{64,67}Cu-based radiopharmaceuticals is not common, due to the lack of consistent, high activity production .

In the medium to long term range, newer irradiation facilities in the form of intermediate energy proton accelerators, high-energy and high-intensity photon sources and spallation neutron sources are expected to be developed [2]. As an alternative to the use of reactors, use of accelerators represents a promising approach- for the production of ^{99}Mo/^{99m}Tc without the requirement for HEU targets and to aid in the sustained availability of theranostic pair ^{64,67}Cu.

The **thesis** includes the following studies on:

- Direct production of ^{99m}Tc via ^{100}Mo(p,2n)^{99m}Tc
- Accelerator based production of ^{99}Mo
- Production and application of low specific activity ^{64}Cu
- Accelerator based production of no carrier added ^{64,67}Cu

The thesis is organized in seven chapters to discuss the different aspects of the present work. The contents of the chapters are summarized as follows.

Chapter 1 comprises a general introduction to nuclear medicine. The application of radionuclides to nuclear medicine are described. The radionuclides are broadly classified into diagnostic and therapeutic radionuclides. The role of ^{99m}Tc – the workhorse of nuclear medicine is described. The easy availability of ^{99}Mo/^{99m}Tc column generators has helped Single Photon Emission Computed Tomography (SPECT) achieve its importance in nuclear medicine. Radionuclides used in Positron Emission Tomography (PET) are introduced. The role of non standard positron emitters like ^{64}Cu in PET are described. For internal radiotherapy β^-, α, Auger electron and X-ray emitters are of great interest. The therapy usually is either brachytherapy, palliative therapy, or internal therapy with β^- emitters involving the radiosynthesis of tumour seeking agents. Copper-67 has been considered as one of the ideal therapeutic

radionuclides. Theranostics utilises a combination of therapeutic emissions such as alpha, beta, or Auger ('thera'-) and diagnostic emissions such as gamma or positrons (-'nostic') [3].The theranostic approach entails a combination of diagnosis and internal radionuclide therapy. Combining a β^- (or Auger electron) and β+ emitting pair of radionuclides, it is possible to measure the uptake kinetics by PET imaging, thereby allowing an accurate dosimetric calculation related to therapy. There are several such pairs, e.g. ^{47}Sc/^{44}Sc; **^{64}Cu/^{67}Cu**; ^{67}Ga/^{68}Ga or ^{66}Ga; ^{89}Sr/^{83}Sr; ^{131}I/^{124}I and ^{161}Tb/^{152}Tb. ^{67}Cu can also be paired with the positron emitter ^{64}Cu to perform low dose molecular imaging with the same radiopharmaceutical and eventually to obtain more effective therapeutic effect by using higher dose. The section on development of newer irradiation technologies for medical radionuclide production highlights aspects of high-energy and high-intensity photon sources and spallation neutron sources.

Chapter 2 describes **studies on direct production of ^{99m}Tc via ^{100}Mo(p,2n)^{99m}Tc**. The direct production of ^{99m}Tc from a cyclotron beam of energetic protons using the ^{100}Mo(p,2n)^{99m}Tc nuclear reaction can make possible the local distribution of ^{99m}Tc [4]. In producing large-scale quantities of ^{99m}Tc for clinical use, knowledge of the cross-sections is essential for optimizing the high current irradiation conditions and verifying the processing and recovery strategies. Given the large cross section discrepancies in the current literature, the cross sections for the ^{100}Mo(p,2n)^{99m}Tc and ^{100}Mo(p,pn)^{99}Mo reactions were re-evaluated. The ^{99m}Tc and ^{99}Mo cross sections were evaluated using ^{100}Mo enriched (95.5%, 1 mg/cm^2) foils. Foils were irradiated in a stackfoil arrangement with Al foil as energy degrader in the BARC-TIFR Pelletron for 2 hours with proton energies from 11.3 to 21 MeV. A copper foil was used for the purpose of monitoring the beam energy and irradiation current. In determining the ^{99m}Tc activity, the 140.5 keV peak was measured. Two additional contributing sources to the 140 keV peak were subtracted prior to evaluation of the direct ^{99m}Tc cross section. Firstly, as

^{99}Mo gives rise to a 140 keV gamma ray upon decay, this peak contribution was calculated from the measured ^{99}Mo activity of each respective foil (the ^{99}Mo activity was determined using the 181 keV and 739 keV peaks) and as ^{99}Mo decays to ^{99m}Tc, the ^{99}Mo associated ^{99m}Tc activity at the start of counting was determined.

Thick target yields calculated from these cross-sections indicate production of 57GBq and 147 GBq of ^{99m}Tc given a 3h, 100μA,15-10 MeV and 21-10 MeV irradiation of 95.9% enriched ^{100}Mo respectively.

Other isotopes, are co – produced due to competing reactions and impurities in the enriched target during the ^{100}Mo(p,2n)^{99m}Tc reaction. These isotopes affect the specific activity of ^{99m}Tc and can potentially produce poor quality images and unnecessary dose to patient. Off line gamma spectrometry measurement of isotopes co- produced by impurities in the target and competing reactions was carried out using a calibrated HPGe detector. The following isotopes of Tc, Mo and Nb were identified- ^{93g}Tc, ^{94g}Tc, ^{95m}Tc ,^{95g}Tc, ^{96g}Tc, ^{97m}Tc, ^{99m}Tc, ^{99}Mo, ^{95g}Nb,^{96g}Nb. The radionuclidic purity defined as the ratio of ^{99m}Tc to all Tc was determined for end of bombardment, and cooling time upto 24 hours. Radionuclidic purity studies carried out as a function of proton energy and cooling time, post EOB, favor lower proton irradiation energies

Chapter 3 describes studies on **production of ^{99}Mo from the ^{100}Mo(γ, n) reaction and chemical separation of ^{99m}Tc**. The easy availability of ^{99m}Tc, from alumina based ^{99}Mo/^{99m}Tc column generators prepared using fission produced ^{99}Mo, complying to pharmacopieal specifications, on an economical scale has been a major factor responsible for the growth of SPECT. The Indian pursuit of gel generator technology involving the development of a user-friendly, column-type ^{99m}Tc generator is based on the conversion of (n, γ) ^{99}Mo as a zirconium [^{99}Mo] molybdate (Zr^{99}Mo) matrix and subsequent elution of ^{99m}Tc from the Zr^{99}Mo gel column with normal saline [5]. However the preparation of Zr^{99}Mo gel generator, involves multi step operations like

precipitation, filtration, drying, gel fragmentation in a hazardous radiation environment necessitating well-equipped hot cells. Inactive ZrMo was prepared at the Technetium column generator production facility at BRIT. The study investigates, irradiating natural Mo in the form of prepared inactive ZrMo and MoO_3 with bremsstrahlung of endpoint energy 15MeV to form ^{99}Mo via the ^{100}Mo(γ, n) route**,** followed by separation of ^{99m}Tc. The ^{99m}Tc yield from the irradiated MoO_3 was ~ 75%, and from the irradiated ZrMo in the range 25 – 35 % in 9 mL of saline / acetone. The separated $Na^{99m}TcO_4$ was of high radionuclidic, radiochemical and chemical purity. The radiochemical purity was > 99%, no extraneous gamma rays were seen and chemical impurities Al, Mo, Zr were less than 10 ppm. Labelling efficacy was demonstrated by labeling with in house kits.

Chapter 4 describes studies on **measurement of ^{99}Mo production cross-section from the ^{100}Mo(n,2n) reaction.** ^{99}Mo produced via ^{100}Mo(n,2n) route is poised as a long term approach for meeting requirements of nuclear medicine centres [6]. The cross section of the ^{100}Mo(n,2n)^{99}Mo reaction at 11<En<18 MeV is quite high – 1.5 barns, which is 10 times larger than the thermal neutron capture cross section of ^{98}Mo. The ^{100}Mo(n,2n) reaction cross-sections within the neutron energies range of threshold energy (8.36 MeV) to 20.5 MeV only are available in EXFOR. In this study, the production cross-section of the medical isotope, ^{99}Mo from the enriched ^{100}Mo(n,2n) reaction with the average neutron energies of 21.9 and 26.5 MeV has been determined for the first time by using an off-line γ-ray spectrometric technique, as 539.6±37.3 and 359.3±37.0 mb. The average neutron energies were generated by using the ^{9}Be(p,n) reaction with the proton energies of 35 and 45 MeV from the MC50 cyclotron of the Korea Institute of Radiological and Medical Sciences (KIRAMS) at Seoul, South Korea. The experimental results are in close agreement with the theoretical values from TALYS-1.8.

Chapter 5 describes **studies on production and application of low specific activity ^{64}Cu**. This study describes the production of low specific activity (LSA) ^{64}Cu in an electron Linac. ^{nat}Cu was irradiated with bremmstrahlung of 15MeV endpoint energy in a 15MV clinical linac, Truebeam , at Tata Memorial Hospital, Mumbai India. Along with the primary photon beam, the samples were simultaneously irradiated by the photoneutrons, produced by photonuclear reactions of the heavy metals of the accelerator head. ^{64}Cu was produced in the mixed field of photons and neutrons via $^{65}Cu(\gamma,n)^{64}Cu$ + $^{63}Cu(n,\gamma)^{64}Cu$. Fluka was used to simulate the fluence spectra of the gamma photons and neutrons and the Fluka calculations estimate 33 % contribution to ^{64}Cu yield by the secondary co-produced neutrons. The ^{64}Cu yield was observed to increase upto 45 % after moderation of the neutrons with varying thickness of a solid water phantom. This study opens the possibility of irradiating natural targets of Cu in a electron Linac to produce ^{64}Cu as a cost saving measure for medical applications.

Copper metabolism is critical for cell proliferation, angiogenesis, and tumor growth. Human copper transporter 1 (CTR1), a 190-amino acid protein of 28 kDa with three transmembrane domains, mainly acts as a copper transporter in mammals. CTR1 has been proven to be over expressed in many types of cancer cells, including melanoma, prostate cancer, liver cancer [7]. CTR1 has been found to mainly and specifically transport Cu(I) instead of Cu(II) [8]. This study compares the biological efficacy of LSA ^{64}Cu as ^{64}Cu(I)Cl and $^{64}Cu(II)Cl_2$, in C57BL/6 mice bearing melanoma tumors in a B16F10 tumor model. Reactor produced ^{64}Cu prepared via $^{63}Cu(n,\gamma)^{64}Cu$ was used in these experiments. For developing tumor model, the cells were subcutaneously injected in C57-BL6 mice at 5 x 10^5 cells/ mice in 200µl PBS. Tumors were allowed to develop for 15 days until they reached a volume of 100 mm^3, when bio-distribution experiment was initiated. The tumor uptake of LSA ^{64}Cu(II) and ^{64}Cu(I) was 5.14 ± 0.52 and 4.71± 0.56 % injected dose / g (ID/g) respectively at 24 hours post injection. Applications of

^{64}Cu in its most simple chemical form of copper chloride, would obviate radiolabeling steps, preclude the need of expensive target specific ligands such as peptides and antibodies, and will lower the cost of molecular imaging.

Chapter 6 describes studies on **Production, separation and supply prospects of ^{67}Cu with the development of fast neutron sources and photonuclear technology.** The current method for producing ^{67}Cu via the ^{68}Zn(p,2p)^{67}Cu reaction method in high energy proton accelerators is cumbersome and also the ^{67}Zn(n,p)^{67}Cu method in reactors with fission neutrons does not meet the requirements of the medical community.

There is an enhanced production possibility of ^{67}Cu, via (n, p) reactions on Zn induced by fast spectral neutrons [9] and the cross sections are three to five times higher than with a fission neutron spectrum. ^{67}Cu was produced via the ^{67}Zn(n,p)^{67}Cu, ^{68}Zn(n,n'p)^{67}Cu and ^{68}Zn(n,d)^{67}Cu reaction routes by irradiating ^{nat}Zn foils with 14.1 MeV DT accelerator neutrons at the Purnima Neutron generator Facility, BARC. The ^{68}Zn(n,x)^{67}Cu cross section was experimentally determined as 4.7 ± 0.81 mb. The ^{67}Cu production yield on irradiation of ^{nat}Zn via ^{67}Zn(n,p)^{67}Cu +^{68}Zn(n,x)^{67}Cu at the end of 2 days irradiation, in a high flux of 10^{11} n/s cm^2 is estimated as 0.9 MBq.

The Giant Dipole region (GDR), of 10 - 30 MeV is characterized by a high photo-absorption cross-section and is suitable for radioisotope production. The Society for Applied Microwave Electronics Engineering and Research (SAMEER) is developing a 30 MeV, 8-10 kW electron LINAC for the radioisotope production, in India. In the first phase, SAMEER has developed a prototype 15 MeV S-band standing wave side coupled linear electron accelerator [10]. Radioactivity 2.33 kBq of ^{67}Cu / g ^{nat}Zn * kW was produced in 45 minutes of irradiation via the ^{68}Zn(γ,p)^{67}Cu route at SAMEER.

The separation of ^{67}Cu from irradiated Zn was carried out via solvent extraction method. The solvent extraction method is based on (1) selective extraction of Cu

dithizonate into organic solvent from a dilute acidic solution of the bulk Zn target and (2) back extraction of Cu into aqueous phase. The radionuclide impurities ^{65}Zn and ^{69m}Zn were not detected in the final ^{67}Cu product, indicating achievement of high radionuclidic purity. The separation yield was determined radiometrically, by comparing the ^{64,67}Cu activity before and after separation. High separation yields of > 90% , with good reproducibility, was observed.

Chapter 7 concludes with a summary of works and discusses briefly the important outcome of the work and future directions.

Highlights of the work include

- Direct production of ^{99m}Tc via ^{100}Mo(p,2n)^{99m}Tc
  - Evaluation of cross sections of ^{100}Mo(p,2n)^{99m}Tc reaction
  - Calculation of thick target yields of ^{99m}Tc
  - Determination of radionuclidic purity of ^{99m}Tc
- Production of ^{99}Mo via ^{100}Mo(γ,n)^{99}Mo
  - Preparation of column generators with Zr^{99}Mo
  - Separation of ^{99m}Tc from ^{99}Mo and
  - Evaluation of ^{99m}Tc for compliance with pharmacopieal specifications
- Cross section measurements of ^{99}Mo produced via ^{100}Mo(n,2n)^{99}Mo
- Alternative route for production of low specific activity ^{64}Cu in an electron linac in a mixed field of photons and neutrons
- Studies on use of low specific activity ^{64}Cu in the form of its chloride as a probe for tumor imaging by Positron Emission Tomography
- Production yields of no carrier added ^{67}Cu produced via irradiation of ^{nat}Zn with 14.1 MeV DT neutrons and bremsstrahlung of end point energy 15 MeV
- Separation of ^{67}Cu from irradiated Zn with high radionuclidic purity and yield

References

1) Non-HEU production technologies for Molybdenum-99 and Technetium-99m IAEA Nuclear Energy Series No. NF-T-5.4 (2013)

2) Qaim, S.M. Nuclear data for production and medical application of radionuclides: Present status and future needs. Nucl. Med. Biol. **44**, 31, (2017)

3) Rösch, F., Herzog,H., Qaim, S.M.:The beginning and development of the theranostic approach in nuclear medicine, as exemplified by the radionuclide pair ^{86}Y and ^{90}Y.Pharmaceuticals **10**, 56(2017).

4) Gagnon K, Bénard F, Kovacs, Ruth TJ, Schaffer P, Wilson JS Cyclotron production of ^{99m}Tc: experimental measurement of the ^{100}Mo(p, x) ^{99}Mo, ^{99m}Tc and ^{99g}Tc excitation function from 8 to 18 MeV, Nucl Med Biol 38:907-916 (2011)

5) Saraswathy P, Sarkar S.K, Arjun G, Nandy S.K, Ramamoorthy N ^{99m}Tc gel generators based on zirconium molybdate- ^{99}Mo: III: Influence of preparatory conditions of zirconium molybdate-^{99}Mo gel on generator performance Radiochim Acta 92, 259 (2004)

6) OECD NEA Review of potential Molybdenum-99/Technetium-99m production technologies. The supply of medical radioisotopes. (2010)

7) Jesper Tranekjær Jørgensen, Morten Persson, Jacob Madsen, Andreas Kjær High tumor uptake of ^{64}Cu: Implications for molecular imaging of tumor characteristics with copper-based PET tracers Nuclear Medicine and Biology 40 **345** (2013)

8) Lei Jiang, Yingfeng Tu, Xiang Hu, Ande Bao, Hao Chen, Xiaowei Ma, Tim Doyle, Hongcheng Shi, ,Zhen Cheng. Pilot Study of 64Cu(I) for PET Imaging of Melanoma Scientific Reports 7: 2574 (2017)

9) Spahn, I., Coenen, H.H., Qaim, S.M. :Enhanced production possibility of the therapeutic radionuclides ^{64}Cu, ^{67}Cu and ^{89}Sr *via* (*n*, *p*) reactions induced by fast spectral neutrons. Radiochim. Acta **92**, 183 (2004)

10) Dixit,T.S., Chavan, S.T., Krishnan, R., Nainwad, C.S., Pethe, S.N., Thakur, K.A., Tiwari, T., Vidwans, M.M., Deshpande, A.: Development of prototype 15 MeV electron Linac , In Proceedings of 1st International Particle Accelerator Conference (IPAC'10), MOPEA50. 187, http://www.jacow.org, Kyoto, Japan (2010)

Publications in Refereed Journal:

a. Published

1) Preparation of ^{99}Mo from the ^{100}Mo(γ, n) reaction and chemical separation of ^{99m}Tc, A.Gopalakrishna, H. Naik, S.V. Suryanarayana, Y. Naik, V.T. Nimje, B.K. Nayak, S.K. Sarkar, S. Padmanabhan, C. Kothalkar, P. Naskar, A.C. Dey, A. Goswami
J Radioanal Nucl Chem 308: 431–438 (2016)

2) Production, separation and supply prospects of ^{67}Cu with the development of fast neutron sources and photonuclear technology, Arjun Gopalakrishna, Saraswatula Venkata Suryanarayana, Haladhara Naik, Tanuja Sushant Dixit, Basant Kumar Nayak, Amit Kumar, Pravind Maletha, Kiran Thakur,Abhay Deshpande, Ramamoorthy Krishnan, Kamaldeep, Sharmila Banerjee and Alok Saxena,
Radiochim. Acta, 106(7): 549-558 (2018)

3) Measurement of ^{99}Mo production cross-section from the ^{100}Mo(n,2n) reaction with quasi mono-energetic neutron based on the ^{9}Be(p,n) reaction , A.Gopalakrishna, G.N. Kim, H. Naik, K. Kim, B.K. Nayak, Muhammad Zaman,
J Radioanal Nucl Chem 316:561–569 (2018)

b. Accepted

1) Production of ^{99}Mo and ^{64}Cu in a mixed field of photons and neutrons in a clinical electron linear accelerator, A. Gopalakrishna, S.V.Suryanarayana, H.Naik, B.K.Nayak, B.J.Patil, S.Devraju, R.R.Upreti, R.Kinhikar, D.D.Deshpande, P.Maletha, Kamaldeep, S.Banerjee, A.Saxena
J Radioanal Nucl Chem (2018)

List of Figures **Page No.**

List of Tables

Chapter 1

Introduction

Radionuclides find application in many fields, their major use being in nuclear medicine, both in diagnosis and internal radiotherapy [1, 2].For in vivo diagnostic investigations involving organ imaging, radionuclides that do not cause much radiation dose and can be efficiently detected from outside of the body are used. Short-lived γ-ray emitters, like ^{99m}Tc and ^{123}I, and positron emitters, like ^{11}C and ^{18}F, are commonly used, the former finding application in Single Photon Emission Computed Tomography (SPECT) and the latter in Positron Emission Tomography (PET) [3].

Single-Photon Emission Computed Tomography (SPECT) and Positron Emission Tomography (PET) are the basis of nuclear medicine imaging tools, allowing precise investigations that are essential not only for early diagnosis but also for prognosis and monitoring of progress, regression or stagnation of a disease upon application of a particular therapy.

In internal radionuclide therapy, a localised, well-defined radiation dose needs to be deposited in a malignant tissue to achieve the desired therapeutic effect. Radionuclides emitting low-range highly-ionising radiation, i.e. α or β^- particles, conversion and/or Auger electrons, are suitable [4].

Theranostics utilise a combination of therapeutic emissions such as alpha, beta, or Auger ('thera'-) and diagnostic emissions such as gamma or positrons (-'nostic').The theranostic approach entails a combination of diagnosis and internal radionuclide therapy. Combining a β^- (or Auger electron) and β+ emitting pair of radionuclides, it is possible to measure the uptake kinetics by PET imaging, thereby allowing an accurate dosimetric calculation related to therapy. There are several such pairs such as ^{44g}Sc/^{47}Sc, ^{64}Cu/^{67}Cu, ^{83}Sr/^{89}Sr, ^{86}Y/^{90}Y, ^{124}I/^{131}I,

^{152}Tb/^{161}Tb and ^{152}Tb/^{149}Tb[5, 6]. The key advantages of theranostics include the personalisation of therapy based on uptake of the lower-dose diagnostic, the optimisation of dose based on personal dosimetry, and more importantly the selection of patients who have a high chance of responding to therapy [5].

1.1 SPECT and PET: The diagnostic applications of nuclides in nuclear medicine

1.1.1 SPECT

A radiopharmaceutical, labelled with a gamma emitter nuclide, is injected in patients and SPECT-cameras (large scintillation crystals connected to Photo-Multiplier Tubes, PMTs) are used for detecting the out-coming gamma rays [7]. The energy of these gamma rays should be high enough to come out from patients' body but low enough to be detected in medium-size crystals. The suitable γ-ray for SPECT-studies has an energy in the range of 100 - 300 keV.; the intensity should be as high as possible and preferably only the useful radiation should be emitted, in order to reduce the dose delivered to patients.

In order to reconstruct the bio distribution (spatial distribution) of the radiopharmaceutical, collimators, select a defined direction absorbing almost all the radiation coming from other directions. Thus, acquiring many views of the patient from different angles, the 3D distribution of the radio-pharmaceutical is reconstructed. Dual / triple headed cameras increase the speed of acquisition. Software algorithms integrate all individual projection views into a composite data set which are re-displayed as tomographic slices. The fusion of CT (Computed Tomography) with SPECT, has improved attenuation corrections.

Fig 1.1 Dual Head SPECT System.

Following radionuclides have been used in SPECT-studies: ^{67}Ga ($T_{½}$ = 3.26 d), ^{99m}Tc ($T_{½}$ = 6.0 h), ^{111}In ($T_{½}$ = 2.8 d), ^{123}I ($T_{½}$ = 13.2 h) and ^{201}Tl ($T_{½}$ = 3.06 d). The radionuclide ^{99m}Tc is by far the most commonly used SPECT radionuclide [8]. It emits a 140.5 keV γ-ray and causes the least radiation dose to the patient. It is available via the ^{99}Mo/^{99m}Tc generator system. Recent estimates reveal that worldwide about 40 million patients per year are investigated using this radionuclide. Also the radionuclide ^{123}I is commonly used. However, due to its lesser availability and higher cost, ^{123}I is much less broadly used than ^{99m}Tc. ^{201}Tl, is extensively utilized for myocardial perfusion measurements. The remaining two radionuclides, i.e. ^{67}Ga and ^{111}In, are less commonly used as SPECT agents.

Applications of SPECT / Planar Imaging

Some typical applications of major interest are:

a) Bone scanning with ^{99m}Tc-MDP for follow up of metastatis of cancer patients.

b) Renography to elicit renal function, study obstruction and evaluate renal transplant.

c) Imaging blood flow (perfusion) to myocardium and brain.

d) Hepatobiliary function imaging for suspected acute cholecystitis.

e) Lung imaging, both perfusion and ventilation functions – pulmonary embolism, chronic obstructive pulmonary disease (COPD).

1.1.1.1 ^{99m}Tc / ^{99}Mo

Technetium-99m (^{99m}Tc) is used in approximately 85% of nuclear medicine diagnostic imaging procedures worldwide. ^{99m}Tc has many favourable properties required for diagnostic use in nuclear medicine. These are:

(a) 140 keV gamma energy of ^{99m}Tc is ideally suited for efficient detection and giving high quality pictures with a gamma camera. The distortion due to attenuation by the body tissues is low.

(b) The decay of ^{99m}Tc is associated with only a small component of particulate emission (internal conversion electrons) and hence upto 30-40 mCi of 99mTc radiopharmaceuticals can be injected safely into patients. Such a large dose helps in getting better quality images and information of greater reliability.

(c) The 6.01 h half-life of ^{99m}Tc is well suited for most of the nuclear medicine studies.

(d) The multiple oxidation states of technetium allow the chemical formulation of a variety of coordinate complexes.

(e) ^{99m}Tc can be conveniently obtained from a generator system.

Almost all the ^{99m}Tc used for this purpose is obtained from the radioactive decay of molybdenum-99 (^{99}Mo), which is produced by processing irradiated uranium targets in Belgium (IRE), Canada (AECL/Nordion), the Netherlands (Covidien) and South Africa (NTP). After irradiation, the uranium targets are processed to extract ^{99}Mo, which in turn is purified for use in ^{99}Mo /^{99m}Tc generators that are shipped to radiopharmacies.

^{99}Mo undergoes beta decay with about a 66 hour half-life. About 87% of these decays result in the production of the metastable isotope ^{99m}Tc , which subsequently decays to the ground state (^{99g}Tc) with about a 6 hour half-life. The present 'gold standard' process for producing ^{99}Mo for medical isotope use involves the neutron fission of ^{235}U (i.e. ^{235}U(n,f) ^{99}Mo) in multipurpose research reactors. About 6.1% of the ^{235}U fissions produce ^{99}Mo. The cross-section for this reaction is large (~584 barns for thermal neutrons) .

Column generators

The wide application of ^{99m}Tc in nuclear medicine was possible due to the availability of ^{99}Mo/^{99m}Tc column generators [9, 10]. These column chromatographic generators use a small bed of acidic alumina to reliably hold the $^{99}MoO_4^{2-}$ ions and allows $^{99m}TcO_4^-$ to be eluted in a pure form in high radioactive concentration. The daughter activity is periodically removed by elution with saline solution (since the $[^{99m}TcO_4]^-$ is less tightly bound to the column than $[^{99}MoO_4]^{2-}$). As shown in Fig 1.3, the daughter ^{99m}Tc grows again after elution. The maximum ^{99m}Tc activity is reached in generator systems in about 23 hours after the previous elution.

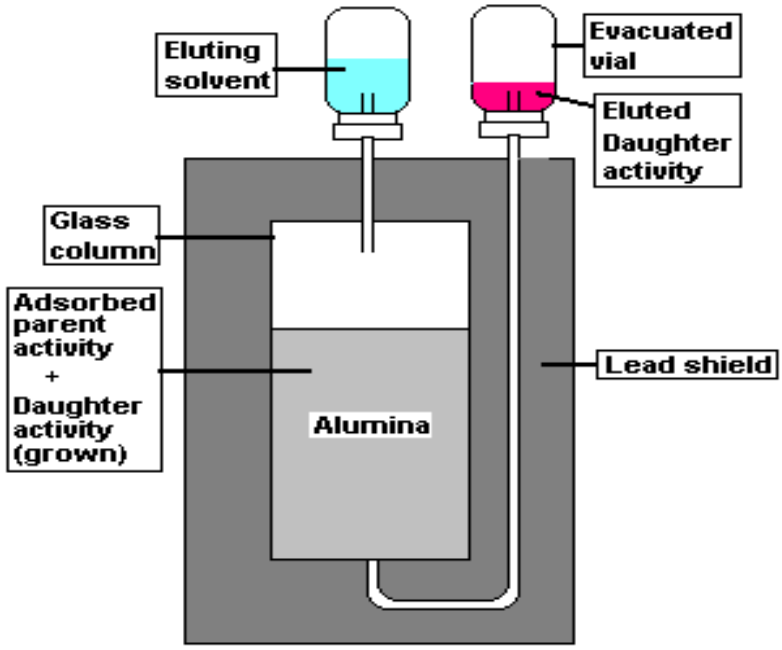

Fig 1.2 $^{99}Mo/^{99m}Tc$ alumina column generator .

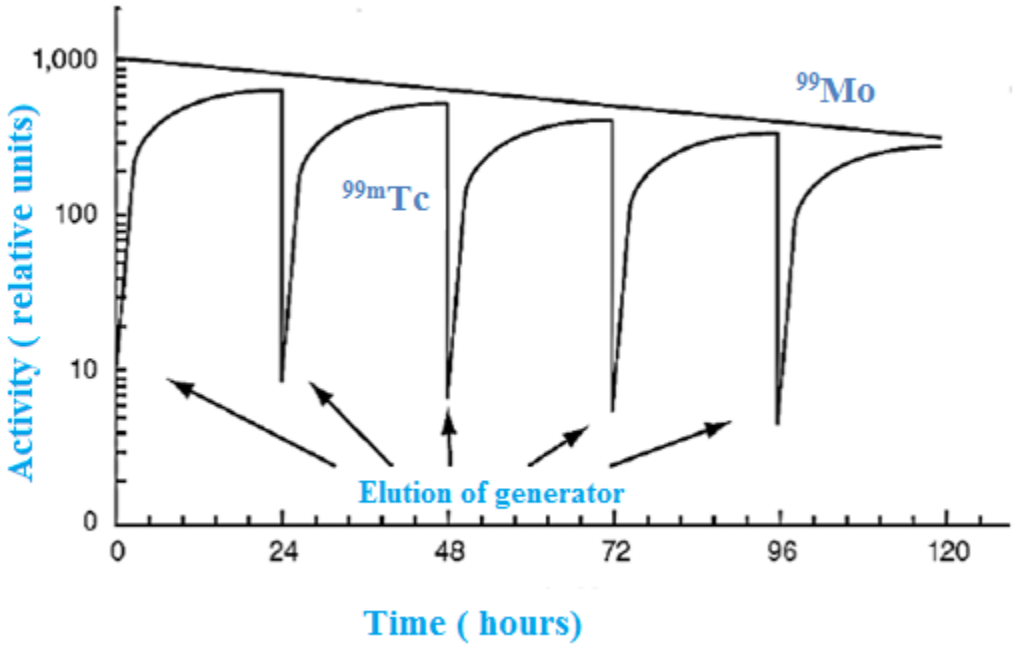

Fig 1.3 Growth and decay of ^{99m}Tc- post elution of $^{99}Mo/^{99m}Tc$ generator.

Kits for ^{99m}Tc-Labeling

The chemical form of ^{99m}Tc available from the Moly generator is sodium pertechnetate (^{99m}Tc-$NaTcO_4$). Chemically the pertechnetate ion, having the oxidation state 7+ is a rather nonreactive species and does not label any compound by direct addition. In ^{99m}Tc-labeling of many compounds, prior reduction of ^{99m}Tc from the 7+ state to a lower oxidation state is required. Among these, stannous chloride is the most commonly used reducing agent in most preparations of ^{99m}Tc-labeled compounds.

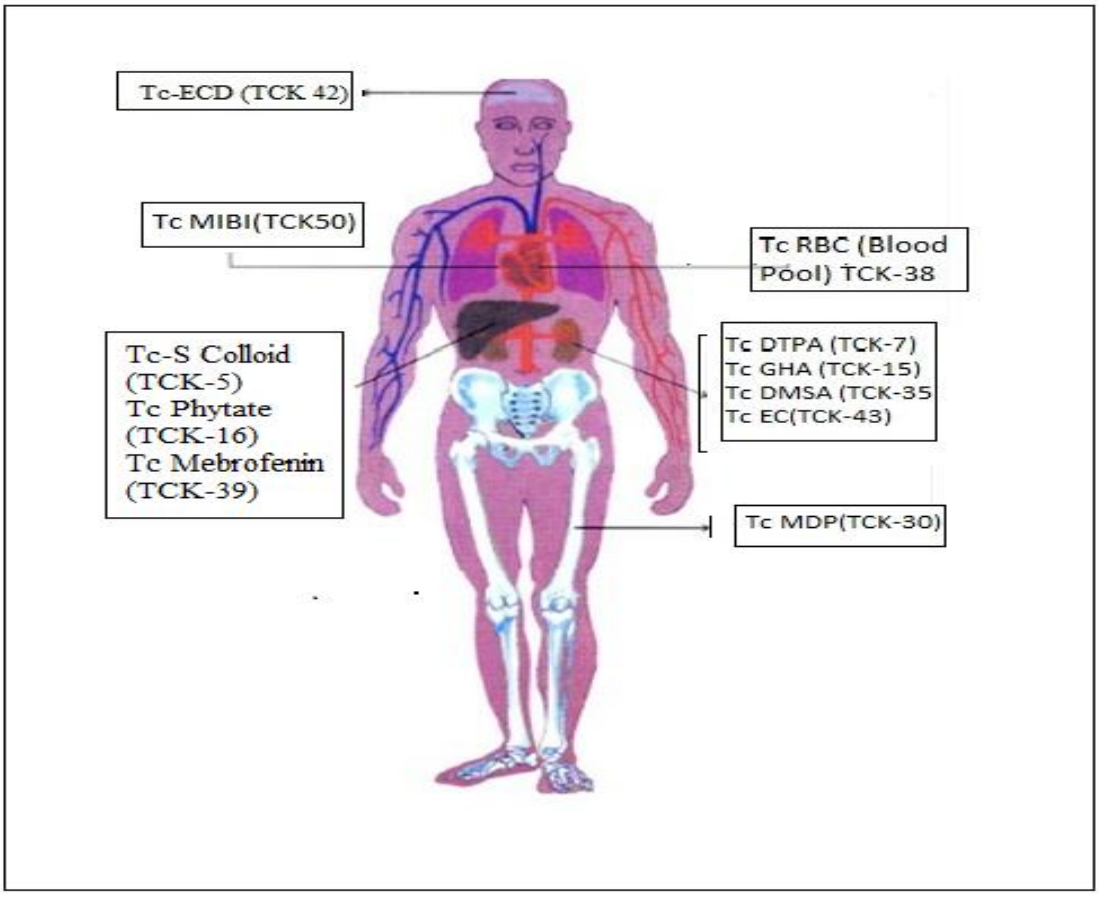

Fig 1.4 Utility of some the Tc cold kits prepared and marketed by Board of Radiation and Isotope Technology (BRIT) India.

Kits for labelling with ^{99m}Tc are easily available and the simplicity of use of these kits have also contributed to the wide spread use of ^{99m}Tc [11]. The kits for ^{99m}Tc-labeling have a long shelf life and can be purchased and stored well ahead of daily preparation; ^{99m}Tc-labeling can be accomplished by adding $^{99m}TcO_4^-$ to most kits. The Fig 1.4 shows utility of some of the Tc cold kits prepared and marketed by Board of Radiation and Isotope Technology (BRIT) India.

Kits for most ^{99m}Tc- radiopharmaceuticals are prepared from a ‘‘master’’ solution consisting of the compound to be labeled mixed with an acidic solution of a stannous compound in appropriate proportions. The pH of the solution is adjusted to 5 to 7 with dilute NaOH, purged with nitrogen, and aliquots of the solution are dispensed into individual kit vials. The solution is then lyophilized (freeze-dried) and the vial flushed and filled with sterile nitrogen. Lyophilization renders the dried material in the vial readily soluble in aqueous solution and thus aids in labeling by chelation.

.

1.1.1.2 Alternative non-HEU ^{99}Mo /^{99m}Tc production methods

The research reactors used to irradiate targets that produce most of the world’s supply of ^{99}Mo are over 40 years old. Planned and unplanned shutdowns of some of these reactors have resulted in several recent ^{99}Mo /^{99m}Tc supply interruptions. These interruptions prompted international organizations and several government agencies to step up efforts to find both short and long term solutions to supply shortages. The IAEA convened a group of experts to initiate a new activity specifically aimed at supporting global efforts to improve ^{99}Mo /^{99m}Tc supply reliability and promoting the conversion of ^{99}Mo production from highly enriched uranium (HEU) to low enriched uranium (LEU). The IAEA’s focus on the conversion of ^{99}Mo production from HEU to LEU is part of a long standing effort to eliminate HEU use in civilian applications [12].This has led to considerable scientific effort to develop alternative production methods for the parent

radionuclide ^{99}Mo as well as the desired product ^{99m}Tc. In general, more use of accelerators has been proposed [13, 14]. The Ref [12], considers fission based (n, f) production, photon based (γ, n) production using electron accelerators, neutron induced process ^{100}Mo(n,2n)^{99}Mo and direct production of ^{99m}Tc using proton accelerators.

In the **Photo-Fission of Uranium Targets** - a photon beam is focused on ^{238}U target to promote fission [15]. After irradiation, the uranium target is processed in the same manner as in the HEU route to recover ^{99}Mo and existing generator technologies can be used. Also a natural uranium target can be used. However, the extremely low cross-section of the reaction route coupled with the expense and challenges in the development of a high power machine are major challenges for the success of this proposition [16]. Also high volumes of waste would be produced. In the **Photo-transmutation of** ^{100}Mo **Targets-** high-intensity photons initiate the ^{100}Mo (g,n)^{99}Mo nuclear reaction to produce ^{99}Mo [15, 16]. The reaction cross-section of this path is approximately 130 mb at 15 MeV. Negligible radioactive waste and no proliferation concerns are the advantages in this method. However, the high cost of ^{100}Mo coupled with the expense and challenges in the development of a high power machine are major challenges for the success of this production route.

The production of ^{99}Mo from a ^{100}Mo target (whether using a photon, neutron or charged-particle induced reaction) would always lead to low specific activity and the generator column loaded with that ^{99}Mo would behave similar to that produced via the ^{98}Mo(n,γ) ^{99}Mo reaction in a nuclear reactor. Furthermore, since the enriched target (^{100}Mo) is expensive, its recovery from the column would be mandatory.

Another possible strategy for producing ^{99}Mo is with an **ADS** [14], which is a unique combination of an accelerator and a subcritical nuclear reactor. The system basically consists of

a proton accelerator that delivers its beam to a high-mass spallation target such as lead, tantalum, tungsten, and uranium to produce a high-intensity spallation neutron flux, which in turn is coupled to a subcritical fast core cooled with liquid metal. The spallation target is surrounded by a subcritical assembly consisting of secondary ^{235}U (LEU) targets. Within this subcritical assembly, one can tailor the neutron spectrum of these irradiation fields for production of ^{99}Mo. Each collision of a proton results in up to 20–30 fast neutrons (with energies mainly between 1 and 10 MeV) that in turn are moderated to produce epithermal neutrons that can be captured by ^{98}Mo to produce ^{99}Mo.

The **direct production of ^{99m}Tc** at a cyclotron appears to be promising for local supply. The production reaction $^{100}Mo(p,2n)^{99m}Tc$ was first suggested about 40 years ago [17].Cyclotron-produced technetium is at present the most mature technology available, and the accelerator and targetry are effectively developed, plus the possible co-use of such facilities to produce other isotopes such as ^{18}F is attractive when considering capital investment and infrastructure development. Despite the promising nature of the $^{100}Mo(p,2n)^{99m}Tc$ reaction, a note of caution has been expressed [18] with respect to the level of radionuclide impurities.

1.1.2 Positron Emission Tomography

The PET is based on the detection in coincidence of the two 511-keV photons emitted in opposite directions after annihilation of a positron from a positron emitter and an electron in the medium. The photons are detected by two detectors in coincidence, and data collected over many angles around the body axis of the patient are used to reconstruct the image of the activity distribution in the slice of interest. Such coincidence counting obviates the need for a collimator to define the field of view, since the detection in coincidence of both -rays simply define their Line Of Response (LOR). The detectors are primarily made of bismuth germanate (BGO),

NaI(Tl), lutetium oxyorthosilicate (LSO), godolinium oxyorthosilicate (GSO), or barium fluoride (BaF2). The PET systems use multiple detectors distributed in two to eight circular, hexagonal, or octagonal circumferential rings around the patient. Each detector is connected to the opposite detector by a coincidence circuit. Thus, all coincident counts from different slices over 360^0 angles around the patient are acquired simultaneously in a 64x64, 128 x128, or higher matrix in a computer. The data are then processed to reconstruct the images depicting the activity distribution in each slice. PET/CT, offers accurate matching of anatomic (CT) and functional (PET) images. Patients are imaged by both PET and CT in the same position of the patient, and images are then aligned to provide accurate diagnosis.

The significance of positron emission tomography (PET) in diagnostic nuclear medicine is increasing and today this non-invasive technique is routinely used in neurology, cardiology, oncology.

Table 1. 1 Selected Positron emitting radionuclides

Radionuclide	**$T_{1/2}$ (min)**	**Production route**
^{11}C	20.3	^{14}N (p,α)
^{13}N	9.9	^{16}O (p,α)
^{15}O	2.0	^{14}N (d,n)
^{18}F	109.8	^{18}O (p,n)
^{64}Cu	12.7 h	^{64}Ni (p,n)
^{68}Ga	68.3	$^{68}Ge/^{68}Ga$

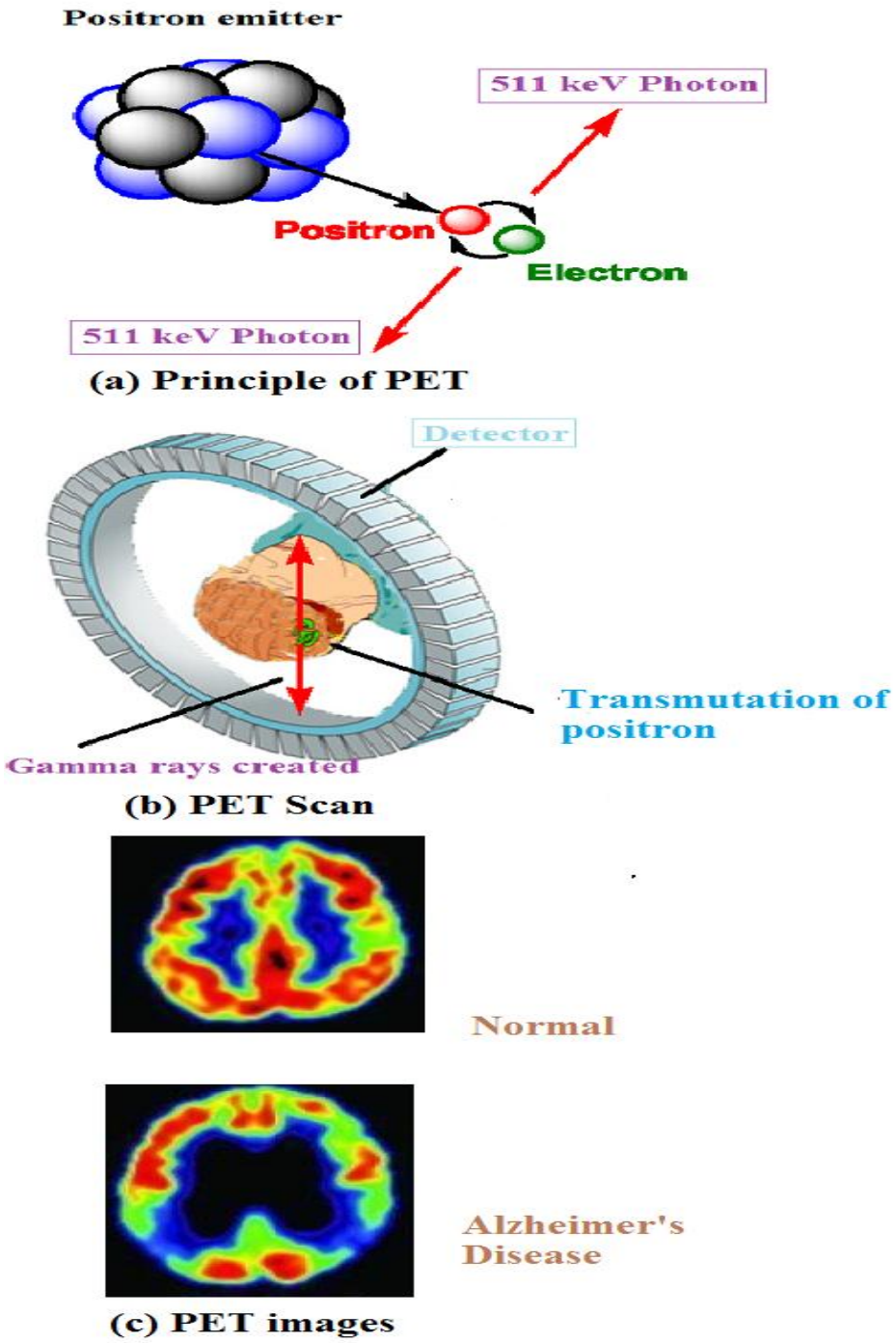

Fig 1.5 (a) Principle of PET (b) PET Scan (c) PET images.

For routine PET investigations [19], mainly the short-lived "organic" positron emitters, *viz.* ^{11}C ($T_{½}$ = 20.4 min) and ^{18}F ($T_{½}$ = 110 min), and to a lesser extent ^{15}O ($T_{½}$ = 2 min) and ^{13}N ($T_{½}$ = 10 min), are used. The radionuclides ^{11}C, ^{13}N and ^{15}O are generally used at the site of production. ^{18}F, is extensively employed because it has a longer half-life, emits a low-energy positron and allows versatile chemistry. All these four positron emitters can be produced in good yields at low-energy cyclotrons (E < 20 MeV), typically via the nuclear reactions shown in Table 1.1. Besides those positron emitters, two other short-lived positron emitters, namely ^{68}Ga ($T_{½}$ = 67.6 min) and ^{82}Rb ($T_{½}$ = 1.3 min), are produced *via* generator systems.

Applications of PET Studies

2-[18F]-fluoro-2-deoxyglucose (FDG) has become synonymous with PET. On entering the cell, FDG gets converted to FDG-6-phosphate by the enzyme hexokinase but, thereafter, not metabolised further. This leads to retention of 18F activity within the cell by metabolic trapping mechanism.

Neurology

^{18}F-^{18}FDG is used to investigate cerebral glucose metabolism, whereas $H_2{}^{15}O$ is used to examine cerebral blood flow. Fundamental aspects of receptor involvement in health and disease have been investigated using ^{11}C-labelled receptor radiopharmaceuticals. The link between blood flow/metabolism with ^{18}F-FDG on one hand and receptor involvement on the other, for example with ^{11}C-N-methylspiperone (for dopamine receptor), has been investigated in neurologic disorders. ^{18}F labelled fluoro-DOPA (6-^{18}F-3,4-dihydroxy phenylalanine) has shown interesting results in patients of Parkinson's disease (PD) with the degree of uptake in D-2 dopamine receptor regions inversely related to the severity of disease.

Cardiology

There is avid accumulation of ^{18}F-FDG in viable but damaged myocardial tissues, i.e. in blood flow starved, but viable tissues, since they shift to glycolytic pathway for availing glucose as source of energy. This is thus an unequivocal marker of myocardial viability. PET tracers, $^{13}NH_4^+$ and $^{82}Rb^+$, can be used for PET imaging of myocardial perfusion. $^{82}Rb^+$ is a generator produced K^+ analogue, ^{82}Sr being the parent nuclide.

Oncology

^{18}F-FDG is used in tumour metabolism investigation as a better grading/ staging indicator of tumour prognosis. The correlation of response in terms of FDG uptake with tumour prognosis in a large number of clinical studies help choose or avoid surgery. The distinction between necrotic (radiation scar) tumour tissue (FDG absent) versus tumour recurrence (FDG uptake) is facilitated by FDG imaging. ^{11}C labelled amino acid, e.g., ^{11}C-methionine, is useful for estimating the efficacy of response to therapy in cancer patients, the increased rate of utilisation of amino acid by the proliferating malignant cells, providing the basis for the selection / rejection of therapeutic strategy under consideration. Functional imaging plays a crucial role in management of neuro endocrine tumors (NETs). PET-CT with ^{68}Gallium (^{68}Ga)-labeled somatostatin analogues has shown excellent results for imaging of NETs.

For studying slow metabolic processes, however, some longer lived positron emitters (half-life between a few hours and a few days) are needed. Presently ^{64}Cu ($T_{1/2}$ = 12.7 h), ^{86}Y ($T_{1/2}$ = 14.7 h) and ^{124}I ($T_{1/2}$ = 4.18 d) are finding worldwide attention [20].The fact that these positron emitters can be produced via the (p, n) reaction using low-energy cyclotrons has given a tremendous impulse to their production at hospital-based cyclotrons.

Many production routes and processes have been reported to obtain no-carrier-added **^{64}Cu** from targets of Ni and Zn [21-24].Among them, the ^{64}Ni(p, n)^{64}Cu reaction is a promising route, because this reaction can be performed by low energy protons from a compact cyclotron at a high production yield [21].

Copper-64 has several unique attributes that make it a multi-purpose radionuclide with many potential applications. It has a complex decay scheme, with electron capture, beta-emission and positron emission branches. The positron emission (18%) has a low energy allowing high resolution images and there are no abundant gamma emissions that impair the imaging properties as with many other positron emitters. The combination of positron and beta-emission (39%) imparts a high local radiation dose at the cellular level making it suitable for targeted radionuclide therapy, while the electron capture decay (43%) is accompanied by emission of high LET Auger electrons which add to the cytotoxic potency if the radionuclide is located inside cells and particularly within or close to cell nuclei. Thus, it may be described as a "theranostic" radionuclide, producing excellent PET molecular imaging at low administered doses without major dosimetry or radiobiological concerns, and having potential for radionuclide therapy at high doses, with radionuclide distribution and accurate dosimetry possible using PET imaging during therapy.

Its half-life of 12.7 h makes it versatile – short enough to be useful for tracers with rapid pharmacokinetics such as small molecules and peptides, yet long enough to be useful for tracers with slow pharmacokinetics, for example those associated with monoclonal antibodies.

Its chemistry offers advantages: although it is less substitutional inert than other transition metals, with well-designed macrocyclic chelators it can be stably attached to targeting molecules such as antibodies, peptides, antibody fragments etc [25, 26].It is also redox active, and the

reduction of Cu(II) to Cu(I) in the biological milieu can be used as a basis for molecular imaging with very simple complexes, allowing blood flow and hypoxia imaging.

1.2 Radionuclides for therapy

Radiation therapy is mostly performed by using external beams of electrons, x-rays and γ-rays from radioactive sources (as ^{60}Co), high-energy γ-rays from accelerators or hadrons as neutron, protons. In addition to external therapy, some radioisotopes are used internally, introducing the therapeutic nuclide in a given part of the body. For internal radiotherapy β^-, α, and Auger electrons are used [1, 4]. In brachytherapy both liquid (conglomerates or colloids) and solid sources (as seeds) can be used, respectively introduced by injection or surgery, which is commonly performed with ^{192}Ir ($T_{½}$ = 73.8 d) [27, 28] in the form of a wire, ^{125}I ($T_{½}$ = 59.4 d) as a stent or ^{103}Pd ($T_{½}$ = 17.0 d) [28] as a seed or a stent. In the case of ^{192}Ir, the strong β^- particles are effective but in the latter two cases, X-rays cause the therapeutic effect. In palliative therapy [33] performed with radionuclides ^{32}P ($T_{½}$ = 14.3 d) and ^{90}Y ($T_{½}$ = 2.7 d), (both pure β^- emitters with high β^- energy), are introduced into joints and cavities as gels, glass microspheres or conglomerates. In case of small joints, ^{169}Er ($T_{½}$ = 9.4 d) with low β^- energy, is used [34].

Table 1.2 Selected radionuclides for therapy

(A) Alpha emitters				
Radionuclide	Half-life	Eα (MeV)		Method of production
^{211}At	7.21 h	6.76		^{209}Bi[α,2n]^{211}At [29, 30]
^{212}Bi	60.55 min	7.8		^{224}Ra(3.8d)^{212}Pb - ^{212}Bi generator [31]
^{213}Bi	45.6 min	5.87		^{225}Ac (10 d) - ^{213}Bi generator [32]
(B) 'Pure' Beta Emitters				
^{32}P	14.2 d	1.71		^{32}S(n, p)^{32}P
^{90}Y	64.0 h	2.27		Decay of ^{90}Sr (28.3 y); ^{90}Sr - ^{90}Y generator
Beta emitters with Gamma Emission				
Radionuclide	Half-life	E_β max (MeV)	Eγ/(keV %)	Method of production
^{153}Sm	46.28 h	0.81	103 (28)	^{152}Sm (n,γ)
^{166}Ho	26.76 h	1.5	81 (6.33)	^{165}Ho (n, γ)
^{186}Re	90.64 h	1.07	137 (9)	^{185}Re (n, γ)
^{188}Re	17.005 h	2.11	155 (15)	^{187}Re (n, γ); Decay of ^{188}W (69.4 d) ^{188}W - ^{188}Re generator ^{186}W (n, γ) ^{187}W (n, γ) ^{188}W
^{131}I	8.0207 d	0.6	364 (81	^{130}Te (n, γ) ^{131}Te →; ^{235}U (n,f)
^{67}Cu	61.83 h	0.57	184 (49) 92 (16)	^{68}Zn(p,2p)^{67}Cu [3] ^{68}Zn(γ,p)^{67}Cu [47]
^{47}Sc	3.35 d	0.6	160 (73)	^{46}Ca(n, γ)^{47}Ca→β$^-$→^{47}Sc ^{48}Ca(p,2n)^{47}Sc
Auger e$^-$ and other Particulate Emitters				
Radionuclide	Half-life	Decay characteristics and major energy, keV		Method of production
^{124}I	4.176 d	β$^+$; EC; Auger e$^-$; E_γ 603		^{124}Te (p,n); ^{125}Te (p,2n)
^{125}I	59.40 d	EC; IC & Auger e$^-$; E_γ 35		^{124}Xe (n, γ) ^{125}Xe →
^{117m}Sn	13.6 d	IT; IC e$^-$ 130, 160; E_γ 159		^{116}Sn (n, γ)
^{169}Er	9.4 d	β$^-$; IC e$^-$ 340		^{168}Er (n, γ)

If a tumor is cancerous, conventional modes of treatments, include surgery, chemotherapy, and radiation. In surgery, a surgeon may be constrained in excising the tumor by the presence of critical structures or organs that cannot be removed. Healthy surrounding tissues are not spared by radiation treatments and even cells remote from the area of the cancer can be affected by chemotherapy treatments. The indiscriminate destruction of normal cells, the toxicity as well as the development of multidrug resistance, support the need to find new effective targeted / biologic treatments.

Among the new forms of biology-based targeted therapies, **radionuclide therapy (RNT)** is a fast growing alternative [35, 36]. It involves, combining a radioisotope (typically a low to medium energy electron emitter) with a bio-conjugate, such as (Peptide Receptor Radio Therapy -PRRT)[37, 38], or antibodies (radio immunotherapy- RIT) [39, 40]. The goal of RNT is to kill tumor cells selectively by delivering high radiation doses to a specific target while minimizing damage to normal cells (Fig 1.6). This enables irradiation and selective destruction of cancer cells, minimizing the side effects that otherwise occur in whole body irradiation procedures. For this purpose the radionuclides ^{89}Sr ($T_{½}$ = 50.5 d), ^{153}Sm ($T_{½}$ = 1.9 d)) [41], ^{177}Lu ($T_{½}$ = 6.7 d), ^{188}Re ($T_{½}$ = 17.0 h) and ^{131}I ($T_{½}$ = 8.02 d) are more commonly used. New radioimmunotherapy (RIT) approaches incorporating α-particle emitters have been considered and have led to the development of both chelating agents and execution of pre-clinical studies. The α-particle has a very short path length (<100 μm), but a very high linear energy transfer (LET), with typical energy deposition of ~100 keV/μm compared to 0.2 keV/μm typically for a β-particle. The relative biological effectiveness of high LET radiation exhibits no dose rate dependence and is effective even under hypoxic conditions. The α-particle, a He nucleus, is quite relatively large compared to a β-particle, and the emission is associated with discrete high energies and a dense

ionization track that is also associated with a high probability of inflicting irreparable and cytocidal DNA double strand breaks. An individual cancer cell can in theory be killed by interaction with only a single α-particle traversing the nucleus of a cell. The fundamental physics and radiobiology of a β-particle emitter provides a poor tumor to normal tissue dose ratio for treatment of single cell disease. On the other hand, delivery of an α-emitting radio nuclide to the cell membrane is sufficient to kill malignant cells, requiring only a few α-particle decays at the cell membrane due to 3 dimensional emission geometry considerations, to effect a 99.99% level of cell kill with correspondingly low normal tissue toxicity. Consequently, α-emitters are well suited for hematologic disease, micrometastatic disease, and tumor cells near the surface of cavities. High homogeneity of antigenic expression is required for the complete destruction of micrometastases with high LET. Conversely, with radiations of low LET with a longer path length, the cross-fire of the β-emitters may make up for the non-homogeneity of antigen expression. A number of pre-clinical studies have concluded that α-emitters may be more effective than β-emitters administered at comparable doses in RIT. However, high cost and/or limited or unresolved availability are major obstacles that have limited the clinical evaluation of mAbs radiolabeled with α-emitters. In α-emitters, the application of ^{211}At ($T_{½}$ = 7.2 h) is still in the research phase [40]. In Auger electron therapy most studies have been performed using ^{125}I [42].

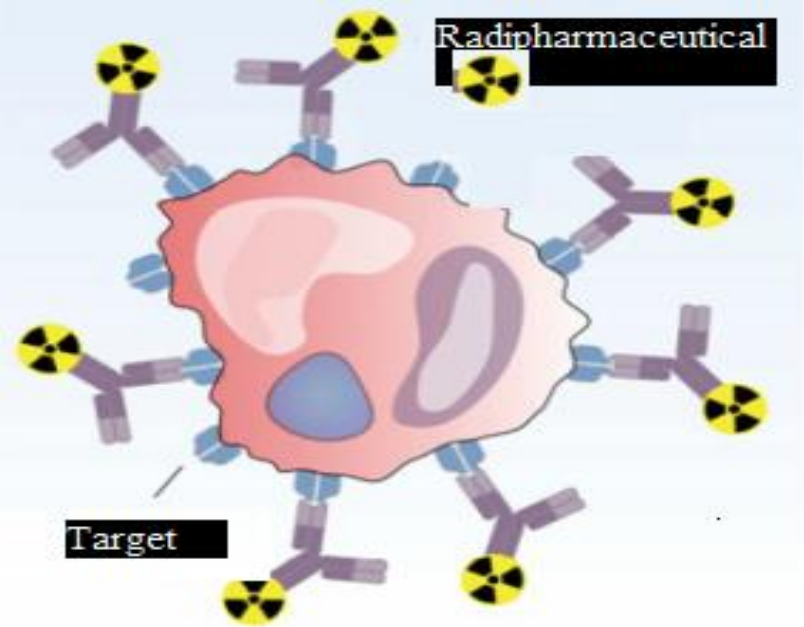

Fig 1.6 Radionuclide therapy: A radiolabelled compound binds to a target that is over expressed on the surface of tumor cells.

The emerging role of ^{67}Cu in radionuclide therapy: Copper-67 has long been considered as one of the ideal therapeutic radionuclides. The 61.83 h half-life of ^{67}Cu is suitable for imaging slow *in vivo* pharmacokinetics with agents such as Monoclonal Antibodies (MAbs) and other carrier molecules (*e.g.* receptor-avid peptides), while the β-particle energy is appropriate for therapy (mean energy 141 keV, corresponding to a range in soft tissue about 200-300 μm). Along with 100% β^-emission, ^{67}Cu also emits γ-radiation with 93 and 185 keV, suitable for pretherapy low dose imaging (SPECT or SPECT/CT) followed by higher dose treatment in the same patient, thus possibly a step towards personalized medicine. In addition, ^{67}Cu can also be paired with the positron emitter ^{64}Cu to perform low dose molecular imaging with the same radiopharmaceutical (PET or PET/CT) and eventually to obtain more effective therapeutic effect by using high dose. The biochemistry of copper is well known. It has no long-term residence in the body and copper is an essential trace nutrient. Furthermore, the complexation chemistry of

copper has been extensively studied, which allows for rapid identification of potential ligands for radiopharmaceuticals and chelators that are suitable for stable coordination of copper are available [43]. Despite these favorable characteristics, the growth and use of ^{67}Cu-based radiopharmaceuticals is not common, due to the lack of consistent supplies [44].

1.3 Radionuclide production

In the medium to long term range, newer irradiation facilities in the following three directions are expected to be developed - intermediate energy proton accelerators, high-energy and high-intensity photon sources and spallation neutron sources [45].

High-energy and high-intensity photon sources

Major advantages of the photon-induced reactions as compared to the charged-particle induced reactions are that large thick samples can be irradiated and heat dissipation is no problem. The Society for Applied Microwave Electronics Engineering and Research (SAMEER) is developing a 30 MeV, 8-10 kW LINAC for radioisotope production, in India [46]. The LINAC, will typically be used for ^{99}Mo production via ^{100}Mo(γ,n)^{99}Mo. The parameters of the proposed 30 MeV LINAC, are shown in Table 1.3.

A 30 MeV electron beam from an accelerator falling on a heavy metal target delivers photons with an energy spectrum extending from about 0.1 MeV to 30 MeV. Over this energy range several nuclear reactions can be induced, resulting in the formation of a few medically interesting radionuclides as shown in Table 1.4 [47]. The accelerator technology can be developed to deliver electron beam currents by a factor of about 10^4 higher than in the presently available accelerators and thus boost up the batch yield [45].

Table 1.3 Parameters of proposed 30 MeV Linac at SAMEER

Energy	30 MeV
$\mathbf{I_{average}}$	166 - 350 µA
Power (beam)	8-10 kW
Pulse width	16.3 µs
Rep rate	Up to 400 Hz
Power (kly.peak)	7 MW
Power (kly.ave)	36 kW
Duty cycle	0.00514

Spallation neutron sources- The irradiation of a heavy mass target with protons of energies above about 150 MeV leads to a spallation neutron spectrum, the energy of which extends from about thermal up to the maximum energy of the proton, with a strong component covering the energy region of 0.5 to 10 MeV. Due to the much harder spectrum of the spallation neutrons as compared to that of the fission neutrons, it is expected that with spallation neutrons several neutron threshold reactions would be advantageously induced [48] e.g. $^{32}S(n, p)^{32}P$; $^{35}Cl(n, p)^{35}S$; $^{47}Ti(n, p)^{47}Sc$; $^{64}Zn(n, p)^{64}Cu$; $^{67}Zn(n, p)^{67}Cu$; $^{89}Y(n, p)^{89}Sr$; $^{90}Zr(n, p)^{90}Y$; $^{105}Pd(n, p)^{105}Rh$; $^{149}Sm(n, p)^{149}Pm$; $^{153}Eu(n, p)^{153}Sm$; $^{159}Tb(n, p)^{159}Gd$; $^{161}Dy(n, p)^{161}Tb$; $^{166}Er(n, p)^{166}Ho$; $^{169}Tm(n, p)^{169}Er$.

Table 1.4 Medical isotopes which can be obtained through photoneutron and photoproton production routes [47]

Nuclide	Half-life	Decay mode	Production route
^{18}F	110 min	β^+	$^{19}F\ (\gamma, n)^{18}F$
^{47}Sc	3.35 d	β^-	$^{48}Ca(\gamma, n)^{47}Ca$; $^{47}Ca(\beta^-)^{47}Sc$
			$^{48}Ti(\gamma, p)^{47}Sc$
^{57}Co	271 d	ε.c.	$^{58}Ni(\gamma, p)^{57}Co$
^{64}Cu	12.7 h	ε.c, β^-, β^+	$^{65}Cu(\gamma, n)^{64}Cu$; $^{66}Zn(\gamma, np)^{64}Cu$
^{67}Cu	61.85 h	β^-	$^{68}Zn(\gamma, p)^{67}Cu$
^{67}Ga	78.3 h	ε.c	$^{69}Ga(\gamma,2n)^{67}Ga$
^{75}Se	120 d	ε.c	$^{76}Se(\gamma, n)^{75}Se$
^{77}Br	57 h	ε.c, β^+	$^{79}Br(\gamma,2n)^{77}Br$
^{90}Y	64 h	β^-	$^{91}Zr(\gamma, p)^{90}Y$
^{99}Mo	66 h	β^-	$^{100}Mo(\gamma, n)^{99}Mo$
^{166}Ho	26.8 h	β^-	$^{167}Er(\gamma, p)^{166}Ho$
^{177}Lu	6.71 d	β^-	$^{178}Hf(\gamma, p)^{177}Lu$
$^{225}Ra/^{225}Ac$	10 d	β^-, ε.c	$^{226}Ra(\gamma, n)^{225}Ra$; $^{225}Ra(\varepsilon, \beta^-)\ ^{225}Ac$

Radioisotope yield

As an energetic charged particle passes through any material, there is some probability that it will interact with a nucleus along its path. The particle may be scattered off the nucleus or, if the

energy is high enough when they collide, they may combine to form a compound nucleus that may decompose along one of several channels, leading to a new nucleus.

The probability of a nuclear reaction to occur is generally described in terms of its cross section (σ), that has units of area and has been traditionally been measured in barn: 1 b = 10^{-28} m^2. The quantity of cross section depends on the type of interaction, the involved particles and their energies. The accurate knowledge of the cross section is difficult to obtain using theoretical calculations and experiments are needed to get precise results.

In the classic sense, a reaction between a charged particle and a nucleus cannot take place if the centre of mass energy of the two particles is less than the Coulomb barrier. In the case that applies to the production of radionuclides with a cyclotron, this implies that the charged particle must have an energy greater than the electrostatic repulsion, which is given by

$$B = Zze^2/R$$

Where *B* is the barrier to the reaction; *Z* and *z* are the atomic numbers of the two species; *e* is the electric charge; and *R* is the separation of the two species (cm).

In any nuclear reaction, the total energy must be conserved, which means that the total energy including the rest mass of the reactants must be equal to the total energy including the rest mass of the products. The ***Q* value** is the mass difference between the compound nucleus and the incoming particles. Any increase in kinetic energy must be accompanied by an equal decrease in the rest masses. The *Q* value of a nuclear reaction may be either positive or negative. If the rest masses of the reactants exceed the rest masses of the products, the *Q* value of the reaction is positive, with the decrease in rest mass being converted into a gain in kinetic energy. The energy equivalent of the mass deficit *Q* is given by:

Q (MeV) = 931.4ΔM

Where $\Delta M = (m_p + M_T) - (m_q - M_R)$ in which m_p is the particle mass; M_T is the target mass; M_R is the product mass; and m_q is the emitted particle mass.

If $Q < 0$ the reaction is called endoergic, and if $Q > 0$ the reaction is said to be exoergic. If the reaction is endoergic, then an energy of an amount greater than this must be supplied in order for the reaction to proceed. The threshold will be the Coulomb barrier plus this difference. Owing to the conservation of momentum, only a fraction of the kinetic energy is available to compensate for the mass deficit. If the reaction is exoergic, the threshold energy will just be the Coulomb barrier. In reality, as a result of quantum mechanical tunnelling, nuclear reactions start to occur at energies below the Coulomb barrier.

The rate of radionuclide production is dependent on a number of factors, including the magnitude of the reaction cross-section as a function of energy, the incident particle energy, the thickness of the target in nuclei per cm^2, which will determine the exit particle energy, and the flux (related to beam current) of incoming particles.

$$-\frac{dn}{dt} = R = nI\left(1 - e^{-\lambda t}\right)\int_{E_S}^{E_o} \frac{\sigma(E)}{dE/dx} dE$$

Where R is the number of nuclei formed per second; n is the target thickness in nuclei/cm^2; I is the incident particle flux per second and is related to the beam current; σ is the reaction cross-section, or probability of interaction, expressed in cm^2 and is a function of energy; E is the energy of the incident particles; x is the distance travelled by the particle; and $\int_{E_S}^{E_o}$ is the integral from the initial energy to the final energy of the incident particle along its path.

As the particle passes through the target material, it loses energy due to the interactions of the particle with the electrons of the target. This is the **stopping power** and represented in the above equation by the term d*E*/d*x* . It depends on the atomic and mass number of the medium, Z and A, and on the specific type and kinetic energy of the incoming particle. The stopping power is composed of two contributions, the electronic and the nuclear stopping power. Considering that a charged particle is surrounded by its Coulomb electric force field, it interacts with one or more electrons of practically every atom it passes; most of these interactions individually transfer only small fractions of the incident particle's kinetic energy, such as in a friction-like process. This gradual kinetic energy loss is described by the Continuous Slowing Down Approximation (CSDA) and explains why the electronic stopping power is much larger than the nuclear one, that can usually be neglected. Many models may be used to describe the energy loss of a charge particle in matter, but the main one is the modern form of the Bethe-Block's formula:

$$-\frac{dE}{dx} = K\frac{z^2 Z\rho}{\beta^2 A}\left[\ln\left(\frac{2m_e\gamma^2\beta^2}{I}\right) - \beta^2 - \frac{\delta}{2} - \frac{\eta}{Z}\right]$$

where K is a constant (0.3071 MeV cm^2/ g), β is the normalized velocity v and γ the relativistic factor of the incoming particle, m_e is the electron mass, I is the ionization potential of the medium, δ and η are correction factors, respectively at high and low energies. The factor δ takes into account the correction at high energy for the polarization of electrons by the electric field of the moving ion, that could shield distant electrons. The factor η is applied at low energy when the collisions are no longer adiabatic and it depends on the orbital velocities of the electrons. The software SRIM [49] is used in the analysis of experimental data, in order to estimate the stopping power.

1.4 Quality control of radiopharmaceuticals

Since radiopharmaceuticals are intended for administration to humans, it is necessary that they undergo strict quality control measures. Quality control involves specific tests and measurements that ensure the purity, potency, product identity, biologic safety, and efficacy of radiopharmaceuticals. The quality control tests fall into two categories: **physicochemical tests and biological tests**. The physicochemical tests indicate the level of radionuclidic and radiochemical impurities and determine the pH, and physical state of the sample, particularly if it is a colloid. The biological tests establish the biodistribution sterility, apyrogenicity, and toxicity of the radiopharmaceutical.

Physicochemical tests

A true solution should not contain any particulate matter. Colloidal or aggregate preparations should have a proper size range of particles for a given purpose. For example, for visualization of the reticuloendothelial system, the colloidal particle should have a mean size around 100 nm. This can be checked by means of a microscope. These observations should be corroborated further by tissue distribution studies in animals, in which colloids of proper size should localize in the liver, while larger aggregated particles would deposit in the lungs. The number of particles in a preparation is equally important and can be determined by counting the particles on a haemocytometer under a light microscope.

All radiopharmaceuticals should have an appropriate hydrogen ion concentration or **pH** for their stability and integrity. The ideal pH of a radiopharmaceutical should be 7.4 (pH of the blood), although it can vary between 2 and 9 because of the high buffer capacity of the blood. The pH of a solution is accurately measured by a pH meter.

Radioactive concentration (RAC) - Assay of radioactivity expressed as activity /ml is determined by measurement in a pre-calibrated ion chamber or dose calibrator.

Radionuclide identification (RNI) – Presence of the radionuclide of interest, is confirmed by determining its energy spectrum and/ or its half life. **Radionuclide purity (RNP)** – It is the fraction of the total radioactivity present in the stated radionuclide form. The route of production of the radionuclide and the separation system determine the presence of the radionuclidic contaminants. Impurities arise from extraneous nuclear reactions due to isotopic impurities in the target material or from fission of heavy elements in the reactor. Some examples are ^{99}Mo in ^{99m}Tc-labeled preparations (this arises due to ^{99}Mo breakthrough from the Moly generator) and many iodine isotopes in ^{131}I-labeled preparations. Presence of radionuclidic impurity in the formulation could lead to additional radiation exposure to the patients and may also have an impact on the quality of images. RNP of a radiopharmaceutical should be generally greater than 99 %.

Radionuclidic purity is determined by measuring the half-lives and characteristic radiations emitted by individual radionuclides. Since a given radiation may belong to a number of radionuclides, determination of radiation energy alone does not establish the identity of a radionuclide, and its half-life must also be established. Radionuclidic purity depends on the relative half-lives and the quantities of the desired radionuclide and other contaminants, and changes with time. The presence of small quantities of a long-lived contaminant radionuclide is difficult to detect in the presence of large quantities of a desired short-lived radionuclide. In these instances, the short-lived radionuclide is allowed to decay and then the long-lived activity is measured.

Radionuclides that emit gamma rays are distinguished from one another by identification of their gamma-ray energies on the spectra obtained on a NaI(T1) or High purity germanium HPGe detector coupled to a multichannel analyzer . Pure β emitters may be checked for purity with a β spectrometer or a liquid scintillation counter.

γ-spectrometry with HPGe detectors - In order to correctly interpret the γ-ray spectrum in terms of energy and amount of activity, it is necessary to calibrate the detector. First, it is necessary to find out the conversion between channels and energy (*Energy calibration*) and then the relation between number of counts and activity (*Efficiency calibration*). As the *Energy calibration* does not depend on the geometry chosen, i.e. it is the same for all distances, while the the *Efficiency calibration* depends on the geometry chosen, i.e. it has to be calculated for each distance detector-source used, since it converts number of counts into activity values.

The evaluation of samples activity, and thus all physical quantities related to it (such as cross section and yield), can be done by using γ-spectrometry. Gamma rays interact with matter by elastic scattering (Rayleigh scattering) and inelastic processes (photoelectric absorption, Compton scattering and pair production). The elastic scattering, where gamma particles interact with the matter atom as a whole, the scattered gamma particles have the same energy as incident gammas. Hence this process does not contribute to detection.

In inelastic processes the energies of gamma rays are absorbed and consequently transferred to the counting system. In **Photoelectric Absorption** - a photon interacts with a bound electron from the inner shell of an atom. This interaction leads to the ejection of a photoelectron. A vacancy left in the atom leads to X-ray fluorescence or ejection of Auger electrons. Eγ is totally absorbed and the energy of the ejected electron $E_e = E_\gamma - E_{\text{shell bind.}}$ The photoelectric absorption, where the gamma deposits its full energy in the detector, results in a photopeak – a single

narrow line in the measured spectrum at the location corresponding to its total energy ($E\gamma$). In **Compton Scattering** - a photon interaction with an outer shell electron of atom of material results in ejection of this outer shell electron (recoil electron) and a scattered photon.

Photon energy after scattering:

$$E_f = \frac{E_\gamma}{1 + \frac{E_\gamma}{0.511}(1 - cos\theta)}$$

The recoil electron energy: $E_e = E_\gamma - E_f$

In a Compton scattering event, only part of gamma energy is transferred to the detector. The energy deposited (E_e) in the detector from a single Compton scattering event can range from near zero to a maximum value of E_{ce} (when θ = 180 degree), which leads to a Compton region (when $E_e < E_{ce}$) and a Compton edge (when $E_e = E_{ce}$) in the gamma spectrum. Moreover, it is possible that a gamma ray may experience more than one Compton scattering that shows in the gamma spectrum as a multiple Compton-scattering region.

Instead of detecting a sharp line of photopeak and a sharp Compton edge, a broad peak and a rounded Compton edge are observed as seen in Fig 1.7 (b). This effect is caused by the imperfect energy resolution of the gamma detecting system. Moreover, a backscatter peak may appear in the spectrum. It is caused by the detection of gamma rays which are scattered toward the detector after undergoing a 180-degree scattering outside the detector. In addition, when lead shielding is employed, X-ray peaks can be created by interactions of gamma rays in lead.

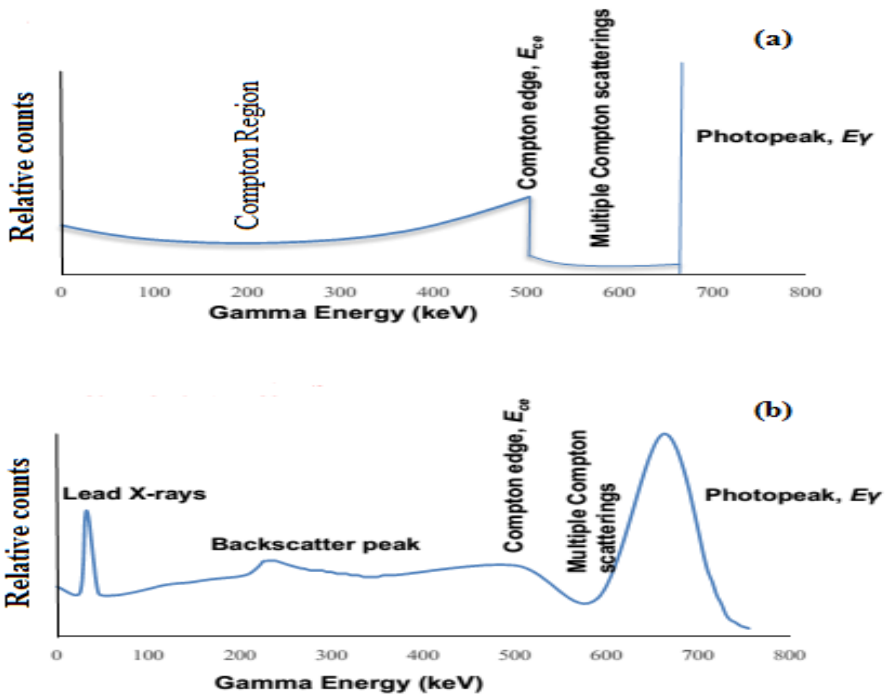

Fig 1.7 (a) Ideal gamma spectrum (b) Real gamma spectrum

Radiochemical purity (RCP) - It is a very important parameter reflecting the integrity and stability of radiopharmaceuticals and, indirectly, its biological efficacy. RCP is the fraction of total radioactivity in the desired radiochemical form. Examples of radiochemical impurity are free $^{99m}TcO_4$ and hydrolyzed ^{99m}Tc in ^{99m}Tc-labeled complexes, free ^{131}I iodide in ^{131}I-labeled proteins. The radiochemical impurity can arise from the method of preparation of the radiopharmaceuticals, radiolytic decomposition or deterioration on storage. Presence of radiochemical impurities can affect the biodistribution of the product, could impart unnecessary radiation dose to the non target tissues and also affect the image quality.

A number of analytical methods are used to detect and determine the radiochemical impurities in a given radiopharmaceutical, such as - precipitation, paper, thin-layer, and gel chromatography,

paper and gel electrophoresis, ion exchange, solvent extraction, high performance liquid chromatography, and distillation.

In **paper and instant thin-layer chromatography**, a small aliquot of the radiopharmaceutical preparation is spotted on a paper (Whatman paper strip) or an instant thin-layer chromatography (ITLC) strip. ITLC strips are made of glass fibre impregnated with silica gel (SG) or polysilicic acid (SA) and then chromatography is carried out by dipping the spotted strip into an appropriate solvent contained in a jar or a chamber. The commonly used solvents for chromatography of ^{99m}Tc-complexes are 85% methanol, acetone, methyl ethyl ketone (MEK), 0.9% NaCl solution. During the chromatographic process, different components of the sample distribute themselves between the adsorbent (paper or silica gel) and the solvent, depending on their distribution coefficients. Electrostatic forces of the stationary phase (adsorbent) tend to retard various components, while the mobile phase (solvent) carries them along. This effect and varying solubilities of different components in a solvent, and polarity of the solvent cause the individual components to move at different speeds and to appear at different distances along the paper or ITLC strip. When the solvent front moves to a desired distance, the strip is removed from the chamber, dried, and divided into several segments, and the radioactivity of each segment is measured in an appropriate counter, particularly in a NaI(Tl) well counter. Alternatively, the activity along the strip can be measured by a radiochromatographic scanner, which, with an automatic integrator device, plots the radioactivity versus the distance along the strip.

Three ^{99m}Tc species may exist in any ^{99m}Tc-labeled preparation: free, hydrolyzed, and bound ^{99m}Tc. Radiochemical impurity is calculated as the ratio (as a percentage) of the radioactivity of the undesirable component to the total activity applied at the origin. RCP of a radiopharmaceutical should be normally greater than 90%.

In **solvent extraction**, a solution containing one or more chemical compounds is shaken with an immiscible liquid and separation of different compounds is effected by the preferential solubility of individual compounds in one solvent or another. Thus, different solutes distribute themselves between two immiscible liquid phases. The ratio of solubilities of a component in two phases is called the distribution or partition coefficient. The efficiency of solvent extraction of a compound from one solvent into another depends primarily on this partition coefficient. Solvent extraction of ^{99m}Tc with MEK from ^{99}Mo has been a successful method of avoiding various radiocontaminants in the ^{99m}Tc-eluate.

The **chemical purity** of a radiopharmaceutical is the fraction of the material in the desired chemical form, whether or not all of it is in the labeled form. Chemical impurities arise from the breakdown of the material either before or after labeling, their inadvertent addition during labeling, and their undue accompaniment in the preparation of the compound. For example, aluminium is a chemical impurity in the ^{99m}Tc-eluate.

Biological tests

Biological tests are carried out essentially to examine the sterility, apyrogenicity, and toxicity of radiopharmaceuticals before human administration. It should be realized that it is quite possible for a particular radiopharmaceutical solution to be sterile but still be highly pyrogenic when injected into patients. While radiopharmaceuticals become unsterile due to bacterial, fungal, and yeast growth, pyrogenicity arises from certain metabolic byproducts (endotoxin) of these microorganisms.

Biodistribution is the in-vivo distribution of the radiopharmaceutical post injection, studied in test animals (usually in mice and rats). This test is performed to confirm the efficacy of the product. It determines the fate of the product in vivo, with respect to the uptake, retention,

excretion and biokinetics of the product. The uptake/localization of radiopharmaceuticals in different tissues/organs is governed by various mechanisms which depend on the physico-chemical nature of the radiopharmaceutical and the physiology/ functional anatomy of the tissue.

Sterility indicates the absence of any viable bacteria or microorganisms in a radiopharmaceutical preparation. Sterility tests are performed by incubating the radiopharmaceutical sample in fluid thioglycollate medium at 30–35^{0}C for 14 days and in soybean–casein digest medium for incubation at 20–25^{0}C for 14 days. If bacterial growth is observed in either test, the radiopharmaceutical is considered to be unsterile. In the case of short lived radiopharmaceuticals, completion of test for the absence of microorganisms in the final product is not possible, prior to its release or use. Hence monitoring and enumeration of environmental microbial contamination, prior and post formulation, sterilization equipment control testing and procedure control testing are mandatory for the quality assurance of the preparation of injectable products.

Pyrogen testing- All radiopharmaceuticals for human administration are required to be pyrogen free. Pyrogens are either polysaccharides or proteins produced by the metabolism of microorganisms. They are 0.05–1 mm in size, and in general, are soluble and heat stable. Bacterial products, the so-called bacterial endotoxins (BE), are the prime examples of pyrogens, but various chemicals also can add pyrogens to a radiopharmaceutical solution. Following administration, pyrogens produce symptoms of fever, chills, malaise, leukopenia, pain in joints, flushing, sweating, headache, and dilation of the pupils. Two methods viz. the in vivo rabbit pyrogen test and the in vitro Bacterial Endotoxin Test (BET), are recommended in the Pharmacopoeias, for detecting pyrogens. BET is generally employed for short lived, ready to use, injectable radiopharmaceuticals whereas pyrogen test (rabbit) is performed in case of non radioactive freeze dried 'cold' kit formulations.

The **stability** of a compound is time-dependent on exposure to light, change in temperature, and radiolysis. The longer a compound is exposed to these conditions, the more it will tend to break down. For this reason, most radiopharmaceuticals are assigned an **expiratory date** after which they are not guaranteed for their intended use. Substances such as sodium ascorbate, ascorbic acid, and sodium sulphite are often added to maintain the stability of radiopharmaceuticals. Some radiopharmaceuticals are stored in the dark under refrigeration to lessen the degradation of the material.

1.5 Concepts of nuclear medicine dosimetry

When radiation (photons and charged particles) pass through matter, energy is deposited. Absorbed radiation dose (D) is defined as the total energy deposited by radiation per unit mass of organ or tissue is

$$D = \frac{dE}{dm}$$

The basic unit of radiation dose is the Gray (Gy), which equals to 1 joule of energy deposited per kilogram of material. Since different types of radiation can cause different levels of biological damage, equivalent dose (H), measured in Sievert (Sv), takes into account the relative biological effects caused by radiation interacting with organ or tissue.

$$H = D \times Q$$

where Q is the weighting factor of a given radiation type. For photons and electrons Q=1; while for α particles, Q=20.

Also different organs or tissues have different radiation sensitivity, proportional to the rate of proliferation of cells and inversely proportional to the degree of cell

differentiation. Considering different probabilities of the occurrence of stochastic radiation effect in various organs and tissues, International Commission on Radiological Protection (ICRP) the effective dose E is defined as as [50]

$$E = \sum_T H_T W_T$$

where the subscript T represents the type of an organ or tissue, while W_T represents tissue weighting factors. The effective dose provides an estimate of the total probability of the occurrence of radiation effects.

The absorbed dose in a target region from a source region is [51, 52]

$$D_{(r_T \leftarrow r_S)} = \widetilde{A_S} \frac{\sum_i n_i E_i \varphi_i (r_T \leftarrow r_S)}{m_T}$$

Where $D_{(r_T \leftarrow r_S)}$ is the mean absorbed dose in the target region T from activity in the source region S, r_T represents the target region and r_S represents the source region, ϕi is the absorbed fraction (the fraction of energy emitted from the source r_S that is deposited in the target r_T), n_i is the number of radioactive emissions with energy E_i (MeV) per nuclear decay, and m_T is the mass of the target region. The summation i is performed over the number of radioactive emissions from the given radioisotope that contribute to the dose. $\widetilde{A_S}$ (MBq-s or uCi-h) is the cumulated activity in the source organ, which represents the total number of nuclear decays, integrated over a time period for which dose is calculated. The dose to a target region from multiple source regions requires summation over all these regions.

The calculations are simplified using Medical Internal Radiation Dose system

$$D_{r_T} = \sum_S \widetilde{A_S} S_{(r_T \leftarrow r_S)}$$

with all terms other than the cumulated activity clubbed in the factor S

$$S_{(r_T \leftarrow r_S)} = \frac{\sum_i n_i E_i \varphi_i(r_T \leftarrow r_S)}{m_T}$$

Thus, the S factor represents the pre-calculated dose per unit of cumulated activity of a given radioisotope.

To estimate the cumulated activity $\widetilde{A_S}$ in a source organ S, injected activity needs to be integrated over total time spent by the radioisotope of interest in this organ considering both the physical and biological half life.

$$\lambda_{eff} = \lambda_{phy} + \lambda_{bio}$$

where λ_{phy} represents the physical decay factor of radioisotopes; λ_{bio} represents the biological washout constant. Thus the cumulated activity in the source organ S is:

$$\widetilde{A_S} = \int_0^\infty A_s(t)dt = \int_0^\infty A_{s0} e^{-\lambda_{eff} t} = \frac{A_{s0}}{\lambda_{eff}}$$

where A_{s0} is the administrated activity.

The ratio of cumulated activity to the administrated activity is presently referred to as the time-integrated-activity-coefficient $\widetilde{a_S}$ (traditional name was residence time).

1.6 Outline of the thesis work

As an alternative to the use of reactors, use of accelerators represents a promising approach- for the production of ^{99}Mo/^{99m}Tc without the requirement for HEU targets and to aid in the sustained availability of theranostic pair ^{64,67}Cu.

The thesis includes studies on:

a) Direct production of ^{99m}Tc via ^{100}Mo(p,2n)^{99m}Tc

^{99}Mo/^{99m}Tc supply interruptions have necessitated development of alternate technologies to obtain ^{99}Mo/^{99m}Tc. The direct production of ^{99m}Tc via ^{100}Mo(p,2n) route is among one of the alternative promising routes The aim of the study in **chapter 2** is to optimize the irradiation parameters and target composition for production of clinical grade ^{99m}Tc. There are discrepancies in the cross section values of the ^{100}Mo (p,2n)^{99m}Tc reaction in the literature. Further, the co-produced Tc isotopes, inseparable from ^{99m}Tc, reduce the specific activity of ^{99m}Tc, potentially impacting the radiochemical quality of ^{99m}Tc-radiopharmaceuticals, and also cause an internal dose increase (DI), compared to pure ^{99m}Tc. Decrease of specific activity, the DI, and % content of co-produced impurities were used to estimate the clinical shelf-life of ^{99m}Tc.

b) Accelerator based production of ^{99}Mo

Chapter 3 presents details of preparation of ^{99}Mo by the photonuclear reaction ^{100}Mo(γ, n) in high energy electron linear accelerators (linac), and of the separation of ^{99m}Tc from the irradiated Mo. The ^{nat}Mo samples for irradiation were in the form of Molybdenum trioxide and in-house prepared Zirconium Molybdate. The evaluation of the quality of these ^{99m}Tc eluates with reference to the Indian Pharmacopeia (IP) pertechnetate monograph have been carried out.

In an assessment of long term technologies for supply of ^{99}Mo by alternative routes, production of ^{99}Mo via the ^{100}Mo(n, 2n)^{99}Mo reaction using fast neutrons from an accelerator has been proposed. **Chapter 4** presents details of the determination of the ^{100}Mo(n,2n) reaction cross-sections at the average neutron energies of 21.9 and 25.5 MeV.

c) Production and application of low specific activity ^{64}Cu

Chapter 5 in this study has investigated the potential of producing low specific activity (LSA) ^{64}Cu in an electron linac. The mixed field of photons along with the neutrons co-produced in the linac head via photonuclear processes, offer a dual reaction route for the production of ^{64}Cu, via the $^{63}Cu(n, \gamma)^{64}Cu$ + $^{65}Cu(\gamma,n)^{64}Cu$ reactions. The effect of change in ^{64}Cu yield with moderation of the neutrons with varying thickness of a solid water phantom is also presented. Administration of ^{64}Cu in the simple chloride form should lower the cost of PET imaging. In animal studies carried out with reactor produced LSA ^{64}Cu, the tumor uptake of LSA $^{64}Cu(II)Cl_2$, in C57BL/6 mice bearing melanoma tumors in a B16F10 tumor model was compared with the uptake of (a) LSA $^{64}Cu(I)Cl$, and (b) of published data of no carrier added $^{64}Cu(II)Cl_2$, at 24 hours post injection.

d) Accelerator based production of ^{67}Cu

^{67}Cu is a promising therapeutic radionuclide, whose limiting factor for a more widespread application in clinical trials is its availability. As an aid to expand the availability of ^{67}Cu and to demonstrate the viability of the production processes, with development of fast spectral neutron sources and photonuclear technology, **chapter 6** presents details of the production of ^{67}Cu. No carrier added ^{67}Cu was separated from the irradiated Zinc by solvent extraction.

Chapter 2

Direct production of ^{99m}Tc via the ^{100}Mo(p,2n) reaction: optimisation of irradiation parameters for obtaining clinically useful ^{99m}Tc

^{99}Mo/^{99m}Tc supply interruptions have necessitated development of alternate technologies to obtain ^{99}Mo/^{99m}Tc. The direct production of ^{99m}Tc via ^{100}Mo(p,2n) route is among one of the alternative promising routes. However there are discrepancies in the cross section values of the ^{100}Mo (p,2n)^{99m}Tc reaction in the literature. Further, the co-produced Tc isotopes, inseparable from ^{99m}Tc, reduce the specific activity of ^{99m}Tc, potentially impacting the radiochemical quality of ^{99m}Tc-radiopharmaceuticals, and also cause an internal dose increase (DI), compared to pure ^{99m}Tc. The aim of the study is to optimise irradiation parameters and target composition for production of clinical grade ^{99m}Tc.

2.1 Introduction

The radionuclide ^{99m}Tc is the work horse of nuclear medicine. The research reactors used to irradiate targets that produce most of the world's supply of ^{99}Mo are over 40 years old. Planned and unplanned shutdowns of some of these reactors have resulted in several recent ^{99}Mo/^{99m}Tc supply interruptions. Further, global efforts to promote ^{99}Mo production from LEU, to eliminate HEU use in civilian applications has led to considerable scientific effort to develop alternative production methods for the parent radionuclide ^{99}Mo as well as the desired product ^{99m}Tc. In general, more use of accelerators has been proposed [13, 14].

Among the alternative routes proposed and investigated for ^{99}Mo production are photo fission of Uranium targets [15], photo transmutation of ^{100}Mo [47, 53], the ^{100}Mo(n,2n)^{99}Mo route using fast neutrons [54, 55] and direct production of ^{99m}Tc [56, 57] via the ^{100}Mo(p,2n)^{99m}Tc route. Cyclotron-produced technetium is at present the most mature technology available, and the

accelerator and targetry are effectively developed, plus the possible co-use of such facilities to produce other isotopes such as ^{18}F is attractive when considering capital investment and infrastructure development. ^{18}F produced via $^{18}O(p,n)^{18}F$ route is converted to [^{18}F]-FDG, packed and transported to nuclear medicine centres in a process taking less than one hour after end of bombardment (EOB). A similar approach of irradiating, processing the ^{100}Mo target and transporting the ^{99m}Tc labelled radiopharmaceutical, can be replicated [57].

However, there are cross section discrepancies of the ^{100}Mo $(p,2n)^{99m}Tc$ reaction in the current literature [18, 58-66]. Knowledge of the cross-sections over a wide range of energies is essential for calculation of the yield and verifying the processing methods. Further the co-produced ^{9x}Tc isotopes due to (p,xn) reactions on the ^{100}Mo and stable ^{9x}Mo impurities in the target are inseparable from ^{99m}Tc [67, 68].This increases the internal dose, compared to pure ^{99m}Tc [69, 70]and the long lived Tc impurities reduce the specific activity of ^{99m}Tc, potentially impacting radiochemical quality of ^{99m}Tc-radiopharmaceuticals [18]. The Table 2.1 shows the Q values and half-lives of Technetium isotopes expected by the $^{100}Mo(p, xn)$ reactions upto Ep = 40 MeV

The aim of the study is to optimise the irradiation parameters, for direct production of clinical grade ^{99m}Tc, via the $^{100}Mo(p,2n)^{99m}Tc$ route. The $^{100}Mo(p,2n)^{99m}Tc$ excitation function was measured from E_p = 11.5 to 21 MeV. In order to assess the possible impact of long-lived nuclides on the radiochemical quality, the radiochemical purity of various technetium cold kits, with different ratios of $\frac{N_{99m_{Tc}}}{N_{99(m+g)_{Tc}}}$ has been determined, using solvent extracted ^{99m}Tc from reactor produced $^{98}Mo(n,\gamma)^{99}Mo$. A programme in Fortran was developed by varying the beam energy, target thickness, target enrichment and composition, irradiation and cooling times to maximise the yield of ^{99m}Tc and minimise impurities and applied to some of the commercially

available targets of ^{100}Mo with different compositions. Estimation of increase in internal dose due to the mix of ^{9x}Tc isotopes, for Tc as pertechnetate was calculated based on the radioisotope content and biokinetic data in humans. Decrease of specific activity, the DI, and % content of co-produced impurities were used to estimate the clinical shelf-life of the ^{99m}Tc obtained.

Table 2.1: Q values and half-lives of Technetium isotopes expected by the $^{100}Mo(p, xn)$ reactions upto Ep = 40 MeV

Nuclear reaction	**Q-value (MeV)**	**Product Nuclide**	**$T_{1/2}$**
(p,n)	-0.95	^{100}Tc	15.8 s
(p,2n)	-7.859	^{99m}Tc	6 h
	-7.716	^{99g}Tc	2.1 x 10^5 y
(p,3n)	-16.682	^{98g}Tc	4.2 x 10^6 y
(p,4n)	-24.056	^{97m}Tc	92.2 d
	-23.960	^{97g}Tc	4.2 x 10^6 y
(p,5n)	-33.475	^{96m}Tc	52 min
	-33.433	^{96g}Tc	4.28 d

2.2 Material, methods and calculations

2.2.1 Measurement of cross sections of $^{100}Mo(p,x)^{99}Mo, ^{99m}Tc$

2.2.1.1 Target and irradiation parameters

Two stacks of foils consisting of enriched ^{100}Mo (Target A of Table 2.2) with ^{nat}Al as degrader and ^{nat}Cu foils as beam current and energy monitors were irradiated in the 6M setup of the BARC-TIFR Pelletron Mumbai India. For the first and second set of stack irradiations the energies were set at 21 and 15 MeV respectively. Both stacks were irradiated for two hours. The

isotopic composition of commercially available enriched ^{100}Mo targets, considered in the study, are shown in Table *2.2*.

Table 2.2: Isotope compositions of the enriched Mo targets considered in the study (isotopic content[a] is expressed in %)

Isotopes	Target A (Trace)	Target B (Trace)	Target C (Isoflex)	Target D (Isoflex)
^{92}Mo	0.6	0.005	0.09	0.003
^{94}Mo	0.23	0.005	0.06	0.003
^{95}Mo	0.4	0.005	0.1	0.003
^{96}Mo	0.81	0.005	0.11	0.003
^{97}Mo	0.36	0.01	0.08	0.003
^{98}Mo	1.69	2.58	0.55	0.17
^{100}Mo	**95.9**	**97.39**	**99.01**	**99.815**

a = The percent abundance of each isotope is as reported on the Certificate of Analysis, by the vendors Trace and Isoflex

The beam current was recorded each second and integrated over the bombardment time The beam energy was determined using SRIM [49] for beam energy degradation in the aluminium foil. To monitor the proton energy and irradiation current, the ^{nat}Cu(p,x)^{63,65}Zn cross-section data recommended by the International Atomic Energy Agency [71] was also used.

2.2.1.2 Activity measurement and estimation of Radioisotopic / Radionuclidic purity

After the EOB, the stacks were dismounted and the activity of radionuclides in each foil was measured using an energy and efficiency calibrated HPGe detector. Decay data of the radionuclides - the half-lives, gamma ray energies and intensities are from Nudat [72], and are shown in Table 2.3. The various gamma lines in the spectra were evaluated using the software Interwinner 7.

Table 2.3: Decay data for the investigated radionuclides [72]. Energies of gamma lines used for quantification of each particular radionuclide are in bold

Radionuclide	Half life	Eγ (keV)	Iγ (%)
^{93g}Tc	2.75 h	**1362.94**	**66.2**
		1477.14	8.7
		1520.28	24.4
^{94g}Tc	293 min	**702.67**	**99.6**
		849.74	95.7
		871.05	99.9
^{95g}Tc	20.0 h	765.789	93.8
^{95m}Tc	61 d	**204.117**	**63.2**
		582.082	30
		835.149	26.6
^{96g}Tc	4.28 d	778.22	99.76
		812.54	**82**
		849.86	98
		1126.85	15.2
^{99m}Tc	6.0067 h	**140.5**	**88.5**
^{99}Mo	65.649 h	**140.5**	**4.72**
		181.09	**6.01**
		739.5	**12.12**
^{95}Nb	34.991 d	**765.8**	**99.808**
^{96}Nb	23.35 h	460.04	26.62
		568.871	**58**
		778.224	96.45
		849.929	20.45
		1091.349	48.5
^{62}Zn	9.187 h	**548.35**	**15.2**
		596.56	**25.7**
^{65}Zn	244.1 d	**1115.55**	**50.75**

Table 2.4: Validation of the optimisation approach- Comparison of the experimental thin target yields (Bq) of the isotopes co-produced in the irradiation of Target A (of Table 2.2) with the expected yields due to the contribution of the various Mo(p, x) channels

Radio-nuclide	**Channels**	**11.5 MeV**	**13.3 MeV**	**15 MeV**	**16.9 MeV**	**18.4 MeV**	**19.8 MeV**	**21 MeV**
^{93}Tc	^{92}Mo(p,g)	67.74	39.78	25.08	17.18	13.93	9.67	6.98
	^{94}Mo(p,2n)	0.00	0.00	1535.37	2855.99	3742.21	3879.15	4048.21
Expected (Bq)		***67.74***	***39.78***	***1560.45***	***2873.17***	***3756.14***	***3888.82***	***4055.19***
Experimental (Bq)		**Not detected**		**592.46**	**3154.31**	**3388.60**	**3635.42**	**3795.33**
^{94}Tc	^{94}Mo(p,n)	2348.06	2258.04	1818.89	1159.18	697.21	406.87	292.50
	^{95}Mo(p,2n)	0.00	582.92	1592.51	2806.27	3555.85	3560.18	3588.20
Expected (Bq)		***2348.06***	***2840.96***	***3411.4***	***3965.45***	***4253.06***	***3967.05***	***3880.7***
Experimental (Bq)		**585.02**	**1339.18**	**1996.95**	**2444.23**	**2792.70**	**2861.48**	**3031.19**
^{95m}Tc	^{95}Mo(p,n)	3.87	2.87	2.02	1.24	0.80	0.51	0.41
	^{96}Mo(p,2n)	0.00	16.23	19.09	19.62	18.89	16.59	15.70
	^{97}Mo(p,3n)	0.00	0.00	0.00	0.00	0.00	0.02	0.22
Expected (Bq)		***3.87***	***19.1***	***21.11***	***20.86***	***19.69***	***17.1***	***16.33***
Experimental (Bq)		**2.29**	**4.82**	**19.12**	**21.30**	**21.80**	**20.43**	**17.10**
^{95g}Tc	^{95}Mo(p,n)	1077.98	940.25	724.27	456.19	274.81	156.13	108.53
	^{96}Mo(p,2n)	0.00	1351.62	1996.92	2608.80	2956.63	2885.77	2941.34
	^{97}Mo(p,3n)	0.00	0.00	0.00	0.00	0.00	17.74	95.86
Expected (Bq)		***1077.98***	***2291.87***	***2721.19***	***3064.99***	***3231.44***	***3059.64***	***3145.73***
Experimental (Bq)		**965.66**	**1809.90**	**2124.99**	**2402.59**	**2666.33**	**2707.75**	**2883.50**
^{96}Tc	^{96}Mo(p,n)	416.90	322.61	231.77	141.57	87.50	53.75	40.80
	^{97}Mo(p,2n)	81.76	166.43	229.69	279.46	299.83	278.13	264.05
	^{98}Mo(p,3n)	0.00	0.00	0.00	0.00	0.00	0.00	50.48
Expected (Bq)		***498.66***	***489.04***	***461.46***	***421.03***	***387.33***	***331.88***	***355.33***
Experimental (Bq)		**635.98**	**507.14**	**436.66**	**332.39**	**337.15**	**361.49**	**468.73**
^{95g}Nb	^{96}Mo(p,α)	***0.92***	***1.85***	***2.56***	***3.02***	***2.99***	***2.34***	***1.99***
Experimental (Bq)		**1.25**	**1.65**	**3.30**	**2.70**	**3.97**	**3.91**	**4.30**
^{96g}Nb	^{100}Mo(p,αn)	***0.00***	***0.00***	***133.39***	***997.89***	***1819.06***	***2398.90***	***3012.87***
Experimental (Bq)		***Not detected***	**50.79**	**179.40**	**1056.11**	**1660.63**	**2368.91**	**3195.45**

The radionuclidic / radioisotopic impurities in the irradiated 95.9 % enriched ^{100}Mo foils were determined using gamma ray spectrometry and were quantified at the gamma lines [56] recommended by the European pharmacopeia. The foils were measured at several time points, post irradiation to quantify shorter lived isotopes, and also assayed approximately 3 months later to quantify the longer-lived isotopes (e.g. ^{95m}Tc and ^{95}Nb). The decay corrected measured values to EOB, were averaged. The isotopes were also identified by their half-life. The isotopes identified are shown in the Table 2.4.

2.2.1.3 ^{100}Mo(p, x)^{99}Mo excitation function

In measuring the excitation function of ^{100}Mo(p, 2n)^{99m}Tc, the measurement of the ^{100}Mo(p,x)^{99}Mo excitation function is also needed to account for ^{99m}Tc produced indirectly from ^{99}Mo decay [18].^{99}Mo production cross sections (mb) are estimated at the various irradiation energies from the measured activities of 181 keV and 739.5 keV lines. Cross-sections for ^{99}Mo formed via ^{100}Mo(p,x)^{99}Mo are determined according to the activation formula given [62].The cross section values for ^{100}Mo(p,x)^{99}Mo are represented in Fig 2.1 and shown in Table 2.5.

2.2.1.4 ^{100}Mo(p, 2n)^{99m}Tc excitation function

The ^{99m}Tc is identified by its 140.5 KeV γ-line. The count rates of the E_γ = 140.5 keV gamma-line, has a complex time dependence due to the formation and decay process of the ^{99m}Tc and ^{99}Mo radionuclides. The counts at the 140.5 keV $[Counts]^{140}_{Total}$ can be considered as the sum of the following independent sources [60, 64] :

- $[Counts]^{140}_{Mo}$ due to prompt gamma radiation that follows the decay of ^{99}Mo,
- $[Counts]^{140}_{m_{Tc-indir}}$ due to indirect production of ^{99m}Tc, from decay of ^{99m}Tc produced from EOB ^{99}Mo + decay of ^{99m}Tc produced during irradiation exclusively by decay of ^{99}Mo

- $[Counts]^{140}_{m_{Tc-dir}}$ due to direct production of ^{99m}Tc

$$[Counts]^{140}_{Total} = [Counts]^{140}_{Mo} + [Counts]^{140}_{m_{Tc}}$$

where $[Counts]^{140}_{mTc}$ includes the direct ^{99m}Tc and indirect ^{99}Mo to ^{99m}Tc decay contributions during irradiation and post irradiation.

To determine the direct production of ^{99m}Tc, the 140.5 keV net peak area counts has to be corrected for, the contribution of ^{99m}Tc as decay product from ^{99}Mo during and after irradiation, and contribution of the 140.5 keV gamma line emitted directly in ^{99}Mo decay. The corrections are performed as described in Ref [62, 64].

The total ^{99m}Tc activity $[A^{Start}_{mTc}]_{Total}$ at the start of counting (*start*)

$$= \frac{[Counts]^{140}_{mTc} - [Counts]^{140}_{Mo}\,\lambda_2 t_R}{(1-e^{-\lambda_2 t_R})\,\varepsilon_{140} I^{140}_{mTc} t_L}$$

Where the contribution of ^{99}Mo decay to 140 keV line intensity, $[Counts]^{140}_{Mo}$ is estimated from measurement of the EOB activity of ^{99}Mo, A^{EOB}_{Mo} from the independent 181 and 739.5 keV ^{99}Mo lines.

$$[Counts]^{140}_{Mo} = \frac{A^{EOB}_{Mo}\, e^{-\lambda_1 t_\Delta}(1-e^{-\lambda_1 t_R})\varepsilon_{140}\, I^{140}_{Mo} t_L}{\lambda_1 t_R}$$

λ_1 and λ_2 are the decay constants of ^{99}Mo and ^{99m}Tc respectively,

t_Δ= elapsed time between EOB and start of counting (*start*),

t_R= real time, t_L = live time, t_b = irradiation time,

ε_{140}= detector efficiency at 140 keV, I^{140}_{Mo} = γ-ray intensity at 140 keV for ^{99}Mo,

I^{140}_{mTc} = γ-ray intensity at 140 keV for ^{99m}Tc

The total ^{99m}Tc activity $\left[A_{mTc}^{Start}\right]_{Total}$ at the start of counting (*start*) includes contributions from both the direct production of ^{99m}Tc, $[A_{mTc}^{Start}]_{Dir}$ and indirect production of ^{99m}Tc, $[A_{mTc}^{Start}]_{Indir}$ arising from ^{99}Mo $\rightarrow$ ^{99m}Tc and is given by

$$[A_{mTc}^{Start}]_{Total} = [A_{mTc}^{Start}]_{Indir} + [A_{mTc}^{Start}]_{Dir}$$

Where $[A_{mTc}^{Start}]_{Indir} = \frac{\lambda_2}{\lambda_2-\lambda_1}(0.87)\,A_{Mo}^{EOB}(e^{-\lambda_1 t_\Delta} - e^{-\lambda_2 t_\Delta}) + [A_{mTc}^{EOB}]_{Indir}\, e^{-\lambda_2 t_\Delta}$ 2-1

and $\left[A_{mTc}^{EOB}\right]_{Indir} = (0.87)\dfrac{A_{Mo}^{EOB}\left(1-\frac{\lambda_2}{\lambda_2-\lambda_1}\right)e^{-\lambda_1 t_b} + \left(\frac{\lambda_1}{\lambda_2-\lambda_1}\right)e^{-\lambda_2 t_b}}{\left(1-e^{-\lambda_1 t_b}\right)}$

In equation 2-1, the first term corresponds to ^{99}Mo $\rightarrow$ ^{99m}Tc production post EOB, and the second term corresponds to ^{99}Mo $\rightarrow$ ^{99m}Tc production during irradiation [62] .

Thus the direct ^{99m}Tc activity at EOB, $[A_{mTc}^{EOB}]_{Dir}$ is given by

$$[A_{mTc}^{EOB}]_{Dir} = ([A_{mTc}^{Start}]_{Total} - [A_{mTc}^{Start}]_{Indir})e^{\lambda_2 t_\Delta} \quad 2\text{-}2$$

The direct ^{99m}Tc production cross sections for this work are calculated using $[A_{Tc}^{EOB}]_{Dir}$ from equation 2-1. The ^{99m}Tc cross sections measured at the various proton energies are given in Table 2.5. Each irradiated foil was measured for 4 – 5 half-lives of ^{99m}Tc, post EOB, to check the consistency of the applied interference corrections for determination of cross section. The Fig 2.2 shows the ^{99m}Tc cross sections measured at the various proton energies. The contributions of the direct and indirect components to the total activity of ^{99m}Tc (Bq) as a function of cooling time for the irradiation time of 2 hours in the various thin foils, have been determined and are shown in Fig 2.3.

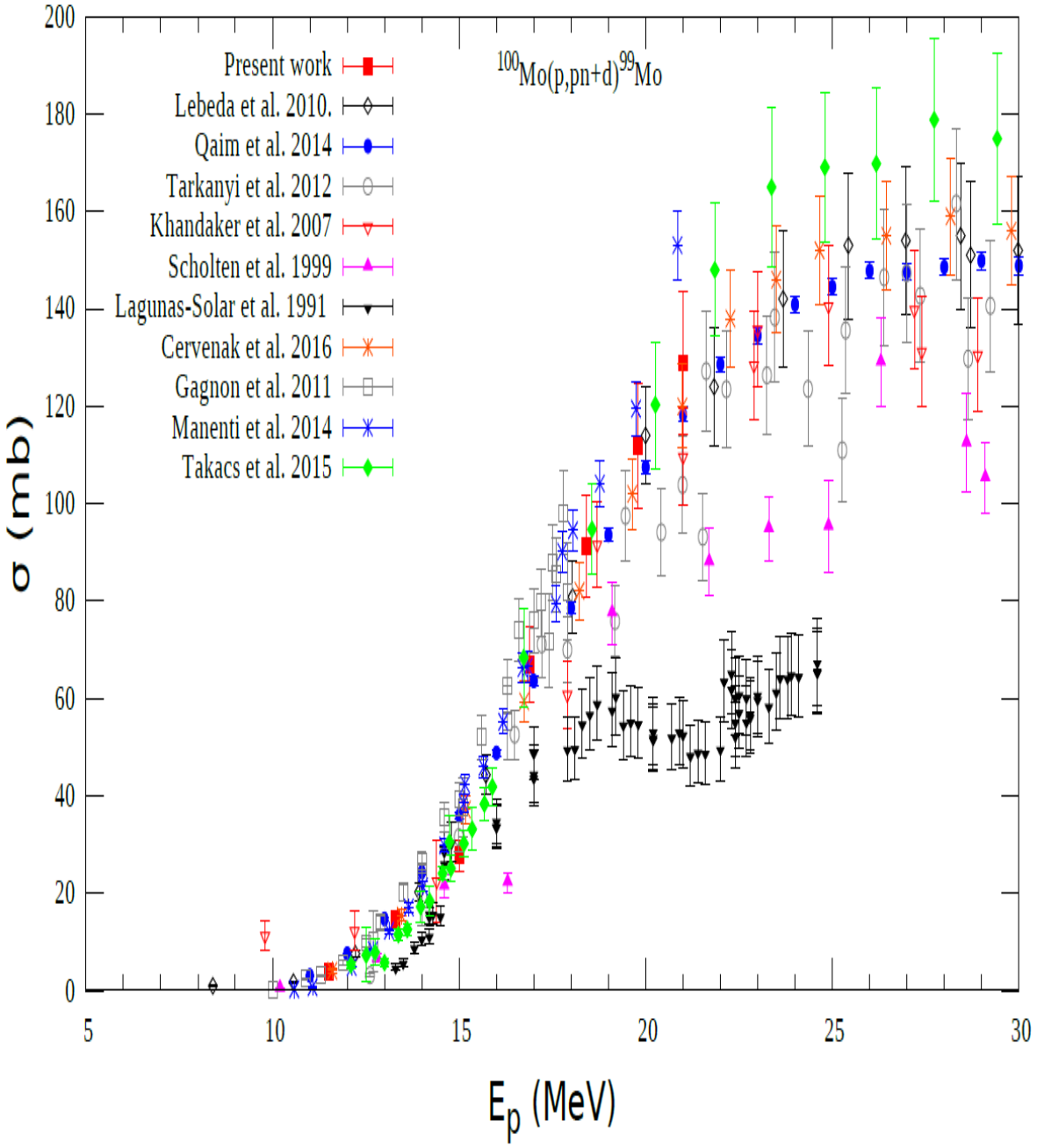

Fig 2.1 Experimental excitation function for the $^{100}Mo(p,x)^{99}Mo$ reaction

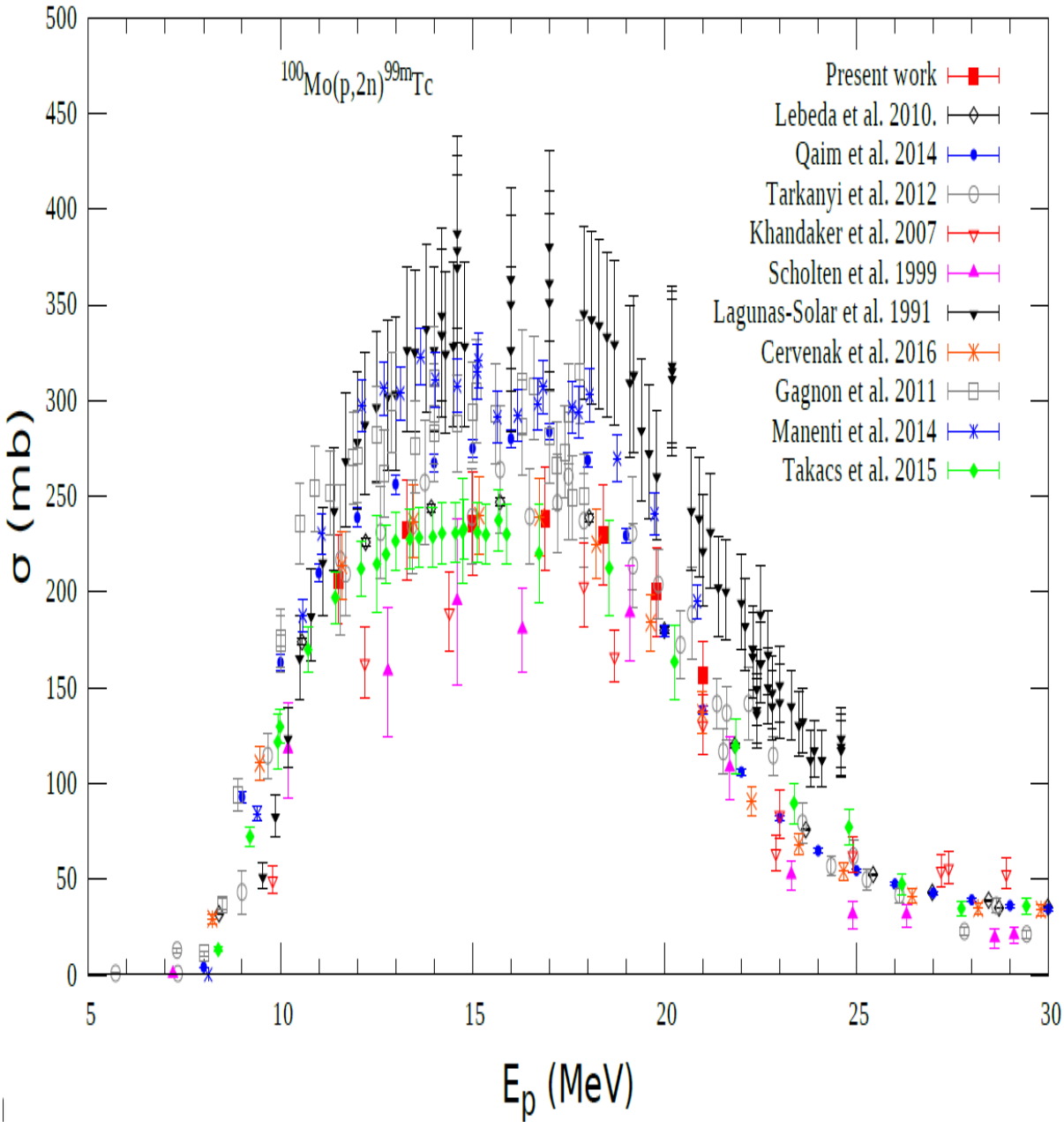

Fig 2.2 Experimental excitation function for the $^{100}Mo(p,2n)^{99m}Tc$ reaction

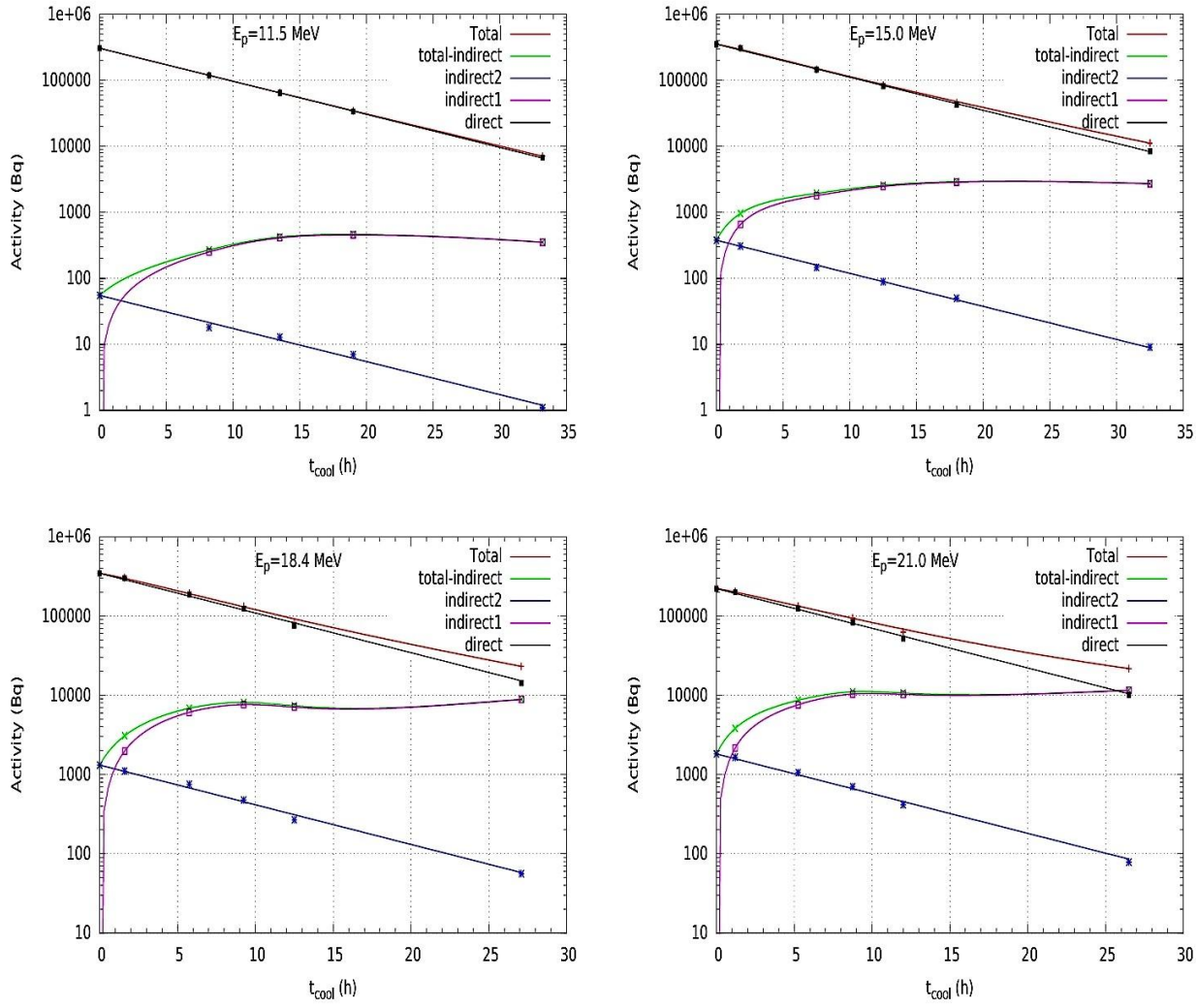

Fig 2.3 **:** The contributions of the direct and indirect components to the total activity of ^{99m}Tc (Bq) as a function of cooling time for the irradiation time of 2 hours in the thin foils of target A.

2.2.2 Assessment of the impact of co-produced long-lived ^{9x}Tc nuclides on the radiochemical quality of technetium cold kits

Long-lived Technetium isotopes ^{97}Tc, ^{98}Tc, ^{99g}Tc formed by the (p,xn) reactions on ^{100}Mo (Table 2.1) have half-lives of 4.2 x 10^6, 4.2 x 10^6 and 2.1 x 10^5 years respectively. These long lived co-produced isotopes, could affect the specific activity of ^{99m}Tc and impair the labelling of technetium cold kits [18]. Evaluation of the radiochemical purity of various technetium cold kits with different atomic ratios of $\frac{N_{99m_{Tc}}}{N_{99(m+g)_{Tc}}}$ was carried out to determine the minimum ratio, that would ensure compliance of labelled ^{99m}Tc radiopharmaceutical to pharmacopoeia specifications.

Solvent extracted ^{99m}Tc from reactor produced $^{98}Mo(n,\gamma)^{99}Mo$ was used in the labelling studies (LS). The methyl ethyl ketone (MEK) solvent extraction method [73] enables obtaining ^{99m}Tc in a high concentration. The multi step process, in the solvent extraction process involves (a) bringing the aqueous ^{99}Mo solution into rigorous contact with MEK (b) separation of the organic and aqueous phases (c) retaining the ^{99}Mo solution for subsequent use (d) evaporation of inflammable MEK (e) leaching of the residue with saline and (f) terminal sterilisation.

The ^{99}Mo as sodium molybdate and the technitium cold kits were obtained from Board of Radiation and Isotope Technology, India. On reciept of the ^{99}Mo, the radionuclide identification and radionuclidic purity of the ^{99}Mo sodium molybdate were determined and the steps a,b,c of the solvent extraction process were carried out, to remove any ^{99g}Tc built up. The ^{99m}Tc was allowed to grow and separated from the ^{99}Mo, via solvent extraction, for the LS.The tests for radionuclide identification, radionuclidic purity, radiochemical purity, pH of the extracted sodium pertechnetate were carried out as per the specifications of the Indian Pharmacopoeia (IP). The kits of Sulphur colloid, DTPA, Glucoheptonate, MDP, Mebrofenin,ECD, EC and

MIBI were labelled as per the labelling recipe. The radiochemical purity of the ^{99m}Tc labelled radiopharmaceuticals were determined, using paper chromatography / thin layer chromatography as specified in the IP.

The LS were sub-divided into 4 groups, LS1 to LS4, depending on ingrowth time, activity used for labelling, age of the eluate, and age of the kit. In LS1, LS2, LS3, and LS4, ^{99m}Tc of ingrowth time of 120, 72, 48, and 48 hours respectively was used. In LS1, LS2, and LS4, labelling was carried out immediately after extraction, whereas in LS3, labelling was carried out upto 3 hours after extraction. In LS4, studies were carried out at the end of the declared shelf life of the kit. Activity levels of ^{99m}Tc used, number of batches tested, and the % compliance to the radiochemical purity specifications of the IP, are shown in Table 2.6.

The levels of $\frac{N_{99m_{Tc}}}{N_{99(m+g)_{Tc}}}$ used in the LS were determined, using decay and buildup kinetics of nuclides in the ^{99}Mo-^{99m}Tc generator system [74, 75].

2.2.3 Optimisation approach

A theoretical approach for (a) calculation of yields, (b) estimation of the influence of co-produced Tc isotopes on the internal dose, and (c) estimation of shelf-life of ^{99m}Tc, has been carried out. A Fortran programme has been developed to optimise the ^{99m}Tc yield by varying the beam energy, target thickness, target enrichment and composition, irradiation and cooling times for thick targets of enriched ^{100}Mo (Targets A, B, C, D of Table 2.2), and various initial beam energies in the range from $E_{p,in}$=24 MeV to exit energy Ep,out =8 MeV. The threshold energies for formation of ^{99m}Tc and long-lived impurities, ^{99g}Tc, ^{98}Tc and ^{97}Tc via ^{100}Mo(p,2n), ^{100}Mo(p,3n) and ^{100}Mo(p,4n) are ~ 8, 8, 16 and 24 MeV respectively. Formation of long lived ^{97}Tc can be minimised by irradiating below the threshold energy ~24 MeV of ^{100}Mo(p,4n)^{97}Tc.

2.2.3.1 Calculation of yields

In order to calculate the thick target yield, the decrease of protons energy through the target is considered, and the cross sections integrated over the energy range upto $E_{p,out}$ = 8 MeV. The saturated thick target reaction yield Y per unit beam current (Bq/μA) [67]:

$$Y = 6.24 \times 10^{12} \times \frac{N}{M} \int_{E_{out}}^{E_{in}} \frac{\sigma(E)}{S(E)} dE$$

where 6.24×10^{12} is the number of protons per second per μA, N is the Avogadro number, M is the target atomic mass (g), $\sigma(E)$ is the reaction cross section (cm^2), and $S(E)$ is the target stopping power (MeV· cm^2/g). The target stopping power is obtained from SRIM [49] and the cross-section values for $^{100}Mo(p, x)^{99}Mo$ and $^{100}Mo(p, 2n)^{99m}Tc$ reactions in the energy range 11.5 to 21 MeV are from the present study, and above 21 MeV and below 11.5 MeV are adapted from [66]. The cross sections for long lived ^{99g}Tc and ^{98}Tc via $^{100}Mo(p,2n)^{99g}Tc$ and $^{100}Mo(p,3n)^{98}Tc$ are taken from Talys 1.8 [76]. The cross section values for other short-lived ^{9x}Tc, Nb and Zr isotopes are adapted from [67]. Contribution of different production routes leading to the formation of the same reaction product are summed up. The indirect contribution of ^{99}Mo to formation of ^{99m}Tc and additional formation of ^{99g}Tc via the chains $^{100}Mo(p,x)^{99}Mo \rightarrow {}^{99m}Tc \rightarrow {}^{99g}Tc$, and $^{100}Mo(p,2n)^{99m}Tc \rightarrow {}^{99g}Tc$ are incorporated following reference [18].Post EOB, the irradiated target would need to be transferred to a hotcell, followed by dissolution of the target and ^{99m}Tc separated from the Mo matrix. Typically the separation process should be initiated in one hour after EOB [57]. Accordingly the calculation of the ^{99m}Tc and ^{99g}Tc yield, incorporates the indirect contribution from the co-produced ^{99}Mo for one hour. The Fig 2.4 shows the number of atoms of ^{99m}Tc, ^{99g}Tc, ^{98}Tc and the atoms ratio Ar defined as

$\frac{N_{99m_{Tc}}}{N(99m_{Tc}+all\ co-produced\ Tc)}$, for all targets of Table 2.2, for a six hour irradiation time, and two initial beam energies ($E_{p,in}$=24, and 18 MeV) to $E_{p,out}$ = 8 MeV.

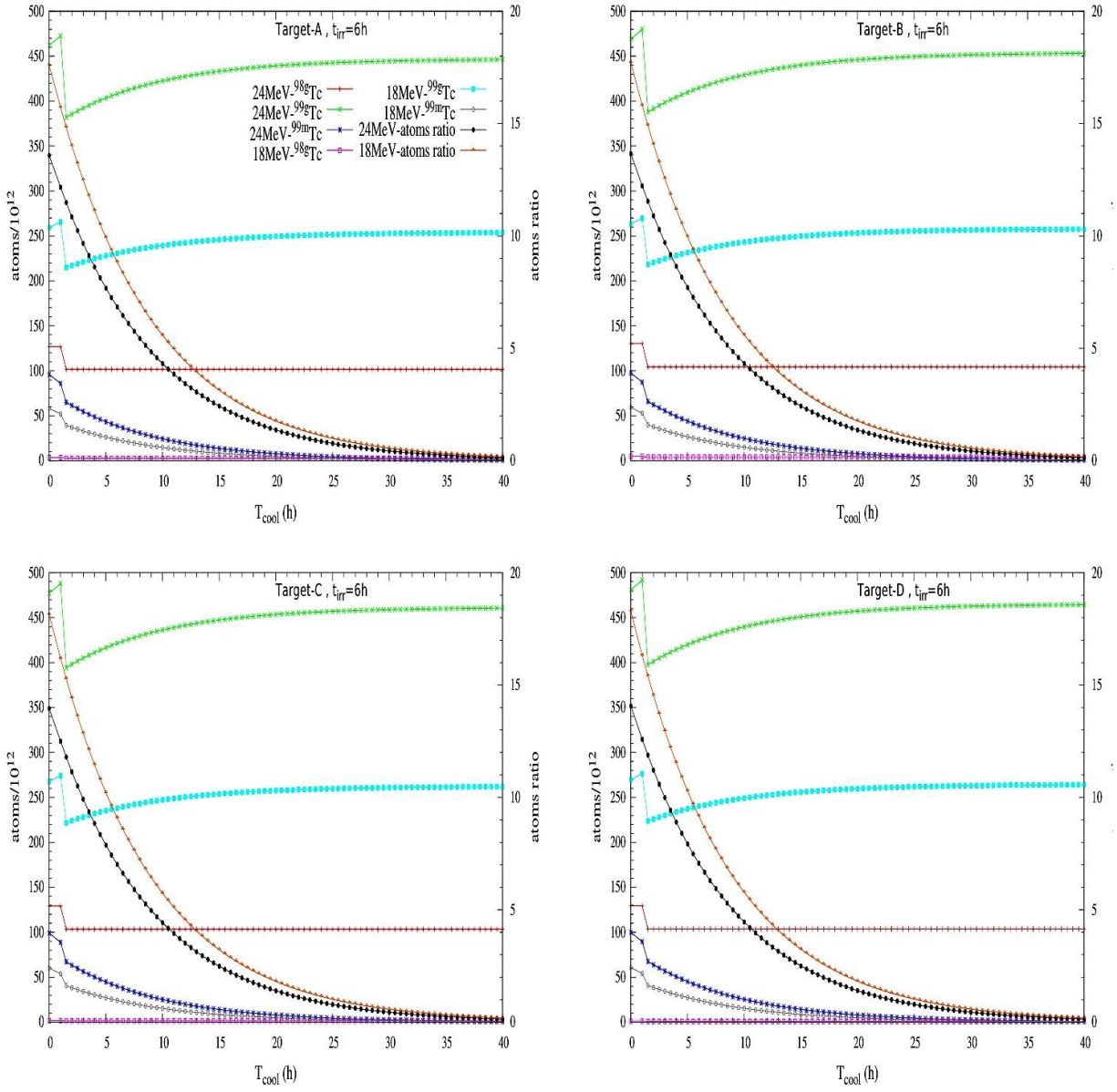

Fig 2.4: Number of atoms of ^{99m}Tc, ^{99g}Tc, ^{98}Tc atoms ratio Ar = $\frac{N_{99m_{Tc}}}{N(99m_{Tc}+all\ co-produced\ Tc)}$, for all targets of Table 2.2, for a six hour irradiation time, and two initial beam energies ($E_{p,in}$=24, and 18 MeV) to $E_{p,out}$ = 8 MeV.

2.2.3.2 Estimation of internal dose

Estimation of internal dose is based on the radioisotopic composition. In this study, absorbed doses were estimated for Tc as pertechnetate, which is used for imaging of the thyroid. Published time-integrated activity coefficients ($\tilde{a}_s$) for each Tc isotope in form of pertechnetate [69] was applied to calculate internal dose that would result if each Tc isotope is injected individually. The dose for each Tc isotope was multiplied by its fraction and partial doses due to each isotope were added together. The calculations were performed using OLINDA/EXM 2 software for an adult male reference phantom [77, 78]. The dose $[Dose]_{Tc-mix}$ from all Tc impurities relative to $[Dose]_{99m_{Tc}}$ from pure ^{99m}Tc, i.e. the dose increase (DI), is defined as $DI = \left(\frac{[Dose]_{Tc-mix}-[Dose]_{99m_{Tc}}}{[Dose]_{99m_{Tc}}}\right) X\ 100\ \%$.

2.2.3.3 Effect of beam energy and isotopic composition on ^{99m}Tc yield, DI and atoms ratio

The performance of the four targets of Table 2.2 for various irradiation times are compared, on the basis of ^{99m}Tc yield, DI and Ar. The Fig 2.5 shows the ^{99m}Tc yield in GBq/ μA at EOB, Ar at 2 hours from EOB, %DI at 26 hours from EOB, for various irradiation times, for four initial beam energies ($E_{p,in}$=24, 22,18 and 16 MeV) to $E_{p,out}$ = 8 MeV.

The % content of the co-produced ^{9x}Tc isotopes, the DI and atoms ratio profile for a six hour irradiation, for four initial beam energies ($E_{p,in}$=24, 22,18 and 16 MeV) to $E_{p,out}$ = 8 MeV, for various cooling times, for the targets A,B,C,D of Table 2.2, are shown in Figures 2.6 to 2.9 respectively.

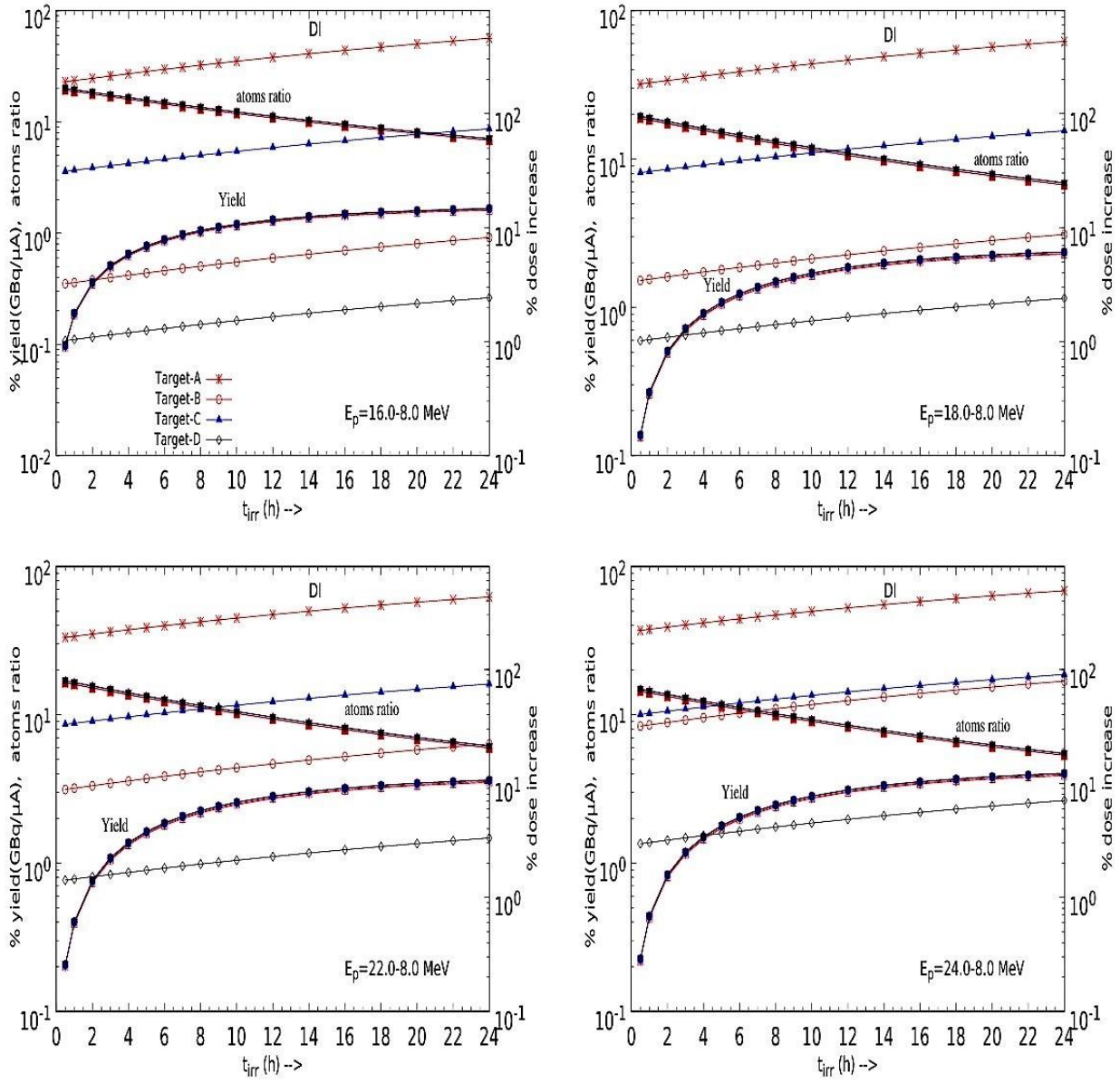

Fig 2.5: Performance of the four targets of Table 2.2 - ^{99m}Tc yield in GBq/ μA at EOB, Ar at 2 hours from EOB, %DI at 26 hours from EOB, for various irradiation times, for four initial beam energies ($E_{p,in}$=24, 22,18 and 16 MeV) to $E_{p,out}$ = 8 MeV.

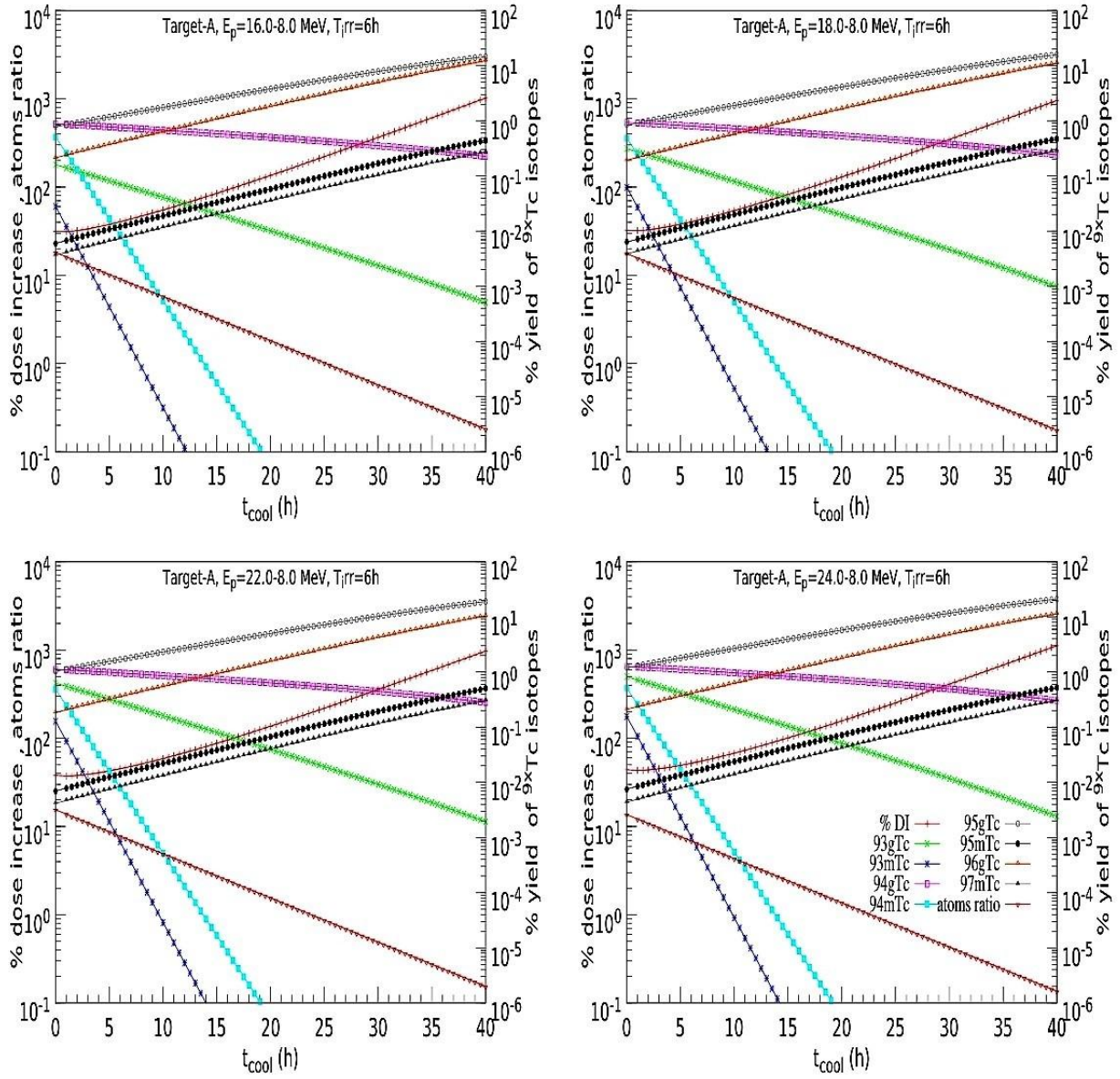

Fig 2.6: The % content of the co-produced ^{9x}Tc isotopes, the DI and atoms ratio profile for a six hour irradiation, for four initial beam energies ($E_{p,in}$=24, 22,18 and 16 MeV) to $E_{p,out}$ = 8 MeV, for various cooling times, for the target A of Table 2.2

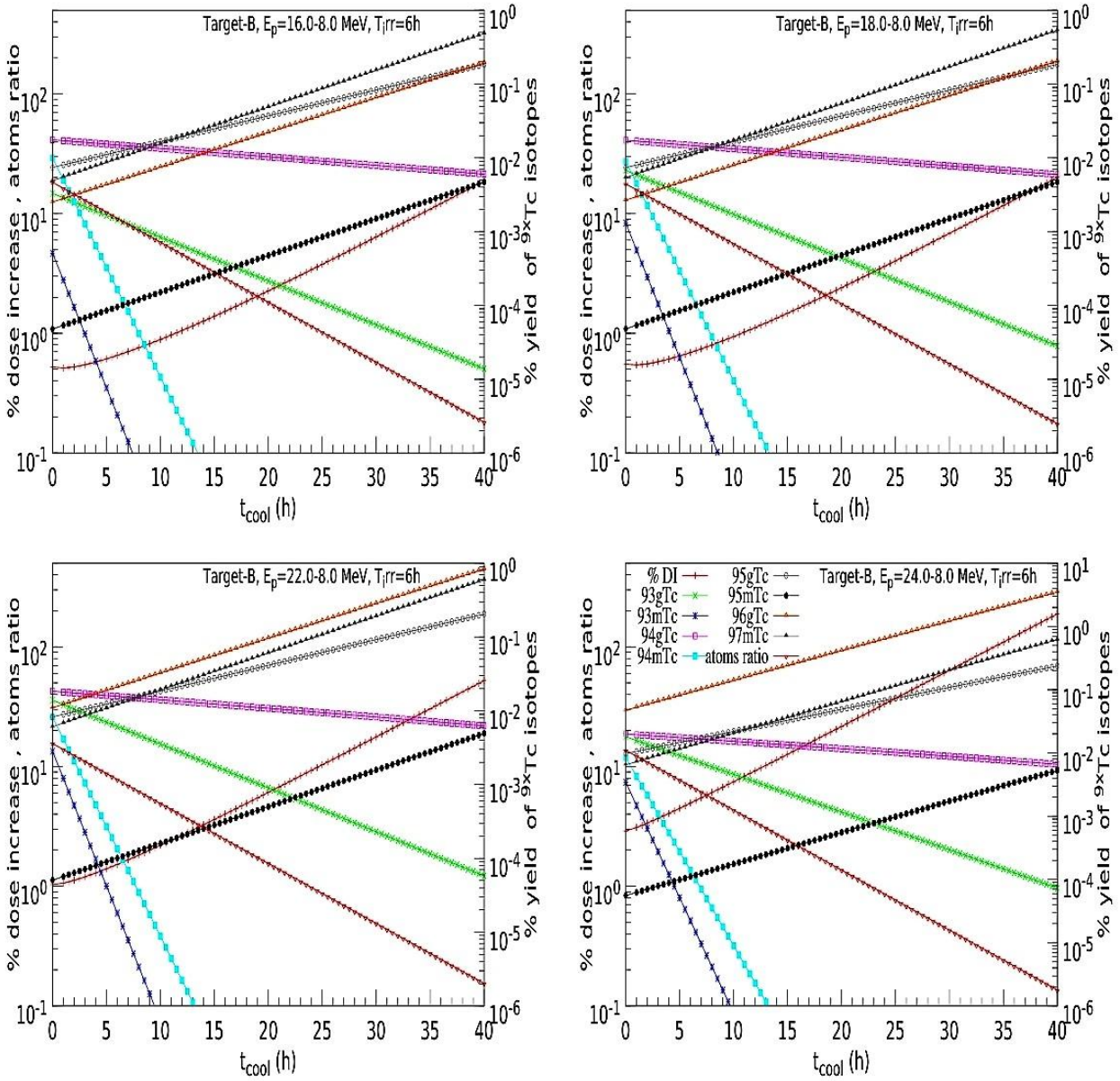

Fig 2.7 : The % content of the co-produced ^{9x}Tc isotopes, the DI and atoms ratio profile for a six hour irradiation, for four initial beam energies ($E_{p,in}$=24, 22,18 and 16 MeV) to $E_{p,out}$ = 8 MeV, for various cooling times, for the target B of Table 2.2

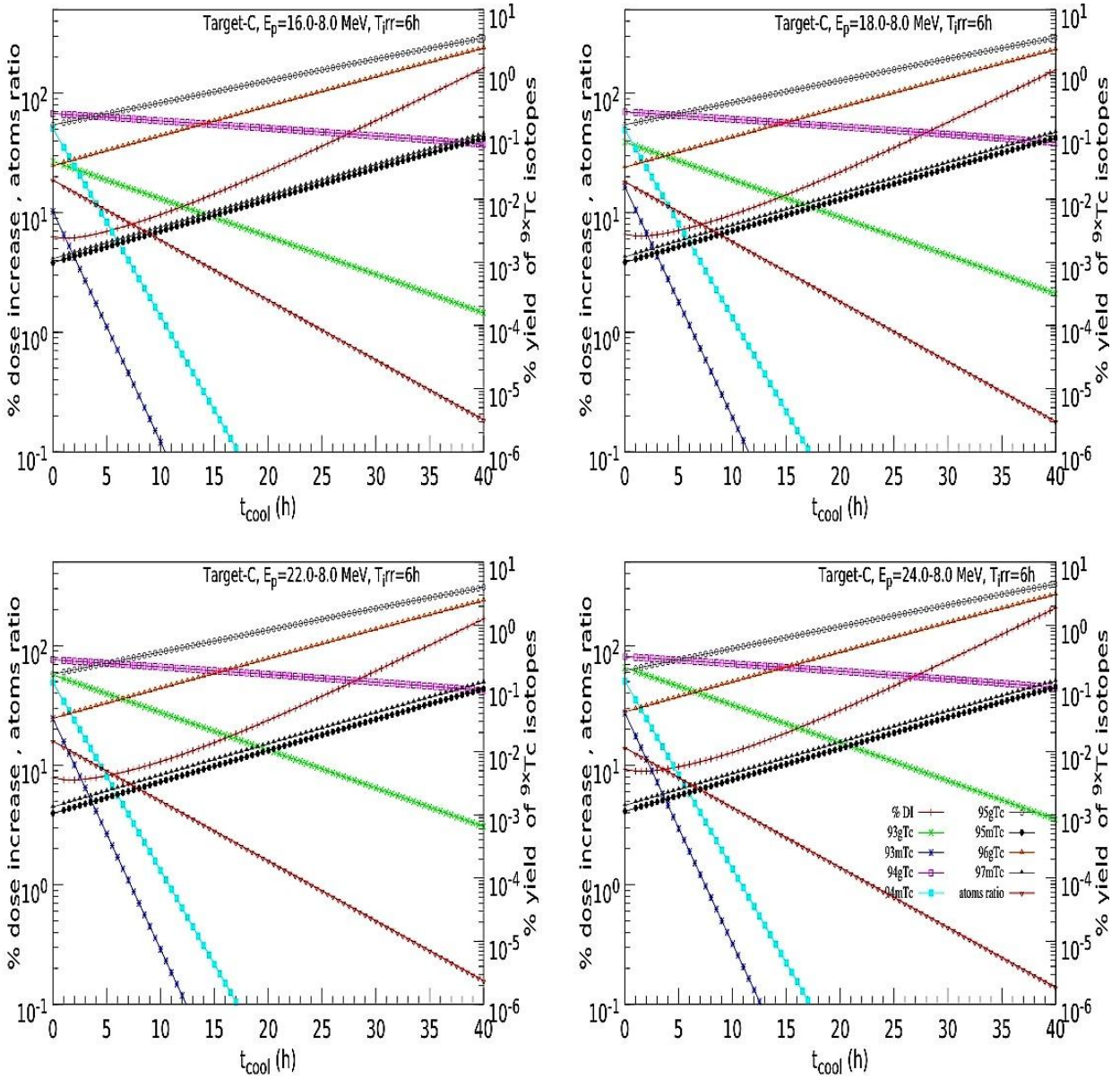

Fig 2.8 : The % content of the co-produced ^{9x}Tc isotopes, the DI and atoms ratio profile for a six hour irradiation, for four initial beam energies ($E_{p,in}$=24, 22,18 and 16 MeV) to $E_{p,out}$ = 8 MeV, for various cooling times, for the target C of Table 2.2

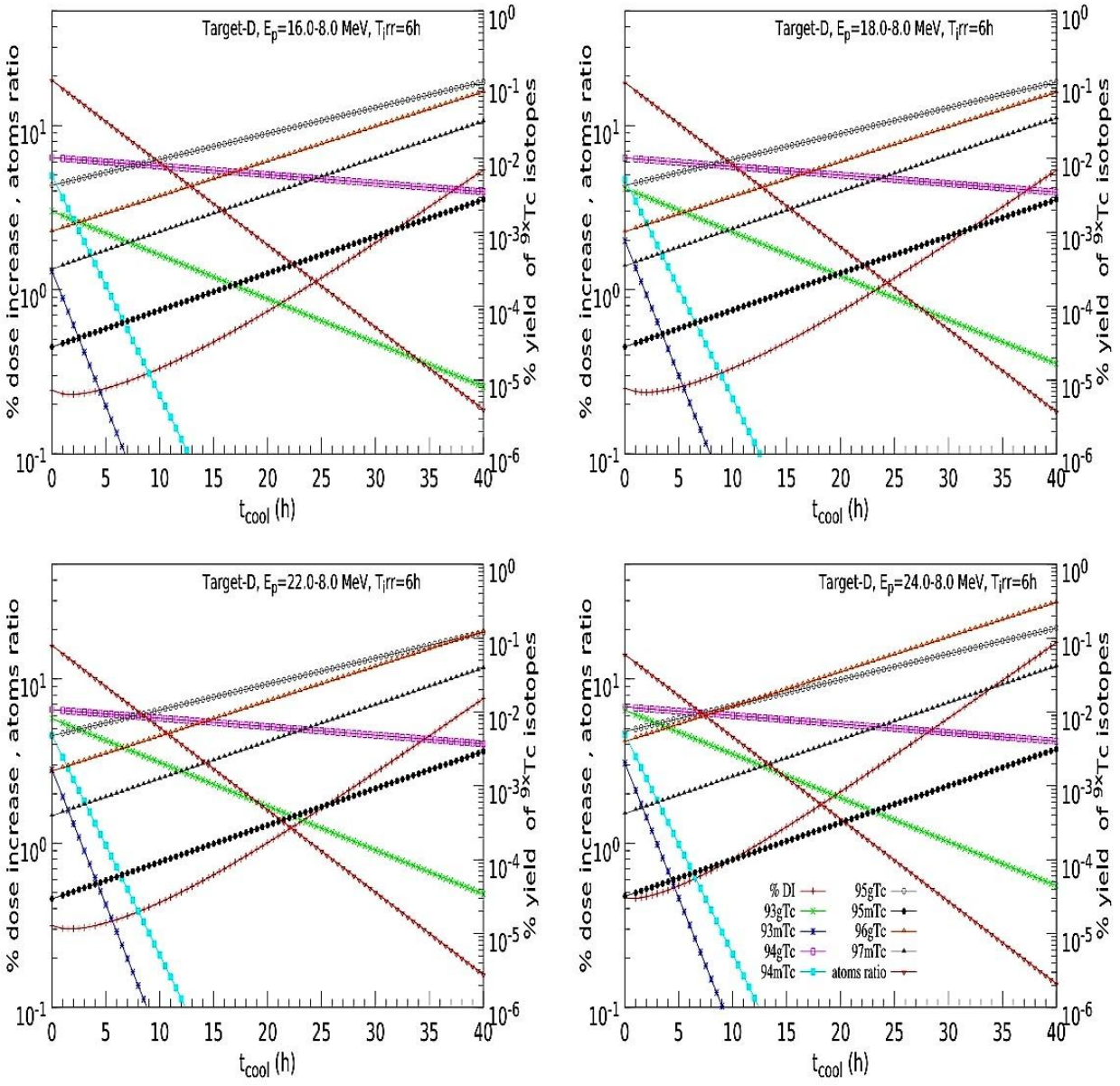

Fig 2.9 : The % content of the co-produced ^{9x}Tc isotopes, the DI and atoms ratio profile for a six hour irradiation, for four initial beam energies ($E_{p,in}$=24, 22,18 and 16 MeV) to $E_{p,out}$ = 8 MeV, for various cooling times, for the target D of Table 2.2

To understand how each of the Mo isotopes present in the target individually influences the DI, an irradiation of six hypothetical thick targets of 99 % enriched ^{100}Mo with a single impurity of 1 %, of each of ^{92,94,95,96,97,98}Mo was considered. The DI at 24 hours post EOB for various irradiation times, and the profile of the DI and % content of the co-produced Tc isotopes for various cooling times, for a six hour irradiation for the various hypothetical targets of 99% enriched ^{100}Mo with a single impurity of 1 %, for $E_{p,in}$ = 24, 22, 18 and 16 MeV to $E_{p,out}$ = 8 MeV are shown in Figs 2.10 to 2.13 respectively.

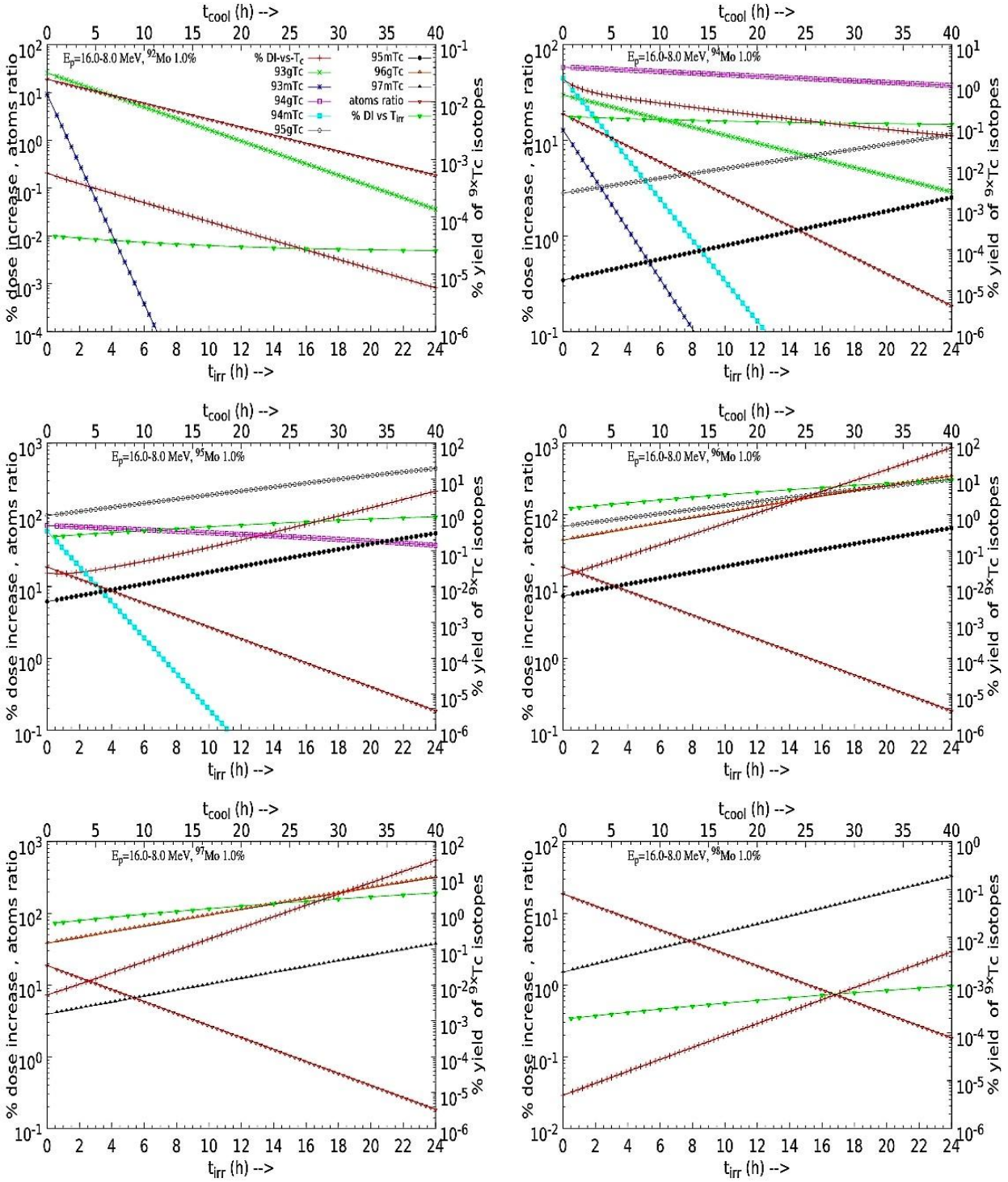

Fig 2.10: The DI at 24 hours post EOB for various irradiation times, and the profile of the DI and % content of the co-produced Tc isotopes vs t_{cool} for a six hour irradiation for the various hypothetical targets of 99% enriched ^{100}Mo with a single impurity of 1 % each of, ^{92,94,95,96,97,98}Mo for $E_{p,in}$ = 16 MeV to $E_{p,out}$ = 8 MeV.

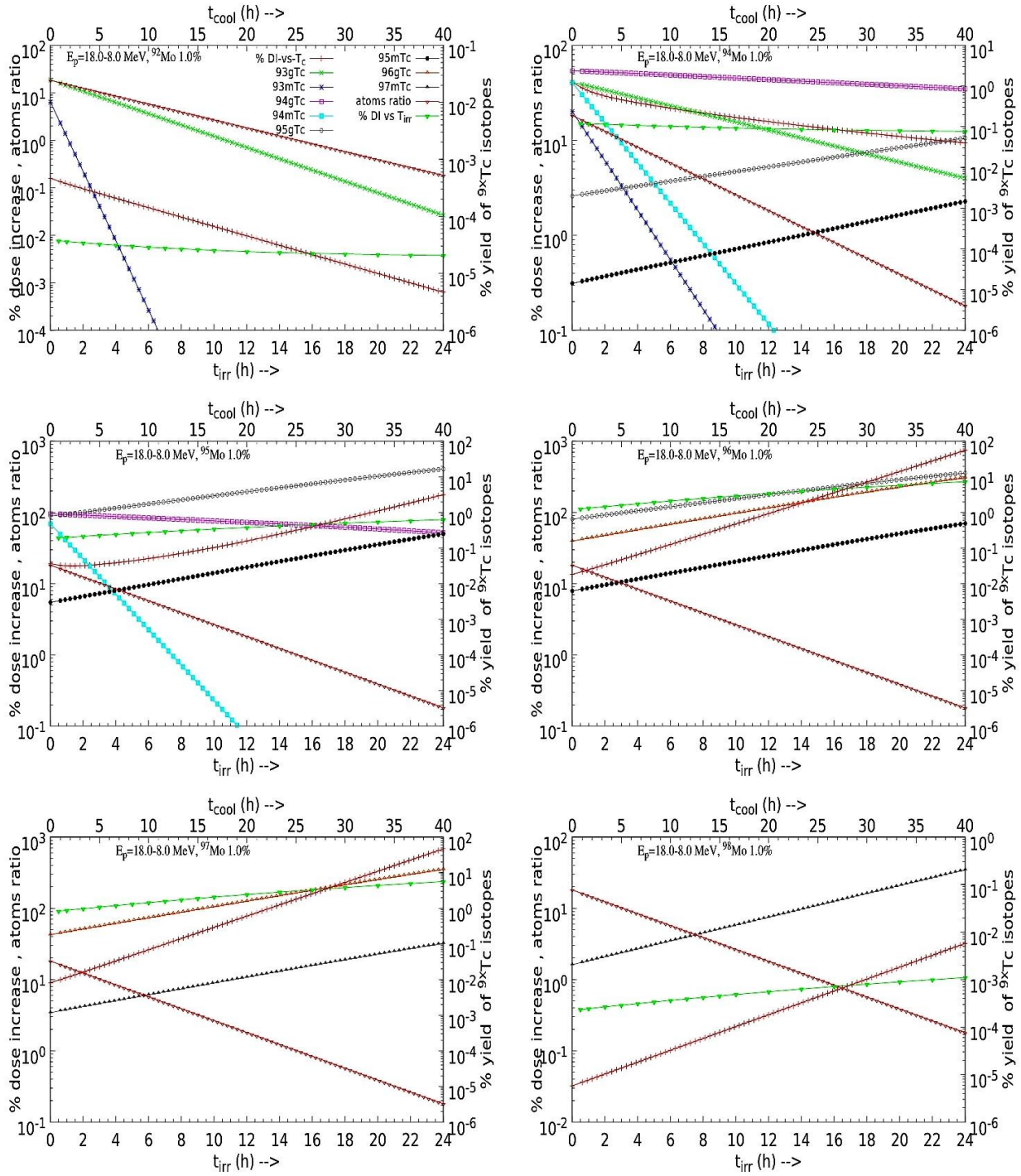

Fig 2.11: The DI at 24 hours post EOB for various irradiation times, and the profile of the DI and % content of the co-produced Tc isotopes vs t_{cool} for a six hour irradiation for the various hypothetical targets of 99% enriched ^{100}Mo with a single impurity of 1 % each of, $^{92,94,95,96,97,98}Mo$ for $E_{p,in}$ = 18 MeV to $E_{p,out}$ = 8 MeV.

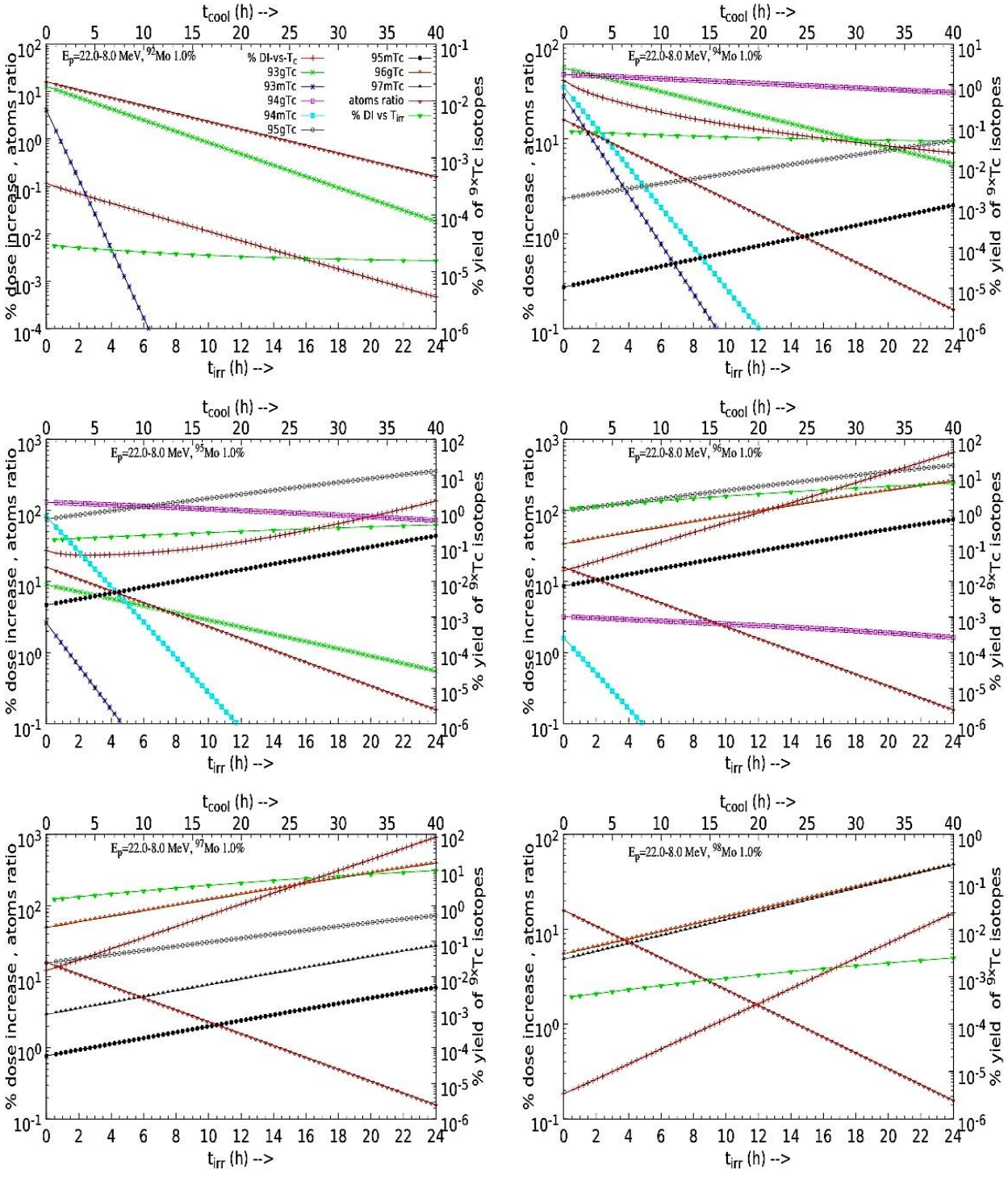

Fig 2.12: The DI at 24 hours post EOB for various irradiation times, and the profile of the DI and % content of the co-produced Tc isotopes vs t_{cool} for a six hour irradiation for the various hypothetical targets of 99% enriched ^{100}Mo with a single impurity of 1 % each of, ^{92,94,95,96,97,98}Mo for $E_{p,in}$ = 22 MeV to $E_{p,out}$ = 8 MeV.

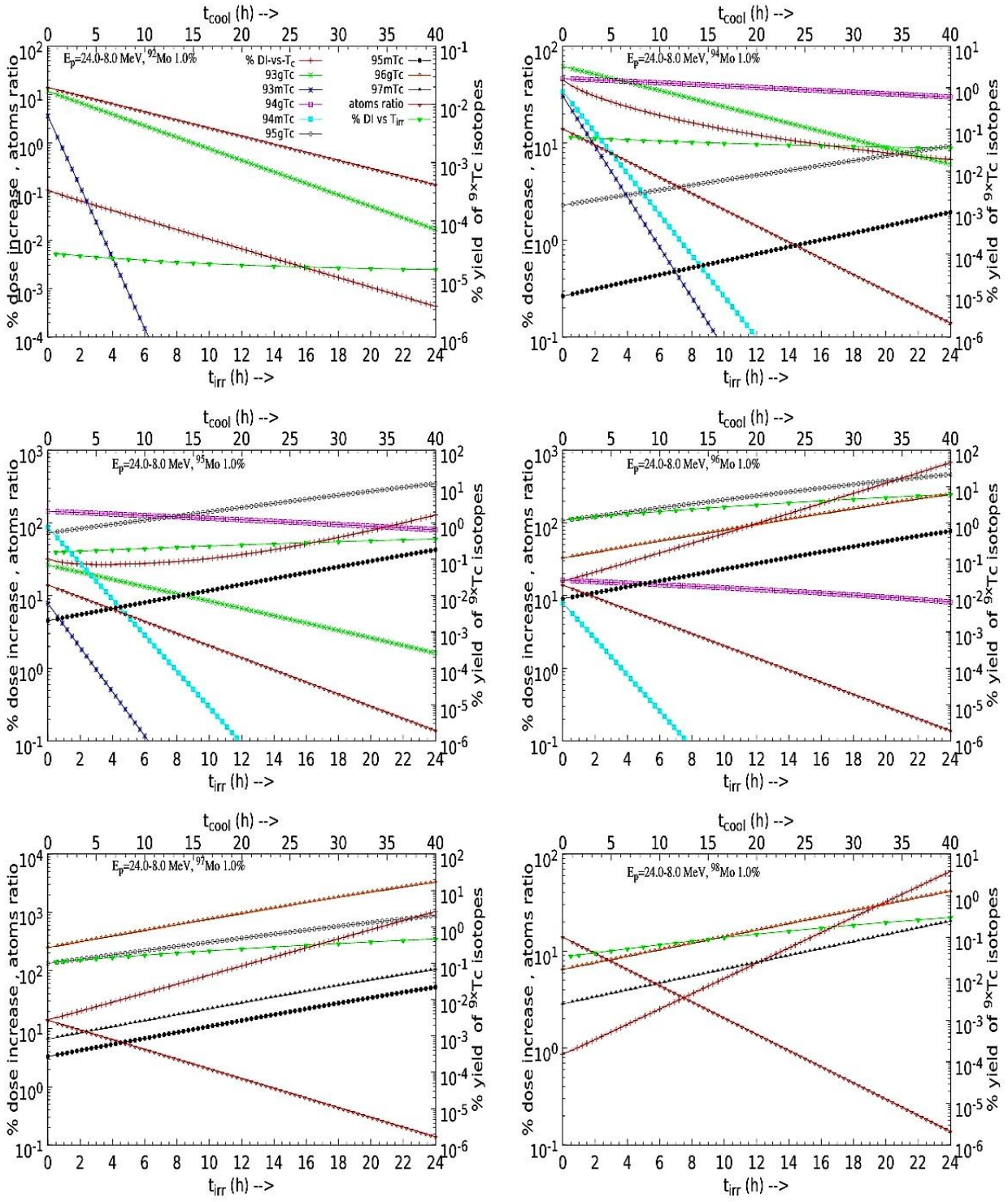

Fig 2.13*:* The DI at 24 hours post EOB for various irradiation times, and the profile of the DI and % content of the co-produced Tc isotopes vs t_{cool} for a six hour irradiation for the various hypothetical targets of 99% enriched ^{100}Mo with a single impurity of 1 % each of, ^{92,94,95,96,97,98}Mo for $E_{p,in}$ = 24 MeV to $E_{p,out}$ = 8 MeV.

2.2.3.4 Validation of the optimisation approach

To validate the optimisation approach (a) the contribution of the various (p, x) channels for the formation of the co-produced Tc and Nb isotopes in the present study are summed up and the calculated cumulative yield for each isotope compared with the experimental yields in Table 2.4. (b) theoretical thick target yields calculated are compared with the published data of [56] and (c) and DI calculated (Fig 2.14) for the irradiation conditions of [70] is shown in Fig 2.14.

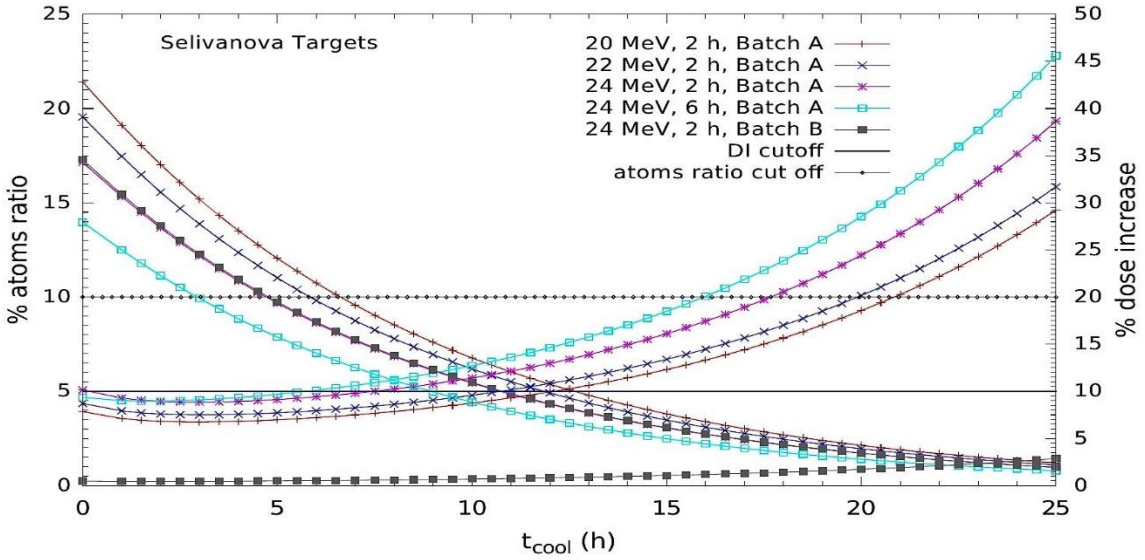

Fig 2.14*:* Validation of optimisation approach - DI calculated for the irradiation conditions of [70]

2.2.3.5 Estimation of the shelf life of ^{99m}Tc

As per the European pharmacopeia (EP), the maximum limits of the shorter lived ^{93m}Tc, ^{93}Tc, ^{94m}Tc, ^{94}Tc, ^{95}Tc, ^{96}Tc are 0.01%, 0.04%, 0.02%, 0.04%, 0.07%, 0.07% and the longer-lived ^{95m}Tc, ^{97m}Tc and other Tc are 0.005%, 0.01% and 0.02% of the total radioactivity respectively. Hou *etal and* Selivanavo *etal* [69, 70] have recommended capping the DI to 10 % in 24 hours from administration.

The shelf-life is defined as the maximum cooling time post EOB,

- where the Ar values are suitable for administering the ^{99m}Tc-radiopharmaceutial,
- the % content of co-produced ^{9x}Tc isotopes are below the specified limits of EP,
- and DI values are < 10 % at 24 hours after administration.

The cutoff for Ar and DI, for various irradiation and cooling times, for $E_{p,in}$= 24,22,18,16 MeV to $E_{p,out}$ = 8 MeV, for targets A, B, C and D of Table 2.2 are shown in Figs 2.15 to 2.18 respectively. The shelf life of the ^{99m}Tc eluates were determined for select irradiation conditions for target B and D, and are shown in Table 2.7. Assuming an optimum 80 % can be separated, the yield of ^{99m}Tc at the end of the shelf-life of the ^{99m}Tc eluates, shown in Table 2.7, incorporates a 20 % loss.

2.3 Results

2.3.1 Cross sections of ^{100}Mo(p,x)^{99}Mo,^{99m}Tc

The cross sections measured in this work, are reported in Table 2.4. Uncertainties due to errors in foil thickness (8-9%), HPGe efficiency error (5%), and nuclear decay data error (1%) and beam current (5%) were added in quadrature.

The Fig 2.1 compares the ^{100}Mo(p,x)^{99}Mo cross sections measured to previously published cross section data. General agreement is noted when comparing with Takács *et al*. [60], Qaim *et al*.[18] The cross sections reported by Gagnon *et al.* [64] and Manenti *et al.* [65] are higher and those reported by Lagunas-Solar *et al.* [58] and Scholten *et al.* [59] are lower than the present data. **The** Fig 2.2 compares the evaluated ^{100}Mo(p,2n)^{99m}Tc cross sections of this work to previously published cross section data. General agreement is noted when comparing with Takács *et al.* [60], Cervenak *et al.* [66]. Cross sections reported by Gagnon *et al.* [64] , Manenti *et al.* [65], Qaim *et al.* [18] , Lagunas-Solar *et al.* [58] are higher and those reported by Scholten

et al. [59] , Khandekar *et al.*[61] are lower than the present data. Increase in efficiency of production of ^{99}Mo with increasing energy is noted.

As seen from the Fig 2.3, the indirect contribution to the activity of ^{99m}Tc, gains significance as the proton energy increases. The indirect contribution is 2 orders more in the thin foil irradiated at 21 MeV as compared to at 11.5 MeV.

Table 2.5 **Experimental cross sections (in mb) of $^{100}Mo(p,x)^{99}Mo$ and of $^{100}Mo\ (p,2n)^{99m}Tc$**

Ep (MeV)	$^{100}Mo(p,x)^{99}Mo$	$^{100}Mo\ (p,2n)^{99m}Tc$
11.5	4.0 ± 0.46	206.5 ± 23
13.3	14.7 ± 1.7	232.5 ± 26
15	27.8 ± 3.2	236.1 ± 27
16.9	67.0 ± 7.6	238.5 ± 27
18.4	91.2 ± 10.4	229.8 ± 26
19.8	111.8 ± 12.7	200.0 ± 23
21	128.9 ± 14.7	156.3 ± 18

Major source of discrepancy between literature reports of the cross section values of the $^{100}Mo(p,2n)^{99m}Tc$ reaction may be due to improper correction of interferences prior to evaluation of the direct ^{99m}Tc cross section. The evaluated ^{99m}Tc cross sections are consistent and independent of the time post-EOB upon which they were evaluated. This builds a confidence in the 140 keV gamma ray peak area corrections performed in this experiment.

2.3.2 Labelling studies of cold kits with various values of $\frac{N_{99m_{Tc}}}{N_{99(m+g)_{Tc}}}$

From Table 2.6 it is seen that **i**n LS1, LS3 and LS4 all ^{99m}Tc radiopharmaceuticals complied to the specifications of the IP for radiochemical purity. In LS2 at 72 hours ingrowth time, 40 % and

Table 2.6: % Compliance of radiochemical purity (determined by Paper Chromatography / Thin Layer Chromatography) of the labelled ^{99m}Tc-radiopharmaceuticals with specifications of Indian Pharmacopoeia

^{99m}Tc-radio pharmaceutical	**LS1 (120 hours [a])**	**LS2 (72 hours [a])**	**LS3 (48 hours [a])**	**LS4 (48 hours [a])**
Sulphur colloid	100 (n= 12; 100-180 MBq[b])	83.3 (n=6; 1.5 – 1.8 GBq[b])	100 (n=6; 1.8 – 2 GBq)	100 (n=6; 1.8-2 Gbq)
DTPA	100 (n= 12; 200-300 MBq)	100 (n=6; 1.5 – 1.8 GBq)	-np-	100 (n=6; 1.8-2 Gbq)
Glucoheptonate	100 (n= 12; 100-180 MBq)	100 (n=6; 1 -1.3 GBq)	-np-	100 (n=6; 1.5 – 1.8 GBq)
MDP	100 (n= 6; 200 - 300 MBq)	60 (n= 15; 4 -5 GBq)	100 (n= 6; 5 - 6 GBq)	100 (n= 6; 5-6 GBq)
Mebrofenin	100 (n= 12; 100-180 MBq)	100 (n=6; 1 -1.3 GBq)	-np-	100 (n=6; 1.5 – 1.8 GBq)
ECD	100(n= 10; 200 - 300 MBq)	100 (n=6; 1.5 – 1.8 GBq)	-np-	100 (n=6; 1.8 - 2 GBq)
EC	100 (n= 6; 100-160 MBq)	83.3 (n=6; 1.5 – 1.8 GBq)	100 (n=6; 1.8 - 2 GBq)	100 (n=6; 1.8 - 2 GBq)
MIBI	100 (n= 6; 200-300 MBq)	40 (n= 10; 5-6 Gbq)	100 (n= 6; 6-7.5 GBq)	100 (n= 6; 6-7.5 GBq)

[a] Ingrowth time is shown in hours , [b] Activity used for labelling is shown in MBq / GBq
n = number of batches tested, np = not performed

60 % failures of MDP and MIBI, and a single failure of sulphur colloid and EC, from testing of 15,10, 6, and 6 batches respectively were observed.

The values of A_r , $\frac{N_{99m_{Tc}}}{N_{99(m+g)_{Tc}}}$ **,** of the ^{99m}Tc used in the LS**,** can never be 100 % because of the branching decay of ^{99}Mo to ^{99m}Tc and ^{99g}Tc (and moreover, ^{99m}Tc also decays to ^{99g}Tc by isomeric transition) which implies that ^{99m}Tc is always diluted with ^{99g}Tc. The A_r with ingrowth time of 48 hours is~ 13 % [74, 75].In LS 3 the time span between elution and the usage of the eluate is upto three hours which reduces the A_r to 10 - 11 % [75]. Also in practical terms, complete separation of all Tc atoms from ^{99}Mo is not possible in the first separation on receipt of the ^{99}Mo; If 10% of Tc is retained it will reduce the value of A_r to around 9 % for LS3 [75]. Further, the levels of activity used for labelling, play a role in determining the radiochemical quality of the Tc-pharmaceutical [79]. The labelling studies in LS3 and 4 have been carried out with activities suitable for 4 -5 patients per kit vial. As an optimum consideration, labelling with moderate activities and administration of the ^{99m}Tc-pharmaceutical within a value of A_r of 10-11% or higher will ensure utilisation of the ^{99m}Tc radiopharmaceutical for intended purpose.

2.3.3 Optimisation approach

2.3.3.1 Validation of the optimisation approach

The co-produced isotopes identified in the 2 hour irradiation of Target A are, ^{93}Tc, ^{94}Tc, ^{95}Tc, ^{95m}Tc, ^{96}Tc, ^{99}Mo, ^{95}Nb, and ^{96}Nb. As seen from Table 2.4 the optimisation approach over estimates the shorter- lived radionuclides ^{93}Tc and ^{94}Tc in the lower energy foils. However, there is a very good agreement with the thin target yields for ^{95m}Tc, ^{95g}Tc, ^{96}Tc and the ^{95,96}Nb isotopes. The thick target yields of ^{99m}Tc, calculated by the optimisation approach, are in good agreement with the Table 2 of Ref [56].The DI calculated (Fig 2.14) are comparable to those obtained in Ref [70].

2.3.3.2 Shelf life of clinical grade ^{99m}Tc

From Fig 2.5, it can be seen that there is only a minimal increase in ^{99m}Tc yield with ^{100}Mo enrichment, in all the energy intervals, across all the four targets. Obtaining high yields and high levels of atoms ratio $\frac{N_{99m_{Tc}}}{N(_{99m_{Tc}+all\ co-produced\ Tc})}$ simultaneously is not possible and there is a trade-off with increasing time of irradiation and energy.

From Fig 2.18 it is seen that for target D, the DI cutoff line is way above the Ar cutoff line, implying the suitability of target D, for all irradiation, and cooling times. From Fig 2.15 and 2.17, it is seen that for target A and target C , the DI rises above 10 % before 24 hours EOB. Target A and C are not suitable in any energy interval, for obtaining clinical grade ^{99m}Tc. The DI cutoff line is below the Ar cutoff line for targets B for $E_{p,in}$ = 22 and 24 MeV . The target B has limited shelf-life, for the $E_{p,in}$ = 22 MeV, case, as the DI crosses 10 % after 26 hours EOB, and is not suitable for Ep,in = 24 MeV. From Fig 2.10 to 2.13 it is seen that, for the hypothetical cases in which impurities $^{92,\ 98}Mo$ are 1 %, the DI levels are low. For ^{98}Mo, the DI levels rise with $E_{p,in.}$. For the hypothetical cases with $^{94,\ 95,\ 96,\ 97}Mo$ as 1%, the DI levels are significantly high.

In targets A and C, the content of these Mo, are 10-100 times more than that in Target B and D. Each Mo isotope undergoes various (p,x), reactions as the proton travels through the target losing energy, producing multiple Tc impurities, which although follow the same bio distribution in the body, deliver different internal dose, based on the physical half life and γ ray energy intensity. Rather than the absolute ^{100}Mo enrichment, the isotopic composition of the target, is more significant for the DI [80] .

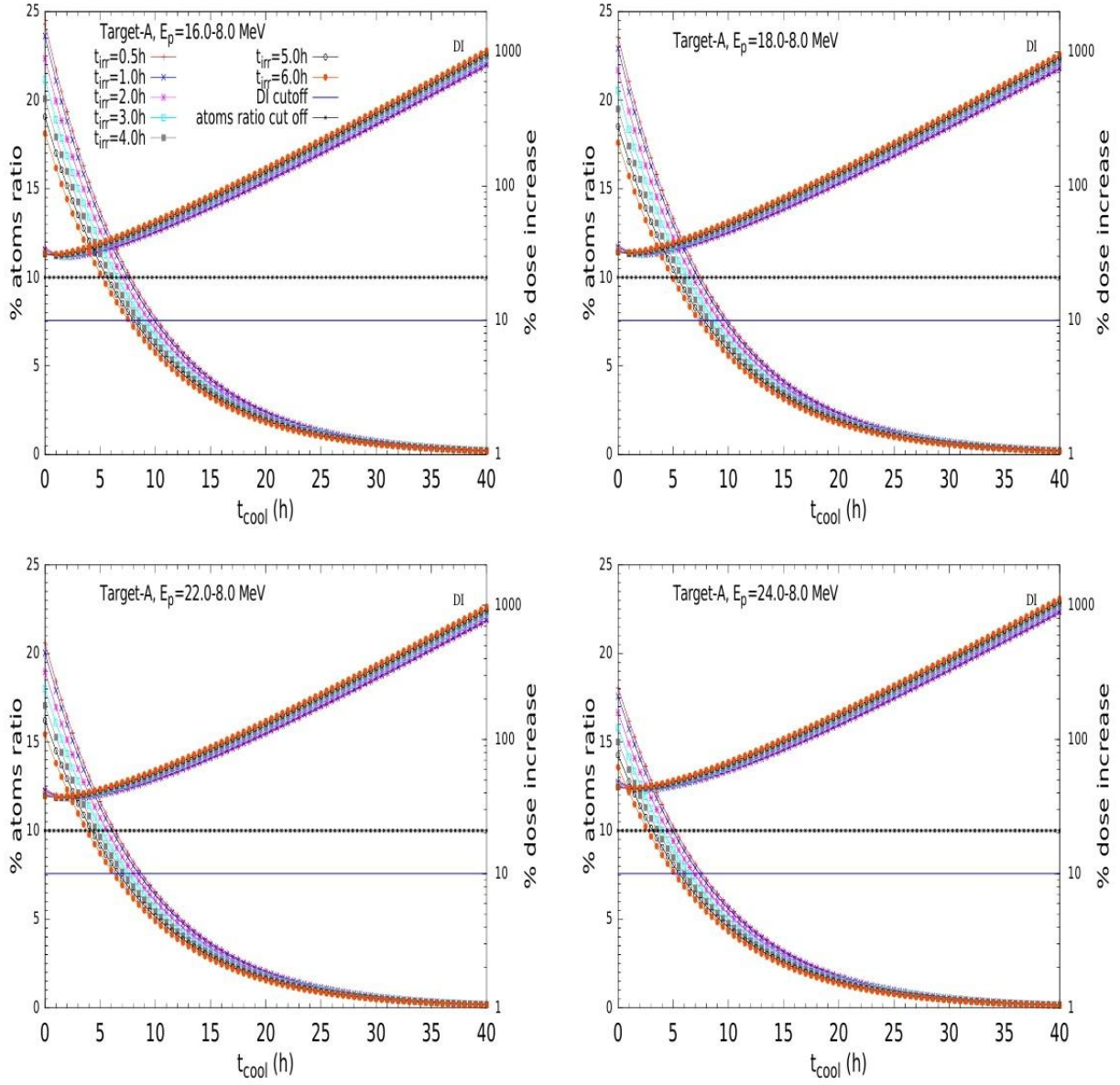

Fig 2.15: Estimation of shelf-life of ^{99m}Tc- The cutoff for Ar and DI, for various irradiation and cooling times, for $E_{p,in}$= 24,22,18,16 MeV to $E_{p,out}$ = 8 MeV for target A of Table 2.2.

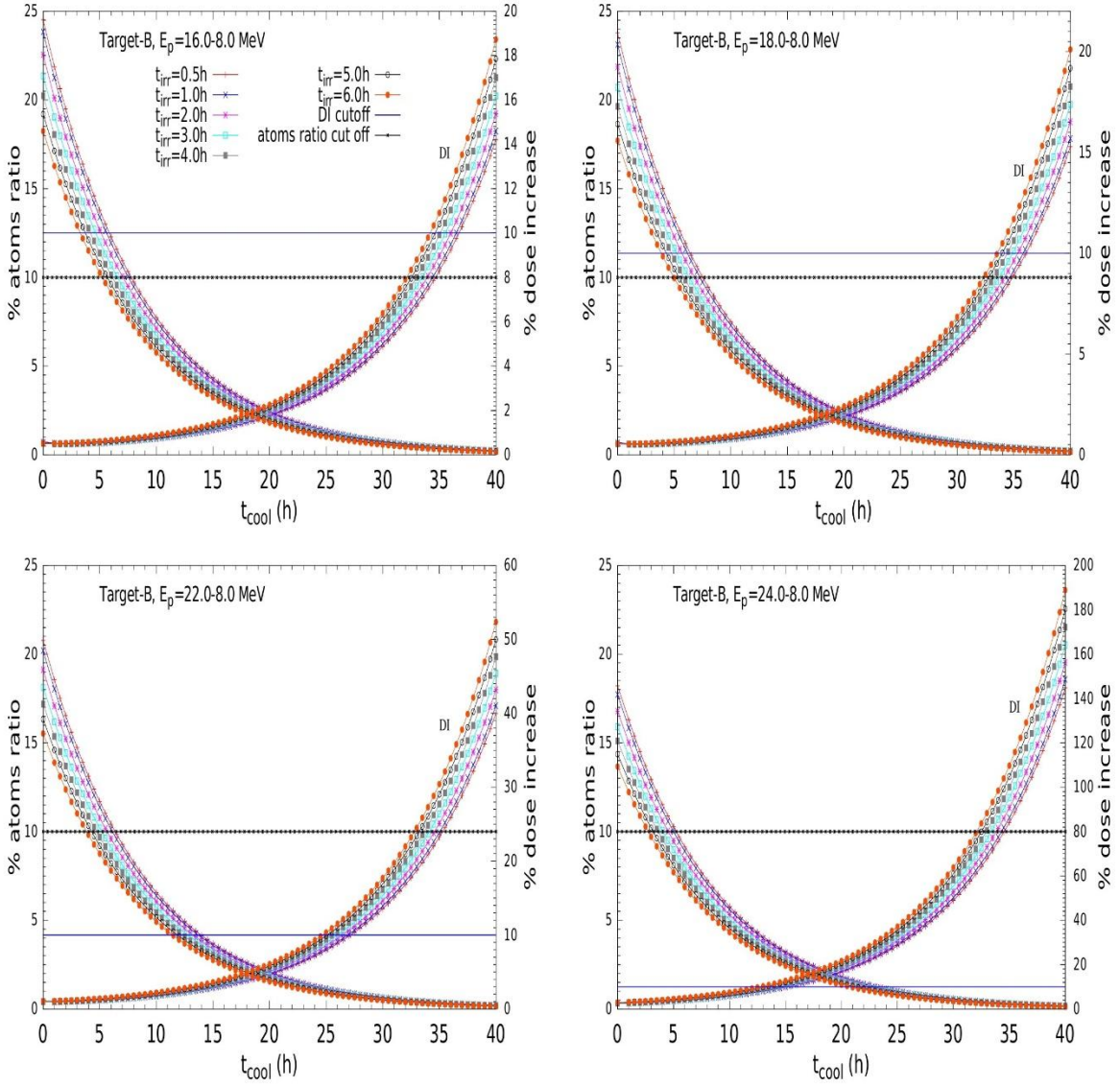

Fig 2.16: Estimation of shelf-life of ^{99m}Tc- The cutoff for Ar and DI, for various irradiation and cooling times, for $E_{p,in}$= 24,22,18,16 MeV to $E_{p,out}$ = 8 MeV for target B of Table 2.2.

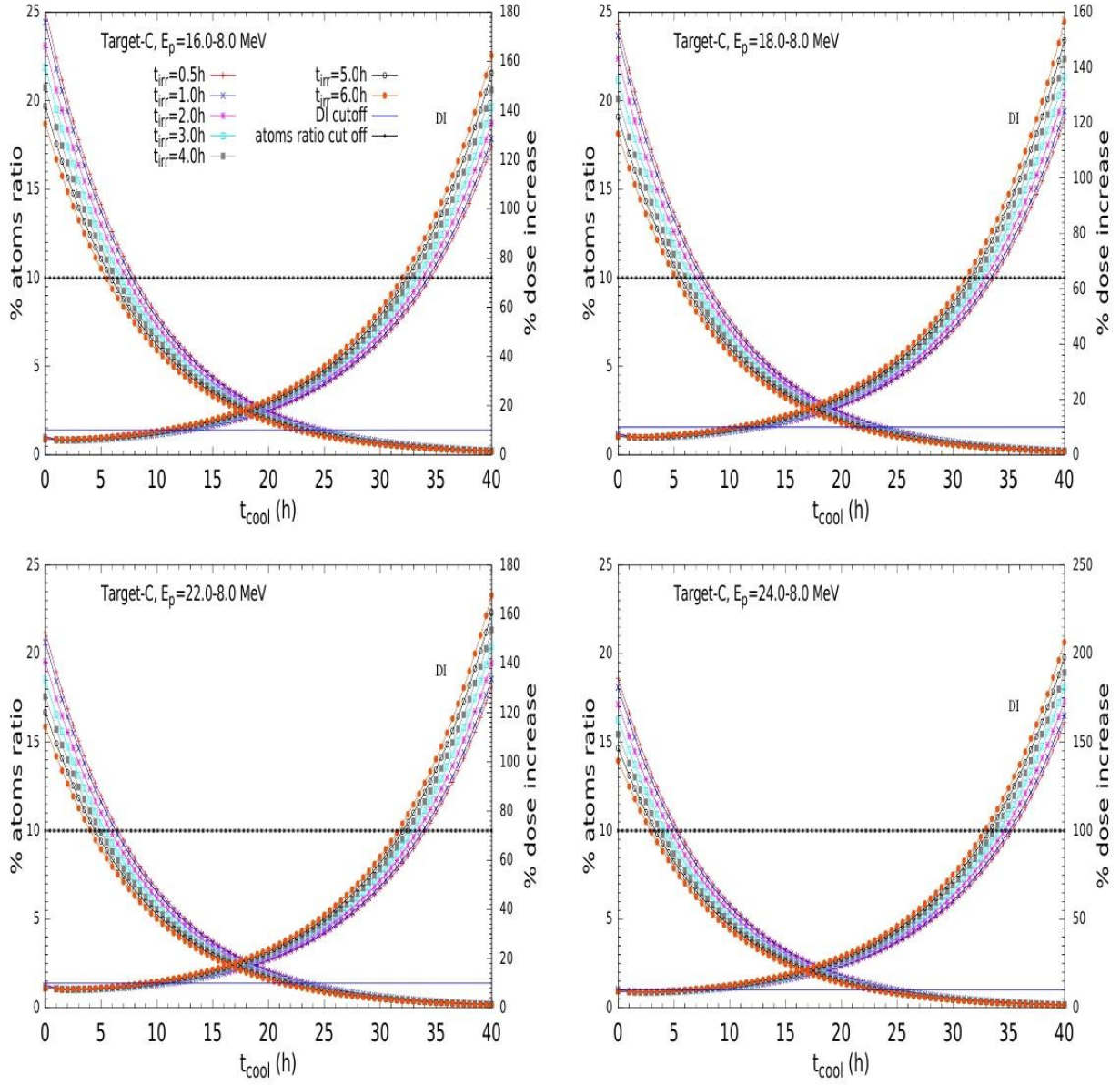

Fig 2.17: Estimation of shelf-life of ^{99m}Tc- The cutoff for Ar and DI, for various irradiation and cooling times, for $E_{p,in}$= 24,22,18,16 MeV to $E_{p,out}$ = 8 MeV for target C of Table 2.2.

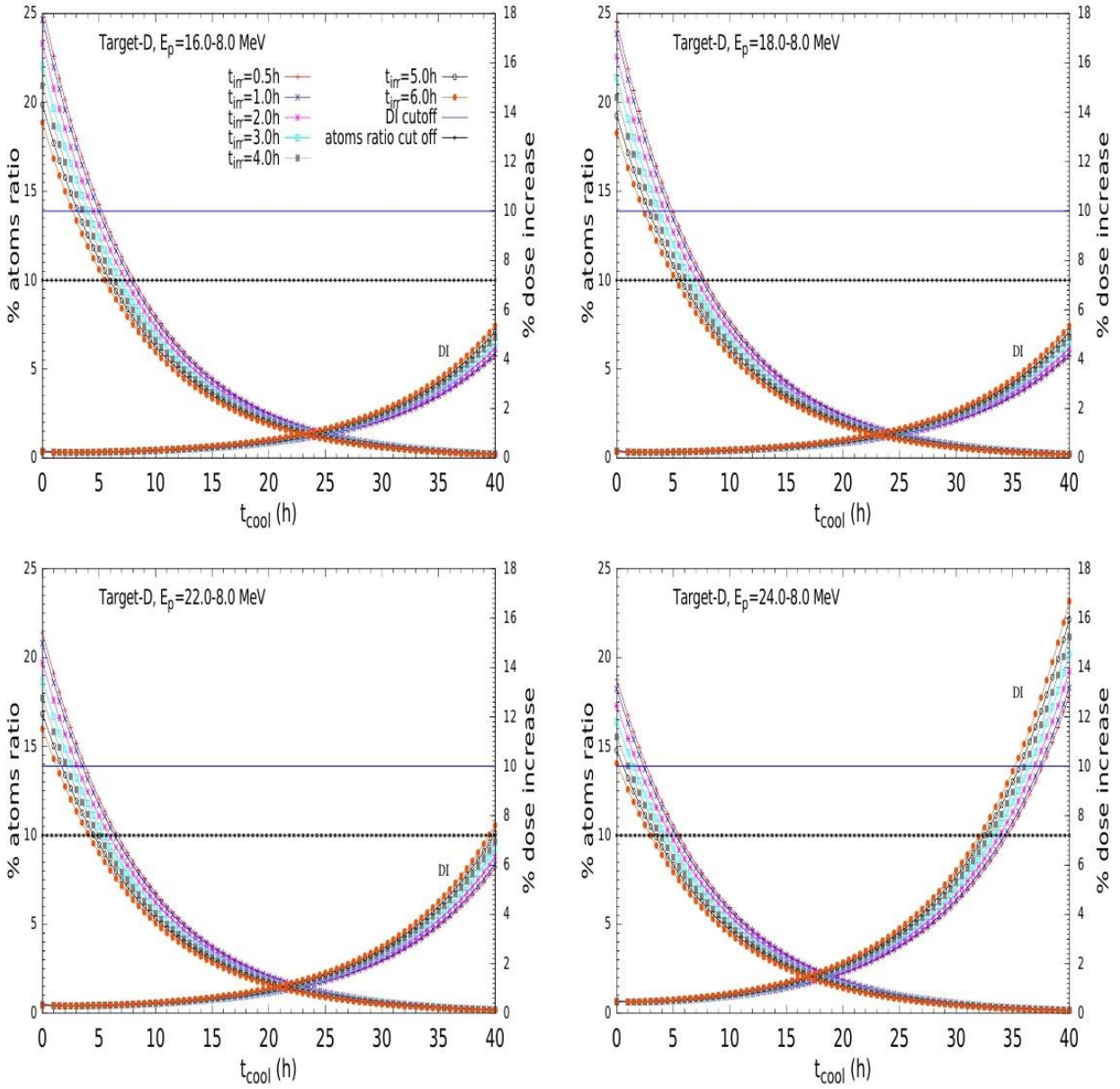

Fig 2.18: Estimation of shelf-life of ^{99m}Tc- The cutoff for Ar and DI, for various irradiation and cooling times, for $E_{p,in}$= 24,22,18,16 MeV to $E_{p,out}$ = 8 MeV for target D of Table 2.2.

Table 2.7: Shelf life of ^{99m}Tc for select irradiation conditions of Target B and D

Target	E_{pin} (MeV)	Irradiation time (h)	Shelf life (Time in hours post- EOB)	At end of shelf life			At Shelf life + 24 hours
				Atoms ratio %	Yield- ^{99m}Tc (Bq/μA)	DI %	DI%
B	22	3	2	14.43	1.06E+09	1.035	10.012
	20	4	5.5	9.99	7.66E+08	0.667	6.231
	20	5	5	10.05	9.64E+08	0.665	6.193
	20	6	4	10.72	1.54E+09	0.644	5.830
	20	7	4	10.20	1.37E+09	0.661	6.098
	20	8	3.5	10.30	1.58E+09	0.659	6.042
	18	5	5.5	9.90	7.07E+08	0.649	6.186
	18	6	5	9.97	8.55E+08	0.646	6.145
	18	7	4.5	10.04	1.01E+09	0.644	6.097
	16	6	5.5	9.68	5.73E+08	0.632	6.058
D	24	4	3.5	10.43	1.27E+09	0.483	4.072
	24	5	3.5	9.91	1.51E+09	0.493	4.258
	24	6	3	9.99	1.82E+09	0.492	4.223
	24	7	2.5	10.09	2.15E+09	0.491	4.183
	22	4	5	9.97	9.74E+08	0.316	2.237
	22	5	4.5	10.04	1.23E+09	0.315	2.222
	22	6	4.5	10.11	1.48E+09	0.315	2.206
	22	7	3.5	10.21	1.75E+09	0.315	2.187
	20	4	5.5	10.30	7.86E+08	0.260	1.704
	20	5	5	10.36	9.88E+08	0.260	1.694
	20	7	4.5	9.93	1.33E+09	0.264	1.754
	20	8	4	10.02	1.53E+09	0.263	1.738
	18	5	5.5	10.21	7.25E+08	0.255	1.750
	18	6	5	10.28	8.76E+08	0.250	1.740
	18	7	4.5	10.36	1.03E+09	0.245	1.730
	16	6	5.5	10.01	5.87E+08	0.256	1.840

Present study suggests a 6 hour irradiation, for thick targets of 24, 22, 18 to 8 MeV would limit the clinical shelf-lives to 3, 4.5, 5 hours, post EOB with ^{99m}Tc yield of 1.8, 1.5, 0.85 GBq/μA at the end of shelf-lives respectively.

2.4 Summary

The $^{100}Mo(p,2n)^{99m}Tc$ excitation function was measured from Ep =11.5 to 21 MeV and compared with literature data. The cross section values presented are consistent independent of time from EOB. This builds a confidence in the 140 keV peak γ-ray area corrections performed in this experiment.

Evaluation of radiochemical purity of Tc-radiopharmaceuticals mimicking different ratios of $\frac{N_{99m_{Tc}}}{N_{99(m+g)_{Tc}}}$, shows labelling of Tc kits with $\frac{N_{99m_{Tc}}}{N_{99(m+g)_{Tc}}}$ of 10-11% or higher will ensure compliance with pharmacopoeia specifications.

In a theoretical approach, to maximise the yield of ^{99m}Tc and minimise the impurities, the beam energy, target thickness, target enrichment and composition, irradiation and cooling times were varied. The optimisation approach was validated by comparing thin target yields and published data [56, 70].

There is only minimal increase in thick target yields of ^{99m}Tc with enrichment. The thick target yields of ^{99}Mo and ^{99m}Tc increases with energy and irradiation time. There is a trade-off between the yield and thick target atoms ratio of $\frac{N_{99m_{Tc}}}{N(99m_{Tc}+all\ co-produced\ Tc)}$ with increasing irradiation time and energy. With cooling time, the composition of Tc-Mix changes and affects the internal dose. Tc isotopes with half-life more than ^{99m}Tc, contribute significantly to the dose with increase in cooling time.

Rather than the absolute ^{100}Mo enrichment, the isotopic composition of the target, i.e the amount of stable impurities of ^{9x}Mo, should be considered as they play a significant role in the increase

of the internal dose. The criteria of dose increase, and decrease of specific activity, can be used to set the shelf life of the ^{99m}Tc obtained and accept/reject ^{100}Mo targets of various compositions. The compliance of the % content of co-produced isotopes to specifications of EP and value of atoms ratio $\frac{N_{99m_{Tc}}}{N_{99m_{Tc}}+N_{all\,Tc}}$ > 10% at administration, subject to DI < 10% at 24 hours after administration, can be used to optimise the irradiation conditions for ^{100}Mo targets of a given composition and ensure the clinical quality of ^{99m}Tc obtained.

Chapter 3

Preparation of ^{99}Mo from the ^{100}Mo(γ, n) reaction: Separation of ^{99m}Tc and evaluation of the ^{99m}Tc eluates

The aim of this study is preparation of ^{99}Mo via the ^{100}Mo(γ, n)^{99}Mo route, separation of ^{99m}Tc, and evaluation of the ^{99m}Tc eluates with reference to the Indian Pharmacopeia (IP) pertechnetate monograph.

3.1 Introduction

3.1.1 ^{99}Mo production by the ^{100}Mo(γ, n) ^{99}Mo route

One of the alternate options of accelerator based production of ^{99}Mo, is the photonuclear reaction^{100}Mo(γ, n) in high energy electron linear accelerators (linac) [15, 47, 81, 82]. Photo producing radioisotopes with electron linacs requires a bremsstrahlung converter. An electron traversing the converter will lose energy by means of emitting photons through the process of bremsstrahlung. Conventional converters are made of solid high-Z metals having a high melting point, such as W or Ta.

Photonuclear reactions can be described as a two-stage process. During the first stage a photon is absorbed, and a nucleus becomes excited. For energies below about 10 MeV only narrow resonance peaks exist, corresponding to exciting a single nuclear level. In general, the resonance lines are very sharp and thus even though the peak cross-section can reach thousands of barns, the integrated cross-section is very small. In the energy range from approximately 10 MeV to about 30 MeV a very broad resonance maximum is observed. This region, called giant dipole resonance (GDR), represents the collective vibrational motion of the neutrons against the protons inside the nucleus. This is the most suitable energy region for photonuclear production. During the second stage, the excitation energy is released – in the form of a photon, neutron, or a charged particle (proton, alpha particle, etc)

The radioactive yield Y depends upon a number of parameters, such as the number of target nuclides that are irradiated N, the threshold energy of the nuclear reaction E_{th}, the maximum energy of photons E_{max}, the photon flux density $\emptyset(E)$, the probability of a photonuclear reaction or cross section $\sigma(E)$, the decay constant of the daughter nuclide λ, and the irradiation time t_i.

$$Y = N \int_{E_{th}}^{E_{max}} \emptyset(E)\sigma(E)dE\left(1 - e^{-\lambda t_i}\right)$$

The simplest photoneutron reaction is (γ, n), however, higher order reactions are also possible: $\sigma(\gamma, n_{total}) = \sigma(\gamma, n) + \sigma(\gamma, np) + \sigma(\gamma, 2n) + \sigma(\gamma, 2np) + \sigma(\gamma,3n) + \text{----}$. Higher order terms start contributing as well once their threshold energy is reached. The Fig 3.1 shows the ^{100}Mo(γ,n)^{99}Mo excitation function. While providing relatively high yield, photoneutron production of most radioisotopes has a drawback of low specific activity. ^{99}Mo decays predominantly to ^{99m}Tc with a half-life of 66 hours. ^{99m}Tc can be extracted periodically via chemical processes, as it accumulates from the decay of the parent ^{99}Mo.

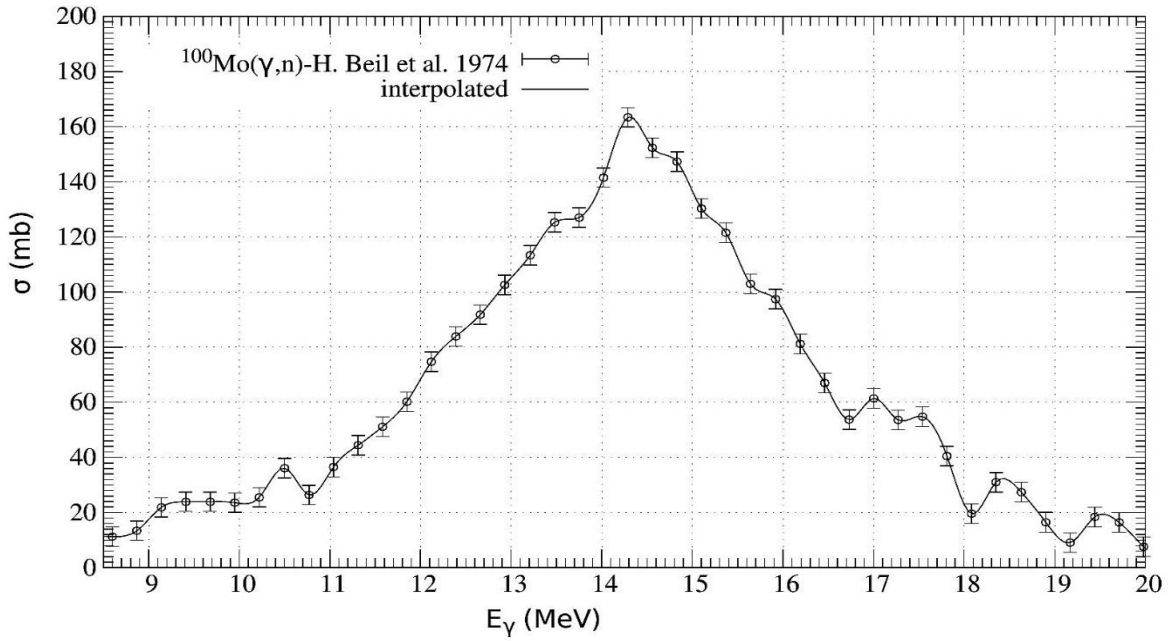

Fig 3.1 The ^{100}Mo(γ, n)^{99}Mo excitation function [82]

3.1.2 ZrMo generators

The ZrMo gel generator has been established as an alternative user friendly column source to obtain ^{99m}Tc from low specific activity ^{99}Mo [83-86].Zirconium molybdate gel generator is a dual column generator system. A primary column of insoluble Zirconium molybdate gel and a secondary column of acidic alumina, which traps any coeluted radionuclidic impurities. The ^{99}Mo ZrMo gel generator system for ^{99m}Tc supply combines the advantages of chromatographic column generators and the use of inexpensive (n, γ) produced ^{99}Mo. The Indian pursuit of gel generator technology based on the conversion of (n, γ) ^{99}Mo as a Zr^{99}Mo matrix and subsequent elution of ^{99m}Tc from the Zr^{99}Mo gel column has been driven by the

(i) reliable, established and ease of production of (n,γ) ^{99}Mo and

(ii) need to replace the solvent (MEK) extraction generator system in use in India since 1970s with a more user-friendly column-type generator system for use in hospitals.

Although the separation of ^{99m}Tc from the Zr^{99}Mo generator is simple in a radiopharmacy, the preparation of the ZrMo gel generator is a multi-step process, complicated by requirements of shielding and automation to handle huge amounts of radioactive ^{99}Mo.

The preparation of Zr^{99}Mo involves mixing of Na_2MoO_4 solution with $ZrOCl_2$ solution, forming a thick, viscous, gelatinous precipitate, followed by filtration of the gel under vacuum, drying of gel cake in a microwave oven, and dispersion of the cake into granules. The Fig 3.2 shows the flow chart of radiochemical operations to prepare a ZrMo generator.

A 100 mm lead-shielded production facility comprising 4 interconnected processing cells has been designed and erected at BRIT, for carrying out the production operations (Fig- 3.3). In the first cell, the sodium molybdate-$^{99/nat}$Mo solution containers are handled and the contents transferred to a pooling vessel under suction. In the second cell (MPC-2), the entire process from precipitation of zirconium molybdate gel to converting it to free flowing granules is

carried out. This cell is equipped with processing vessels - mixing vessel, filters, cake collection dish, granule receiver vessel, microwave oven, an IR lamp (250W) for drying, a peristaltic pump for solution/slurry transfers. and a pneumatic powered material handling system.

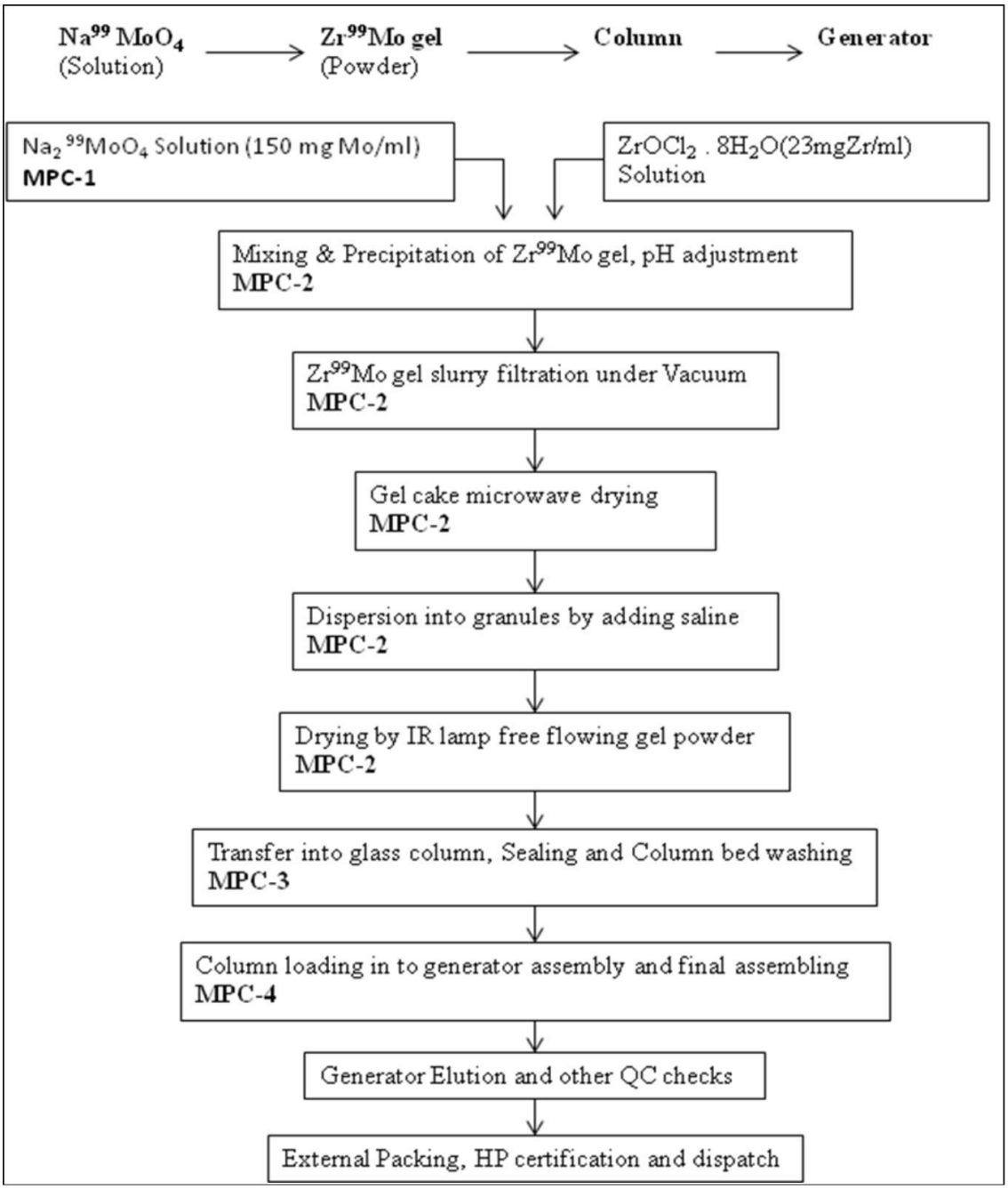

Fig 3.2 Flow chart for preparation of ZrMo gel.

The pneumatic powered material handling system can move to different pre-programmed stations such as microwave drying station and IR drying station with three-dimensional (x,y,z co-ordinates) controlled movement. For filtration, an oil-free, moisture–free diaphragm type vacuum pump is used. After filtration, the gelcake is discharged into a collection vessel and dried in a domestic microwave oven made amenable for remote operations. Special ducting is connected to the oven to exhaust the moisture laden air during drying of the gel cake. The dried lumps are transferred into another vessel and rendered into granular form using a shower arrangement for spraying saline.

Fig 3.3 A 100mm lead-shielded production facility comprising 4 interconnected processing cells for carrying out the production of Zr^{99}Mo gel [87].

The granules are converted into free flowing form by drying under an IR lamp. In the third cell (MPC-3), the ZrMo granules are dispensed into individual glass columns. The rubber

closure and aluminum cap are inserted to seal the column using special pick and place devices and the columns crimped remotely using a crimper. In the fourth cell (MPC-4), the activity containing glass columns are transferred into pre-assembled cold generator assembly, the top shielding plug is inserted in place and the generator is moved outside the MPC-4 to elution testing station through a conveyor system. Fig. 3.4 shows an assembled gel generator.

Fig 3.4 Assembled gel generator [87].

3.2 Experimental details

3.2.1 Irradiation parameters

The experiment was carried out using the 10 and 15 MeV electron linac of the Electron Beam Centre (EBC) and of SAMEER respectively at, Kharghar,Navi-Mumbai, India . The 10 MeV electron linac facility is vertical type and has a scanning frequency 10 times/s for the electron beam in the exit window. The bremsstrahlung radiation was generated by impinging an electron beam of 10 MeV on a tantalum metal foil situated in front of the scanning electron beam. The thickness of Ta target was 0.25 mm with a size of 100 mm x 100 mm. It was placed on a suitable stand at a distance 7 cm from the beam exit window. The 15 MeV electron linac is an S band electron linac of 1.2 m length. The bremsstrahlung with end-point

energy of 15 MeV was generated by impinging an electron beam on water cooled circular tungsten metal foil of 4 mm thick and 6 mm diameter.

Natural Mo in the form of natural molybdenum trioxide and in-house prepared natural zirconium molybdate gel were used for irradiation with bremsstrahlung of end-point energies 10 and 15 MeV. Different sample packets were made for the irradiations in the 10 and 15 MeV electron linacs. In each packet of sample about 0.23 to 0.6 g of molybdenum trioxide powder and 0.98–6 g of zirconium molybdate gel were wrapped separately with 0.025 mm thick aluminum metal foil. Then they were combinedly wrapped with additional aluminum foil of same thickness.

In the 10 MeV electron linac, the target assembly was irradiated for 2–3 h with the bremsstrahlung radiation produced by bombarding the electron beam on 0.25 mm thick tantalum metal foil. The peak current of the electron beam during irradiation was 50 mA, at a frequency of 200–400 Hz and a pulse width of 10 μs. Thus the average continuous current was only 0.4 mA resulting from beam power of 1–2 kW at electron energy of 10 MeV. During the irradiation, the electron to bremsstrahlung converter was cooled by using a water flow cooling arrangement.

In the case of 15 MeV electron linac, the target assembly was irradiated only for 30–45 min with the bremsstrahlung radiation produced by bombarding the electron beam on the water cooled 4 mm thick tungsten metal foil. The peak current of the electron beam during irradiation was 65 mA, at a frequency of 20–150 Hz, a pulse width of 6 μs, beam power 117–878 W.

3.2.2 Offline gamma spectrometry

The irradiated targets of aluminum wrapped molybdenum trioxide and zirconium molybdate were mounted separately on different perspex plates. The γ-ray counting of the reaction products in the irradiated samples was done by using an energy- and efficiency-calibrated 80

cm^3HPGe detector coupled to a PC based 4 K-channel analyser in live time mode. The counting dead time was always kept less than 5 % by placing the irradiated samples at a suitable distance from the detector to avoid pileup effect. The energy and efficiency calibration of the detector system was done by counting the γ-ray energies of standard ^{152}Eu source keeping the same geometry, where the summation error was negligible. The efficiency of the HPGe detector used was 20 % at 1332.5 keV relative to 3' diameter x 3' length NaI(Tl) detector. The uncertainty in the efficiency was 2–3 %. The resolution of the detector system was 1.8 keV (FWHM) at 1332.5 keV of ^{60}Co. Atypical γ-ray spectrum of the irradiated zirconium molybdate gel and molybdenum trioxide are shown in Fig. 3.5a and 3.6a respectively.

3.2.3 Radiochemical separation

3.2.3.1 Separation of ^{99m}Tc from irradiated MoO_3

The irradiated molybdenum trioxide was dissolved in 5 mL of 5 M NaOH. The irradiated solution was estimated by offline γ spectrometry. The solution obtained after the dissolution of the irradiated target was thoroughly mixed with 5 mL of methylethylketone (MEK).

After standing for few minutes, the two layers got separated. The upper organic layer containing the ^{99m}Tc was collected in a counting vial. ^{99m}Tc was estimated by offline γ spectrometry. A typical γ ray spectrum of the separated ^{99m}Tc solution from the irradiated molybdenum trioxide is given in Fig 3.5 b.

To obtain ^{99m}Tc of clinical quality, the MEK is passed through an alumina column to trap any coeluted Mo. The purified MEK containing the ^{99m}Tc is evaporated to dryness and reconstituted in physiological saline. Sterility is typically ensured by passing the ^{99m}Tc in saline through a 0.22 μ filter into a sterile vial.

3.2.3.2 Separation of ^{99m}Tc from irradiated ZrMo

The irradiated zirconium molybdate, was transferred to a polypropylene barrel of dimension 6 cm x 1 cm, with a sintered frit at the bottom. A frit was also placed on the top to prevent disturbance of the column during passage of eluents. The ^{99m}Tc was eluted out with 5 mL of

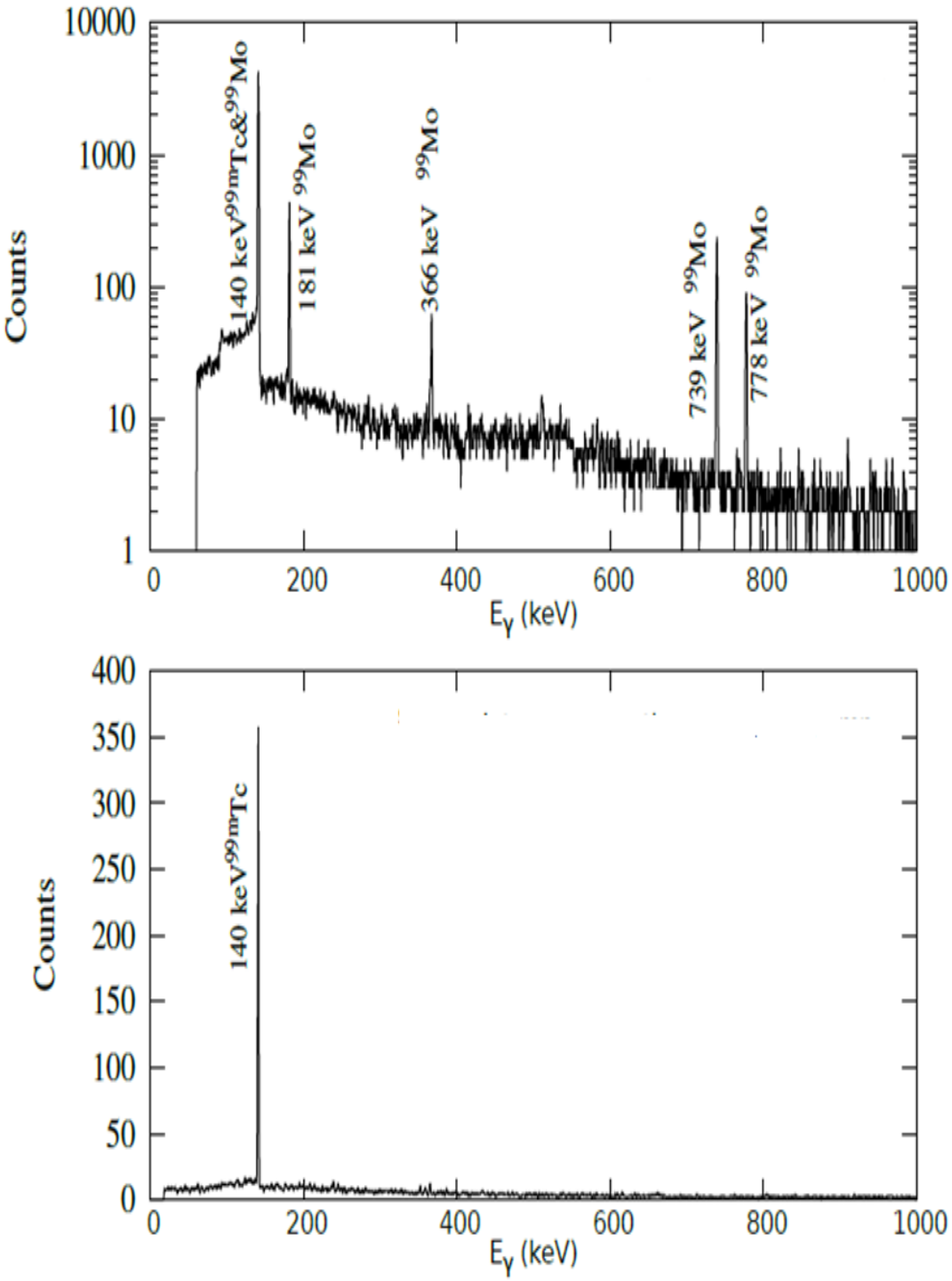

Fig 3.5 Gamma ray spectrum of (a) Irradiated MoO_3 (b) ^{99m}Tc separated and eluted in saline.

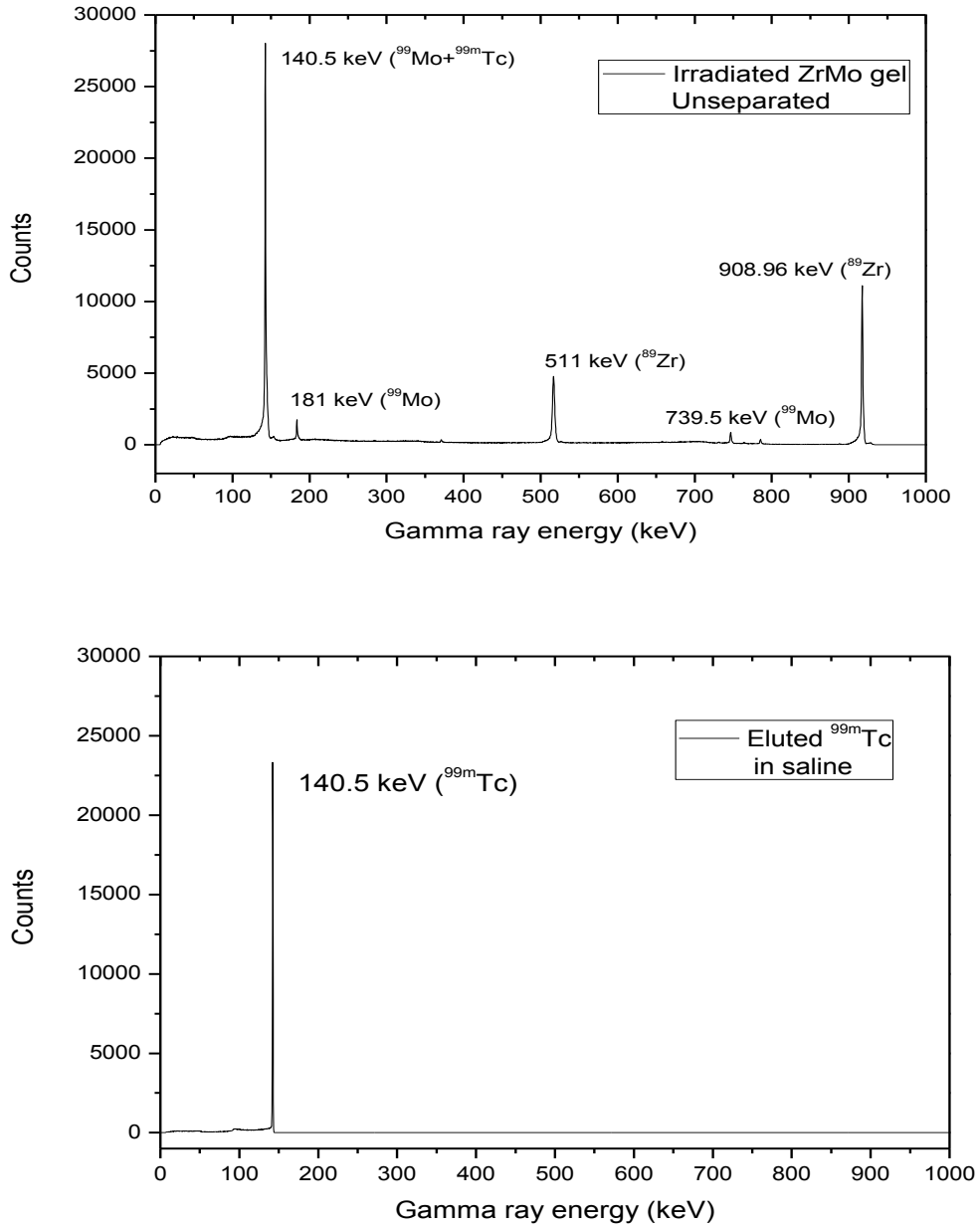

Fig 3.6 Gamma ray spectrum of (a) Irradiated ZrMo (b) ^{99m}Tc separated and eluted in saline.

saline for 1 g of gel and 2 x 5 mL for the 3 and 6 g gel. The eluted ^{99m}Tc was purified by passing it through an acidic alumina column (6 x 1 cm). Commercially available acidic alumina (100–200 mesh) was soaked overnight in dilute nitric acid (0.1 M) and washed with

sufficient double-distilled water till the pH of the final washing reached a 3–4 range. The conditioned and wet alumina was dried to get free flowing particles. The dried acidic alumina (2 g) was used to prepare the acidic alumina column (6 cm x 1 cm).The purified ^{99m}Tc solutions in counting vials were analysed by γ-ray spectrometric technique. A typical γ ray spectrum of the purified ^{99m}Tc solution from the irradiated zirconium molybdate is given in Fig 3.6b.

The ZrMo columns are autoclavable and the entire process is amenable to supply of sterile sodium pertechnetate and supply of ZrMo gel. The supply of sterile sodium pertechnetate-^{99m}Tc solution from Geltech generator has been already established [87].

3.2.4 Elution Yield

The elution yield (Y_C) of ^{99m}Tc was obtained from the ratio of the photo-peak activity of 140.5 keV γ ray in the separated sample (A_S) to the dissolved unseparated sample (A_U)

$Y_C = A_s / A_u$, Where $A_i = N_{obs}(CL/LT)\lambda / [I.\varepsilon_\gamma.e^{-\lambda t}(1-e^{-\lambda CL})]$

N_{obs} is the observed activity of the 140.5 keV γ-ray, λ is the decay constant ($\lambda = \ln 2/T_{1/2}$) of the radionuclide of interest with half-life = $T_{1/2}$, t, CL and LT are the cooling, clock and live time, respectively, I_γ is the branching ratio of the γ-ray and ε is the efficiency of the detector system, which depends on the geometry of the sample and the detector to sample distance. The efficiency has been determined using standard ^{152}Eu source of similar geometry of sample. The nuclear spectroscopic data of ^{99}Mo and ^{99m}Tc are taken from the refs[72, 88]. The elution yields of ^{99m}Tc, post separation from the irradiated molybdenum trioxide and zirconium molybdate are shown in Table 3.1 and 3.2 respectively.

3.2.5 Evaluation of the ^{99m}Tceluate

The evaluation of ^{99m}Tc eluates from the bremsstrahlung irradiation of 15 MeV were carried out as detailed below. The typical results are shown in Table3.3, 3.4 and 3.5.

3.2.5.1 Radionuclide identification

Radionuclide identity of ^{99m}Tc was determined by identification of the 140 keV photopeak and/or measurement of the half-life, by following sample assay on a HPGe detector. The

half-life was evaluated by two repeated assay measurements on a HPGe detector typically performed 2–3 hours apart.

3.2.5.2 pH

One drop from the product sample vial was applied to universal pH indicator papers. The colors of the wet areas were immediately compared to the reference color indicator chart supplied with each lot of pH paper.

3.2.5.3 Radiochemical purity

Radiochemical purity (RCP) was evaluated by ITLC. 1–2 drops of $^{99m}TcO_4^-$ were dispensed at the origin of a pre-marked commercially available, 1 x 8 cm silica gel coated strip (ITLC-SG) with acetone as the mobile phase. The strips were divided into 2 sections and counted. The detected activity was associated with two well-defined areas on the strip - the origin peak represented technetium complexes, hydrolyzed reduced technetium, and/or colloidal technetium, while the peak near the solvent front represented the free pertechnetate $^{99m}TcO_4^-$. Areas under each peak were integrated, and the radiochemical purity given as a percentage of the total integrated area.

3.2.5.4 Radionuclidic purity

The relative radionuclidic impurities in the ^{100}Mo and ^{99m}Tc aliquots were determined via γ-ray spectroscopy using an HPGe detector as detailed in 3.2.2 .

3.2.5.5 Chemical purity: Aluminium

Al content in the eluate was determined by a spot test based on the reaction of Al ions with Chromazural S. 10 µl of ^{99m}Tc eluate was applied in a well of spot plate. 30 µl acetate buffer pH 4.6 and 10 µl of 0.1 % w/v Chromazural S were added to the spot plate. The test sample colour (reddish pink) intensity was visually compared to a reference standard colour intensity obtained similarly using 10 µl of aluminum standard solution.

3.2.5.6 Chemical purity: Molybdenum

Mo content in the eluate was determined by a spot test based on the reaction of Mo with KSCN and $SnCl_2$. 50 µl of ^{99m}Tc eluate was applied in a well of spot plate. 50 µl of KSCN and $SnCl_2$were also added to the spot plate. The test sample color (orange) intensity was visually compared to a reference standard color intensity obtained similarly using 50 µl of molybdenum standard solution.

3.2.5.7 Chemical purity: Zirconium

Zr content in the eluate was determined by a spot test based on the reaction of Zr with Alizarin-S.10 µl of ^{99m}Tc eluate was applied in a well of spot plate. 80 µl of 2N HCl and 10 µl of 0.05% Alizarin-S and were also added to the spot plate. The test sample color (reddish yellow) intensity was visually compared to the reference standard color intensity.

3.2.5.8 Chemical purity: Methyl Ethyl Ketone (MEK)

In a test tube 200µl of 1 M sodium hydroxide solution was added, followed by addition of 200 µl of 0.1 % iodine solution. 50 µl of ^{99m}Tc eluate was applied followed by addition of 150 µl of double distilled water . The turbidity developed was visually compared with a standard MEK solution (0.1 % v/v) prepared at the same time.

3.2.5.9 Evaluation of labelled ^{99m}Tc-pharmaceuticals

MDP and ECD kits used in these studies were procured from Board of Radiation and Isotope Technology, Mumbai. The kits were labelled with ^{99m}Tc as per the recipe and radiochemical purity determined as per the specifications of the IP.

3.3 Results and Discussion

3.3.1 Radiochemical Separation

In the gamma ray spectrum of the irradiated Molybdenum trioxide (Fig 3.5 a), the 140.5, 181.0 and 739.5 keV γ-ray energies of ^{99}Mo are seen. The separated ^{99m}Tc in fig 3.5 b shows only the 140.5 keV γ-ray of ^{99m}Tc. In the gamma ray spectrum of the irradiated ZrMo (Fig

3.6 a), the 140.5, 181.0 and 739.5 keV γ-ray energies of ^{99}Mo and the 908.9 keV γ-ray of ^{89}Zr are seen. In the γ-ray spectrum of the separated sample (Fig. 3.6 b), only the 140.5 keV γ-ray of ^{99m}Tc is seen. The absence of radionuclidic impurities implies the high radionuclidic purity of the ^{99m}Tc eluates and the very good separation of ^{99m}Tc from ^{99}Mo and/or ^{89}Zr.

3.3.2 Elution yield

As seen from Table 3.1 and 3.2, the elution yields of the ^{99m}Tc obtained are in the range of 71–75 %, in the first extraction, and 19–43 % from the irradiated molybdenum trioxide and Zirconium molybdate respectively.

Table 3.1 ^{99m}Tc elution yield in the MEK phase from the irradiated MoO_3.

Weight	Elution No.	Time after EOB (hours)	Expected ^{99m}Tc (KBq)	Eluted ^{99m}Tc (KBq)	Elution Yield (%)
Irradiation 1 (10 MeV)					
0.23grams	1	24	.028	.0198	70.7
Irradiation 2 (15 MeV)					
0.53 grams	1	46	7.9	5.61	71
Irradiation 3 (15 MeV)					
0.6 grams	1	45	5.8	4.2	72.4
Irradiation 4 (15 MeV)					
0.5 grams	1	52	12.1	9.1	75.2

Table 3.2 ^{99m}Tc elution yield from irradiated ZrMo .

Generator	Elution No.	Time between elutions / EOB (hours)	Expected ^{99m}Tc (KBq)	Eluted ^{99m}Tc (KBq)	Elution Yield (%)
Irradiation 1 (10 MeV)					
1 gram; eluent saline	1	47	.0469	.00896	19.1
Irradiation 2 (15 MeV)					
6 grams; Eluent - saline	1	45	45.1	15.17	33.6
	2	21	33.4	10.36	31
	3	55	25.6	6.12	23.8
	4	19.5	14.4	4.14	28.75
	5	25	11.7	3.075	26.3
Irradiation 3 (15 MeV)					
3 grams; Eluent - Acetone	1	44	14.53	4.3	29.6
	2	24	10.4	3.65	35
	3	11	6.5	2.28	35.1
3 grams; Eluent - Saline	1	42	14.5	3.85	26.55
	2	24	10.5	3.81	36.2
	3	11	6.6	1.857	28.1
Irradiation 4 (15 MeV)					
3 grams; Eluent - Saline	1	50	36.89	12.2	32.99
	2	36	23.9	7.1	29.7
	3	31	17.4	4.27	24.5
	4	41	10.2	2.93	28.7
	5	72	4.8	1.58	33
	6	96	1.4	0.61	43

The ^{99m}Tc-elution performance of the gel is based on the the gel synthesis conditions such as the molar ratios of zirconium to molybdenum and the drying conditions i.e. time, temperature [83, 84, 89, 90].The typical yield from ZrMo generators prepared with (n, γ)^{99}Mo is 70 % [84, 86]. The average yield from the ZrMo system is ~ 28 % from the 15 MeV irradiations. This is higher than the value of 12% elution yield from the neutron induced irradiation of pre-formed ZrMo [91]. It is postulated that the neutron flux modifies the structure of the gel, obstructing the free diffusion of ^{99m}Tc.

3.3.3 Evaluation as per IP specifications

As seen from table 3.3 and 3.4 all the ^{99m}Tc eluates from the MoO_3 and ZrMo were clear solutions with a pH of 6-7 and 5-6 respectively. The radiochemical purity test showed that the ^{99m}Tc eluted was in the pertechnetate form, as $Na^{99m}TcO_4$. The radiochemical purity was > 99 % . The colorimetric spot test (limit test) for Al, and Mo showed less than 10 ppm of these chemical impurities in the ^{99m}Tc eluates. The Zr content and the MEK content in the ^{99m}Tc eluates from the irradiated ZrMo and MoO_3 samples were less than 10 ppm and 0.1 % v/v respectively. Labelling efficiencies > 98 % for both ^{99m}Tc-MDP and ^{99m}Tc-ECD were observed as seen from Table 3.5.

Table 3.3 Summary of test results to evaluate IP specifications for ^{99m}Tc eluates from the irradiated MoO_3

Irradiation No	Half life (h)	pH	RCP (%)	Chemical purity		
				Al	Mo	MEK
Specifications	***5.7 – 6.3***	***4 – 8***	***> 95***	***< 10 ppm***	***< 10 ppm***	***< 0.1 % v/v***
15 MeV- 1	6.13	6 -7	99.4	< 10 ppm	< 10 ppm	< 0.1 % v/v
15 MeV- 2	6.02	6 -7	99.2	< 10 ppm	< 10 ppm	< 0.1 % v/v
15 MeV- 3	5.98	6 -7	99.3	< 10 ppm	< 10 ppm	< 0.1 % v/v

Table 3.4 Summary of test results to evaluate IP specifications for ^{99m}Tc eluates from the irradiated ZrMo

Irradiation No	Half life (h)	pH	RCP (%)	Chemical purity		
				Al	Mo	Zr
Specifications	***5.7 – 6.3***	***4 – 8***	***> 95***	***< 10 ppm***	***< 10 ppm***	***< 10 ppm***
15 MeV- 1	5.9	5 - 6	99.1	< 10 ppm	< 10 ppm	< 10 ppm
15 MeV- 2	6.1	5 - 6	99.5	< 10 ppm	< 10 ppm	< 10 ppm
15 MeV- 3	6.04	5 - 6	99.3	< 10 ppm	< 10 ppm	< 10 ppm

Table 3.5 Labelling efficiency for MDP and ECD for ^{99m}Tc eluates from the irradiated MoO_3 and ZrMo

^{99m}Tc-radiopharmaceutical	^{99m}Tc source	
	MoO_3	ZrMo
MDP	98.5	98.2
ECD	98.6	98.7

3.4. Summary

In this study, ^{99}Mo has been prepared by bremsstrahlung irradiation of endpoint energies 10 and 15 MeV on ^{nat}Mo via the ^{100}Mo(γ, n)^{99}Mo reaction. The ^{nat}Mo samples were in the form of Molybdenum trioxide and in-house prepared Zirconium Molybdate. The ^{99m}Tc has been separated from the irradiated ^{nat}Mo samples and the elution yield of ^{99m}Tc determined. The typical elution yield of ^{99m}Tc from the irradiated molybdenum trioxide in the first pass via solvent extraction was in the range 70 to 75 %. In an aid to reduce complexities in preparation of Zr^{99}Mo with ^{99}Mo [83, 84], preformed natural zirconium molybdate has been

irradiated and converted to Zr^{99}Mo column generators. The typical elution yield of ^{99m}Tc from the irradiated zirconium molybdate was in the range 19 to 43 %. The evaluation of the quality of the ^{99m}Tc eluates with reference to the Indian Pharmacopeia (IP) pertechnetate monograph have been carried out. The eluates complied with the specifications of the IP. The eluates were of high radiochemical, chemical and radionuclidic purity. The $^{99m}TcO_4^-$ eluate was further assessed by evaluating its labelling efficiency with kits of MDP and ECD. It may be noted, that the IP monograph is specific to $^{99m}TcO_4^-$ obtained following the decay of the parent ^{99}Mo which is, in turn, produced either via neutron bombardment of ^{98}Mo, or as a product of uranium fission.

The present work has been carried out with natural targets under un-optimised conditions to demonstrate the feasibility of ^{99}Mo–^{99m}Tc production through ^{100}Mo(γ,n) route and its chemical separation. The yield of ^{99m}Tc obtained in this study is only in the kBq/mL or kBq/g order, whereas typical patient injection doses are~ 300–1000 MBq. The scaling up of ^{99}Mo–^{99m}Tc activity to clinical levels would be achievable with increase of target material, enrichment, beam power, irradiation time, scanning electron beam etc[15]. Commercialization of ^{99}Mo production via this route would need implementation of ^{100}Mo recovery and reuse due to its limited availability and the high cost [92, 93].

Chapter 4

Measurement of the ^{100}Mo(n,2n) reaction cross sections

The ^{100}Mo(n,2n) reaction cross-sections at the average neutron energies of 21.9 and 25.5 MeV have been determined by using an activation and off-line γ-ray spectrometric technique. The results along with the literature data for the ^{100}Mo(n,2n) reaction, are compared with the theoretical values from the TALYS-1.8 code.

4.1 Introduction

In an assessment of long term technologies for supply of ^{99}Mo by alternative routes, production of ^{99}Mo via the ^{100}Mo(n, 2n)^{99}Mo reaction using fast neutrons from an accelerator [54, 94] has been proposed. This route has the following characteristics : (a) the (n,2n) reaction cross section is large, about 1.5 b at a neutron energy of 14 MeV, which is about ten times larger than the thermal neutron capture cross section of^{98}Mo in a reactor, (b) the radioactive waste production reaction cross sections, such as (n,γ), (n, np), (n, p), and (n,α), however, are small, less than 0.2% of the^{100}Mo(n,2n)^{99}Mo cross section, (c) ^{100}Mo samples of more than 200 g can be used, since incident neutrons do not lose their energy in the sample via electromagnetic interactions, contrary to the production of^{99}Mo or ^{99m}Tc using a charged particle-induced reaction (d) high-intensity fast neutrons can be obtained via ^{3}H(d, n)^{4}He or ^{12}C(d, n)^{13}N.

With a 5 mA 40 MeV deuteron beam (200 kW) one may obtain about 190 Ci of ^{99}Mo for 250 g enriched ^{100}Mo in two days of bombardment [95]. Such an accelerator (40 MeV 5 mA) is currently under construction in France to produce exotic neutron rich radioactive nuclei via the fission reaction of a natural uranium target for nuclear physics interests [96].The ^{99}Mo produced by this method would be of low specific activity. In the work carried out by Hashimoto *etal* [97],^{99m}Tc was separated by thermochromatographic method (by

sublimation) from a MoO_3 sample irradiated with 14 MeV accelerator neutrons. Radionuclidic and radiochemical purities of the separated ^{99m}Tc and its aluminum concentration met the United States Pharmacopeia regulatory requirements for ^{99m}Tc from the fission product ^{99}Mo. The biodistribution of ^{99m}Tc-radiopharmaceutical (^{99m}Tc-MDP) in mouse was determined by single photon emission computed tomography (SPECT). The SPECT images are comparable to the image produced with fission produced ^{99}Mo. These results provide important evidence that the ^{99m}Tc-radiopharmaceutical formulated using the (n,2n)^{99}Mo can be a promising substitute for the fission product ^{99}Mo.

The ^{100}Mo(n,2n) reaction cross-section within the neutron energy ranges from the threshold energy (8.36 MeV) to 20.5 MeV only are available in the EXFOR [98] from the experimental work of various authors [99-106]. At higher neutron energies, the ^{100}Mo(n,2n) reaction cross section data are very much limited. In fact, only one set of data above neutron energy of 16 and below 20.5 MeV are available based on the work of Reimer et al. [101]. Most of the earlier ^{100}Mo(n,2n) reaction cross section data are for the neutron energies based on the D + D and D + T reaction neutron sources except one set of data, which is from the ^{7}Li(p,n) reaction neutron source [106]. In the D + D and D + T reactions, the neutrons are mono-energetic within small energy range. In the ^{7}Li(p,n) reaction, the neutrons have a spectrum with a sharp peak at E_P-1.881 MeV. However, the use of lithium is not so easy due to its low melting point and pyrophoric nature. In the ^{9}Be(p,n) reaction, the neutrons have a broad spectrum but is more accessible from the safety point of view. However, the cross-section data for the ^{100}Mo(n,2n) reaction are not available above the neutron energy of 20.5 MeV by using any of the above neutron sources.

In the present work, the ^{100}Mo(n,2n) reaction cross-sections at the average neutron energies of 21.9 and 25.5 MeV have been determined by using an activation and off-line γ-ray

spectrometric technique. The results along with the literature data [99-106] for the ^{100}Mo(n,2n) reaction are also compared with the theoretical values from the TALYS-1.8 code [76].

4.2 Experimental details

The quasi monoenergetic neutrons were produced from the ^{9}Be(p, n) reaction by impinging proton beams of 35 and 45 MeV on a Be-target (purity 99%) at the MC-50Cyclotron of the Korean Institute of Radiological and Medical Sciences (KIRAMS), Korea [107]. The thickness of ^{9}Be metallic foil used was 2 mm thick and 25 mm x 25mm in size. A 12 mm thick graphite plate behind the Be target was used to stop the lower energy proton beam. Two set of enriched (99.99%) metallic powered sample of ^{100}Mo weighing 33.8 and 38.6 mg were separately wrapped with 0.025-mm-thick Al foil of purity 99.99%. The weights of Al wrapper were 67.4 and 62.5 mg, respectively. The Al wrapper was used to stop reaction products recoiling out from the ^{100}Mo sample during the irradiation and to avoid the radioactive contamination to the surrounding. In addition to this, the ^{27}Al(n,α)^{24}Na reaction of the Al wrapper was used as the neutron flux monitor. The sample assemblies were positioned one at a time at a distance of 3.5 cm behind the Be target in zero degree with respect to the direction of the proton beam and irradiated for 60 min each. The proton beam current during irradiation was about 200 nA. The diameter of proton beam and neutron beam collimator was 10 mm. The beam energy and current were persistent during the irradiation. The irradiated ^{99}Mo samples along with ^{27}Al wrapper were taken out from the irradiated assemblies after cooling time of 1.5–2 h.

The irradiated samples were mounted on different perspex (acrylic glass, 1.5 mm thick) plates. The γ-ray counting of the mounted sample was done by using an energy- and efficiency-calibrated HPGe detector coupled to a PC-based 4 K-channel analyzer. The

resolution of the HPGe detector was 1.8 keV full-width at half maximum (FWHM) at the 1332.5 keV γ-ray photo-peak of ^{60}Co. A standard source ^{152}Eu with the γ-ray energy range of 121.8–1408.0 keV was used for the energy and the efficiency calibration. The detector efficiency was 20% at the 1332.5 keV γ-ray photo-peak relative to a 7.6 cm diameter x 7.6 cm length NaI (Tl) detector. The dead time of the HPGe detector during the γ-ray counting was always kept less than 5% by placing the sample at a suitable distance to avoid pile up and coincidence-summing effect.

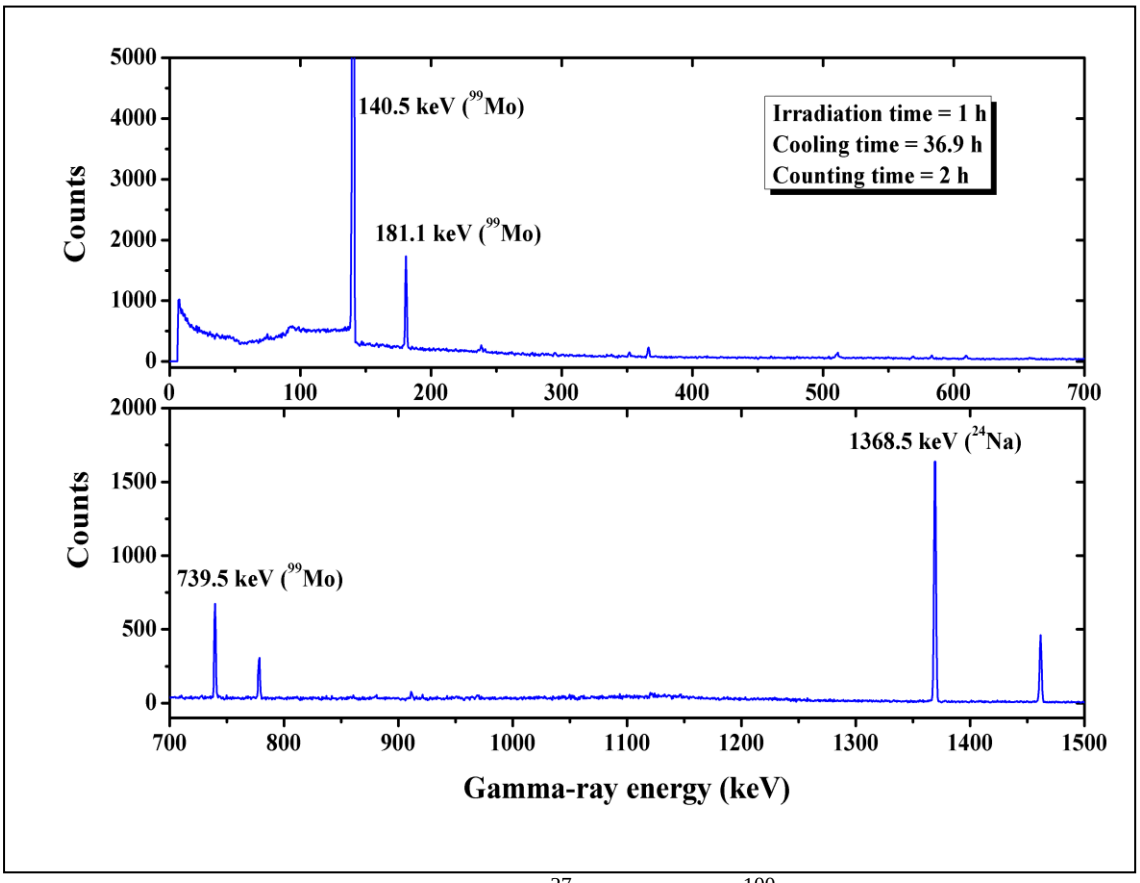

Fig. 4.1 Typical gamma-ray spectrum of ^{27}Al wrapped ^{100}Mo sample irradiated with the neutron beam from the ^{9}Be(p,n) reaction with the proton energy of 45 MeV.

A typical γ-ray spectrum from the ^{99}Mo sample and ^{27}Al wrapper irradiated with the fast neutrons based on the ^{9}Be(p,n) reaction for the proton beam of 45 MeV is shown in Fig.4.1. The nuclear spectroscopic data for the reaction products such as ^{99}Mo and ^{24}Na from the

^{100}Mo(n,2n) and ^{27}Al(n,α) reactions were taken from Refs. [72, 108-110] and are given in Table 4.1.

Table 4.1 Nuclear reactions, their threshold energies and nuclear spectroscopic data [72, 108, 109] of ^{99}Mo from the ^{100}Mo(n,2n) reaction and ^{24}Na from the ^{27}Al(n,α) [72, 110].

Reaction	Threshold energy (MeV)	Q-value (MeV)	Nuclide	Half-life	Decay mode (%)	γ-ray energy* (keV)	γ-ray intensity (%)
^{100}Mo(n,2n)	8.3738	-8.2897	^{99}Mo	65.976 h	β$^-$ (100)	**181.1** **739.5**	**6.05** **12.2**
			daughter ^{99m}Tc	6.007 h	IT (100) β$^-$ (3.7E-3)	**140.5**	**90.2**
^{27}Al(n,α)	3.2494	-3.1321	^{24}Na	14.997 h	β$^-$ (100)	**1368.6** 2754.0	**99.9936** 99.855

*The γ-ray energy marked with bold letters are used in the present calculation

4.3 Data analysis

4.3.1 Generation of neutron spectrum and calculation of average neutron energy

The neutron energy spectra from the ^{9}Be(p,n) reaction for the proton energies of 35 and 45 MeV generated by using the MCNPX 2.6.0 code [111] is shown in Fig. 4.2.The flux weighted average neutron energies (<En>) for the ^{100}Mo(n,2n)^{99}Mo and ^{27}Al(n,α)^{24}Na reactions from the respective threshold energy (E_{th}) to the maximum neutron energy (E_{max}) based on the neutron spectra in Fig. 4.2 were estimated for two proton energies as follows:

$$\langle E_n \rangle = \int_{E_{th}}^{E_{max}} E_n \emptyset(E_n) dE_n \Big/ \int_{E_{th}}^{E_{max}} \emptyset(E_n) dE_n \qquad 4.1$$

where $\emptyset(E_n)$is the neutron flux as a function of neutron energy (En) estimated with the MCNPX 2.6.0 code [111]. The flux-weighted average neutron energies for the ^{100}Mo(n,2n)^{99}Mo and ^{27}Al(n,α)^{24}Na reactions for the proton energies of 35 and45 MeV are given in Table 4.2.

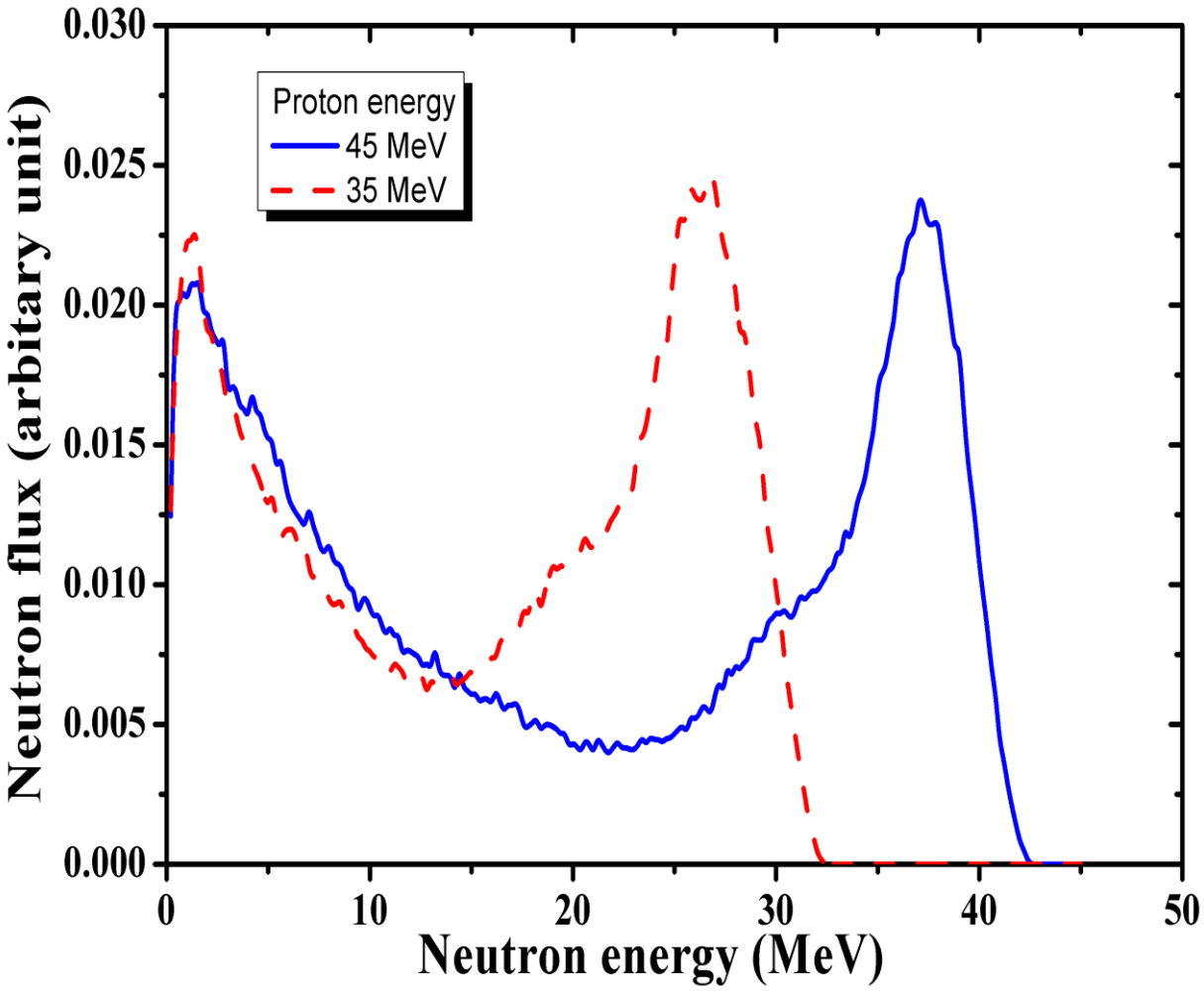

Fig. 4.2 Neutron spectrum from the ^{9}Be(p,n) reaction for the proton energies of 35 and 45MeV calculated by using the MCNP 2.6.0 code [111].

4.3.2 Calculation of neutron flux

The ^{27}Al(n,α)^{24}Na reaction was used as the neutron flux monitor. The net photo-peak area (A_{net}) corresponding to the 1368.6 keV γ line of ^{24}Na was calculated from the sum full energy

peak and subtracting the linear Compton background. The net photo peak activity (A_{net}) of the 1368.6 keV γ line from the ^{24}Na is related to the neutron flux $\emptyset_M$ from the threshold energy of the monitor reaction (E_{Mth}) to the maximum neutron energy (E_{max}) by the following relation:

$$\emptyset_M = \int_{M_{th}}^{E_{max}} \emptyset(E_n) dE_n$$

$$= \frac{A_{net}(CL/LT)\lambda}{N\langle\sigma^M\rangle I_\gamma \varepsilon_\gamma (1 - e^{-\lambda t_i}) e^{-\lambda T}(1 - e^{-\lambda CL})} \qquad 4.2$$

where N is the number of target atoms and $\langle\sigma^M\rangle$ the average cross-section of the ^{27}Al(n,α)^{24}Na monitor reactions, I_γ the branching intensity of the analyzed γ-rays, ε_γ the detection efficiency of the γ-ray of interest, λ is the decay constant for the isotope of interest t_i, T, CL, and LT are the irradiation time, cooling time, clock time and counting time, respectively. In the above equation, the photo-peak area has been corrected for dead time by multiplying by CL/LT factor. The γ-ray energies and the decay data for the residual nuclide such as branching ratio and half-lives were taken from Table 4.1 based on the Refs. [72, 108-110].

4.3.3 Calculation of flux weighted average cross section $\langle\sigma^M\rangle$ of the ^{27}Al(n,α)^{24}Na reaction

The ^{27}Al(n,α)^{24}Na reaction cross-section ($\sigma(E_n)$) data below the neutron energy of 20 MeV are available from EXFOR [112]. The ^{27}Al(n,α)^{24}Na reaction cross section values at the higher neutron energy are very much limited and scattered [107]. The ^{27}Al(n, α)^{24}Na reaction cross-section has been calculated by using computer code TALYS-1.8 [76], which follows a similar trend of experimental data [112] and also gives a very good estimate within the neutron energy of present work. The flux-weighted average cross-section $\langle\sigma^M\rangle$ of the ^{27}Al(n, α)^{24}Na monitor reaction was calculated with the reaction cross-sections $\sigma^M(E_n)$ of mono-

energetic neutron from reaction threshold energy (E_{Rth}) to maximum neutron energy (E_{max}) by using the following relation.

$$\langle \sigma^M \rangle = \frac{\int_{E_{Rth}}^{E_{max}} \sigma^M(E_n)\emptyset(E_n)dE_n}{\int_{E_{Rth}}^{E_{max}} \emptyset(E_n)dE_n} \qquad 4.3$$

The neutron flux distribution $\emptyset(E_n)$ was taken from Fig. 4.2. The flux-weighted average cross-section$\langle \sigma^M \rangle$ for the ^{27}Al(n, α)^{24}Na monitor reaction at the average neutron energies corresponding to the proton energies of 35 and 45 MeV are given in Table 4.2. The $\langle \sigma^M \rangle$values of ^{27}Al(n,a)^{24}Na reaction at the average neutron energies of 21.9 and 26.5 MeV were used in Eq. 4.2 to obtain the neutron flux $\emptyset_M$.

4.3.4 Calculation of flux conversion factor C_f:

The threshold value of ^{27}Al(n, α)^{24}Na monitor reaction is 3.25 MeV, whereas the threshold value for the ^{100}Mo(n,2n)^{99}Mo reaction is 8.37 MeV. Thus the neutron flux obtained from the ^{27}Al(n,a)^{24}Na monitor reaction has to be modified for the^{100}Mo(n,2n)^{99}Mo reaction based on its threshold value to the maximum neutron energy. In order to modify the neutron flux obtained with the ^{27}Al(n, α)^{24}Na monitor reaction from the threshold value to the maximum neutron energy, the flux conversion factor (C_f) is defined as follows

$$C_f = \frac{\int_{E_{thr}^R}^{E_{max}} \emptyset(E_n)dE_n}{\int_{E_{thr}^M}^{E_{max}} \emptyset(E_n)dE_n} \qquad 4.4$$

where $\emptyset(E_n)$ is neutron flux as a function of neutron energy En, which was calculated by using the MCNPX 2.6.0 code [111] and shown in Fig.4.2.E_{thr}^R and E_{thr}^M are the reaction and monitor threshold energy and E_{max} is the maximum neutron energy.

The different ratio used for the conversion of the neutron flux for the ^{100}Mo(n,2n)^{99}Mo reaction to the total flux of ^{27}Al(n, α)^{24}Na reaction based on the threshold values to the maximum neutron energies are given in the Table 4.2.

Table 4.2 Flux conversion factor ($^{C}_{f}$) used to obtain the neutron flux for ^{100}Mo(n,2n)^{99}Mo reaction from the total flux based on the ^{27}Al(n, α)^{24}Na reactions flux monitor.

Proton energy (MeV)	Reactions	35	45
Average neutron energy (MeV)	^{27}Al(n, α)^{24}Na	18.72	23.62
Flux-weighted average cross-section ($<\sigma^{M}>$) (b)	^{27}Al(n, α)^{24}Na	0.027	0.0324
Average neutron energy (MeV)	^{100}Mo(n,2n)^{99}Mo	21.9	26.5
$^{C}_{f}$	^{100}Mo(n,2n)^{99}Mo	0.809	0.804

4.3.5 Calculation of ^{100}Mo(n,2n)^{99}Mo reaction cross section

The produced radioisotope ^{99}Mo from the ^{100}Mo(n,2n) reaction has a half-life of 65.976 h [72, 108, 109] and the primary γ-ray energies of 181.1 and 739.5 keV with good branching intensities. The radionuclide ^{99}Mo undergoes β- decay to ^{99m}Tc, which has the main γ ray energy of 140.5 keV. Once the ^{99}Mo-^{99m}Tc equilibrium is achieved the γ-ray energy of 140.5 keV, which has very good branching intensity can also be used. The net photopeak area (A_{net}) corresponding to these γ lines of 140.5, 181.1 and 739.5 were calculated from the sum full energy peak area after subtracting the linear Compton background. From the net photo-peak

area (A_{net}) of the γ rays of ^{99}Mo, the average cross-sections $\langle\sigma^R\rangle$ of the ^{100}Mo(n,2n) reaction was obtained by using the following relation

$$\langle\sigma^R\rangle = \frac{A_{net}(CL/LT)\lambda}{N\phi_R I_\gamma \varepsilon(1-e^{-\lambda t_i})e^{-\lambda T}(1-e^{-\lambda CL})} \qquad 4.5$$

All terms in Eq. 4.5 have the similar meaning as in the Eq. 4.2. $\phi_R = \emptyset_M$ x C_f is the modified neutron flux using the flux conversion factor C_f and the measured neutron flux based on the monitor reaction. The ^{100}Mo(n,2n)^{99}Mo reaction cross-sections measured in the present work at the average neutron energies of 21.9 and 26.5 MeV based on the three different γ-ray energies and their average values are given in Table 4.3.

4.4 Results and Discussion

The average neutron energies corresponding to the proton energies of 35 and 45 MeV are 21.9 and 26.5 MeV. As seen from Table 3, the flux conversion factors are 0.809 and 0.804 for the ^{100}Mo(n,2n)^{99}Mo reaction at the average neutron energies of 21.9 and 26.5 MeV respectively. The weighted average flux obtained from the ^{27}Al(n,α)^{24}Na reaction is multiplied by these factors.

Table 4.3 Experimentally determined flux-weighted ^{100}Mo(n,2n)^{99}Mo reaction cross-sections from the present work and values from TALYS-1.8 [76] at different average neutron energies

Average neutron energy (MeV)	Average reaction cross-section ($<\sigma^R>$) (mb)	
	Experiment	TALYS-1.8
21.9	539.6±58.3	490.5
26.5	359.3±38.8	334.9

The average values of the ^{100}Mo(n,2n)^{99}Mo reaction cross-sections measured in the present work at the average neutron energies of 21.9 and 26.5 MeV are 539.6 ± 58.3 and 359.3 ± 38.8 respectively. The overall uncertainty is the quadratic sum of both statistical and systematic

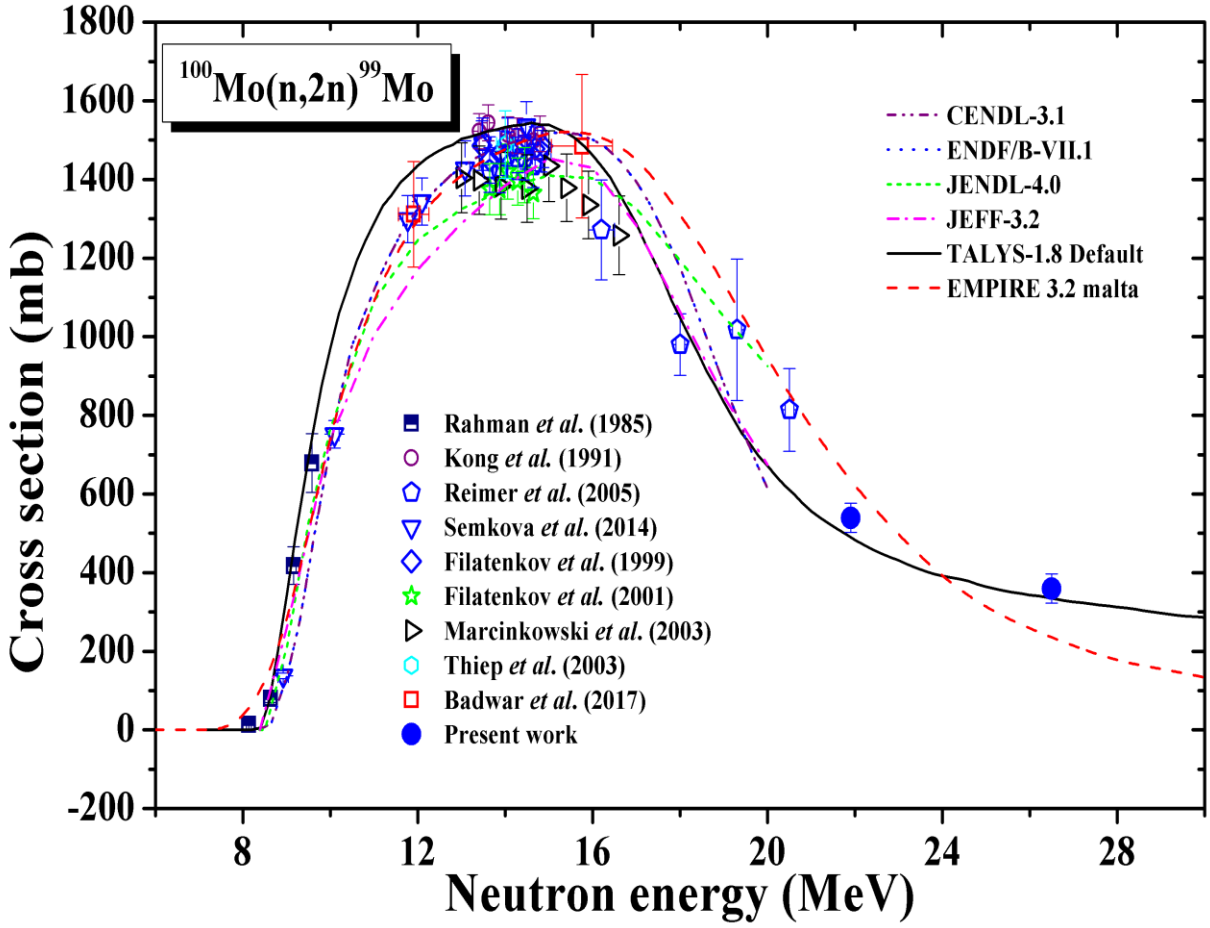

Fig. 4.3 Cross-sections of^{100}Mo(n,2n)^{99}Mo reaction as a function of neutron energy obtained by the existing experimental data [99-106], present work and calculated values from TALYS-1.8 [76].

uncertainties. The random uncertainty in the observed activity is primarily due to counting statistics, which is estimated to be 5–10%. This can be determined by accumulating the data for an optimum time period that depends on the half-life of the nuclides of interest. The systematic uncertainties are due to the uncertainties of the neutron flux estimation (~ 2%), the

irradiation time (~ 0.25%), the detection efficiency calibration (~ 3%) and the half-life of the reaction products and the γ-ray abundance or branching intensity (~ 2%). Thus, the total systematic uncertainty is about ~ 4.13%. The overall uncertainty is found to be in between 6.5 and 10.8%, coming from the combination of a statistical uncertainty of 5–10% and a systematic uncertainty of 4.13%.

The ^{100}Mo(n,2n)^{99}Mo reaction cross-sections in the average neutron energies of 21.9 and 26.5 MeV from the present work, are the first time measurement. The ^{100}Mo(n,2n)^{99}Mo reaction cross sections available in literature [99-106] as a function of neutron energy are plotted in Fig.4.3 .The cross sections calculated by using the computer code TALYS-1.8 [76] with default parameters are also plotted in Fig. 4.3 and compared with the evaluated ^{100}Mo(n,2n)^{99}Mo reaction cross-section data of ENDF/BVII.1 [113], CENDL-3.1[114], JEFF-3.2 [115], JENDL- 4.0 [116] and that calculated from Empire 3.2 malta [117]. The theoretical values from TALYS-1.8 [76] at the neutron energies of 21.9 and 26.5 MeV are also given in Table 4.3.

It can be seen from Fig. 4.3 that the theoretical values from TALYS-1.8 follows a similar trend as of the experimental literature data [99-106] and that the present data at the average neutron energies of 21.9 and 26.5 MeV are in good agreement with the value from TALYS-1.8.

4.5 Summary

The ^{100}Mo(n,2n)^{99}Mo reaction cross-sections at the average neutron energies of 21.9 and 26.5 MeV have been determined for the first time by using activation and off-line γ ray spectrometric technique. The ^{100}Mo(n,2n)^{99}Mo reaction cross-sections as a function of mono-energetic neutron energy were theoretically calculated using the computer code TALYS-1.8 and are found to be in close agreement with the data of literature and from the present work.

Chapter 5
Production and application of Low Specific activity ^{64}Cu

The utilization of ^{64}Cu is mostly limited to studies, sourcing no carrier added ^{64}Cu, produced via $^{64}Ni(p, n)^{64}Cu$ reaction in a medical cyclotron. This study investigates the potential of producing low specific activity (LSA) ^{64}Cu in an electron linac via the $^{65}Cu(\gamma,n)$ ^{64}Cu reaction route. Natural targets of copper were irradiated in a clinical 15 MV electron linac, in Tata Memorial Hospital, Mumbai, India. The mixed field, of photons along with the neutrons co-produced in the linac head (via photonuclear processes), offers a dual reaction route for the production of ^{64}Cu, via the $^{63}Cu(n, \gamma)^{64}Cu$ + $^{65}Cu(\gamma, n)^{64}Cu$ reactions. A solid water phantom was used to moderate the secondary neutrons and enhance the yields of ^{64}Cu. The contribution of secondary neutrons to the yields of ^{64}Cu via the $^{63}Cu(n, \gamma)^{64}Cu$ reactions was estimated by Fluka.

Administration of ^{64}Cu in the simple chloride form should lower the cost of PET imaging. In animal studies carried out with reactor produced LSA ^{64}Cu, the tumor uptake of LSA $^{64}Cu(II)Cl_2$, in C57BL/6 mice bearing melanoma tumors in a B16F10 tumor model was compared with the uptake of (a) LSA $^{64}Cu(I)Cl$, and (b) of published data of no carrier added $^{64}Cu(II)Cl_2$, at 24 hours post injection.

5.1 Introduction

^{64}Cu is unique as it decays by three different routes, namely, electron capture (EC) and $\beta-$ and $\beta+$ decays (Fig 5.1). Due to simultaneous emission of both $\beta+$ and $\beta-$particles, this radioisotope holds promise toward development of PET imaging probes for noninvasive visualization of diseases and can also be used in targeted radiotherapy.

Its half-life of 12.8 h makes it versatile – short enough to be useful for tracers with rapid pharmacokinetics such as small molecules and peptides, yet long enough to be useful for tracers with slow pharmacokinetics, for example those associated with monoclonal

antibodies, and for the tracking of cell migration. Its chemistry offers advantages: although it is less substitutional inert than other transition metals, with well-designed macrocyclic chelators it can be stably attached to targeting molecules such as antibodies, peptides, antibody fragments etc.

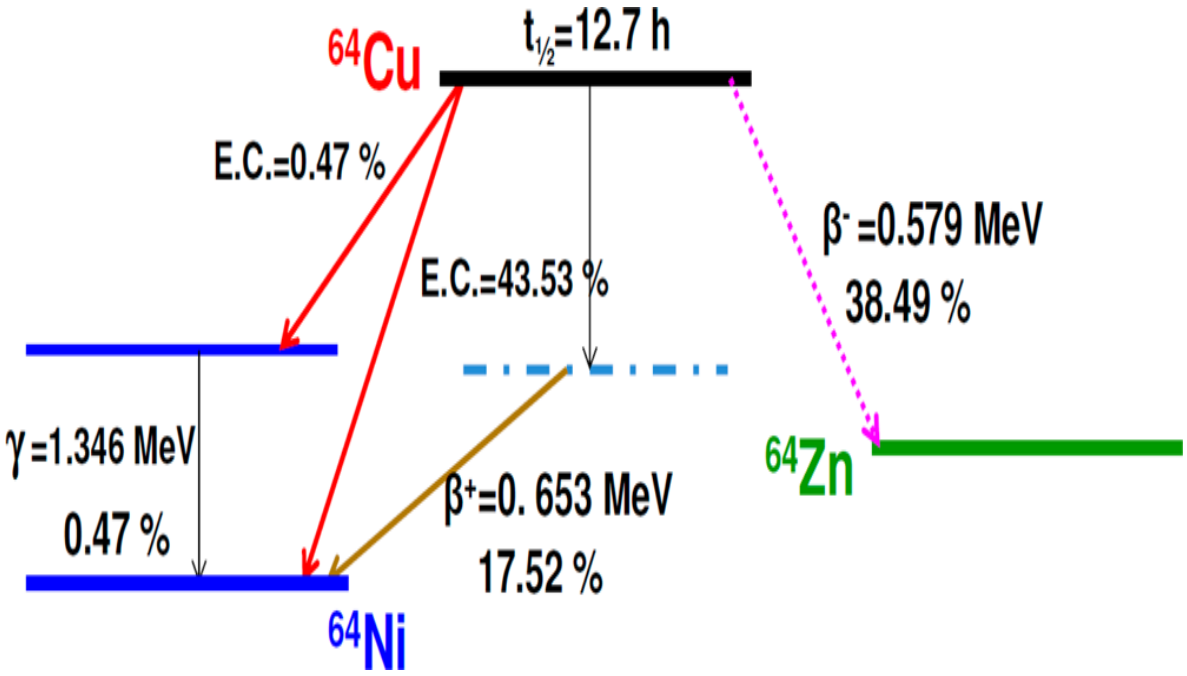

Figure 5.1 Nuclear decay scheme of ^{64}Cu. The radioisotope decays to either ^{64}Ni by β+ emission or EC or to ^{64}Zn by β− decay [ ]

5.1.1 No carrier added (NCA) ^{64}Cu production

^{64}Cu can be produced in a NCA form by $^{64}Ni(p,n)^{64}Cu$ nuclear reaction in a cyclotron [21, 22].The target for producing ^{64}Cu is enriched ^{64}Ni. The ^{64}Ni (typically 10–50 mg) is prepared and electroplated onto a gold disk and bombarded in a cyclotron. After bombardment, the ^{64}Cu is separated from the target nickel in a one-step procedure using an ion exchange column. Nowadays, "state-of-the-art" automated modules are available for fast and highly efficient separation of ^{64}Cu from ^{64}Ni and other extraneous radioisotopes adopting ion

exchange chromatography [20]. Typically, 18.5 GBq of ^{64}Cu are produced with a 40 mg ^{64}Ni target and a bombardment time of 4 h. The specific activity of the ^{64}Cu ranges from 47.4 to 474 GBq/μmol (1280 to 12,800 mCi/μmol). The typical yields for ^{64}Cu productions are 0.2 mCi/μA·h per mg ^{64}Ni. The recovery of enriched ^{64}Ni is ~ 85–95%.

Another method of ^{64}Cu production is the $^{64}Zn(n,p)^{64}Cu$ reaction [23, 24]. High-specific activity ^{64}Cu production of ^{64}Cu by fast neutron reaction of $^{64}Zn(n,p)^{64}Cu$ is possible with small amounts of ^{67}Cu co-production (^{67}Zn natural abundance 4%).However, a major concern includes the coproduction of high levels of the long-lived ^{65}Zn ($t_{1/2}$= 244 days) by the neutron capture $^{64}Zn(n,\gamma)^{65}Zn$ reaction. This can be reduced by shielding thermal neutrons (using, for example, boron nitride) [23]. The production of ^{65}Zn could be prohibitive for the recycling of the enriched target material.

Both $^{64}Zn(n,p)^{64}Cu$ and $^{64}Ni(p,n)^{64}Cu$ reactions lead to high specific activity ^{64}Cu. Proton irradiation of enriched Ni target yields far higher quantities of ^{64}Cu.

5.1.2. Low specific activity (LSA) ^{64}Cu production

LSA ^{64}Cu production in a nuclear reactor via thermal neutron capture via the $^{63}Cu(n, \gamma)^{64}Cu$ reaction has been reported [118]. ^{63}CuO targets were irradiated in research reactors at a neutron flux of 6.6 x10^{12} n cm-2 s -1 for duration of 3 days. Average specific activity of 254 GBq ^{64}Cu per g Cu and 348 GBq ^{64}Cu per g Cu was recorded at the end of irradiation from natural and enriched CuO (99.9% ^{63}Cu) targets respectively.

5.1.3 Clinical Applications of ^{64}Cu

Molecular carriers for ^{64}Cu, like monoclonal antibodies, peptides, and nanoparticles, have been developed and the labeling of peptides and antibodies with Cu radionuclides, requires the use of bifunctional chelators [25, 26]. Copper metabolism has also been known to be critical for cell proliferation, angiogenesis, and tumor growth [119, 120]. ^{64}Cu in the chemical

form of copper chloride $^{64}CuCl_2$ has been identified as a potential theranostic agent for using the human copper transporter 1 (hCTR1) as a molecular target. CTR1 has been proven to be overexpressed in many types of cancer cells, including melanoma, prostate cancer [121, 122]. hCtr1 a 190-amino acid protein of 28 kDa with three transmembrane domains, transports copper with high affinity in a time-dependent, energy-independent process and is stimulated by extracellular acidic pH and high K^+ concentrations [123]. CTR1 has been found to mainly and specifically transport Cu(I) instead of Cu(II) [124]. In the body, Cu^{2+} ions are bound to plasma proteins, which carry them to the cell surface, where the enzyme reductase, reduces Cu^{2+} ions to Cu^+ ions before their uptake into cells. In its reduced form, Cu^+ ions are then transported across the cell membrane by CTR1 [120].

Preclinical studies using $^{64}CuCl_2$ in human cancer xenograft models in mice, such as glioblastoma multiforme (U-87MG) and malignant melanoma (B16F10, A375M), demonstrated its potential as a therapeutic agent [122, 125, 126]. Eighteen patients diagnosed with GBM were administered with $^{64}CuCl_2$ (13 MBq/kg) and brain PET/CT imaging was performed [127]. Copper-64 chloride clearly visualized brain cancerous lesions within 1 hour after injection, with stable retention of radioactivity at 3 and 24 hours. Valentini et al. evaluated the potential of $^{64}CuCl_2$ as a therapeutic agent in two patients with metastatic prostate and uterine cancer [128] and observed a significant reduction in volume of lesions and an improvement in overall condition following a single cycle treatment with 3700 MBq of $^{64}CuCl_2$.

5.2 Material, methods and calculations

5.2.1 Production of ^{64}Cu in a clinical linac

5.2.1.1 Clinical Linac

A clinical electron linac is used for external beam radiation treatments for cancer patients. The linac customizes high energy bremsstrahlung or electrons to conform to a tumor's shape

and destroys cancerous cells while sparing surrounding normal tissue. It has been reported that a

clinical linac, in combination with its extremely stable operation, ensures that photoactivation studies can be performed with very limited beamtime [129].The transition energies and half-lives of isotopes created by photonuclear reactions with Zinc [130] and the energy levels of ^{92m}Nb via the photonuclear reaction have been determined [131] in clinical linacs.

Table 5.1 Specifications of clinical electron Linac *TrueBeam*

Wave Guide	Standing
Length-wave guide	140 cm
RF power source	Klystron
RF Frequency	3000 MHz
RF Power	5.5 MW
*Field Size*Minimum (cm)	0.5 X 0.5
*Field Size*Maximum (cm)	40 X 40
Jaws	Asymmetric
X1 and X2	(-2 cm to + 20 cm)
Y1 and Y2	(-10.0 cm to +20 cm)
MLC	120 Leaves, 60 pairs
Photon (MV)	6,10,15,6FFF, 10FFF*
Dose Rate(MU/min)	100-600(FF**),1600, 2400(FFF)
Electrons (MeV)	6,9,12,15,18

*FFF: Flattening filter free ; ** Flattening filter

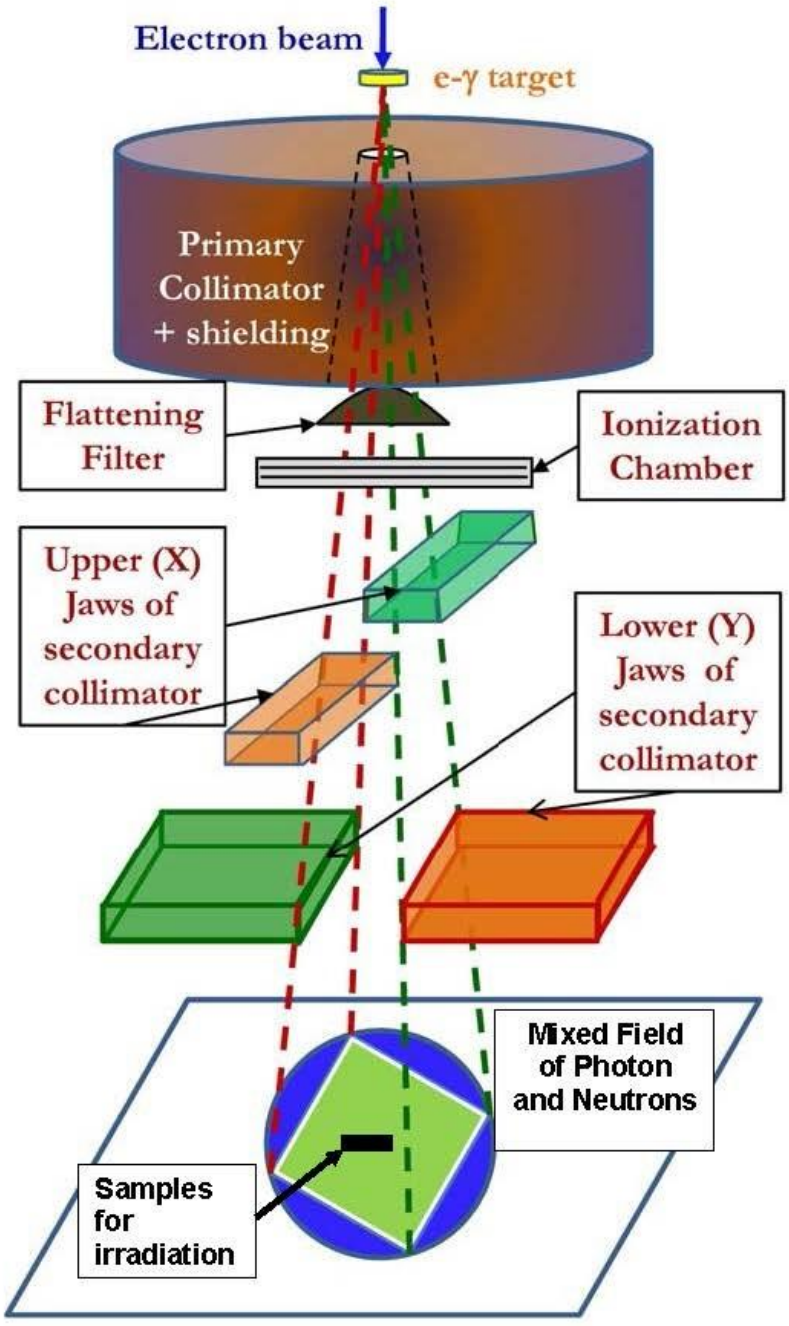

Fig 5.2 Schematic of the electron linac and experimental set up for irradiation.

TrueBeam, is a clinical linear accelerator, manufactured by Varian. The TrueBeam control system dynamically synchronises imaging, patient positioning, motion management beam delivery and shaping to facilitate image guided- radiotherapy and radiosurgery . Among the key features of this linac are the availability of two types of photon beams- standard flattened filtered beams and flattening filter free beams [132] and the availability of multiple X-ray energies, with high-intensity modes that can deliver dose rates up to 2400 monitor units per minute. Typical specifications of TrueBeam are shown in Table 5.1

Figure 5.2 shows the geometry of the linac. Its main components are the target, primary collimator, ion chamber, secondary collimators and multi-leaf collimator (MLC) [133]. Thermally excited primary electrons enter a horizontal accelerating cavity waveguide where high-frequency electromagnetic field waves are used for acceleration to energy of 15 MeV maximum. The linac uses a klystron as a radiofrequency power source. A 270^0 bending magnet primarily consisting of steel and copper with an outer tungsten and lead shielding is used to direct the horizontal beam in vertical direction (for patient treatment) on to a 3 mm thick tungsten target disc to create bremsstrahlung photons. A primary tungsten collimator absorbs the photons that are scattered out of the treatment field and defines the maximum field size. The dose distribution is forward peaked and a flattening filter, made of steel, creates a flat dose profile. Afterwards the photon beam is collimated by focusing Y-jaws and a multi-leaf collimator (MLC) made of tungsten to create individual field geometry.

5.2.1.2 Electron Linac: a photoneutron generator

Medical linear accelerators (linacs) for high energy photon therapy produce neutrons through photonuclear reactions [134] with the elements present in the linear accelerator head such as W, Pb, Cu and Fe. Table 5.2 shows the common elements typically found in the linac head (target, field-flattening filters, and beam collimators) and their associated (γ,n) reaction

Table 5.2 Energy thresholds for (γ,n) reactions in the nuclides typically found in an electron linac head [135].

Isotope	Abundance %	(γ,n) threshold energy
^{182}W	26.30	8.07
^{184}W	30.70	7.41
^{186}W	28.60	7.19
^{206}Pb	24.10	8.09
^{207}Pb	22.10	6.74
^{208}Pb	52.40	7.37
^{56}Fe	91.72	11.20
^{63}Cu	69.17	10.85
^{65}Cu	30.83	9.91

threshold energy [135]. The main sources for photoneutrons in an electron linac head are high atomic number components, including target, primary collimator, secondary collimators, wedges, blocks and multi-leaf collimators. The photoneutron yield depends upon the target material, the strength and spectrum of the photon target and the cross-section of photodisintegration process, which is dependent on the photon energy. In order to produce photoneutrons, the energy of the high intensity photon source must exceed the binding energy of the neutron in a particular target material. The tungsten (W) and lead (Pb) with high cross sections for (γ,n) reaction are major sources of photoneutrons in medical linacs. The probability of photoneutron interaction increases with photon energy and its maximum value

has been found in the therapy range of 13–18 MeV photons for the materials used in the linac head. Also both tungsten and lead have, very low, fast neutron absorption cross section.

5.2.1.3 Dual route of ^{64}Cu production in an electron linac

The secondary collimator jaws were adjusted in such a way that it redirects a beam of 20 x 20 cm^2 field size. The accelerator was operated at 15 MV in photon mode and a set of ^{nat}Cu samples were placed at various SSD and yields of ^{64}Cu were determined by offline γ-ray spectrometry and is shown in Table 5.3

In further experiments to study the effect of moderation of neutrons on the ^{64}Cu yield, ^{nat}Cu and Au foils, alternating with the solid water phantom RW3 (30 cm X 30 cm(L X B)) were irradiated in a stack foil arrangement for 1380 seconds and dose 150 Gy at isocentre. The density and composition of the moderator, solid water phantom RW3 is: ρ= 1.045 g/cm^3, H(7.59 %), C(90.41 %), O(0.80 %), Ti(1.20 %). Au foils were used as a flux monitor for both γ-rays and slow neutrons. The experimental yields of ^{196}Au, ^{198}Au (Bq / g Au) and of ^{64}Cu (Bq/g ^{nat}Cu) are shown in Table 5.4.

5.2.1.4 Fluka estimations of ^{64}Cu yield

Accelerator head assembly has been simulated in Fluka for the determination of fluence and energy spectra of primary beam and secondary particle [136]. A water phantom of 30 × 30 cm^2 was designed in Fluka to study the dose distribution. At different source to surface distances (SSD) the solid water phantom was simulated in Fluka to estimate the fluence spectra of γ-rays and neutrons. An electron beam of size 3 mm diameter was allowed to pass on a tungsten target having thickness 3 mm to generate bremsstrahlung radiation. Source to surface distance (SSD) is measured from the centre of tungsten target. Accelerator head assembly was designed using FLUKA geometry card and MATERIAL cards were used to

define materials in the different regions of the geometry. PHOTONUC card was used to start the photonuclear reaction while determining the dose distribution study in the water phantom.

Natural copper comprises two stable isotopes, ^{63}Cu (69.17%) and ^{65}Cu (30.83%). The mixed field of neutrons and photons in the electron linac offers a dual route of production of ^{64}Cu, via the ^{63}Cu(n, γ)^{64}Cu + ^{65}Cu(γ,n) ^{64}Cu reactions from ^{nat}Cu irradiation.

The ^{64}Cu formation rate via the ^{65}Cu(γ,n) ^{64}Cu reaction is as follows.

$$Y_{(\gamma,n)} = N_0 \int_{E_{th}}^{E_{max}} \varphi_\gamma . \sigma_{(\gamma,n)} dE \qquad 5.1$$

Similarly ^{64}Cu formation rate via the ^{63}Cu(n, γ)^{64}Cu is as follows

$$Y_{(n,\gamma)} = N_0 \int_{0}^{E_{max}} \varphi_n . \sigma_{(n,\gamma)} dE \qquad 5.2$$

where N_0 is the number of target nuclides, φ_γ and φ_n are the photon and neutron flux densities, and σ is the reaction cross section [98, 137]. The excitation functions of ^{65}Cu(γ,n)^{64}Cu and ^{63}Cu(n,γ)^{64}Cu are shown in Figs 5.3 and 5.4 respectively. The cross-sections are grouped over energy intervals and weighted according to the neutron / photon energy spectrum obtained using Fluka. Fluka estimations of ^{64}Cu yield are shown in Table 5.5.

5.2.1.5 Offline gamma spectrometry and radionuclidic purity

After irradiation, activities of radionuclides were measured by offline gamma spectrometry. The γ-peaks were analyzed using a calibrated, low background and high-purity Germanium detector (HPGe). The spectral analysis was performed using the software package Interwinner 7. Radioisotope levels were determined by the quantification of the photo-peak counts of the γ-line 1345.77keV, ^{196}Au (355, 333 keV) and ^{198}Au (411 keV) by using the following equation:

Activity in Bq= $(N_{obs}).D(RT) / (\varepsilon . I_\gamma.LT)$ 5.3

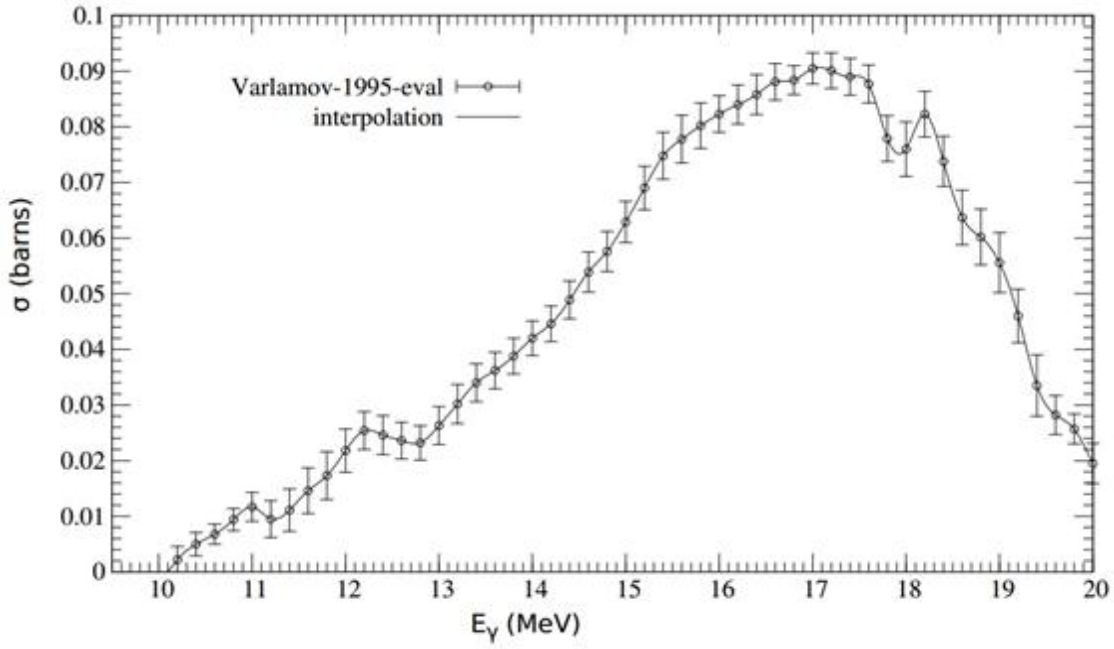

Fig 5.3 $^{65}Cu(g,n)^{64}Cu$ excitation function [137].

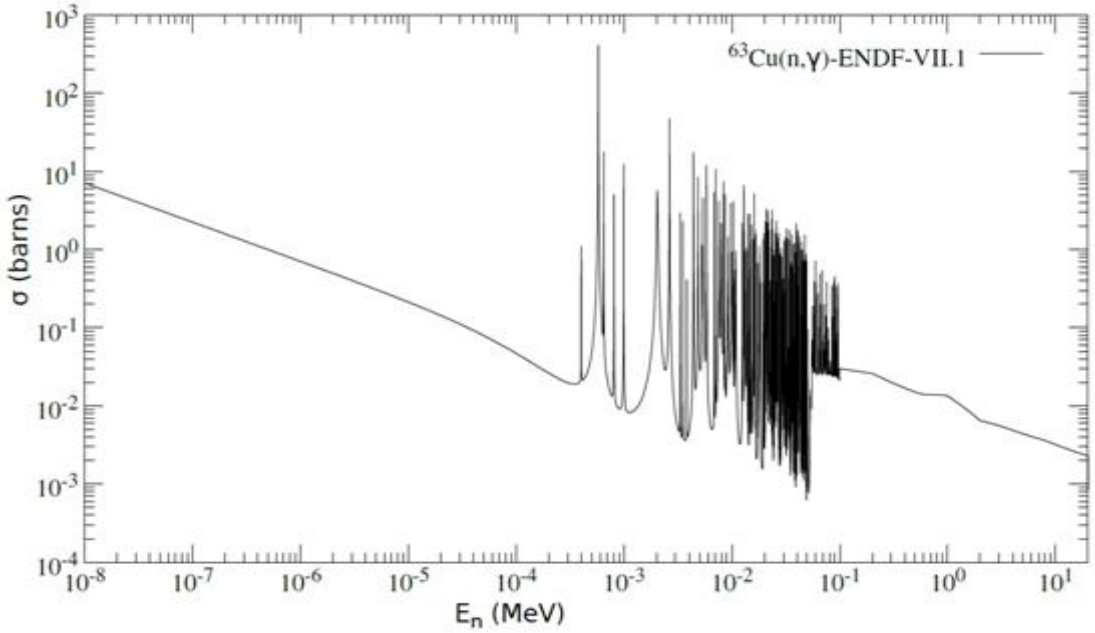

Fig 5.4$^{63}Cu(n,g)^{64}Cu$ excitation function [98].

where N_{obs}= number of detected photo-peak counts of the γ-ray energy, D(RT)= decay factor to correct decay during counting time = λ / (1-e-$^{\lambda}{}_{RT}$), I_γ= the branching intensity or the

abundance of the γ-ray of interest, ε = experimental efficiency of the HPGe detector for the γ-ray energy considered, LT= Live counting time, RT= Real time, λ = decay constant (=0.693/$T_{1/2}$) of the radionuclide of interest with half-life $T_{1/2}$.

5.2.2 Biodistribution studies in tumor bearing mice

5.2.2.1 Preparation of radiotracer

LSA ^{64}Cu was prepared in the Dhruva research reactor, BARC, India via $^{63}Cu(n, \gamma)^{64}Cu$ [118, 138] and procured in the form of $^{64}CuCl_2$ solution. This was diluted with phosphate-buffered saline buffer (PBS, 0.01 M, pH 7.4). It is reported that with antioxidants VitC or DTT, $^{64}Cu(II)$ can be reduced to $^{64}Cu(I)$ [139-141]. $^{64}CuCl$ was prepared by adding 2.96–3.33 MBq [80–90 μCi] $^{64}CuCl_2$ with VitC.

5.2.2.2 Cell Culture and in-vivo tumor model

Mouse melanoma cell line B16-F10 (C57-BL6 mice origin) was obtained from the National Centre for Cell Sciences (Pune, India). It was maintained in monolayer culture at 37ºC and 5% CO_2 in IMDM supplemented with 10% FCS, 100 U/mL of penicillin G, 100 μg/mL of streptomycin, and 0.25 μg/mL of amphotericin B. The cells were grown up to 80% confluence for performing all studies. For developing tumor model, the cells were subcutaneously injected in C57-BL6 mice at 5 x 10^5 cells/ mice in 200μl PBS. Tumors were allowed to develop for 15 days until they reached a volume of 100 mm^3, when bio-distribution experiment was initiated.

5.2.2.3 Biodistribution study

Anesthetized B16F10 tumor-bearing mice (n = 4 for each group) were injected with approximately (2.96–3.33 MBq [80–90 μCi]) via the tail vein . After the injections of the tracer, the animals were returned into their cages where they remained with access to food and water until the time points of evaluation. The animals were sacrificed by cardiac puncture

24 hours post-anesthesia post-injection (p.i.). Various organs, tissues, and tumors were excised after sacrifice, and the weight of each organ and tumor was also determined by using an analytical balance. The radioactivity associated with each organ and tissue was determined with a NaI(Tl) counter .The results are expressed as percentages of injected radioactivity dose per gram of tissue (%ID/g).

5.3 Results and Discussion

5.3.1 ^{64}Cu yield

Electron linear accelerators today constitute the core of the equipment of a modern radiation therapy department. Photon beams of about 6-20 MeV have, in general, a sufficient penetration in the tissues to treat most of the tumors with an adequate physical selectivity. This energy range of the photons overlaps with the GDR region of 10-30 MeV, where (γ, n) and (γ, p) reactions typically have a high cross section. Table 5.3 shows that the radioactivity of ^{64}Cu produced was 13.5 ± 1.06 Bq per gram of ^{nat}Cu, respectively per gray-sec irradiation.

Table 5.3 ^{64}Cu yield (Bq) per g Cu /gray/sec on irradiation of ^{nat}Cu in a 15 MV clinical electron linac

Sample	Weight (g)	Source to surface distance (cm)	Dose (Gy)	Time of irradiation (s)	Activity at EOB (Bq)	^{64}Cu Activity (Bq) per g Cu/gray-sec
1	0.2	55	112	240	235	12.35
2	0.26	60	40	240	125	13.77
3	1	70	266	1380	2350	14.43

Table 5.4 Yields (Bq)of^{196}Au Bq/g Au, ^{198}Au Bq/g Au, ^{64}Cu/ g ^{nat}Cu at EOB obtained on irradiation of ^{nat}Au and ^{nat}Cu foils alternating with the solid water phantom RW3 (30 cm X 30 cm (L X B)) in a stack foil arrangement for 1380 seconds and dose 150 Gy at isocentre in the 15 MV clinical electron linac.

SSD (cm)	Moderator Thickness (cm)	^{196}Au Bq/g Au via ^{197}Au(γ, n)^{196}Au	^{198}Au Bq/g Au via ^{197}Au(n, γ)^{198}Au	^{64}Cu Bq/g Cu via $^{65}Cu(\gamma,n)^{64}Cu$ +$^{63}Cu(n,\gamma)^{64}Cu$
70	0	1385	737	1421
71.5	1	1329	2473	1673
74.5	3	1282	4203	2290
77.5	5	1194	4810	2067

The ratio of neutron to photon fluxes and their energy distributions, may be varied by adjusting the electron beam energy and the converter/target design. The spectrum of neutrons available from an accelerator target is typically much harder than that available from a reactor and, with appropriate shaping with a moderator, can be used to enhance the rate of neutron capture in a nuclide's resonance region. Fig. 5.5 shows that ^{198}Au yield increased by 55 % and Table 5.4 shows that ^{64}Cu yield increased upto 46 % with increase in thickness of moderators.

Table 5.5 Fluka estimation of ^{64}Cu yield and % neutron contribution to ^{64}Cu yield for irradiation conditions described in Table 5.4.

Thickness of moderator (cm)	Fluka estimated		
	^{64}Cu / g ^{nat}Cu via $^{63}Cu(n,g)^{64}Cu$ (Bq)	^{64}Cu / g ^{nat}Cu via $^{65}Cu(g,n)^{64}Cu$ (Bq)	% Neutron contribution to ^{64}Cu yield
0	515 ± 78	1029 ± 156	33.3 ± 6.3
1	861 ± 130	1009 ± 153	46.0 ± 8.7
3	524 ± 79	922 ± 140	36.2 ± 6.8
5	652 ± 99	900 ± 136	42.01 ± 7.9

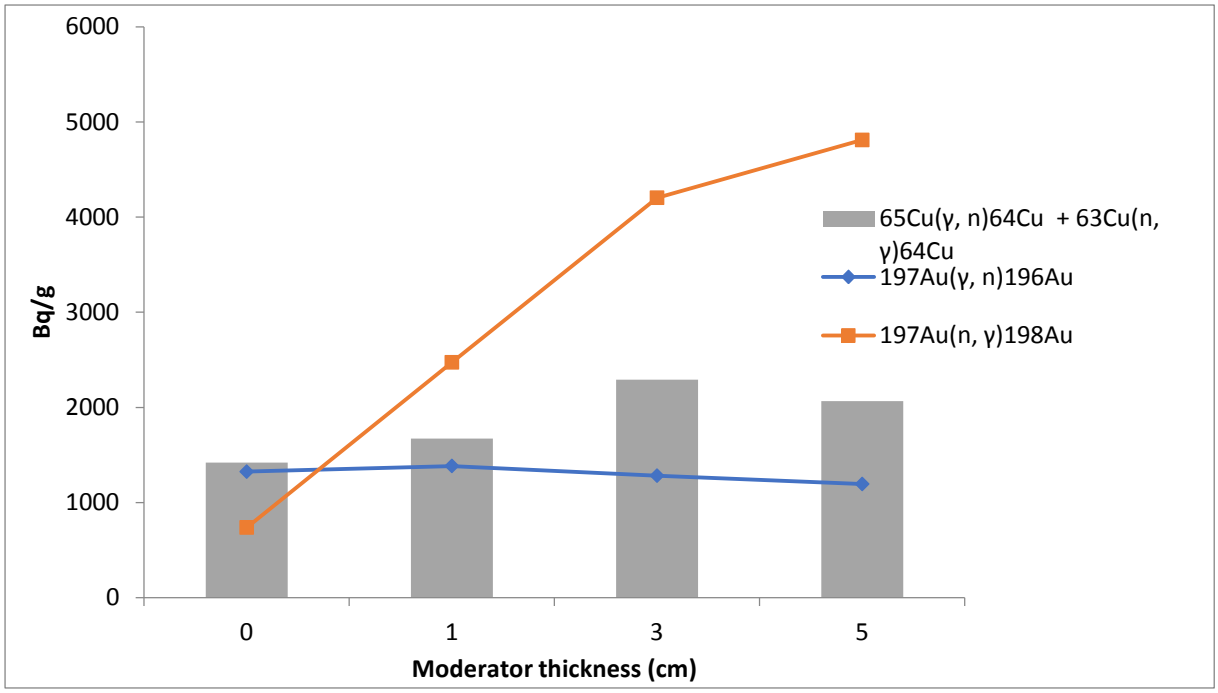

Fig. 5.5 Yield (Bq/g) ^{64}Cu, ^{196}Au, ^{198}Au with variation in solid water phantom thickness.

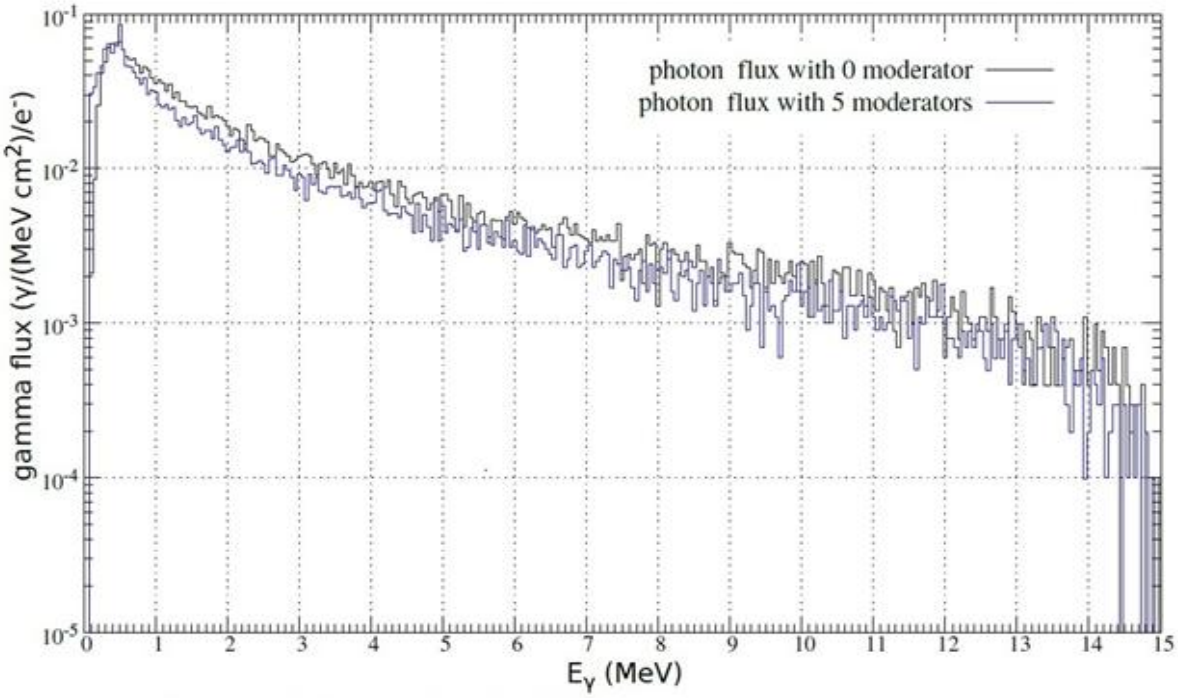

Fig. 5.6 Bremsstrahlung spectra in the 15 MV clinical electron linac with variation in solid water phantom thickness**.**

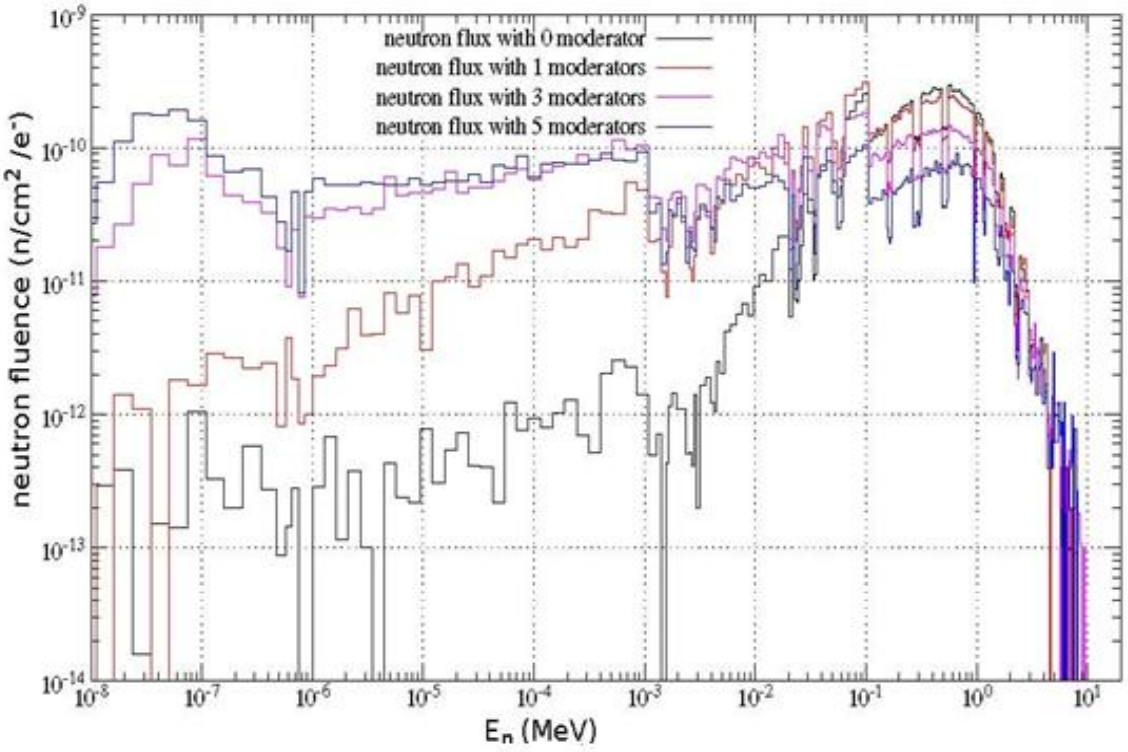

Fig. 5.7 The neutron energy spectra in the 15 MV clinical electron linac with variation in solid water phantom thickness.

The components consisting of materials with high atomic numbers in the accelerator head have a high cross section for photonuclear reactions. Neutron spectrum measurement is a complicated process to perform with the standard nuclear instrumentation, due to the high fluence rate of γ-rays with respect to neutrons. Therefore a code which allows the entire process of photo-neutron generation and transport across the accelerator head represents a useful tool to estimate neutron spectra. As Fluka can handle the accurate electron-nucleus, electron-electron bremsstrahlung and photonuclear interactions over the whole energy range it is suitable for simulation[142]. The Fluka estimation of ^{64}Cu yield and % neutron contribution to ^{64}Cu yield for irradiation conditions described in Table 5.4 is shown in Table 5.5

Figs. 5.6 and 5.7 show the effect of the solid water phantom on the photon and neutron flux and the enhancement of the neutron flux in the slow neutron region. The increase in yield of ^{64}Cu is primarily due to increased contribution via the reaction route $^{63}Cu(n,\gamma)^{64}Cu$ to the total yield of ^{64}Cu. The 69.17% natural abundance of ^{63}Cu, and thermal neutron cross section of 4.1 b indicate favourable conditions for the production of reasonable amounts of ^{64}Cu activity.

5.3.2 **Radionuclidic purity**

Possible co-produced radionuclide impurities are ^{66}Cu and ^{65}Zn. ^{64}Cu decays to stable ^{64}Zn by β^- decay and to stable ^{64}Ni by β^+ decay. ^{64}Zn can undergo neutron activation to form long lived ^{65}Zn ($t_{1/2}$ = 244 d) and short lived ^{65}Ni ($t_{1/2}$ = 2.5 h) respectively. ^{66}Cu ($t_{1/2}$=5.1 min) will be produced by neutron activation of ^{65}Cu. The γ-ray spectrum in Fig. 5.8 shows the annihilation peak of 511 keV and γ-ray peak of 1345.8 keV characteristic photopeak of ^{64}Cu.No extraneous γ-ray peaks were recorded indicating high radionuclide purity.

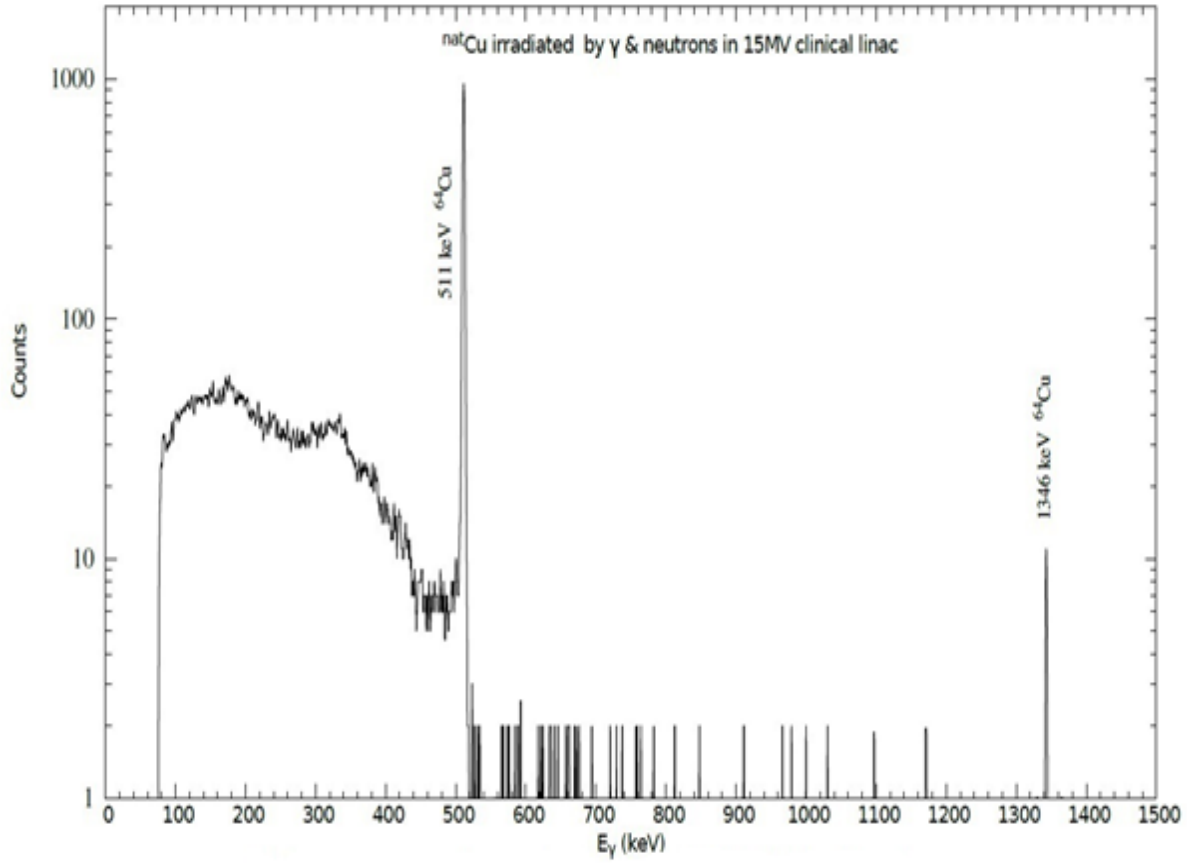

Fig. 5.8 Gamma-ray spectrum of ^{nat}Cu irradiated in 15 MV clinical electron linac.

5.3.3 Biodistribution study

The tumor uptake of LSA $^{64}Cu(II)$ and $^{64}Cu(I)$ was 5.14 ± 0.52 and 4.71± 0.56 % injected dose / g (ID/g) at 24 hours post injection. This is comparable to the tumor uptake of high specific activity $^{64}Cu(II)$ and $^{64}Cu(I)$ as 6.56% ± 0.61 and 5.95% ± 0.24 % ID/g respectively, in B16F10 tumor-bearing mice at 24 hour post injection [141]. Fig 5.9 shows no significant difference in biodistribution between $^{64}Cu(I)$ and $^{64}Cu(II)$. This could happen because of the dilution of VitC, and oxidation reaction under physiological conditions resulting in the quick changing from Cu(I) to Cu(II) *in vivo* [141]. Both $^{64}CuCl_2$ and $^{64}CuCl$ displayed high tumor-to-muscle ratios and small uptake in brain. The biodistribution data indicated that $^{64}CuCl_2$ and $^{64}CuCl$ were excreted through both the liver and kidneys.

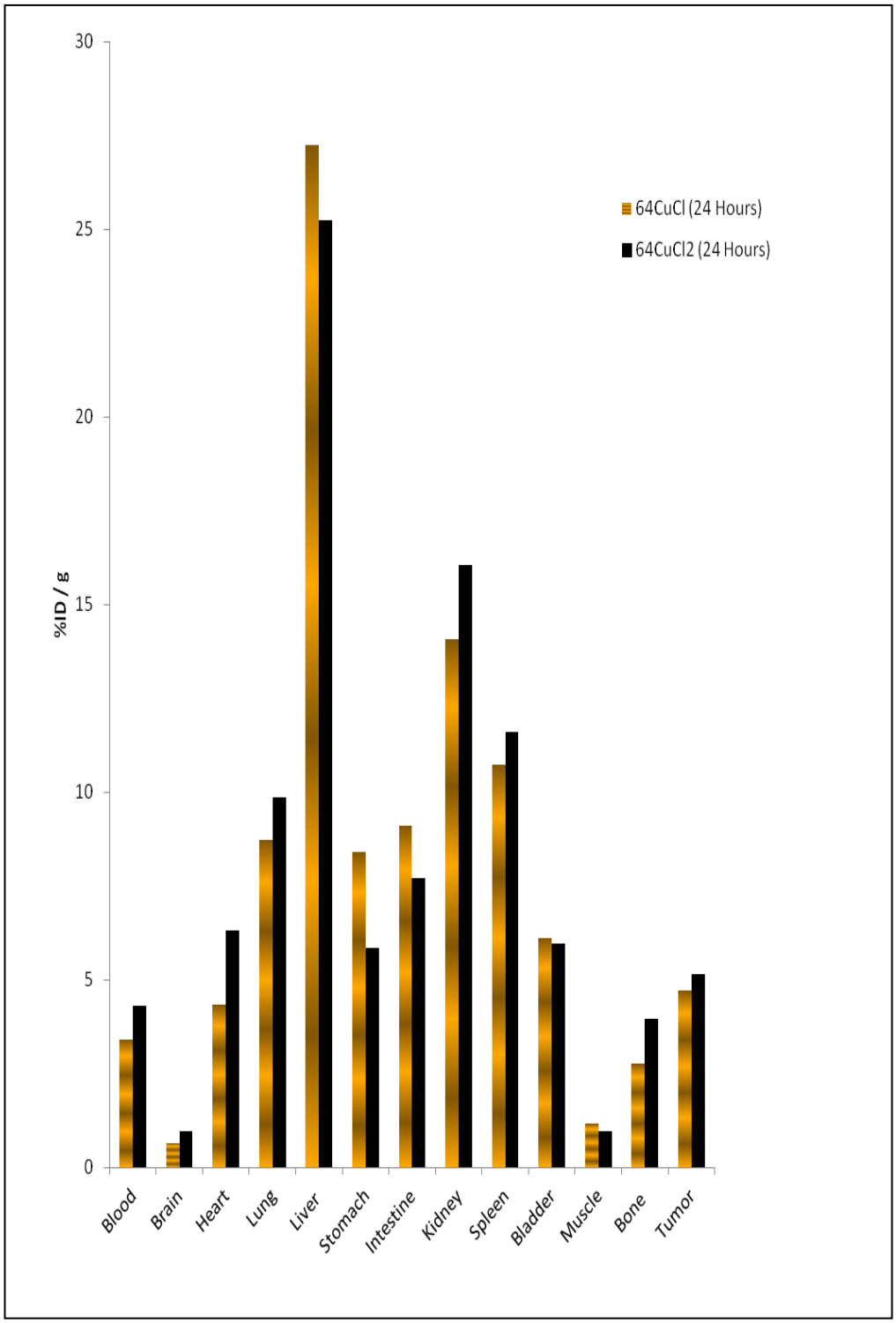

Fig 5.9 Biodistribution data of LSA $^{64}Cu(II)$ and $^{64}Cu(I)$ at 24 hours post injection.

5.4 Summary

It has been demonstrated that a clinical linac, can be used for photoactivation studies. Radioactivity of ^{64}Cu produced was about 13.5 ± 1.06 Bq per gram of ^{nat}Cu per gray-sec irradiation. The ^{64}Cu yield increased up to 46% after moderation of the neutrons by a solid water phantom.

In the comparison study of the biological efficacy of LSA^{64}Cu as $^{64}Cu(I)Cl$ and $^{64}Cu(II)Cl_2$, in C57BL/6 mice bearing melanoma tumors in a B16F10 tumor model, no significant difference in biodistribution between $^{64}Cu(I)$ and $^{64}Cu(II)$ at 24 hours post injection was observed. Also the % tumor uptake of LSA ^{64}Cu ions was similar, to published uptake values no carrier added ^{64}Cu ions.

This production route of LSA ^{64}Cu via $(\gamma,n) + (n,\gamma)$ interactions, obviates the need for costly targets, and direct administration in the chloride form should lower the cost of PET imaging. In the biodistribution study reactor produced ^{64}Cu was used. However, an accelerator offers advantages over a reactor – generation of reduced waste, much safer to operate, cheaper decommissioning costs and does not pose a nuclear weapon proliferation risk.

The present study opens the possibility of irradiating natural targets of Cu in an electron linac to produce ^{64}Cu as a cost saving measure for medical applications.

Chapter 6

Production, separation and supply prospects of ^{67}Cu with the development of fast neutron sources and photonuclear technology

^{67}Cu is a promising therapeutic radionuclide. The use of ^{67}Cu-based radiopharmaceuticals is not common, due to the lack of consistent, high activity production of ^{67}Cu. Growth and development of intense fast neutron sources and photonuclear technology, can possibly aid in the sustained supply of ^{67}Cu. Experimental investigations have been carried out on the production of ^{67}Cu via the ^{67}Zn(n,p)^{67}Cu,^{68}Zn(n,x)^{67}Cu, and ^{68}Zn(γ,p)^{67}Cu reaction routes. Natural Zn metal foils were irradiated with 14.1 MeV neutrons and bremsstrahlung of end-point energy 15 MeV. No carrier added ^{67}Cu was separated from the irradiated Zinc by solvent extraction.

6.1 Introduction

Among the β^-emitting radionuclides, ^{47}Sc ($T_{1/2}$= 3.35 d; E_{β^-} = 610 keV), ^{67}Cu ($T_{1/2}$= 2.58 d; E_{β^-} = 577 keV), ^{105}Rh ($T_{1/2}$= 1.47 d; E_{β^-} = 560 keV), ^{161}Tb ($T_{1/2}$ = 6.90 d; E_{β^-} = 590 keV), ^{175}Yb ($T_{1/2}$= 4.19 d; E_{β^-} = 466 keV) and ^{186}Re ($T_{1/2}$= 3.72 d; E_{β^-} = 1070 keV) have been receiving enhanced attention for internal therapy [4].

The overexpression of the human copper transporter protein (hCtr1) in a variety of cancers [143], and the specific role of copper, as a trace metal, in various metabolic pathways of human physiology [144], make ^{67}Cu a promising therapeutic radionuclide. It has decay characteristics that make it well suited for in vivo studies and treatments [145]. It is suitable for Single Photon Emission Computed Tomography (SPECT) due to its soft gamma-ray emission (Eγ = 184.58 keV, 48.6%) [72] and for the therapeutic effect due to its average 141 keV β- particle (0.61 mm tissue range). The half-life of ^{67}Cu (2.58 d) is shorter, compared to those of clinically established radiotherapeutic radionuclides ^{131}I(8.04 d) and ^{177}Lu (6.65 d),and thus ^{67}Cu can be used to label

molecules that exhibit a more rapid washout from tumor tissues [146].Studies using ^{67}Cu-labeled antibodies [147], and in the simple form of its chloride $^{67}CuCl_2$ [148], indicate the immense potential of ^{67}Cu for cancer radiotherapy. The complexation chemistry of copper has been extensively studied, and chelators that are suitable for stable coordination of copper are available [149].

6.1.1 Various production methods for ^{67}Cu

Many studies [3, 145] have been carried out to produce ^{67}Cu using reactors and accelerators via the $^{67}Zn(n,p)^{67}Cu$ [44, 150, 151], $^{68}Zn(p,2p)^{67}Cu$[152-156], $^{70}Zn(p,\alpha)^{67}Cu$[157-159], $^{70}Zn(d,\alpha n)^{67}Cu$[160], $^{68}Zn(n,x)^{67}Cu$ [161] and $^{68}Zn(\gamma,p)^{67}Cu$[47, 162] reactions. Among all the above reactions, the $^{68}Zn(p,2p)^{67}Cu$ reaction is currently the best route for the production of ^{67}Cu [3].

The production of ^{67}Cu via the $^{nat}Zn(p,2p)^{67}Cu$ reaction has been carried out at high-energy proton beam facilities. Yield of 503.2 kBq/μAh is reported via 200 MeV proton irradiation on natural ZnO targets [152]. The isotopic composition of ^{nat}Zn is $^{64}Zn(48.6\%)$,$^{66}Zn(27.9\%)$,$^{67}Zn(4.1\%)$,$^{68}Zn(18.8\%)$, and$^{70}Zn(0.62\%)$. Thus, in the ^{nat}Zn sample, the production of ^{67}Cu is accompanied by the co-production of isotopes of nickel, cobalt, manganese and chromium, $^{64,65}Cu$ and ^{67}Ga [153]. This increases complexity of the separation and radiochemical processing. The ^{67}Ga co-produced has a comparable half-life and identical gamma-ray energies to ^{67}Cu. Thus estimation of ^{67}Cu activity can be carried out only after the radiochemical separation. The shorter-lived ^{64}Cu isotope ($T_{1/2}$ =12.7 h) reduces the purity of ^{67}Cu and must be allowed to decay to ensure the required radionuclidic purity of ^{67}Cu.Also the formation of ^{65}Cu decreases the specific activity, rendering the ^{67}Cu unsuitable for antibody therapy [153]. The proton irradiation of enriched ^{68}Zn to produce ^{67}Cu via the $^{68}Zn(p,2p)^{67}Cu$

reaction results in increased yield and specific activity of ^{67}Cu, and is currently the best choice [3, 153, 154]. Averaged ^{67}Cu production yield of 1.08 MBq/μAh per g ^{68}Zn in 24h irradiation with~100 MeV proton beam has been reported and the enriched ^{68}Zn target was recovered [154].However the concurrent production of ^{65}Zn can restrict the reuse of recovered enriched ^{68}Zn target [161].

The $^{70}Zn(p,\alpha)^{67}Cu$ reaction has a Q value of 2.62 MeV and the production, can be feasible at medical cyclotron facilities. Using evaluated and recommended cross section data [163], Qaim [3] has compared the ^{67}Cu yields from the two production reactions $^{68}Zn(p, 2p)^{67}Cu$ and $^{70}Zn(p, \alpha)^{67}Cu$, and the former reaction is more suitable. In the case of preparation of ^{67}Cu based on deuteron irradiation of enriched ^{70}Zn, the integral yield in the energy window of 20 → 10 MeV, on 95 % enriched ^{70}Zn, was estimated as 4.2 MBq/μAh or 375 MBq/μA at saturation [160]. However, the availability of high-intensity 20 MeV deuteron beam and the economics of using enriched target material ^{70}Zn may be limiting factors in the use of this method.

The production of ^{67}Cu via the $^{67}Zn(n,p)^{67}Cu$ reaction, in nuclear reactors, with ^{nat}Zn, is accompanied by co-production of high levels of ^{64}Cu impurity. Using a 93.2% enriched ^{67}ZnO target, yields of 3.33MBq/mg of ^{67}Zn are reported [150]. However, limited accesses to reactors and low cross-section values of ~1 mb [151] have resulted in reduced application of this method. A fast spectral neutron source is more effective than a fission reactor for the production of ^{67}Cu [48, 161, 164, 165]. The $^{68}Zn(n,n'p+d)^{67}Cu$ reaction route reported in Refs.[161, 165], produced ^{67}Cu of high radionuclidic purity by using neutrons obtained by irradiating a carbon target with the deuteron beam of 40 MeV energy and 5 mA current. In the experiments, using enriched ^{68}ZnO target (^{68}Zn 99.3%, 0.33 g), with I_d=1.84 μA, for 5 h irradiation, the $^{64}Cu/^{67}Cu$ activity ratio of < 0.016 at the EOB is reported. The bio-distribution studies of $^{67}CuCl_2$ in colorectal

tumor bearing mice, using ^{67}Cu produced via the $^{68}Zn(n,n'p+d)^{67}Cu$ reaction, indicated high uptake of ^{67}Cu in the tumor[148].

The photonuclear reaction method for the ^{67}Cu production uses the $^{68}Zn(\gamma,p)^{67}Cu$ reaction induced by bremsstrahlung radiation in a linear electron accelerator (LINAC). The use of an enriched target ^{68}Zn can significantly reduce the co-produced radioimpurities, ^{63}Zn, ^{65}Zn, and ^{64}Cu. The ^{67}Cu yield of 47.73 kBq/μAh per 100 mg enriched ^{68}ZnO (99%) via 60 MeV bremsstrahlung induced reaction has been reported [162]. The Society for Applied Microwave Electronics Engineering and Research (SAMEER) is developing a 30 MeV, 8-10 kW electron LINAC for the radioisotope production in India [46]. The electron LINAC will typically be used for ^{99}Mo production via the $^{100}Mo(\gamma,n)^{99}Mo$ reaction. In the first phase, SAMEER has developed a prototype 15 MeV S-band standing wave side coupled linear electron accelerator of 1.2 m length **[**166**].**

The (p,2p) reaction method for the production of ^{67}Cu isotope in high energy proton accelerators is cumbersome and the (n,p) method in reactors with fission neutrons does not meet the requirements of the medical community. Despite favorable characteristics, the growth and use of ^{67}Cu-based radiopharmaceuticals is not common, due to the lack of consistent, high activity production of ^{67}Cu. The electron LINACs have been underutilized for medical isotope production and may offer an affordable route to an expanded supply of ^{67}Cu and other isotopes [167]. Also recent advances in accelerator technology could allow us to use a neutron intensity as high as 10^{13} n/s at an average neutron energy of E_n =14 MeV [168].

As an aid to expand the availability of ^{67}Cu and to demonstrate the viability of the production processes, with development of fast spectral neutron sources and photonuclear technology, this study investigates the production of ^{67}Cu via (a) the $^{67}Zn(n,p)^{67}Cu$, $^{68}Zn(n,n'p)^{67}Cu$ and

$^{68}Zn(n,d)^{67}Cu$ reaction routes by irradiating ^{nat}Zn foils with 14.1 MeV DT accelerator neutrons at the Purnima Neutron generator Facility, BARC, and (b) the $^{68}Zn(\gamma,p)^{67}Cu$ route by irradiating ^{nat}Zn foils with 15 MeV bremsstrahlung in a prototype LINAC at SAMEER.

No carrier added ^{67}Cu was separated from the irradiated zinc by solvent extraction. The radioactivity levels of ^{67}Cu and other radioisotopes co-produced were determined by the quantification of γ-ray photo-peaks by off-line gamma-ray spectrometry.

6.2 Experimental methods

6.2.1 Materials

Analytical grade reagents were used at all the times unless specified. Reagents were prepared with18MΩ deionized water. Dithizone and CCl_4were obtained from Sigma-Aldrich.

6.2.2 Irradiation with neutrons

Purnima neutron generator (PNG) [169] operates in DT and DD reaction modes to produce mono-energetic neutrons of 14.1MeV and 2.45MeV, respectively. The deuterium gas is supplied to ion source through a gas inlet and its flow is controlled by a motorised needle valve, which is connected with the deuterium gas cylinder. The plasma is produced using capacitor coupled 100 MHz, 200W RF power. D^+ ion beam is extracted from ion source by applying extraction voltage, which is focused by 30 kV DC electrostatic Einzel lens. Beam is accelerated up to 300 keV and bombarded on a titanium-tritiated target with copper backing plate. The beam power dissipated in the TiT is removed with chilled water circulating around the target. The neutron production is regulated by acceleration voltage and RF ion source parameters. The Zn samples were placed at a distance of 1 cm from the neutron source and irradiated for 20 minutes. The operating parameters during irradiation were 200 μA of D+ current and high voltage of 90 kV. Table 6.1 shows the nuclear spectroscopic data of the reaction products produced in the neutron induced

reactions on ^{nat}Zn [72, 170, 171]. Table 6.2 shows the experimental conditions and end of bombardment (EOB) activity of ^{67}Cu and other radioisotopes co-produced.

Table 6.1: Nuclear spectroscopic data of the reaction products produced in the neutron induced and photonuclear reactions on zinc [72, 162, 170, 171].

Product radio nuclide	Neutron induced reactions		Photon induced reactions		Half - life	Decay mode	Gamma ray energy (keV)	Gamma ray abun-dance (%)
	Reaction	Energy threshold (MeV)	Reaction	Q Value (MeV)				
^{67}Cu	^{67}Zn (n,p)	0.0	^{68}Zn (γ,p)	- 9.99	2.58 d	β^- (100 %)	91.3 93.3 184.6	7.0 16.1 48.7
	^{68}Zn (n,d)	7.87						
	^{68}Zn (n,n+p)	10.12						
^{65}Zn	^{64}Zn (n,γ)	0.0	^{66}Zn (γ,n)	-11.05	244 d	EC(98.5%) β^+(1.5%)	1115.5	50.04
	^{66}Zn (n,2n)	11.23						
^{69m}Zn	^{70}Zn (n,2n)	9.4	^{70}Zn (γ,n)	- 9.21	13.8 h	IT (96.7%) β^- (3.3%)	438.6	94.85
^{64}Cu	^{64}Zn (n,p)	0.0			12.7 h	EC(43.8%) β^+(17.8%) β^-(38.4%)	511.0 1345.8	35.6 0.475†

†- This is an evaluated value. A new measurement [171] gives a value of 0.54%.

6.2.3 Irradiation with photons

The bremsstrahlung with end-point energy of 15 MeV was generated by impinging an electron beam on water cooled circular tungsten metal 4.0 mm thick and 6.0 mm in diameter. The Zn samples were irradiated at a distance of 24.5 cm from the tungsten convertor for 45 min. The peak current of the electron beam during irradiation was 65 mA, at a frequency of 150 Hz, with a pulse width of 6 μs. The schematic diagram of the experimental arrangement is shown in Fig. 6.1.Table 6.1gives the nuclear spectroscopic data of the reaction products produced in the photonuclear reactions on ^{nat}Zn [72, 162, 171]. Table 6.3 shows the experimental conditions and EOB activity of ^{67}Cu and other radioisotopes co-produced.

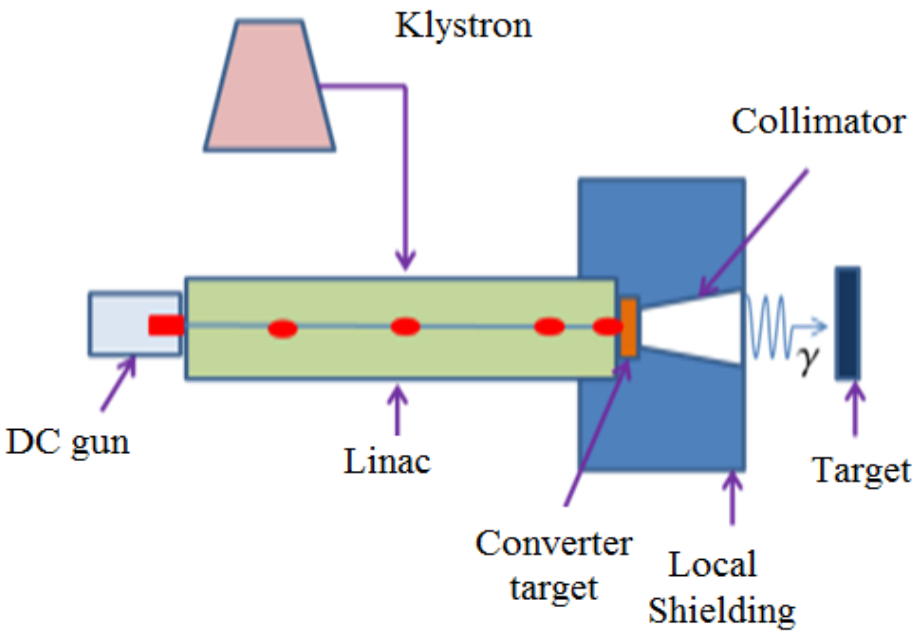

Fig 6.1: Schematics of experimental arrangement for irradiation at the 15 MV LINAC.

6.2.4 Off-line gamma-ray spectrometry

Radioactivity levels of ^{67}Cu and other radioisotopes co-produced were determined by the quantification of photo-peak areas by using the off-line gamma-ray spectrometric technique. The

γ-ray counting of radionuclides was performed using a pre-calibrated HPGe detector coupled to a PC based 4K channel analyzer. The energy resolution of the detector system was 1.8 keV FWHM at the 1332.5 keV γ-ray peak of ^{60}Co. The energy and efficiency calibration of the detector system was done by using a standard ^{152}Eu source. Spectroscopy software, Interwinner 7 was used for the analysis. In order to avoid pile up effect, the dead time of γ-ray counting was always kept less than 5% by placing the samples at a suitable distance from the end cap of the detector. Radioactivity levels were determined by the quantification of the following photo-peak counts of the γ-lines: ^{65}Zn (1115.5keV), ^{69m}Zn (438.6 keV),^{67}Cu (184.6keV) and ^{64}Cu (1345.8 keV) by using the following equation.

$$\text{Activity in Bq} = (N_{obs}).D(RT) / (\varepsilon . I_{\gamma}.LT) \qquad 6.1$$

where N_{obs}= number of detected photo-peak counts of the γ-ray energy, D(RT) = decay factor to correct decay during counting time = $\lambda / (1\text{-}e^{-\lambda RT})$, I_{γ}= the branching intensity or the abundance of the γ-ray of interest, ε = experimental efficiency of the HPGe detector for the γ-ray energy considered, LT= Live counting time, RT= Real time, λ = decay constant = $0.693/T_{1/2}$ of the radionuclide of interest with half-life $T_{1/2}$.

Figures 6.2 (a) and 6.3(a) show the gamma-ray spectra of irradiated ^{nat}Zn via the (n,x) reaction route and via the (γ, p) reaction route, respectively.

6.2.5 Separation of ^{67}Cu from irradiated zinc

Techniques reported to separate the radionuclides $^{64,67}Cu$ from the irradiated zinc matrices include solvent extraction [152, 155, 159], anion exchange chromatography [162, 164, 172], electrolysis [150] and sublimation [167]. The solvent extraction method is based on (1) selective extraction of Cu dithizonate into organic solvent from a dilute acidic solution of the bulk Zn

target and (2) back extraction of Cu into aqueous phase. The solvent extraction procedure was adapted, in this work, with reduction of reagent volumes.

The irradiated Zn foils were transferred into a beaker. Then 5 mL of conc HCl was added to the beaker and the solution was evaporated to dryness. The white residue obtained was then redissolved in 0.5 M HCl, evaporated again to dryness and redissolved in 20 mL of 0.5 M HCl. The solution was transferred into a 60 mL separating funnel. A freshly prepared 5 mL volume of 0.01% dithizone solution in CCl_4 was added to the solution containing the dissolved Zn foils. This mixture was thoroughly mixed for about 2-3 minutes and the layers were then allowed to settle for another 3 minutes. The bottom organic layer (green in color) containing Cu isotopes was separated and collected in a beaker. This extraction was repeated three more times to ensure complete separation. The colorless aqueous solution containing the zinc isotope can be used for the recovery of the enriched target. The four organic extracts (green colored) were then transferred into another separating funnel and treated with (2 x 5 mL) 7M HCl containing 4 drops of 30% H_2O_2 solution. The phases were thoroughly mixed for about 3 minutes. The hydrogen peroxide causes oxidation of the dithizone complex, and the color of the organic layer changes from green to orange. Both phases were separated and collected. The organic phase was transferred back to the separating funnel and back extracted again with a second portion of 7M HCI containing the hydrogen peroxide. The aqueous layer containing ^{67}Cu was collected in a beaker and evaporated to dryness and redissolved in phosphate buffer saline. Figures 6.2 (b) and 6.3(b) show the γ-ray spectra, of the separated ^{67}Cu, produced via the $^{nat}Zn(n,x)$ and $^{nat}Zn(\gamma,p)$ reaction routes, respectively.

6.3 Results and Discussion

6.3.1 Production yields in neutron induced reactions

As seen from Table 6.2 and Figure 6.2(a), in the neutron irradiation experiments on ^{nat}Zn, the radioisotopes ^{67}Cu, ^{64}Cu, ^{65}Zn and ^{69m}Zn, were co-produced. The neutron flux was of the order of 10^7n/s cm^2 at a distance of 1 cm from the source .

Table 6.2: End of bombardment (EOB) activity of radioisotopes produced with 14.1 MeV neutrons via the $^{nat}Zn(n,x)$ reaction route with D^+ current =200μA and irradiation time 20 minutes.

Zn weight (g)	(Bq/ g) at end of bombardment (EOB)			
	^{67}Cu	^{64}Cu	^{69m}Zn	^{65}Zn
3.3	1.51±0.26	175±29.7	12±2	1.84±0.32

End of bombardment (EOB) radioactivity, 1.5 Bq/gram ^{nat}Zn of ^{67}Cu, via the $^{67}Zn(n,p)^{67}Cu$ + $^{68}Zn(n,x)^{67}Cu$ reactions, (where (n,x) denotes (n,n`p) + (n,d)), and 175Bq of ^{64}Cu, per gram of ^{nat}Zn has been obtained, in the 20 minutes of irradiation. Irradiation of Zn with the accelerator neutrons, is useful for the production of ^{64}Cu [164], and conversely, ^{67}Cu becomes a contaminant, in the (n,p) route, when ^{64}Cu is the targeted product.^{64}Cu is an attractive radionuclide in nuclear medicine for both positron emission tomography (PET) and radiotherapy because of its intermediate half-life and a unique decay process. [3, 21, 22, 171].

In the neutron energy region around 14 MeV, several measurements of the cross section of the $^{67}Zn(n,p)^{67}Cu$ reaction have been reported using a neutron generator and these experimental cross section data can be accessed from the EXFOR database [98]. Al-Abyad*etal* [173], have

analyzed the EXFOR data and in conjunction with the study carried out by Qaim [174], have recommended the cross section values aided by the nuclear model calculations STAPRE, for the $^{67}Zn(n,p)^{67}Cu$ reaction. Using the recommended cross section value of 35mb, at En =14.1 MeV, 0.94Bq of ^{67}Cu / g of ^{nat}Zn is expected at EOB via the $^{67}Zn(n,p)^{67}Cu$ reaction. The remaining ^{67}Cu is hence formed via the $^{68}Zn(n,x)$ reaction, with a cross section of 4.71 ± 0.8 mb. Using these cross sections of $^{67}Zn(n,p)^{67}Cu$ and $^{68}Zn(n,x)^{67}Cu$ reactions at the end of 2 days irradiation, in a high flux of 10^{11} n/s cm^2, 164 MBq^{67}Cu (184 g ^{nat}Zn), can be obtained. This is comparable to 152 MBq^{67}Cu (184 g ^{nat}Zn), estimated using the cross sections of Konno *etal*.[175].

Spahn et al [48] have reported on the enhanced production possibility of $^{64,67}Cu$ via (n, p) reactions on Zn induced by spallation neutrons. Considering enriched$^{67,68}Zn$ targets, Kin *etal*.[165] have estimated 3 orders higher production yields of ^{67}Cu by fast neutrons from $^{nat}C(d,n)$ reaction with a deuteron beam of 40MeV energy and 5mA current. They report 249 GBq (184 g enriched ^{67}Zn) via the $^{67}Zn(n,p)^{67}Cu$ reaction and 287 GBq (186 g enriched ^{68}Zn) via the $^{68}Zn(n,x)^{67}Cu$ reaction at the end of 2 days of irradiation. These neutrons have a wide energy distribution from thermal energy to 40MeV with a most probable energy of 14 MeV [176]. Also the cross section of the $^{68}Zn(n,x)^{67}Cu$ reaction, is over 100 mb [165], in the higher energy region of 25–30 MeV, enabling larger production yields.

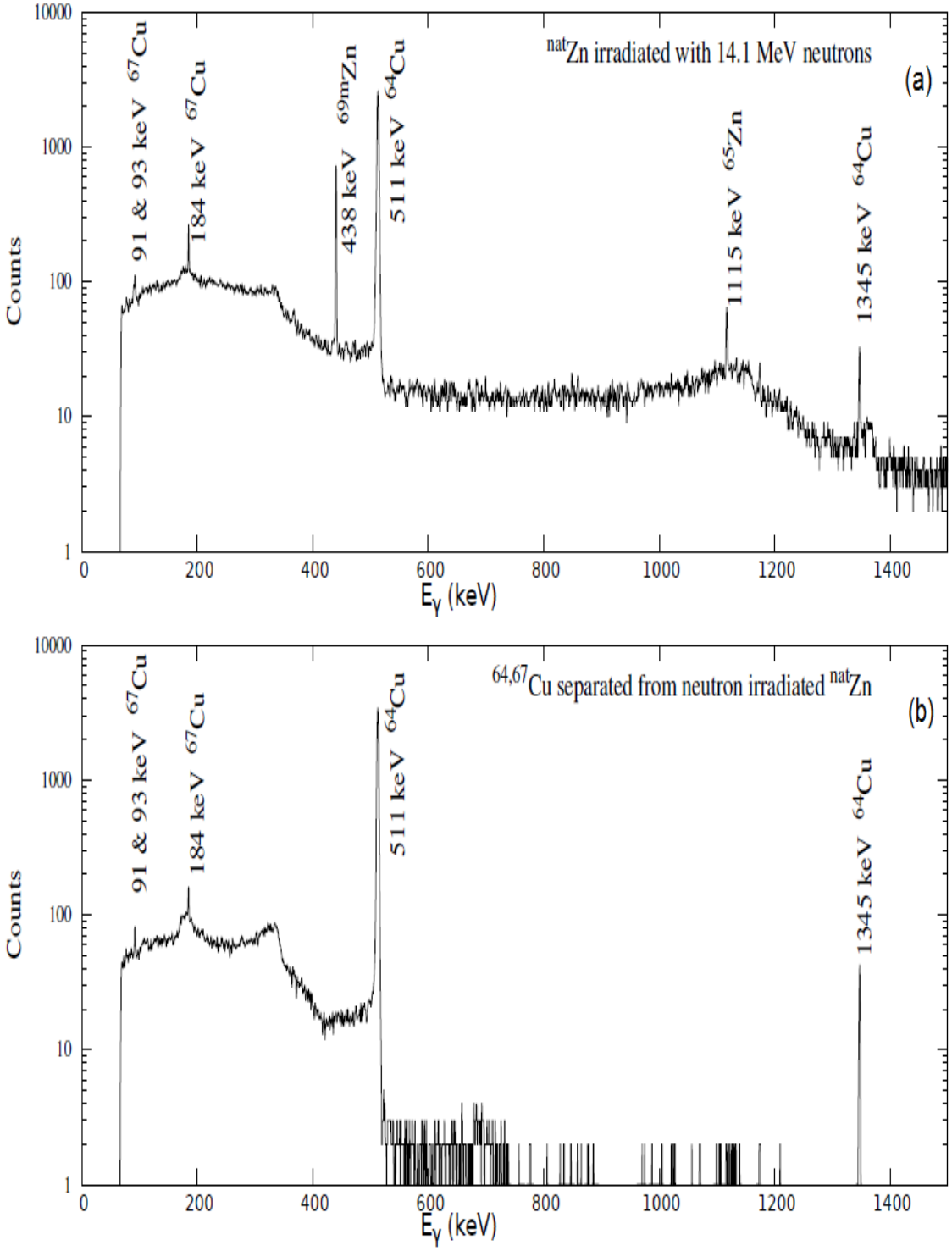

Fig 6.2: Gamma-ray spectra of irradiated ^{nat}Zn with 14.1 MeV neutrons (a) before and (b) after the radiochemical separation.

6.3.2 Production yields in photon induced reactions

As seen from Table 6.3 and Figure 6.3(a), in the photon irradiation with the bremsstrahlung end-point energy of 15 MeV on ^{nat}Zn, the radioisotopes ^{67}Cu,^{65}Zn and ^{69m}Zn were co-produced. From Table 6.3, it is seen that an EOB radioactivity of 2 kBq of ^{67}Cu per gram ^{nat}Zn was obtained in 45 minutes photon irradiation with the bremsstrahlung end-point energy of 15 MeV, despite the small cross section. The Giant Dipole region (GDR) of 10 -30 MeV is characterized by a high photo-absorption cross section and is suitable for radioisotope production.

Table 6.3: End of bombardment (EOB) activity of radioisotopes produced with the bremsstrahlung end-point energy of 15 MeV via the $^{nat}Zn(\gamma,p)$ reaction route with beam power 0.88kW and irradiation time 45 minutes.

Zn weight (g)	(kBq/ g) at end of bombardment (EOB)		
	^{67}Cu	^{69m}Zn	^{65}Zn
0.21	2.17±0.37	3.86±0.66	1.47±0.25
0.20	2.14±0.36	3.57±0.61	1.5±0.26

Considering a power of 1 kW, 30 MeV electron beam, hitting a 4 mm thick tungsten converter and a 1 g target of natural zinc, placed behind the converter, the activity of ^{67}Cu was estimated, by calculating the integral of the product of photon flux and the $^{68}Zn(\gamma,p)^{67}Cu$ reaction cross section (see Fig. 6.4). Geant4 simulations [177] were used to determine the photon flux. The activity of ^{67}Cu after 10 h of irradiation is estimated to be about 14 MBq /(g*kW). This prediction is comparable to the production rate of around 1 MBq/ (g*kW*h) [47].

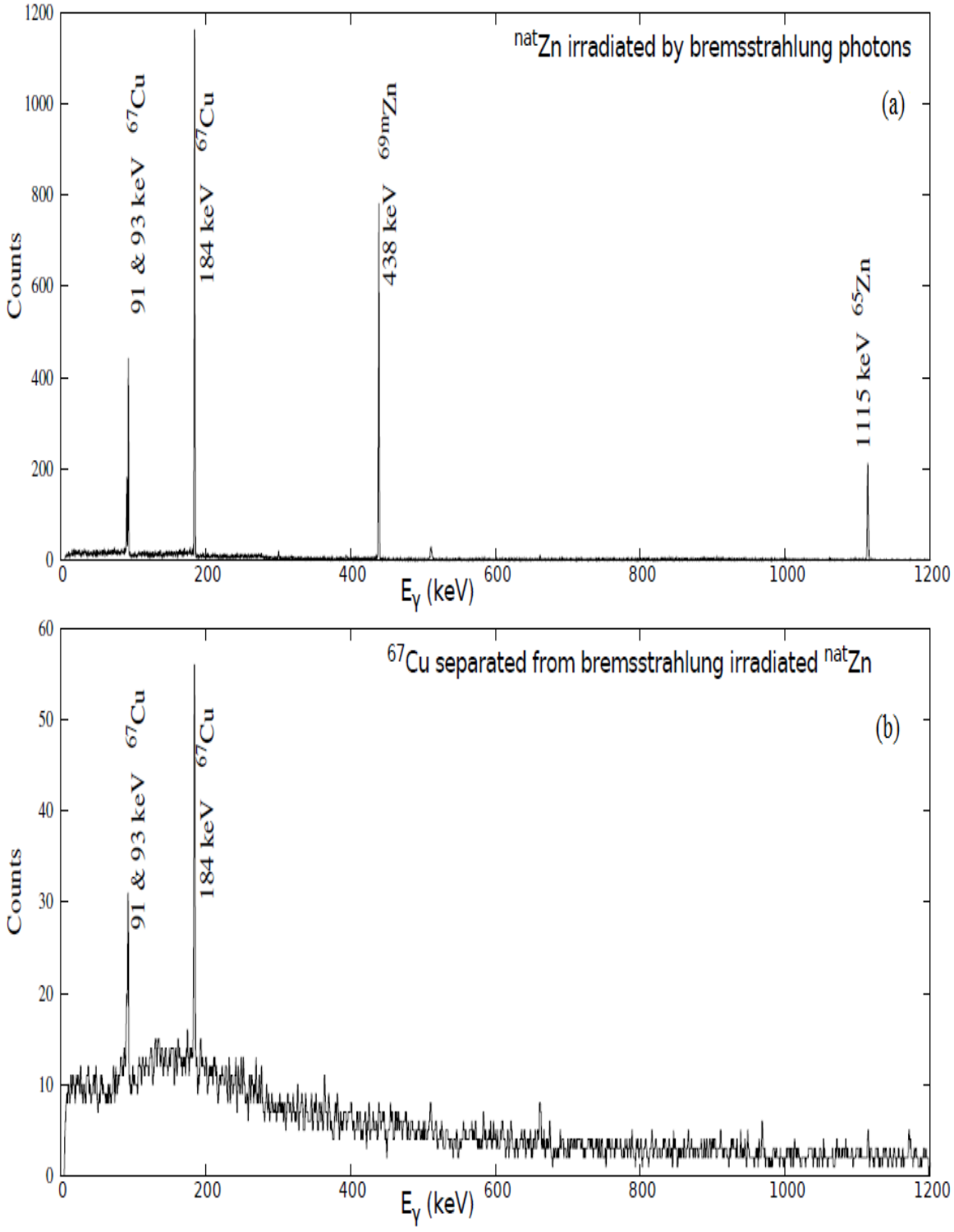

Fig 6.3: Gamma-ray spectra of irradiated ^{nat}Zn with the bremsstrahlung of end-point energy 15 MeV (a) before and (b) after the radiochemical separation.

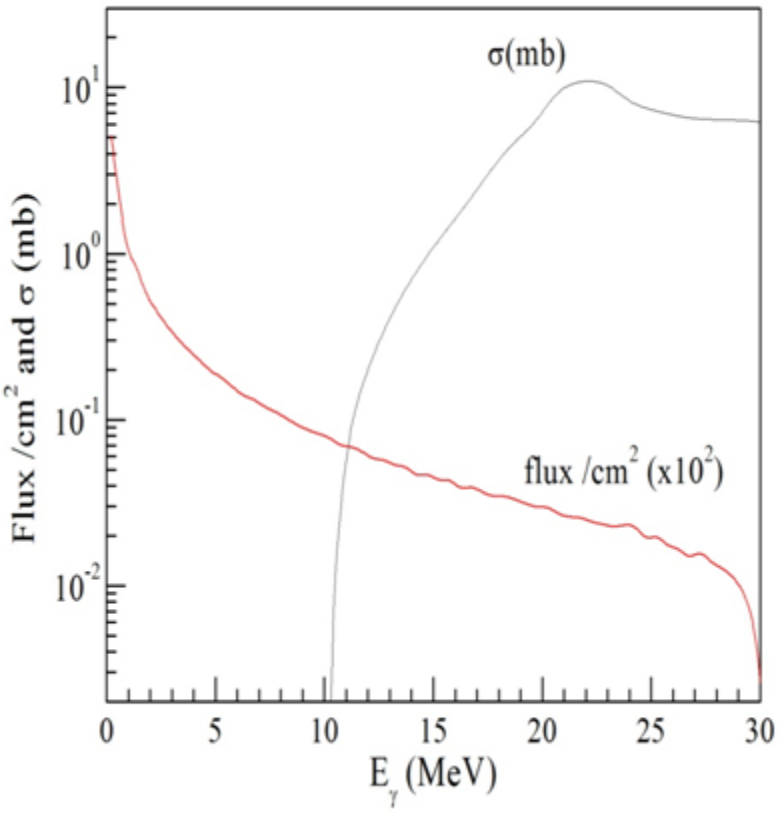

Fig 6.4: $^{68}Zn(\gamma,p)^{67}Cu$ reaction cross section σ (adopted from International Atomic Energy Agency(IAEA) Photonuclear Data Handbook) and simulated photon flux for the proposed 30MeV LINAC.

6.3.3 Purity of the product

The pH ranges for dithizonate formation of specific ions are Co: 6.5-10.5, Cu: 2- 5, Fe: 7.5-8.5, Ni: 6-9, and Zn: 6.5-9.5 [178]. Copper can be selectively complexed over other metals from dilute acidic solution if dithizone is dissolved in an immiscible medium, e.g. CCl_4, $CHCl_3$. The Cu is back extracted into an aqueous phase by the dissociation of Cu-chelate, by shaking the organic solution with 7 M HCl mixed with H_2O_2. A schematic diagram of the separation process is shown in Figure 6.5.

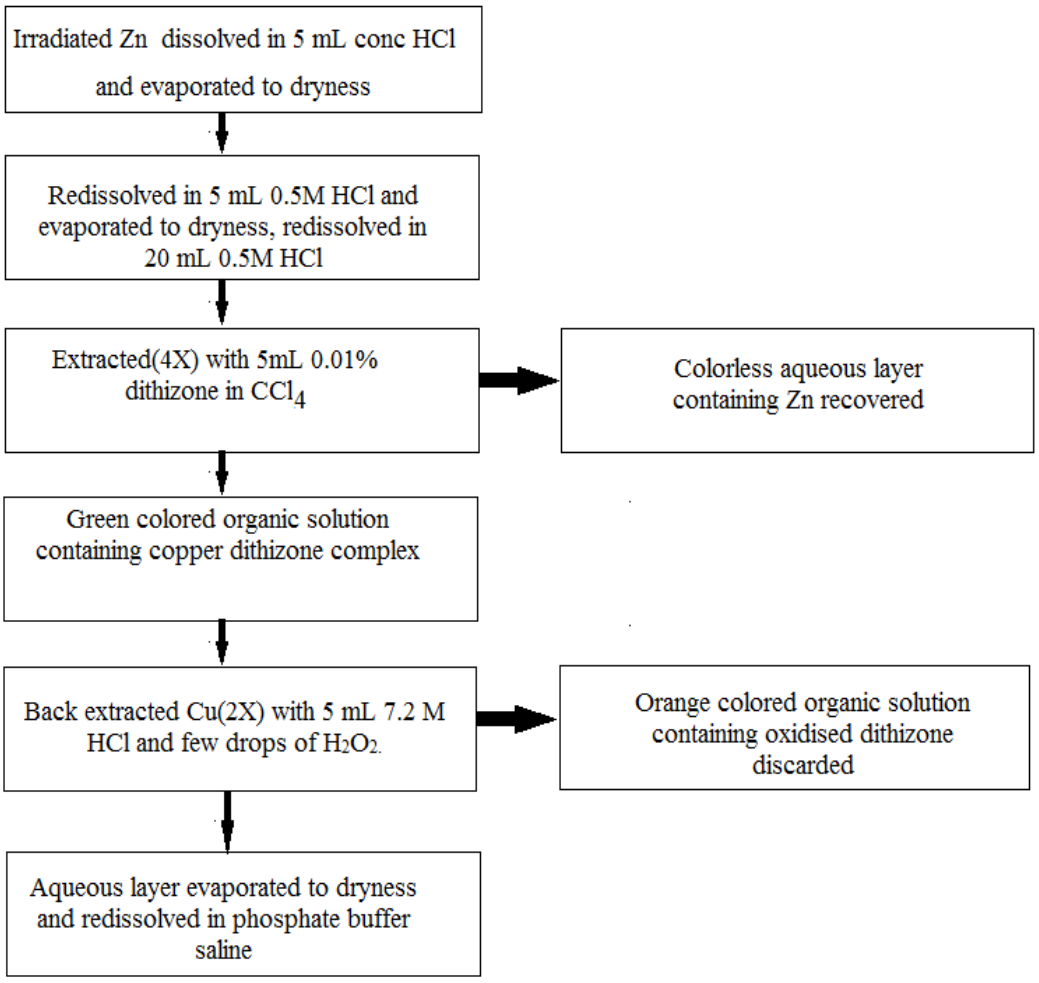

Fig 6.5: Schematic of the radiochemical separation process.

It can be seen from figures 6.2(b) and 6.3(b) that the radionuclide impurities ^{65}Zn and ^{69m}Zn are not detected in the final ^{67}Cu product, indicating achievement of high radionuclidic purity. The separation yield was determined radiometrically, by comparing the $^{64,67}Cu$ activity before and after separation. High separation yields of > 90% , with high radionuclidic purity and good reproducibility, were observed by adapting the procedure given in [152] with reduction of reagent volumes.Automation using the dithizone method [152] and a solid phase extraction

procedure [178] using a modified dithizone XAD-8 chelating resin have been reported for the purification of the Cu radionuclides, making this radiochemical separation procedure attractive.

6.4 Summary

Experimental investigations have been carried out on the production of a promising therapeutic radionuclide ^{67}Cu via the $^{67}Zn(n,p)^{67}Cu$, $^{68}Zn(n,x)^{67}Cu$, and $^{68}Zn(\gamma,p)^{67}Cu$ reaction routes. Natural Zn metal foils were irradiated with 14.1 MeV neutrons and bremsstrahlung of end-point energy 15 MeV. Radioactivity levels of ^{67}Cu and other radioisotopes co-produced were determined by the quantification of photo-peaks by off-line gamma-ray spectrometry. In order to have a final product of sufficient radionuclidic purity, the use of enriched target material is mandatory, followed by recovery of the target material, regardless of the reaction involved. No carrier added ^{67}Cu was separated from the irradiated Zinc by solvent extraction. Yields > 90 % and high levels of radionuclidic purity were achieved.

These studies indicate that the growth and development of intense fast neutron sources and photonuclear technology, will possibly aid in the sustained supply of ^{67}Cu.

Chapter 7

Conclusion and future works

7.1 Conclusion

Technetium-99m (^{99m}Tc) is the principal radioisotope used in medical diagnostics worldwide. ^{99}Mo/^{99m}Tc supply interruptions have necessitated development of alternate technologies to obtain ^{99}Mo/^{99m}Tc.

The direct production of ^{99m}Tc via ^{100}Mo(p,2n) route is among one of the alternative promising routes. However there are discrepancies in the cross section values of the ^{100}Mo (p,2n)^{99m}Tc reaction in the literature, and ^{9x}Tc isotopes (Tc-mix) inseparable from ^{99m}Tc are co-produced. The Tc-mix reduces the specific activity (SA) of ^{99m}Tc, potentially impacting the radiochemical quality of ^{99m}Tc-radiopharmaceuticals, and also cause an internal dose increase (DI), compared to pure ^{99m}Tc. The composition of the Tc-mix changes with cooling time, impacting the clinical shelf-life of the ^{99m}Tc. The aim of the study in chapter 2 was to optimise irradiation parameters and target composition for production of clinical grade ^{99m}Tc.

The ^{100}Mo(p,2n)^{99m}Tc cross section values was measured from E_p = 11.5 to 21 MeV and compared with literature data. The cross section values presented were consistent independent of time from EOB. This builds a confidence in the 140 keV peak γ-ray area corrections performed in this experiment.

The radiochemical purity of various Tc-radiopharmaceuticals mimicking different ratios of $\frac{N_{99m_{Tc}}}{N_{99(m+g)_{Tc}}}$ were evaluated. Labelling of Tc kits with $\frac{N_{99m_{Tc}}}{N_{99(m+all\ co-produced)_{Tc}}} \geq$ 10-11% with ^{99m}Tc activity suitable for 4 – 5 patient studies will ensure compliance with pharmacopoeia specifications.

In a theoretical approach, to maximise the yield of ^{99m}Tc and minimise the impurities, the beam energy, target thickness, target enrichment and composition, irradiation and cooling times were varied. The optimisation approach was validated by comparing thin target yields and published data [56, 70]. There is only minimal increase in thick target yields of ^{99m}Tc with enrichment. The thick target yields of ^{99}Mo and ^{99m}Tc increases with energy and irradiation time. There is a trade-off between the yield and thick target atoms ratio (Ar) = $\frac{N_{99m_{Tc}}}{N(99m_{Tc}+all\ co-produced\ Tc)}$ with increasing irradiation time and energy.

Rather than the absolute ^{100}Mo enrichment, the isotopic composition of the target, i.e the amount of stable impurities of ^{9x}Mo, should be considered as they play a significant role in the increase of the internal dose. From the study of the hypothetical cases of 99% enriched ^{100}Mo and 1% ^{9x}Mo impurity, it is understood that the impurities ^{94,95,96,97}Mo in the enriched ^{100}Mo contribute the maximum to the DI.

The criteria of dose increase, and decrease of specific activity, can be used to set the shelf life of the ^{99m}Tc obtained and accept/reject ^{100}Mo targets of various compositions. The shelf-life is defined as the maximum cooling time post EOB,

- where the Ar values are suitable for administering the ^{99m}Tc-radiopharmaceutial,
- the % content of co-produced ^{9x}Tc isotopes are below the specified limits,
- and DI values are < 10 % at 24 hours after administration.

Present study suggests a 6 hour irradiation, for thick targets of 24, 22, 18 to 8 MeV would limit the clinical shelf-lives to 3, 4.5, 5 hours post EOB , with ^{99m}Tc activities 1.8, 1.5, 0.85 GBq/μA at end of shelf-lives respectively.

Chapter 3 presents details of preparation of ^{99}Mo by the photonuclear reaction ^{100}Mo(γ, n) in high energy electron linear accelerators (linac), and of the separation of ^{99m}Tc from the irradiated Mo. The ^{nat}Mo samples for irradiation were in the form of Molybdenum trioxide

and in-house prepared Zirconium Molybdate. The typical elution yield of ^{99m}Tc from the irradiated molybdenum trioxide in the first pass via solvent extraction was in the range 70 to 75 %.

In an aid to reduce complexities in preparation of Zr^{99}Mo with ^{99}Mo [83], preformed natural zirconium molybdate was irradiated and converted to Zr^{99}Mo column generators. Elution of the column generator is a simpler separation procedure with minimal radioactive waste generation. Simplicity of utilisation of column generators has accelerated the spread and use of SPECT. The typical elution yield of ^{99m}Tc from the irradiated zirconium molybdate was in the range 19 to 43 %.

The evaluation of the quality of these ^{99m}Tc eluates with reference to the Indian Pharmacopeia (IP) pertechnetate monograph show that the eluates comply with the specifications of the IP. The eluates were of high radiochemical, chemical and radionuclidic purity. It may be noted, that the IP monograph is specific to $^{99m}TcO_4^-$ obtained following the decay of the parent ^{99}Mo which is, in turn, produced either via neutron bombardment of ^{98}Mo, or as a product of uranium fission.

The scaling up of ^{99}Mo–^{99m}Tc activity to clinical levels would be achievable with increase of target material, enrichment, beam power, irradiation time etc. SAMEER is setting up a 30 MV electon linac for radioisotope production in India.

In an assessment of long term technologies for supply of ^{99}Mo by alternative routes, production of ^{99}Mo via the ^{100}Mo(n, 2n)^{99}Mo reaction using fast neutrons from an accelerator [94] has been proposed. The (n,2n) reaction cross section is large, about 1.5 b at a neutron energy of 14 MeV, which is about ten times larger than the thermal neutron capture cross section of ^{98}Mo in a reactor. The ^{100}Mo(n,2n) reaction cross-section within the neutron energy ranges from the threshold energy (8.36 MeV) to 20.5 MeV only are available in EXFOR . Chapter 4 presents details of the determination of the ^{100}Mo(n,2n) reaction cross-

sections at the average neutron energies of 21.9 and 25.5 MeV generated by using the ^{9}Be(p,n) reaction at the MC50 cyclotron of the Korea Institute of Radiological and Medical Sciences (KIRAMS) at Seoul, South Korea. The cross sections have been determined by using an activation and off-line γ-ray spectrometric technique.The experimental results are in close agreement with the theoretical values from TALYS-1.8.

Commercialization of ^{99}Mo/^{99m}Tc production via the routes considered in the study would need implementation of ^{100}Mo recovery and reuse due to its limited availability.

Copper plays a role as a cofactor for numerous enzymes, such as Cu/Zn-superoxide dismutase, cytochrome c oxidase, tyrosinase, ceruloplasmin, and other proteins, crucial for respiration, iron transport and metabolism, cell growth, and hemostasis. The complexation chemistry of copper has been extensively studied, and chelators that are suitable for stable coordination of copper are available. Copper radionuclides offer a varying range of half-lives and decay modes suitable for molecular imaging applications (^{60}Cu, ^{61}Cu, ^{62}Cu, and ^{64}Cu), and in vivo targeted radiation therapy (^{64}Cu and ^{67}Cu).

The utilization of ^{64}Cu is mostly limited to studies, sourcing no carrier added ^{64}Cu, produced via ^{64}Ni(p, n)^{64}Cu reaction in a medical cyclotron. Chapter 5 in this study has investigated the potential of producing low specific activity (LSA) ^{64}Cu in an electron linac. The mixed field of photons along with the neutrons co-produced in the linac head via photonuclear processes, offers a dual reaction route for the production of ^{64}Cu, via the ^{63}Cu(n, γ)^{64}Cu + ^{65}Cu(γ,n)^{64}Cu reactions. Radioactivity of ^{64}Cu produced was about 13.5 ± 1.06 Bq per gram of ^{nat}Cu per gray-sec irradiation. The ^{64}Cu yield increased up to 46% after moderation of the neutrons by a solid water phantom RW3. The increase in yield of ^{64}Cu is primarily due to increased contribution via the route ^{63}Cu(n,γ)^{64}Cu. The 69.17% natural abundance of ^{63}Cu, and thermal neutron cross section of 4.1 b indicate favourable conditions for the production of reasonable amounts of ^{64}Cu activity. The production route of LSA ^{64}Cu, via (γ,n) + (n,γ)

interactions by irradiation of natural targets of Cu, obviates the need for costly targets and opens the possibility of an electron linac to produce ^{64}Cu as a cost saving measure for medical applications.

The copper transporter CTR1 has been found to mainly and specifically transport Cu(I) instead of Cu(II) [124]. However in the comparison study of the biological efficacy of LSA ^{64}Cu as ^{64}Cu(I)Cl and ^{64}Cu(II)Cl_2, in C57BL/6 mice bearing melanoma tumors in a B16F10 tumor model, no significant difference in biodistribution between ^{64}Cu(I) and ^{64}Cu(II) at 24 hours post injection was observed. LSA ^{64}Cu used in the animal study was prepared in the Dhruva research reactor, BARC, India via ^{63}Cu(n, γ)^{64}Cu. The tumor uptake of LSA ^{64}Cu(II) and ^{64}Cu(I) of 5.14 ± 0.52 and 4.71± 0.56 % injected dose / g at 24 hours post injection, was also comparable to the reported tumor uptake of high specific activity ^{64}Cu(II) and ^{64}Cu(I) [141]. This comparable tumor uptake of LSA ^{64}Cu ions to no carrier added ^{64}Cu ions should lower the cost of PET imaging.

Although reactor produced ^{64}Cu was used in the animal study, an accelerator offers advantages over a reactor – generation of reduced waste, much safer to operate, cheaper decommissioning costs and does not pose a nuclear weapon proliferation risk.

^{67}Cu is a promising therapeutic radionuclide, whose limiting factor for a more widespread application in clinical trials is its availability. As an aid to expand the availability of ^{67}Cu and to demonstrate the viability of the production processes, with development of fast spectral neutron sources and photonuclear technology, chapter 6 presents details of the production of ^{67}Cu via (a) the ^{67}Zn(n,p)^{67}Cu, ^{68}Zn(n,n'p)^{67}Cu and ^{68}Zn(n,d)^{67}Cu reaction routes by irradiating ^{nat}Zn foils with 14.1 MeV DT accelerator neutrons at the Purnima Neutron generator Facility, BARC, and (b) the ^{68}Zn(γ, p)^{67}Cu route by irradiating ^{nat}Zn foils with 15 MeV bremsstrahlung in a prototype LINAC at SAMEER. No carrier added ^{67}Cu was

separated from the irradiated Zinc by solvent extraction. Separation yields > 90 % and high levels of radionuclidic purity were achieved.

The radioisotopes ^{67}Cu and ^{64}Cu are a theranostic pair [5, 45], as the availability of ^{64}Cu enables PET pretherapy imaging, and a measure of the uptake, thereby, tailoring an accurate dose calculation related to therapy with ^{67}Cu.The concept of personalized medicine and targeted radiation therapy is becoming increasingly clinically relevant and the ensured supply and availability of ^{64,67}Cu will aid in the same.

7.2 Future work

Recycling of enriched ^{100}Mo targets would be mandatory for viable commercial operations. Simple and reliable methods of recycling with an understanding on the number of times, a recycled target can be irradiated to obtain pharmacopeia grade ^{99m}Tc, would need to be worked out. Development of new materials with higher Mo affinity and / or post elution concentration techniques will enable inclusion of LSA ^{99}Mo, produced via proton, photon, or neutron activation in routine use.

Human copper transporter 1 (CTR1) is overexpressed in a variety of cancers. The validation / equivalence of LSA ^{64}Cu to no carrier added ^{64}Cu in these cancers, would be necessary to enable acceptance and widespread utilisation of LSA ^{64}Cu. Development of new copper complexes for therapy, and further investigation into the potential of theranostic pairing of ^{64}Cu and ^{67}Cu would need to be carried out.

References

[1] G. Stöcklin, S. Qaim, F. Rösch, The Impact of Radioactivity on Medicine Metallic, Radiochimica Acta, 70 (1995) 249-272.

[2] S.M. Qaim, Nuclear data for medical radionuclides, Journal of radioanalytical and nuclear chemistry, 305 (2015) 233-245.

[3] S.M. Qaim, The present and future of medical radionuclide production, Radiochimica Acta, 100 (2012) 635-651.

[4] S.M. Qaim, Therapeutic radionuclides and nuclear data, Radiochimica Acta, 89 (2001) 297-304.

[5] F. Rösch, H. Herzog, S.M. Qaim, The beginning and development of the theranostic approach in nuclear medicine, as exemplified by the radionuclide pair 86Y and 90Y, Pharmaceuticals, 10 (2017) 56.

[6] S.M. Qaim, B. Scholten, B. Neumaier, New developments in the production of theranostic pairs of radionuclides, Journal of Radioanalytical and Nuclear Chemistry, (2018) 1-17.

[7] M.L. James, S.S. Gambhir, A molecular imaging primer: modalities, imaging agents, and applications, Physiological reviews, 92 (2012) 897-965.

[8] W.C. Eckelman, Unparalleled contribution of technetium-99m to medicine over 5 decades, JACC: Cardiovascular Imaging, 2 (2009) 364-368.

[9] R. Boyd, Technetium generators: status and prospects, Radiochimica Acta, 41 (1987) 59-64.

[10] V.J. Molinski, A review of 99mTc generator technology, The International Journal of Applied Radiation and Isotopes, 33 (1982) 811-819.

[11] J. Mallol, I. Zolle, Preparation of Technetium 99m Tc Pharmaceuticals, in: Technetium-99m Pharmaceuticals, Springer, 2007, pp. 95-98.

[12] E. Bradley, Non-HEU production technologies for molybdenum-99 and technetium-99m, International Atomic Energy Agency, 2013.

[13] T. Ruth, Accelerating production of medical isotopes, Nature, 457 (2009) 536.

[14] M. Pillai, A. Dash, F. Knapp Jr, Sustained availability of 99mTc: possible paths forward, J Nucl Med, 54 (2013) 313-323.

[15] H. Naik, S. Suryanarayana, K. Jagadeesan, S. Thakare, P. Joshi, V. Nimje, K. Mittal, A. Goswami, V. Venugopal, S. Kailas, An alternative route for the preparation of the medical isotope 99Mo from the 238U (γ, f) and 100Mo (γ, n) reactions, Journal of Radioanalytical and Nuclear Chemistry, 295 (2013) 807-816.

[16] National Research Council Medical isotope production without highly enriched uranium, National Academies Press, 2009.

[17] J. Beaver, H. Hupf, Production of 99mTc on a medical cyclotron: a feasibility study, Journal of Nuclear Medicine, 12 (1971) 739.

[18] S. Qaim, S. Sudár, B. Scholten, A. Koning, H. Coenen, Evaluation of excitation functions of 100Mo (p, d+ pn) 99Mo and 100Mo (p, 2n) 99mTc reactions: estimation of long-lived Tc-impurity and its

implication on the specific activity of cyclotron-produced 99mTc, Applied Radiation and Isotopes, 85 (2014) 101-113.
[19] S.M. Qaim, J.C. Clark, C. Crouzel, M. Guillaume, H.J. Helmeke, B. Nebeling, V.W. Pike, G. Stöcklin, PET radionuclide production, in: Radiopharmaceuticals for positron emission tomography, Springer, 1993, pp. 1-43.
[20] IAEA, Cyclotron Produced Radionuclides: Emerging Positron Emitters for Medical Applications: 64Cu and 124I, INTERNATIONAL ATOMIC ENERGY AGENCY,, AEA Radioisotopes and Radiopharmaceuticals (2016).
[21] D.W. McCarthy, R.E. Shefer, R.E. Klinkowstein, L.A. Bass, W.H. Margeneau, C.S. Cutler, C.J. Anderson, M.J. Welch, Efficient production of high specific activity 64Cu using a biomedical cyclotron, Nuclear medicine and biology, 24 (1997) 35-43.
[22] F. Szelecsényi, G. Blessing, S. Qaim, Excitation functions of proton induced nuclear reactions on enriched 61Ni and 64Ni: possibility of production of no-carrier-added 61Cu and 64Cu at a small cyclotron, Applied Radiation and Isotopes, 44 (1993) 575-580.
[23] K.R. Zinn, T.R. Chaudhuri, T.P. Cheng, J. Steven Morris, W.A. Meyer Jr, Production of no-carrier-added 64Cu from zinc metal irradiated under boron shielding, Cancer, 73 (1994) 774-778.
[24] K. Vimalnath, A. Rajeswari, K. Jagadeesan, C. Viju, P. Joshi, M. Venkatesh, Studies on the production feasibility of 64Cu by (n, p) reactions on Zn targets in Dhruva research reactor, Journal of Radioanalytical and Nuclear Chemistry, 294 (2012) 43-47.
[25] Z. Cai, C.J. Anderson, Chelators for copper radionuclides in positron emission tomography radiopharmaceuticals, Journal of labelled compounds and radiopharmaceuticals, 57 (2014) 224-230.
[26] C.J. Anderson, R. Ferdani, Copper-64 radiopharmaceuticals for PET imaging of cancer: advances in preclinical and clinical research, Cancer Biotherapy and Radiopharmaceuticals, 24 (2009) 379-393.
[27] K. Hilgers, S. Sudár, S. Qaim, Experimental study and nuclear model calculations on the 192Os (p, n) 192Ir reaction: Comparison of reactor and cyclotron production of the therapeutic radionuclide 192Ir, Applied radiation and isotopes, 63 (2005) 93-98.
[28] G.S. Merrick, W.M. Butler, A.T. Dorsey, H.L. Walbert, Prostatic conformal brachytherapy: 125I/103Pd postoperative dosimetric analysis, Radiation Oncology Investigations: Clinical and Basic Research, 5 (1997) 305-313.
[29] R.M. Lambrecht, S. Mirzadeh, Cyclotron isotopes and radiopharmaceuticals—XXXV astatine-211, The International journal of applied radiation and isotopes, 36 (1985) 443-450.
[30] M. R Zalutsky, M. Pruszynski, Astatine-211: production and availability, Current radiopharmaceuticals, 4 (2011) 177-185.
[31] R.W. Atcher, A.M. Friedman, J.J. Hines, An improved generator for the production of 212Pb and 212Bi from 224Ra, International Journal of Radiation Applications and Instrumentation. Part A. Applied Radiation and Isotopes, 39 (1988) 283-286.

[32] M.R. McDevitt, R.D. Finn, G. Sgouros, D. Ma, D.A. Scheinberg, An 225Ac/213Bi generator system for therapeutic clinical applications: construction and operation, Applied Radiation and Isotopes, 50 (1999) 895-904.
[33] F.R. Knapp Jr, S. Mirzadeh, A. Beets, M. O'doherty, P.J. Blower, E. Verdera, J. Gaudiano, J. Kropp, J. Guhlke, H. Palmedo, Reactor-produced radioisotopes from ORNL for bone pain palliation, Applied radiation and isotopes, 49 (1998) 309-315.
[34] F. Rösch, Radionuclide Generator Systems for PET, Der Nuklearmediziner, 27 (2004) 227-236.
[35] A. Dash, F. F Russ Knapp, M. RA Pillai, Targeted radionuclide therapy-an overview, Current radiopharmaceuticals, 6 (2013) 152-180.
[36] A.I. Kassis, S.J. Adelstein, Radiobiologic principles in radionuclide therapy, Journal of Nuclear Medicine, 46 (2005) 4S-12S.
[37] J. L Parus, R. Mikolajczak, Beta-emitting radionuclides for peptide receptor radionuclide therapy, Current topics in medicinal chemistry, 12 (2012) 2686-2693.
[38] L. Bodei, Cremonesi, M., Grana, C.M., Fazio, N., Iodice, S., Baio, S.M., Bartolomei, M., Lombardo, D., Ferrari, M.E., Sansovini, M. and Chinol, M.,, Peptide receptor radionuclide therapy with 177 Lu-DOTATATE: the IEO phase I-II study., European journal of nuclear medicine and molecular imaging, 38 (2011) 2125-2135.
[39] R.B. Wilder, G.L. DeNardo, S.J. DeNardo, Radioimmunotherapy: recent results and future directions, Journal of clinical oncology, 14 (1996) 1383-1400.
[40] M.R. Zalutsky, D.A. Reardon, O.R. Pozzi, G. Vaidyanathan, D.D. Bigner, Targeted α-particle radiotherapy with 211At-labeled monoclonal antibodies, Nuclear medicine and biology, 34 (2007) 779-785.
[41] D. Handkiewicz-Junak, T.D. Poeppel, L. Bodei, C. Aktolun, S. Ezziddin, F. Giammarile, R.C. Delgado-Bolton, M. Gabriel, EANM guidelines for radionuclide therapy of bone metastases with beta-emitting radionuclides, European journal of nuclear medicine and molecular imaging, 45 (2018) 846-859.
[42] L. Bodei, A.I. Kassis, S.J. Adelstein, G. Mariani, Radionuclide therapy with iodine-125 and other auger–electron-emitting radionuclides: Experimental models and clinical applications, Cancer Biotherapy and Radiopharmaceuticals, 18 (2003) 861-877.
[43] P.J. Blower, J.S. Lewis, J. Zweit, Copper radionuclides and radiopharmaceuticals in nuclear medicine, Nuclear medicine and biology, 23 (1996) 957-980.
[44] A.M. Johnsen, B.J. Heidrich, C.B. Durrant, A.J. Bascom, K. Ünlü, Reactor production of 64Cu and 67Cu using enriched zinc target material, Journal of Radioanalytical and Nuclear Chemistry, 305 (2015) 61-71.
[45] S.M. Qaim, Nuclear data for production and medical application of radionuclides: present status and future needs, Nuclear medicine and biology, 44 (2017) 31-49.

[46] A. Deshpande, Dixit,T., Krishnan, R, Conceptual design of linac based radio isotope generation system, Proceedings of the seventh DAE-BRNS Indian particle accelerator conference , Bhabha Atomic Research Centre, India InPAC (2015,) ID 272.
[47] V.N. Starovoitova, L. Tchelidze, D.P. Wells, Production of medical radioisotopes with linear accelerators, Applied Radiation and Isotopes, 85 (2014) 39-44.
[48] I. Spahn, H.H. Coenen, S.M. Qaim, Enhanced production possibility of the therapeutic radionuclides 64Cu, 67Cu and 89Sr via (n, p) reactions induced by fast spectral neutrons, Radiochimica Acta, 92 (2004) 183-186.
[49] J.F. Ziegler, M.D. Ziegler, J.P. Biersack, SRIM–The stopping and range of ions in matter (2010), Nuclear Instruments and Methods in Physics Research Section B: Beam Interactions with Materials and Atoms, 268 (2010) 1818-1823.
[50] P. Mountford, D. Temperton, Recommendations of the international commission on radiological protection (ICRP) 1990, in, Springer, 1992.
[51] R. Loevinger, T.F. Budinger, E.E. Watson, MIRD primer for absorbed dose calculations, Society of Nuclear Medicine, 1988.
[52] W.E. Bolch, K.F. Eckerman, G. Sgouros, S.R. Thomas, MIRD pamphlet No. 21: a generalized schema for radiopharmaceutical dosimetry--standardization of nomenclature, Journal of Nuclear Medicine, 50 (2009) 477.
[53] A. Gopalakrishna, H. Naik, S. Suryanarayana, Y. Naik, V. Nimje, B. Nayak, S. Sarkar, S. Padmanabhan, C. Kothalkar, P. Naskar, Preparation of 99 Mo from the 100 Mo (γ, n) reaction and chemical separation of 99m Tc, Journal of Radioanalytical and Nuclear Chemistry, 308 (2016) 431-438.
[54] Y. Nagai, Y. Hatsukawa, Production of 99Mo for Nuclear Medicine by 100Mo (n, 2 n) 99Mo, Journal of the Physical Society of Japan, 78 (2009) 033201.
[55] A. Gopalakrishna, G. Kim, H. Naik, K. Kim, B. Nayak, M. Zaman, Measurement of 99 Mo production cross-section from the 100 Mo (n, 2n) reaction with quasi monoenergetic neutron based on the 9 Be (p, n) reaction, Journal of Radioanalytical and Nuclear Chemistry, (2018) 1-9.
[56] J. Andersson, B. Thomas, S. Selivanova, E. Berthelette, J. Wilson, A. McEwan, K. Gagnon, Robust high-yield~ 1 TBq production of cyclotron based sodium [99mTc] pertechnetate, Nuclear medicine and biology, 60 (2018) 63-70.
[57] F. Bénard, K.R. Buckley, T.J. Ruth, S.K. Zeisler, J. Klug, V. Hanemaayer, M. Vuckovic, X. Hou, A. Celler, J.-P. Appiah, Implementation of multi-curie production of 99mTc by conventional medical cyclotrons, J Nucl Med, 55 (2014) 1017-1022.
[58] M.C. Lagunas-Solar, P.M. Kiefer, O.F. Carvacho, C.A. Lagunas, Y.P. Cha, Cyclotron production of NCA 99mTc and 99Mo. An alternative non-reactor supply source of instant 99mTc and 99Mo→ 99mTc generators, International Journal of Radiation Applications and Instrumentation. Part A. Applied Radiation and Isotopes, 42 (1991) 643-657.

[59] B. Scholten, R.M. Lambrecht, M. Cogneau, H.V. Ruiz, S.M. Qaim, Excitation functions for the cyclotron production of 99mTc and 99Mo, Applied radiation and isotopes, 51 (1999) 69-80.
[60] S. Takács, Z. Szűcs, F. Tárkányi, A. Hermanne, M. Sonck, Evaluation of proton induced reactions on 100Mo: New cross sections for production of 99mTc and 99Mo, Journal of Radioanalytical and Nuclear Chemistry, 257 (2003) 195-201.
[61] M. Khandaker, M. Uddin, K. Kim, Y. Lee, G. Kim, Measurement of cross-sections for the (p, xn) reactions in natural molybdenum, Nuclear Instruments and Methods in Physics Research Section B: Beam Interactions with Materials and Atoms, 262 (2007) 171-181.
[62] O. Lebeda, M. Pruszyński, New measurement of excitation functions for (p, x) reactions on natMo with special regard to the formation of 95mTc, 96m+ gTc, 99mTc and 99Mo, Applied radiation and isotopes, 68 (2010) 2355-2365.
[63] F. Tárkányi, F. Ditrói, A. Hermanne, S. Takács, A. Ignatyuk, Investigation of activation cross-sections of proton induced nuclear reactions on natMo up to 40 MeV: New data and evaluation, Nuclear Instruments and Methods in Physics Research Section B: Beam Interactions with Materials and Atoms, 280 (2012) 45-73.
[64] K. Gagnon, F. Bénard, M. Kovacs, T.J. Ruth, P. Schaffer, J.S. Wilson, S.A. McQuarrie, Cyclotron production of 99mTc: experimental measurement of the 100Mo (p, x) 99Mo, 99mTc and 99gTc excitation functions from 8 to 18 MeV, Nuclear medicine and biology, 38 (2011) 907-916.
[65] S. Manenti, U. Holzwarth, M. Loriggiola, L. Gini, J. Esposito, F. Groppi, F. Simonelli, The excitation functions of 100Mo (p, x) 99Mo and 100Mo (p, 2n) 99mTc, Applied Radiation and Isotopes, 94 (2014) 344-348.
[66] J. Cervenák, O. Lebeda, Experimental cross-sections for proton-induced nuclear reactions on natMo, Nuclear Instruments and Methods in Physics Research B, 380 (2016) 32-49.
[67] A. Celler, X. Hou, F. Bénard, T. Ruth, Theoretical modeling of yields for proton-induced reactions on natural and enriched molybdenum targets, Physics in Medicine & Biology, 56 (2011) 5469.
[68] O. Lebeda, E.J. van Lier, J. Štursa, J. Ráliš, A. Zyuzin, Assessment of radionuclidic impurities in cyclotron produced 99mTc, Nuclear medicine and biology, 39 (2012) 1286-1291.
[69] X. Hou, A. Celler, J. Grimes, F. Benard, T. Ruth, Theoretical dosimetry estimations for radioisotopes produced by proton-induced reactions on natural and enriched molybdenum targets, Physics in Medicine & Biology, 57 (2012) 1499.
[70] S.V. Selivanova, É. Lavallée, H. Senta, L. Caouette, J.A. Sader, E.J. van Lier, A. Zyuzin, J.E. van Lier, B. Guérin, É. Turcotte, Radioisotopic purity of sodium pertechnetate 99mTc produced with a medium-energy cyclotron: implications for internal radiation dose, image quality, and release specifications, J. Nucl. Med, 56 (2015) 1600-1608.
[71] IAEA, Charged-particle cross section database for medical radioisotope production, Monitor reactions. http://www-nds.iaea.org/medical/monitor_reactions.html (2009).
[72] NNDC, Information extracted from the NuDat2 Database, National Nuclear Data Center Available athttp://www.nndc.bnl.gov/nudat2/ (2016).

[73] M.K. Das, S.S. Das, M.A. Nayer, S. Chattopadhyay, L. Barua, S. Datta, Separation of Mo from Nb, Zr and Y: applicability in the purification of the recovered enriched 100 Mo used in the direct production of 99m Tc in cyclotrons, Journal of Radioanalytical and Nuclear Chemistry, 311 (2017) 643-647.

[74] M. Lamson, C.E. Hotte, R.D. Ice, Practical generator kinetics, Journal of Nuclear Medicine Technology, 4 (1976) 21-27.

[75] Z.B. Alfassi, F. Groppi, M.L. Bonardi, J.J. de Goeij, On the “artificial” nature of Tc and the “carrier-free” nature of 99mTc from 99Mo/99mTc generators, Applied radiation and isotopes, 63 (2005) 37-40.

[76] A. Koning, S. Hilaire, M. Duijvestijn, TALYS-1.8, A nuclear reaction program, NRG-1755 ZG petten. The Netherlands http://www.talys.eu, (2015).

[77] M.G. Stabin, R.B. Sparks, E. Crowe, OLINDA/EXM: the second-generation personal computer software for internal dose assessment in nuclear medicine, The Journal of Nuclear Medicine, 46 (2005) 1023.

[78] Radiation dose to patients from radiopharmaceuticals, Annals of the ICRP Publication 53, 18 (1987).

[79] J.C. Hung, T.J. Herold, M.E. Wilson, R.J. Gibbons, Generator eluate effects on the labeling efficiency of 99mTc-sestamibi, Nuclear medicine and biology, 22 (1995) 949-951.

[80] X. Hou, J. Tanguay, K. Buckley, P. Schaffer, F. Bénard, T. Ruth, A. Celler, Molybdenum target specifications for cyclotron production of 99mTc based on patient dose estimates, Physics in Medicine & Biology, 61 (2015) 542.

[81] Y. Danon, R. Block, R. Testa, H. Moore, Medical isotope production using a 60 MeV linear electron accelerator, TRANSACTIONS-AMERICAN NUCLEAR SOCIETY, 98 (2008) 894.

[82] H.Beil, R.Bergere, P.Carlos, A. Lepretre, A.De Miniac, A.Vevssiere,) A study of the photoneutron contribution to the giant dipole resonance in doubly even Mo isotopes, Nucl Phys A 227 (1974) 427

[83] P. Saraswathy, S. Sarkar, R. Patel, S. Arora, D. Narasimhan, 99m Tc gel generators based on 33zirconium molybdate-99 Mo. Pt. 1. Process standardisation for production, Radiochimica Acta, 83 (1998) 97-102.

[84] P. Saraswathy, S. Sarkar, R. Patel, S. Arora, G. Arjun, D. Narasimhan, N. Ramamoorthy, Evaluation of preparation and performance of gel column 99 Tc m generators based on zirconium molybdate-99 Mo, in, 1998.

[85] P. Saraswathy, S. Sarkar, N. Ramamoorthy, G. Arjun, R. Patel, 99mTc gel generators based on zirconium molybdate-99Mo: II. Evaluation of preparation and performance, Radiochimica Acta, 83 (1998) 103-107.

[86] S. Sarkar, P. Saraswathy, G. Arjun, N. Ramamoorthy, High radioactive concentration of 99mTc from a zirconium [99Mo] molybdate gel generator using an acidic alumina column for purification and concentration, Nuclear medicine communications, 25 (2004) 609-614.

[87] S.K. Sarkar, C. Kothalkar, P. Naskar, S. Joshi, P. Saraswathy, A.C. Dey, G.L. Vispute, V.V. Murhekar, N. Pilkhwal, Indigenous technology development and standardization of the process for obtaining ready to use sterile sodium pertechnetate-Tc-99m solution from Geltech generator, Indian journal of nuclear medicine: IJNM: the official journal of the Society of Nuclear Medicine, India, 28 (2013) 70.
[88] E. Browne, R. Firestone, V. Shirley, Table of radioactive isotopes. 1986.
[89] F. Monroy-Guzman, L. Díaz-Archundia, A.C. Ramírez, Effect of Zr: Mo ratio on 99mTc generator performance based on zirconium molybdate gels, Applied radiation and isotopes, 59 (2003) 27-34.
[90] M. Davarpanah, S.A. Nosrati, M. Fazlali, M.K. Boudani, H. Khoshhosn, M.G. Maragheh, Influence of drying conditions of zirconium molybdate gel on performance of 99mTc gel generator, Applied Radiation and Isotopes, 67 (2009) 1796-1801.
[91] L.V. So, Preparation of chromatographic and solid-solvent extraction exp 99 m Tc generators using gel-type targets, in: 1999 Workshop on the Utilization of Research Reactors, Tokai & Mito, Japan, 1999.
[92] R. Galea, C. Ross, R. Wells, Reduce, reuse and recycle: A green solution to Canada's medical isotope shortage, Applied Radiation and Isotopes, 87 (2014) 148-151.
[93] K. Gagnon, J. Wilson, C. Holt, D. Abrams, A. McEwan, D. Mitlin, S. McQuarrie, Cyclotron production of 99mTc: recycling of enriched 100Mo metal targets, Applied Radiation and Isotopes, 70 (2012) 1685-1690.
[94] OECD, The Supply of Medical Radioisotopes: An Economic Study of the Molybdenum-99 Supply Chain, NEA, 6967 (2010).
[95] F. Minato, Y. Nagai, Estimation of Production Yield of 99Mo for Medical Use using Neutrons from natC (d, n) at E d= 40 MeV, Journal of the Physical Society of Japan, 79 (2010) 093201.
[96] M. Fadil, B. Rannou, About the production rates and the activation of the uranium carbide target for SPIRAL 2, Nuclear Instruments and Methods in Physics Research Section B: Beam Interactions with Materials and Atoms, 266 (2008) 4318-4321.
[97] K. Hashimoto, Y. Nagai, M. Kawabata, N. Sato, Y. Hatsukawa, H. Saeki, S. Motoishi, M. Ohta, C. Konno, K. Ochiai, SPECT Imaging of Mice with 99mTc-Radiopharmaceuticals Obtained from 99Mo Produced by 100Mo (n, 2 n) 99Mo and Fission of 235U, Journal of the Physical Society of Japan, 84 (2015) 043202.
[98] IAEA-EXFOR, Database, http://www-nds.iaea.org/exfor/.
[99] M. Rahman, S. Qaim, Excitation functions of some neutron threshold reactions on isotopes of molybdenum, Nuclear Physics A, 435 (1985) 43-53.
[100] X. Kong, Y. Wang, J. Yuan, J. Yang, X. Wang, J. Wang, The cross section measurements for 100 Mo (n, 2n) 99 Mo, 96 Mo (n, p) 96 Nb and 92 Mo (n, α) 89m+ g Zr reactions, Physica Energiae Fortis et Physica Nuclearis, 15 (1991) 549-555.

[101] P. Reimer, V. Avrigeanu, S. Chuvaev, A. Filatenkov, T. Glodariu, A. Koning, A. Plompen, S. Qaim, D. Smith, H. Weigmann, Reaction mechanisms of fast neutrons on stable Mo isotopes below 21 MeV, Physical Review C, 71 (2005) 044617.
[102] V. Semkova, B. Pritychenko, Summary Report of the Workshop on the Experimental Nuclear Reaction Data Database, in, International Atomic Energy Agency, 2014.
[103] A. Filatenkov, Neutron activation cross sections measured at KRI in neutron energy region 13.4–14.9 MeV, Report, USSR report to the INDC, (2016).
[104] A. Marcinkowski, K. Stankiewicz, U. Garuska, M. Herman, Cross sections of fast neutron induced reactions on molybdenum isotopes, Zeitschrift für Physik A Atomic Nuclei, 323 (1986) 91-96.
[105] T.D. Thiep, N. Van Do, T.T. An, N.N. Son, Nuclear reactions with 14 MeV neutrons and bremsstrahlungs in giant dipole resonance (GDR) region using small accelerators, Nuclear Physics A, 722 (2003) C568-C572.
[106] S. Badwar, R. Ghosh, B.M. Lawriniang, V. Vansola, Y. Sheela, H. Naik, Y. Naik, S.V. Suryanarayana, B. Jyrwa, S. Ganesan, Measurement of formation cross-section of 99Mo from the 98Mo (n, γ) and 100Mo (n, 2n) reactions, Applied Radiation and Isotopes, 129 (2017) 117-123.
[107] H. Naik, G. Kim, K. Kim, M. Zaman, M. Nadeem, M. Sahid, Neutron-induced reaction cross-sections of 93Nb with fast neutron based on 9Be (p, n) reaction, Nuclear Physics A, 970 (2018) 156-168.
[108] E. Browne, J. Tuli, Nuclear Data Sheets for A= 99, Nuclear Data Sheets, 145 (2017) 25-340.
[109] V.P. Chechev, M.-M. Bé, Radioactive equilibrium: 99Mo/99mTc decay characteristics, Applied Radiation and Isotopes, 87 (2014) 132-136.
[110] R.B. Firestone, Nuclear data sheets for A= 24, Nuclear Data Sheets, 108 (2007) 2319-2392.
[111] J.S. Hendricks, G.W. McKinney, M.L. Fensin, M.R. James, R.C. Johns, J.W. Durkee, J.P. Finch, D.B. Pelowitz, L.S. Waters, M.W. Johnson, MCNPX 2.6. 0 Extensions, Los Alamos National Laboratory, (2008).
[112] http://www.nds.iaea.org/exfor.
[113] M. Chadwick, M. Herman, P. Obložinský, M.E. Dunn, Y. Danon, A. Kahler, D.L. Smith, B. Pritychenko, G. Arbanas, R. Arcilla, ENDF/B-VII. 1 nuclear data for science and technology: cross sections, covariances, fission product yields and decay data, Nuclear data sheets, 112 (2011) 2887-2996.
[114] Z. Ge, Z. Zhao, H. Xia, Y. Zhuang, T. Liu, J. Zhang, H. Wu, The updated version of Chinese evaluated nuclear data library (CENDL-3.1), J. Korean Phys. Soc, 59 (2011) 1052-1056.
[115] A. Koning, E. Bauge, C. Dean, E. Dupont, U. Fischer, R. Forrest, R. Jacqmin, H. Leeb, M. Kellett, R. Mills, Status of the JEFF nuclear data library, J. Korean Phys. Soc, 59 (2011) 1057-1062.
[116] K. Shibata, O. Iwamoto, T. Nakagawa, N. Iwamoto, A. Ichihara, S. Kunieda, S. Chiba, K. Furutaka, N. Otuka, T. Ohsawa, JENDL-4.0: a new library for nuclear science and engineering, Journal of Nuclear Science and Technology, 48 (2011) 1-30.

[117] M. Herman, M. Herman, R. Capote, M. Sin, A. Trkov, B. Carlson, P. Oblozinsky, C. Mattoon, H. Wienke, S. Hoblit, EMPIRE-3.2 Malta modular system for nuclear reaction calculations and nuclear data evaluation Users Manual, in, Brookhaven National Laboratory (BNL) National Nuclear Data Center, 2013.
[118] R. Chakravarty, S. Chakraborty, K. Vimalnath, P. Shetty, H.D. Sarma, P. Hassan, A. Dash, 64 CuCl 2 produced by direct neutron activation route as a cost-effective probe for cancer imaging: the journey has begun, RSC Advances, 5 (2015) 91723-91733.
[119] T. Theophanides, J. Anastassopoulou, Copper and carcinogenesis, Critical reviews in oncology/hematology, 42 (2002) 57-64.
[120] M.L. Turski, D.J. Thiele, New roles for copper metabolism in cell proliferation, signaling, and disease, Journal of Biological Chemistry, 284 (2009) 717-721.
[121] H. Cai, J.-s. Wu, O. Muzik, J.-T. Hsieh, R.J. Lee, F. Peng, Reduced 64Cu uptake and tumor growth inhibition by knockdown of human copper transporter 1 in xenograft mouse model of prostate cancer, Journal of nuclear medicine: official publication, Society of Nuclear Medicine, 55 (2014) 622.
[122] C. Qin, H. Liu, K. Chen, X. Hu, X. Ma, X. Lan, Y. Zhang, Z. Cheng, Theranostics of malignant melanoma with 64CuCl2, Journal of nuclear medicine: official publication, Society of Nuclear Medicine, 55 (2014) 812.
[123] J. Lee, M.M.O. Peña, Y. Nose, D.J. Thiele, Biochemical characterization of the human copper transporter Ctr1, Journal of Biological Chemistry, 277 (2002) 4380-4387.
[124] I.F. Tsigelny, Y. Sharikov, J.P. Greenberg, M.A. Miller, V.L. Kouznetsova, C.A. Larson, S.B. Howell, An all-atom model of the structure of human copper transporter 1, Cell biochemistry and biophysics, 63 (2012) 223-234.
[125] J.T. Jørgensen, M. Persson, J. Madsen, A. Kjær, High tumor uptake of 64Cu: implications for molecular imaging of tumor characteristics with copper-based PET tracers, Nuclear medicine and biology, 40 (2013) 345-350.
[126] C. Ferrari, A. Niccoli Asabella, C. Villano, B. Giacobbi, D. Coccetti, P. Panichelli, G. Rubini, Copper-64 dichloride as theranostic agent for glioblastoma multiforme: a preclinical study, BioMed research international, 2015 (2015).
[127] P. Panichelli, C. Villano, A. Cistaro, A. Bruno, F. Barbato, A. Piccardo, A. Duatti, Imaging of brain tumors with copper-64 chloride: early experience and results, Cancer Biotherapy and Radiopharmaceuticals, 31 (2016) 159-167.
[128] G. Valentini, P. Panichelli, C. Villano, G. Pigotti, D. Martini, 64CuCl2: new theranostic agent, Nuclear Medicine and Biology, 41 (2014) 638.
[129] P. Mohr, S. Brieger, G. Witucki, M. Maetz, Photoactivation at a clinical LINAC: The Au (γ, n) 196197Au reaction slightly above threshold, Nuclear Instruments and Methods in Physics Research Section A: Accelerators, Spectrometers, Detectors and Associated Equipment, 580 (2007) 1201-1208.

[130] I. Boztosun, H. Đapo, M. Karakoç, S. Özmen, Y. Çeçen, A. Çoban, T. Caner, E. Bayram, T. Saito, T. Akdoğan, Photonuclear reactions with zinc: A case for clinical linacs, The European Physical Journal Plus, 130 (2015) 185.
[131] M. Aygun, A. Cesur, M. Dogru, I. Boztosun, H. Dapo, M. Kanarya, M. Kuluozturk, S. Bal, S. Karatepe, Using a clinical linac to determine the energy levels of 92mNb via the photonuclear reaction, Applied Radiation and Isotopes, 115 (2016) 97-99.
[132] C. Glide-Hurst, M. Bellon, R. Foster, C. Altunbas, M. Speiser, M. Altman, D. Westerly, N. Wen, B. Zhao, M. Miften, Commissioning of the Varian TrueBeam linear accelerator: a multi-institutional study, Medical physics, 40 (2013) 031719.
[133] E. Brunckhorst, Experimental investigations of the neutron contamination in high-energy photon fields at medical linear accelerators, (2009).
[134] G. Tosi, A. Torresin, S. Agosteo, A.F. Para, V. Sangiust, L. Zeni, M. Silari, Neutron measurements around medical electron accelerators by active and passive detection techniques, Medical physics, 18 (1991) 54-60.
[135] M.S.C. 60, Neutron Contamination from Medical Electron Accelerators: Recommendations of the National Council on Radiation Protection and Measurements, Ncrp, 1984.
[136] B. Patil, S. Chavan, S. Pethe, R. Krishnan, V. Bhoraskar, S. Dhole, Estimation of neutron production from accelerator head assembly of 15 MV medical LINAC using FLUKA simulations, Nuclear Instruments and Methods in Physics Research Section B: Beam Interactions with Materials and Atoms, 269 (2011) 3261-3265.
[137] V. Varlamov, N. Efimkin, B. Ishkhanov, V. Sapunenko, M. Stepanov, Evaluation of Cu-63, 65 (7, np) and Cu-63, 65 (7, p) reaction cross sections in the energy range of giant dipole resonance and isospin splitting of the G DR of Cu nuclei, Izv. Akad. Nauk SSSR, ser. Fiz, 59 (1995) 222.
[138] K. Vimalnath, A. Rajeswari, V. Chirayil, P. Sharad, K. Jagadeesan, P. Joshi, M. Venkatesh, Studies on preparation of 64Cu using (n, γ) route of reactor production using medium flux research reactor in India, Journal of Radioanalytical and Nuclear Chemistry, 290 (2011) 221-225.
[139] K. Thiel, T. Klamroth, P. Strauch, A. Taubert, On the interaction of ascorbic acid and the tetrachlorocuprate ion [CuCl 4] 2− in CuCl nanoplatelet formation from an ionic liquid precursor (ILP), Physical Chemistry Chemical Physics, 13 (2011) 13537-13543.
[140] C. Wang, L. Lu, W. Ye, O. Zheng, B. Qiu, Z. Lin, L. Guo, G. Chen, Fluorescence sensor for Cu (II) in the serum sample based on click chemistry, Analyst, 139 (2014) 656-659.
[141] L. Jiang, Y. Tu, X. Hu, A. Bao, H. Chen, X. Ma, T. Doyle, H. Shi, Z. Cheng, Pilot Study of 64 Cu (I) for PET Imaging of Melanoma, Scientific Reports, 7 (2017) 2574.
[142] A. Fasso, A. Ferrari, J. Ranft, P. Sala, Intermediate energy nuclear data: models and codes, in: Proceedings of a Specialists Meeting, Issy les Moulineaux (France), 1994, pp. 271.
[143] F. Peng, X. Lu, J. Janisse, O. Muzik, A.F. Shields, PET of human prostate cancer xenografts in mice with increased uptake of 64CuCl2, Journal of Nuclear Medicine, 47 (2006) 1649-1652.
[144] M.A. Johnson, S.E. Kays, Copper: its role in human nutrition, Nutrition Today, 25 (1990) 6-14.

[145] N.A. Smith, D.L. Bowers, D.A. Ehst, The production, separation, and use of 67Cu for radioimmunotherapy: a review, Applied Radiation and Isotopes, 70 (2012) 2377-2383.
[146] C. Champion, M.A. Quinto, C. Morgat, P. Zanotti-Fregonara, E. Hindié, Comparison between Three Promising ß-emitting Radionuclides, 67Cu, 47Sc and 161Tb, with Emphasis on Doses Delivered to Minimal Residual Disease, Theranostics, 6 (2016) 1611.
[147] I. Novak-Hofer, A.P. Schubiger, Copper-67 as a therapeutic nuclide for radioimmunotherapy, European journal of nuclear medicine and molecular imaging, 29 (2002) 821-830.
[148] Y. Sugo, K. Hashimoto, M. Kawabata, H. Saeki, S. Sato, K. Tsukada, Y. Nagai, Application of 67Cu Produced by 68Zn (n, n' p+ d) 67Cu to Biodistribution Study in Tumor-Bearing Mice, Journal of the Physical Society of Japan, 86 (2016) 023201.
[149] E.W. Price, C. Orvig, Matching chelators to radiometals for radiopharmaceuticals, Chemical Society Reviews, 43 (2014) 260-290.
[150] S. Mirzadeh, L. Mausner, S. Srivastava, Production of no-carrier added 67Cu, International journal of radiation applications and instrumentation. Part A. Applied radiation and isotopes, 37 (1986) 29-36.
[151] M.S. Uddin, M. Rumman-uz-Zaman, S.M. Hossain, S.M. Qaim, Radiochemical measurement of neutron-spectrum averaged cross sections for the formation of 64Cu and 67Cu via the (n, p) reaction at a TRIGA Mark-II reactor: Feasibility of simultaneous production of the theragnostic pair 64Cu/67Cu, Radiochimica Acta, 102 (2014) 473-480.
[152] A. Dasgupta, L. Mausner, S. Srivastava, A new separation procedure for 67Cu from proton irradiated Zn, International Journal of Radiation Applications and Instrumentation. Part A. Applied Radiation and Isotopes, 42 (1991) 371-376.
[153] S.C. Srivastava, Paving the way to personalized medicine: production of some theragnostic radionuclides at Brookhaven National Laboratory, Radiochimica Acta International journal for chemical aspects of nuclear science and technology, 99 (2011) 635-640.
[154] D.G. Medvedev, L.F. Mausner, G.E. Meinken, S.O. Kurczak, H. Schnakenberg, C.J. Dodge, E.M. Korach, S.C. Srivastava, Development of a large scale production of 67Cu from 68Zn at the high energy proton accelerator: closing the 68Zn cycle, Applied Radiation and Isotopes, 70 (2012) 423-429.
[155] T. Stoll, S. Kastleiner, Y.N. Shubin, H.H. Coenen, S.M. Qaim, Excitation functions of proton induced reactions on 68Zn from threshold up to 71 MeV, with specific reference to the production of 67Cu, Radiochimica Acta, 90 (2002) 309-313.
[156] F. Szelecsényi, G. Steyn, S. Dolley, Z. Kovács, C. Vermeulen, T. Van der Walt, Investigation of the 68Zn (p, 2p) 67Cu nuclear reaction: New measurements up to 40 MeV and compilation up to 100 MeV, Nuclear Instruments and Methods in Physics Research Section B: Beam Interactions with Materials and Atoms, 267 (2009) 1877-1881.

[157] D. sr Jamriska, W. Taylor, M. Ott, R. Heaton, D. Phillips, M. Fowler, Activation rates and chemical recovery of67Cu produced with low energy proton irradiation of enriched70Zn targets, Journal of Radioanalytical and Nuclear Chemistry, 195 (1995) 263-270.
[158] S. Kastleiner, H. Coenen, S. Qaim, Possibility of production of 67Cu at a small-sized cyclotron via the (p, α)-reaction on enriched 70Zn, Radiochimica Acta, 84 (1999) 107-110.
[159] K. Hilgers, T. Stoll, Y. Skakun, H. Coenen, S. Qaim, Cross-section measurements of the nuclear reactions natZn (d, x) 64Cu, 66Zn (d, α) 64Cu and 68Zn (p, αn) 64Cu for production of 64Cu and technical developments for small-scale production of 67Cu via the 70Zn (p, α) 67Cu process, Applied radiation and isotopes, 59 (2003) 343-351.
[160] J. Kozempel, K. Abbas, F. Simonelli, A. Bulgheroni, U. Holzwarth, N. Gibson, Preparation of 67Cu via deuteron irradiation of 70Zn, Radiochimica Acta International journal for chemical aspects of nuclear science and technology, 100 (2012) 419-424.
[161] N. Sato, K. Tsukada, S. Watanabe, N.S. Ishioka, M. Kawabata, H. Saeki, Y. Nagai, T. Kin, F. Minato, N. Iwamoto, First Measurement of the Radionuclide Purity of the Therapeutic Isotope 67Cu Produced by 68Zn (n, x) Reaction Using natC (d, n) Neutrons, Journal of the Physical Society of Japan, 83 (2014) 073201.
[162] M. Yagi, K. Kondo, Preparation of carrier-free 67Cu by the 68Zn (γ, p) reaction, The International Journal of Applied Radiation and Isotopes, 29 (1978) 757-759.
[163] S.M. Qaim, F. Tárkányi, R. Capote, Nuclear data for the production of therapeutic radionuclides, Citeseer, 2011.
[164] M. Kawabata, K. Hashimoto, H. Saeki, N. Sato, S. Motoishi, K. Takakura, C. Konno, Y. Nagai, Production and separation of 64Cu and 67Cu using 14 MeV neutrons, Journal of Radioanalytical and Nuclear Chemistry, 303 (2015) 1205-1209.
[165] T. Kin, Y. Nagai, N. Iwamoto, F. Minato, O. Iwamoto, Y. Hatsukawa, M. Segawa, H. Harada, C. Konno, K. Ochiai, New production routes for medical isotopes 64Cu and 67Cu using accelerator neutrons, Journal of the Physical Society of Japan, 82 (2013) 034201.
[166] T.S. Dixit, S.T. Chavan, R. Krishnan, C.S. Nainwad, S.N. Pethe, K.A. Thakur, T. Tiwari, M.M. Vidwans, A. Deshpande, Development of a prototype 15 MeV electron linac, in: Proceedings of the International Particle Accelerator Conference-2010 (IPAC'10), Kyoto, Japan, 2010, pp. 23-28.
[167] D. Ehst, N. Smith, D. Bowers, V. Makarashvili, Copper-67 production on electron linacs—Photonuclear technology development, in: AIP Conference Proceedings, AIP, 2012, pp. 157-161.
[168] Y. Nagai, K. Hashimoto, Y. Hatsukawa, H. Saeki, S. Motoishi, N. Sato, M. Kawabata, H. Harada, T. Kin, K. Tsukada, Generation of radioisotopes with accelerator neutrons by deuterons, Journal of the Physical Society of Japan, 82 (2013) 064201.
[169] S. Bishnoi, R. Paul, T. Patel, P. Sarkar, P. Adhikari, A. Sinha, Source characterization of Purnima neutron generator (PNG), in: DAE Symp. Nucl. Phys., 2011, pp. 1102-1103.

[170] L. Auditore, E. Amato, S. Baldari, Theoretical estimation of 64Cu production with neutrons emitted during 18F production with a 30 MeV medical cyclotron, Applied Radiation and Isotopes, 122 (2017) 229-234.
[171] S.M. Qaim, T. Bisinger, K. Hilgers, D. Nayak, H.H. Coenen, Positron emission intensities in the decay of 64Cu, 76Br and 124I, Radiochimica Acta, 95 (2007) 67-73.
[172] T.H. Bokhari, A. Mushtaq, I.U. Khan, Production of low and high specific activity 64Cu in a reactor, Journal of radioanalytical and nuclear chemistry, 284 (2010) 265-271.
[173] M. Al-Abyad, I. Spahn, S. Sudár, M. Morsy, M. Comsan, J. Csikai, S. Qaim, H. Coenen, Nuclear data for production of the therapeutic radionuclides 32P, 64Cu, 67Cu, 89Sr, 90Y and 153Sm via the (n, p) reaction: Evaluation of excitation function and its validation via integral cross-section measurement using a 14 MeV d (Be) neutron source, Applied radiation and isotopes, 64 (2006) 717-724.
[174] S. Qaim, A systematic study of (n, d),(n, n'p) and (n, pn) reactions at 14.7 MeV, Nuclear Physics A, 382 (1982) 255-268.
[175] C. Konno, Activation cross section measurements at neutron energy from 13.3 to 15.0 MeV using the FNS facility, JAERI1329, (1993).
[176] G. Lhersonneau, T. Malkiewicz, K. Kolos, M. Fadil, H. Kettunen, M. Saint-Laurent, A. Pichard, W. Trzaska, G. Tyurin, L. Cousin, Neutron yield from carbon, light-and heavy-water thick targets irradiated by 40 MeV deuterons, Nuclear Instruments and Methods in Physics Research Section A: Accelerators, Spectrometers, Detectors and Associated Equipment, 603 (2009) 228-235.
[177] S. Agostinelli, J. Allison, K.a. Amako, J. Apostolakis, H. Araujo, P. Arce, M. Asai, D. Axen, S. Banerjee, G. Barrand, GEANT4—a simulation toolkit, Nuclear instruments and methods in physics research section A: Accelerators, Spectrometers, Detectors and Associated Equipment, 506 (2003) 250-303.
[178] S. Dolley, T. van der Walt, Isolation of Cu radionuclides with dithizone impregnated XAD-8, Radiochimica Acta, 102 (2014) 263-269.